



National Library
of Canada

Acquisitions and
Bibliographic Services Branch

395 Wellington Street
Ottawa, Ontario
K1A 0N4

Bibliothèque nationale
du Canada

Direction des acquisitions et
des services bibliographiques

395, rue Wellington
Ottawa (Ontario)
K1A 0N4

Your file *Votre référence*

Our file *Notre référence*

NOTICE

The quality of this microform is heavily dependent upon the quality of the original thesis submitted for microfilming. Every effort has been made to ensure the highest quality of reproduction possible.

If pages are missing, contact the university which granted the degree.

Some pages may have indistinct print especially if the original pages were typed with a poor typewriter ribbon or if the university sent us an inferior photocopy.

Reproduction in full or in part of this microform is governed by the Canadian Copyright Act, R.S.C. 1970, c. C-30, and subsequent amendments.

AVIS

La qualité de cette microforme dépend grandement de la qualité de la thèse soumise au microfilmage. Nous avons tout fait pour assurer une qualité supérieure de reproduction.

S'il manque des pages, veuillez communiquer avec l'université qui a conféré le grade.

La qualité d'impression de certaines pages peut laisser à désirer, surtout si les pages originales ont été dactylographiées à l'aide d'un ruban usé ou si l'université nous a fait parvenir une photocopie de qualité inférieure.

La reproduction, même partielle, de cette microforme est soumise à la Loi canadienne sur le droit d'auteur, SRC 1970, c. C-30, et ses amendements subséquents.

UNIVERSITY OF ALBERTA

**Trace element and Isotopic Constraints for the
Origin of Mesozoic Granitoids in the
Southern Canadian Cordillera**

by

Alan D. Brandon



A thesis submitted to the Faculty of Graduate Studies and Research
in partial fulfillment of the requirements for the degree of Doctor of
Philosophy

Department of Geology

Edmonton, Alberta

Fall, 1992



National Library
of Canada

Bibliothèque nationale
du Canada

Canadian Theses Service Service des thèses canadiennes

Ottawa, Canada
K1A 0N4

The author has granted an irrevocable non-exclusive licence allowing the National Library of Canada to reproduce, loan, distribute or sell copies of his/her thesis by any means and in any form or format, making this thesis available to interested persons.

The author retains ownership of the copyright in his/her thesis. Neither the thesis nor substantial extracts from it may be printed or otherwise reproduced without his/her permission.

L'auteur a accordé une licence irrévocable et non exclusive permettant à la Bibliothèque nationale du Canada de reproduire, prêter, distribuer ou vendre des copies de sa thèse de quelque manière et sous quelque forme que ce soit pour mettre des exemplaires de cette thèse à la disposition des personnes intéressées.

L'auteur conserve la propriété du droit d'auteur qui protège sa thèse. Ni la thèse ni des extraits substantiels de celle-ci ne doivent être imprimés ou autrement reproduits sans son autorisation.

ISBN 0-315-77229-8

Canada

UNIVERSITY OF ALBERTA

RELEASE FORM

NAME OF AUTHOR: Alan D. Brandon
TITLE OF THESIS: Trace Element and Isotopic Constraints
for the Origin of Mesozoic Granitoids in
the Southern Canadian Cordillera
DEGREE: Doctor of Philosophy
YEAR THIS DEGREE GRANTED: 1992

Permission is hereby granted to the University of Alberta to reproduce single copies of this thesis and to lend or sell such copies for private, scholarly or scientific research purposes only.

The author reserves all other publication and other rights in association with the copyright in the thesis, and except as hereinbefore provided neither the thesis nor any substantial portion thereof may be printed or otherwise reproduced in any material from whatever without the author's prior written permission.



3321 17th Place

Forest Grove, Oregon

United States of America 97116

UNIVERSITY OF ALBERTA

FACULTY OF GRADUATE STUDIES AND RESEARCH

The undersigned certify that they have read, and recommend to the Faculty of Graduate Studies and Research for acceptance, a thesis entitled Trace Element and Isotopic Constraints for the Origin of Mesozoic Granitoids in the Southern Canadian Cordillera submitted by Alan D. Brandon in partial fulfillment of the requirements for the degree of Doctor of Philosophy.

R.S.J. Lambert

Dr. R.StJ. Lambert

Supervisor

[Signature]
Dr. R.W. Luth

[Signature]
Dr. T. Chacko

[Signature]
Dr. R.A. Creaser

G.L. Cumming
Dr. G.L. Cumming

[Signature]
Dr. P.J. Patchett

External Examiner

August 14, 1992

ABSTRACT

The trace element and isotopic compositions of Mesozoic granitoids in southeast British Columbia constrain the timing and mechanisms for granitoid production in the Cordilleran interior in western North America. Mesozoic granitoid rocks in the southeast Canadian Cordillera are exposed within Paleozoic-Mesozoic rocks of Terrane I, Paleozoic metasediments of the Kootenay arc, and Proterozoic Purcell-Windermere metasediments. Rb-Sr whole rock and whole rock plus apatite isochrons for several of the batholiths give the following ages : Raft - 164 +/- 4 Ma for whole rock; Bugaboo - 107 +/- 1 Ma for whole rock-apatite (WRA); Horsethief Creek - 109 +/- 14 Ma for WRA; Fry Creek - 115 +/- 7 Ma for WRA; and White Creek - 106 +/- 1 Ma for WRA. These ages fall within the ranges for a Middle Jurassic magmatic pulse from 175 to 162 Ma and a mid-Cretaceous magmatic pulse from 115 to 110 Ma defined from a compilation of crystallization ages for all granitoid rocks from southeast British Columbia.

The mid-Cretaceous Bugaboo, Fry Creek, and Horsethief batholiths are composed of two types of granite; weakly peraluminous hornblende-biotite granite found in all three, and strongly peraluminous 2-mica granite found in Fry Creek. The White Creek batholith is a zoned pluton with quartz monzodiorite on the rim grading into hornblende-biotite granodiorite, which in turn is crosscut by 2-mica granites. The hornblende-biotite granitoids have initial ϵ_{Sr} ranging from +36 to +80, initial ϵ_{Nd} ranging from -5 to -9, and initial $^{206}Pb/^{204}Pb$, $^{208}Pb/^{204}Pb$, and $^{207}Pb/^{204}Pb$ ranging from 18.3 to 19.2, 15.58 to 15.72, and 38.3 to 39.8, respectively. These granites have high Nb and Rb, and low Ba abundances relative to granites found in volcanic arcs. The 2-mica granites have ϵ_{Sr} ranging from +150 to +470, ϵ_{Nd} ranging from -12 to -21, and more radiogenic initial Pb isotope ratios than the hornblende-biotite

granitoids. Their trace element compositions are similar to granites found in continental interiors. O and Sr isotopes, and REE modelling are consistent with crustal anatexis of Precambrian basement gneisses and Proterozoic metapelites producing the hornblende-biotite granitoids and 2-mica granites, respectively. The sequence of intrusion in the White Creek batholith constrains the timing of melting. A zone of anatexis proceeded upwards through the crust, melting basement gneisses followed by melting of overlying metapelites. Crustal anatexis was likely a response to crustal thickening because of terrane accretion and collision.

The Middle Jurassic Raft, Galena Bay, and Mt. Toby plutons have compositional features similar to other Middle Jurassic granitoids in SEBC. They generally have lower initial ϵ_{Sr} and higher ϵ_{Nd} and less radiogenic initial $^{206}Pb/^{204}Pb$, $^{208}Pb/^{204}Pb$, and $^{207}Pb/^{204}Pb$ ratios than the mid-Cretaceous granitoids. These isotopic features are consistent with mixing between mantle-derived basalt and Precambrian crust. Their trace element compositions are similar to granitoids found within volcanic arcs. In particular, they have high Ba and low Rb and Nb relative to the mid-Cretaceous granitoids. The compositional relationships for the Middle Jurassic granitoids suggest that these rocks were associated with a volcanic arc. They formed on Terrane I as subduction of ocean crust and accretion of Terrane II occurred westwards from Early to Middle Jurassic.

ACKNOWLEDGEMENTS

Many people have had an integral part in helping me complete this study. They are: Gordon G. Goles, R.StJ. Lambert, Dana Johnston, Rob Creaser, Reidar Trøttes, Jonathan Patchett, Alan Smith, Bob Luth, Tom Chacko, George Cumming, Peter Hooper, Kevin Urbanczyk, Rob King, Halfdan Baadsgaard, Dragan Krstic, Len Tober, Don Resultay, Brian Chatterton, Bruce Nesbitt, Andrew Locock, Paul Wagner, John Stimac, and Eric Sonnenthal. Each of these people are thanked for their contributions. Funding from the University of Alberta and NSERC grants to R.StJ. Lambert are acknowledged.

I wish to especially thank G³ for all of his enthusiasm and creativity for which were an inspiration to me during this study. I may have never gotten this far without his advice. I also want to thank Richard for his supervisorship. Through all of the tough times during the past four years, he always remained a supporter and a friend. Thanks everyone!

TABLE OF CONTENTS

Chapter	Page
1. Introduction.....	1
Reference.....	4
2 Rb-Sr Ages on Mesozoic Granitoids in the Southern Canadian Cordillera.....	5
Introduction.....	5
Geology.....	6
Analytical Techniques.....	7
Results.....	8
Discussion and Conclusions.....	11
3. Geochemical Characterization of Mid-Cretaceous Granitoids of the Kootenay Arc in the Southern Canadian Cordillera.....	30
Introduction.....	30
Geology.....	32
Petrography.....	33
Analytical Methods.....	36
Results.....	37
Major and trace element geochemistry.....	37
Isotope geochemistry.....	41
Sources for the BFH Granites.....	44
Isotopic constraints.....	44
Phase equilibrium constraints.....	47
Conclusions.....	49
Appendix 3.1.....	69
Appendix 3.2.....	70

References.....	72
4. Crustal Melting in the Cordilleran Interior: The Mid-Cretaceous White Creek Batholith in the Southern Canadian Cordillera.....	81
Introduction.....	81
Geology.....	83
Petrography.....	85
Analytical Methods.....	87
Results.....	89
Major and trace element geochemistry.....	89
Isotope geochemistry.....	92
Constraints on WCB Source Materials.....	97
Isotopic constraints.....	97
Trace element and phase equilibrium constraints on crustal melting.....	101
Discussion.....	106
Evolution of the White Creek magmatic system.....	106
A model for crustal melting.....	108
Conclusions.....	111
Appendix 4.1.....	143
Appendix 4.2.....	144
References.....	145
5. Mesozoic Granitoid Magmatism in the Omineca Belt on Southeast British Columbia: Implications for the Generation of Silicic Magmas in the North American Cordillera.....	156

Introduction.....	156
Geology.....	158
Sampling, Lithologies, and Petrography.....	160
Analytical Techniques.....	161
Compositional Features of the SEBC	
Granitoids.....	162
Major and trace element compositions.....	162
Isotopic compositions.....	168
Discussion.....	171
Origin of the southern Omineca Belt	
Mesozoic granitoids.....	171
Development of the Omineca Belt in the late-Mesozoic.....	174
Conclusions.....	180
Appendix 5.1.....	203
References.....	204
6. Concluding Remarks	215

LIST OF TABLES

Table	Page
2.1 Rb-Sr results for whole rock powders and apatite separates from Bugaboo, Fry Creek, Horsethief Creek, White Creek, and Raft intrusions.....	14
2.2 Crystallization age determinations for Mesozoic granitoids in the southern Canadian Cordillera.....	15
3.1 Major and trace element abundances of the Bugaboo, Fry Creek, and Horsethief Creek batholiths.....	52
3.2 Isotopic standard data analyzed during this study.....	56
3.3 Rb-Sr and Sm-Nd isotopic relations for the Bugaboo, Fry Creek, and Horsethief Creek batholiths.....	57
3.4 U-Th-Pb isotopic relations for Bugaboo, Horsethief Creek, and Fry Creek samples.....	59
4.1 Modal mineralogical proportions (%) of the main lithologic zones of the White Creek batholith.....	113
4.2 Major and trace element abundances of the White Creek batholith.....	114
4.3 Rb-Sr and Sm-Nd isotopic relations for the White Creek batholith.....	117
4.4 U-Th-Pb isotopic compositions for the White Creek samples.....	119
4.5 Whole rock and quartz oxygen isotope compositions for selected White Creek samples.....	120
4.6 A comparison between amphibolite and tonalite starting material in melting experiments with mafic and felsic Precambrian basement rocks in SE British	

Columbia.....	121
5.1 Major and trace element abundances for samples from the Raft, Galena Bay, and Mt. Toby plutons.....	183
5.2 Rb-Sr and Sm-Nd isotopic compositions for samples from the Raft, Galena Bay, and Mt. Toby plutons.....	188
5.3 U-Th-Pb isotopic compositions of samples from the Raft, Galena Bay, and Mt. Toby plutons.....	190

LIST OF FIGURES

Figure	Page
2.1 Tectono-magmatic map of the southern Omineca Crystalline Belt.....	17
2.2 Rb-Sr age relations for the Raft batholith.....	18
2.3 Rb-Sr age relations for the Bugaboo batholith.....	19
2.4 Rb-Sr age relations for the Fry Creek batholith.....	20
2.5 Rb-Sr age relations for the Horsethief Creek batholith.....	21
2.6 Rb-Sr age relations for the White Creek batholith core.....	22
2.7 Rb-Sr age relations for the White Creek batholith rim and center.....	23
3.1 Generalized geologic map for southeast British Columbia along the Kootenay arc.....	60
3.2 Alumina-saturation index versus Fe ratio and AKN for the BFH granites.....	61
3.3 SiO ₂ versus ASI and Fe ratios for the BFH samples.....	62
3.4 Trace element normalized diagrams for selected BFH samples.....	63
3.5A Nb + Y versus Rb tectonic discrimination diagram plotting the BFH granites.....	64
3.5B Y versus Nb tectonic discrimination diagram plotting the BFH granites.....	65
3.6 Initial ϵ_{Sr} versus ϵ_{Nd} diagram for crustal rocks and Mesozoic granites from SEBC.....	66
3.7 Initial $^{206}Pb/^{204}Pb$ versus $^{208}Pb/^{204}Pb$ and $^{207}Pb/^{204}Pb$ for the BFH samples and SEBC metasediments.....	67
3.8 $^{147}Sm/^{144}Nd$ versus ϵ_{Nd} for the BFH samples and SEBC	

basement rocks.....	68
4.1 Generalized geologic map for southeast British Columbia.....	122
4.2 Lithologic map for the White Creek batholith.....	124
4.3 Harker variation diagrams for major element compositions of samples from the WCB.....	126
4.4 Alumina-saturation index versus AKN for the WCB samples.....	127
4.5 Harker variation diagrams for selected trace elements for WCB samples.....	129
4.6 Rare earth element compositions of the WCB samples.....	130
4.7 A) Ce/Yb versus Eu/Eu* for the WCB samples. B) Eu versus Sr for the WCB samples.....	131
4.8 Initial ϵ_{Sr} versus ϵ_{Nd} diagram for the WCB granitoid and Precambrian crustal rocks from SE British Columbia.....	132
4.9 Initial $^{206}Pb/^{204}Pb$ versus $^{208}Pb/^{204}Pb$ and $^{207}Pb/^{204}Pb$ for the WCB granitoid whole rock samples and alkali feldspars.....	134
4.10 Initial $^{207}Pb/^{204}Pb$ versus ϵ_{Nd} for the WCB samples.....	135
4.11 $\delta^{18}O$ versus ϵ_{Sr} for the WCB samples.....	136
4.12 AFC and mixing calculated models for $\delta^{18}O$ and $1/Sr$ versus ϵ_{Sr} using various end-member compositions.....	138
4.13 Calculated REE compositions of source materials for the WCB and SE British Columbia basement rocks.....	140
4.14 Ce/Sm versus Ce/Yb ratios for mafic sources calculated for 30 to 50% melting of amphibolite.....	141
4.15 Harker variation diagrams for compositions produced by amphibolite melting at 1-6.8 kbar and 8 and 16 kbar....	142

5.1	Tectono-magmatic map of southern British Columbia and surrounding regions.....	191
5.2	Tectono-magmatic map of the southern Omineca Crystalline Belt.....	192
5.3	SiO ₂ versus FeO*/(FeO*+MgO) for the Mesozoic granitoids in SEBC.....	193
5.4	SiO ₂ versus Al ₂ O ₃ /(Na ₂ O + K ₂ O + CaO) for the Mesozoic granitoids in SEBC.....	194
5.5	Incompatible trace element normalized plots for representative Middle Jurassic and mid-Cretaceous granitoids.....	195
5.6	Rb versus Nb + Y diagram showing abundances from SEBC granodiorites and granites.....	196
5.7	Nb versus Y diagram showing the abundances from SEBC granodiorites and granites.....	197
5.8	Ce/Nb versus Ba/Nb.....	198
5.9	ε ₈₇ versus ε _{Nd} for the SEBC granitoids.....	199
5.10	Initial ²⁰⁶ Pb/ ²⁰⁴ Pb versus ²⁰⁸ Pb/ ²⁰⁴ Pb and ²⁰⁷ Pb/ ²⁰⁴ Pb for the Mesozoic granitoids in the Omineca Belt.....	200
5.11	ε _{Nd} versus SiO ₂ for Mesozoic granitoids in the Omineca Belt..	120
5.12	²⁰⁶ Pb/ ²⁰⁴ Pb versus ε _{Nd} for Mesozoic granitoids from the Omineca Belt.....	202

Chapter 1

Introduction

"This indicates to my mind that there is no unique solution to the problem - there are granites and granites"

H.H. Read 1948

The "granite problem" is the ever changing dilemma for the origin of plutonic rocks consisting of essentially quartz and alkali feldspar. When H. Read addressed the world's petrologists at a meeting of the Geological Society of America on the Origin of Granites in 1947, the granite problem was one of fundamental importance to the understanding of how the crust of the Earth was formed and how magmas evolved during cooling and migration (Read 1948). By the 1940's, two hypotheses for the origin of granitic rocks were favored above the rest. One group of petrologists believed that granites were the result of granitization, where country rocks were changed into granite without undergoing a melting stage. Another group, led by N.L. Bowen, argued that granites were igneous rocks derived directly by partial melting of sialic crust, or through fractional crystallization of basaltic melts leaving granitic residual melts. It was believed that evidence supporting each hypothesis could be found in granite rocks from almost every geological terrain on the continents, and led Read (1948) to conclude that there are granites and granites.

After a half-century of field, geochemical, and experimental study, it is now apparent that most granites are of igneous origin, and granitization is unlikely to represent a major process in the production of granite. The granite problem today is primarily one of evaluating whether any given granite is a primary melt of the crust, or a mixture of mantle-derived and

crustal melts. An additional problem is concerned with determining the relative proportions of melt and restite present in a granite body. Identifying the physical and chemical factors that control the production of granites is important to determining possible solutions to the granite problem. In this dissertation, I have studied Mesozoic granites and associated plutonic rocks from southeast British Columbia (SEBC). The primary focus of this study is to use trace element and isotopic evidence to constrain the origins of these granitoid rocks and to determine the factors involved in producing the observed range of chemical variation. The SEBC granitoids are of special interest because they were formed in a continental interior during a time when exotic terranes were being accreted to the continental margin, and during crustal thickening in response to large-scale thrusting in the interior. The mechanisms that produce large volumes of granitoid magma in these tectonic regimes are poorly understood.

In Chapter 2, I have used Rb-Sr isotopes to obtain crystallization ages for several of the batholiths. The granitoid rocks from these batholiths, for the most part, have a restricted range in Rb/Sr ratios, and I use associated aplites and pegmatites with higher Rb/Sr ratios, and apatite with lower Rb/Sr ratios, to constrain their ages. A compilation of published radiometric dates and those I acquired indicate that there were two discrete magmatic pulses which produced large volumes of granitoids in southeast British Columbia in the Mesozoic. The first pulse occurred during the Middle Jurassic from about 175 to 160 Ma, and the second pulse in the mid-Cretaceous from about 115 to 105 Ma. It is apparent from the clustering of ages that the processes that produced large volumes of magma in SEBC during this time were episodic.

In Chapter 3, geochemical data for the mid-Cretaceous Bugaboo, Fry Creek, and Horsethief Creek batholiths are presented. These batholiths are

composed of hornblende-biotite granites and 2-mica granites. Their major and trace element, and Sr, Nd, and Pb isotopic compositions are consistent with derivation of the hornblende-biotite granites by anatexis of mafic and tonalitic basement gneisses exposed in SEBC. The 2-mica granites may be melts from metapelites overlying the basement gneisses.

The absence of contemporaneous basalt is difficult to reconcile with a model for magmatic underplating as a primary cause of anatexis of the crust during the mid-Cretaceous magmatic episode. Alternatively, a model of crustal thickening is favored as a mechanism to promote melting of the crust which would have resulted in the mid-Cretaceous granites.

The geochemical variation of the mid-Cretaceous White Creek batholith is considered in Chapter 4. The White Creek batholith is a zoned pluton. Distinct jumps in major, trace element, and isotopic compositions across the zones are consistent with a model where pulses of magmas were generated as a zone of melting proceeded upward through the crust, producing plutons ranging from hornblende-biotite granodiorites from more mafic source lithologies to 2-mica granites from pelitic schists. These inferences are consistent with a crustal thickening model to produce anatexis.

Finally, in Chapter 5 the variation in granitoid geochemistry from the Middle Jurassic and the mid-Cretaceous is addressed. The granitoids from the Middle Jurassic in SEBC have lithological and geochemical characteristics similar those of granitoids found in relict volcanic arcs. A model where basaltic magmas infiltrated and interacted with lower crust, followed by the evolved magmas assimilating middle to upper crust en route to emplacement, can produce the range in lithological and geochemical variation observed in the Middle Jurassic suite. These granitoids are geochemically distinct from the granitoids in the mid-Cretaceous suite, which result from crustal melting.

This change in character in granitoid composition from the Middle Jurassic to the mid-Cretaceous marks a period during which the tectonic regime changed from growth of the continental margin by subduction of ocean crust and associated accretion of exotic terranes to stabilization of these rocks as part of the continent and north south compression resulting in crustal thickening. The granitoids in SEBC therefore yield important clues to large-scale mechanisms which control the generation of silicic plutonic rocks.

In conclusion, this dissertation study confirms what granite petrologists have known for decades. There are granites and granites. In the decades to follow, I hope that studies such as this one will lay the foundations for new additions and insights to the granite problem.

Reference

Read, H.H., 1948. Granites and granites. *In* Origin of Granite, *Edited* by J.

Gilluly, Geological Society of America, Memoir 28, 1-19.

Chapter 2

Rb-Sr Ages of Mesozoic Granitoids in the Southern Canadian Cordillera

Alan D. Brandon and Richard St J. Lambert
Department of Geology,
University of Alberta, Edmonton,
Alberta, T6G 2E3

Submitted to Canadian Journal of Earth Sciences, February 20, 1992

Introduction

Granitoid rocks in the southeast Canadian Cordillera intrude at the presently exposed surface within several geologic formations ranging from Proterozoic age Purcell-Windermere metasediments in the eastern part of this region to Paleozoic-Mesozoic age rocks of Terrane 1 within the Omineca Belt further west (Fig. 1). Within the present geochronological framework, it is thought that the majority of these granitoids were intruded and crystallized in two phases during the Mesozoic, one in the Middle Jurassic and the other in mid-Cretaceous (Armstrong 1988). These conclusions are based on field relations and a limited radioisotope age database. In many instances, the major batholiths only have K-Ar biotite and muscovite ages reported, which have been interpreted as representing metamorphic and uplift ages rather than crystallization ages (Archibald et al. 1983, Archibald et al. 1984). Furthermore, Rb-Sr mineral isochron ages are discordant with U-Pb zircon ages and Rb-Sr whole rock ages for the Raft and White Creek batholiths, respectively (Wanless et al. 1968a, Calderwood et al. 1990); the mineral isochron dates appear to have been affected by resetting as a result of thermal overprinting after crystallization.

It is important to constrain precisely the range of crystallization ages for Mesozoic batholiths in the southeast Canadian Cordillera to test models of physical and thermal conditions that led to the generation of granite, and to relate these granitoids to possible metamorphic and tectonic events that have affected this complex region of continental crust. In this paper, we report Rb-Sr ages of several major batholiths in the region including the Raft, Fry Creek, White Creek, Bugaboo, and Horsethief Creek intrusions. For the most part, our results, combined with earlier studies, confirm that most of the Mesozoic granitoids in this region were produced in two discrete events at approximately 175 to 160 Ma and 115 to 105 Ma, respectively. However, one U-Pb zircon age of 77 Ma for Whatshan (Carr 1991a, 1991b) does not fall within either of those time periods, and demonstrates that sporadic granitoid magmatism occurred throughout the Late Cretaceous.

Geology

During the Mesozoic, terranes were accreted to the North American Plate along its western edge. Monger et al. (1982) proposed that the Canadian Cordillera west of the autochthonous, North American craton was composed of two allocthonous composite terranes (Terranes I and II). Within the southern Canadian Cordillera, Terrane I includes four smaller terranes, including Quesnellia, which has been intruded by granitoid plutons during the Mesozoic and Cenozoic (Fig. 1).

Armstrong (1988) delineated several magmatic episodes from the early Triassic to Eocene in the Canadian Cordillera, based on K-Ar, U-Pb, and Rb-Sr radiometric ages. Within southeast British Columbia (SEBC), three of these magmatic episodes are of Mesozoic age (Fig. 1). The earliest episode is represented by the Rossland volcanic group within Quesnellia which ranges

in age from about 205 to 190 Ma (Tipper 1984). The second magmatic episode within SEBC comprises plutons with ages from 175 Ma (Spruce Grove, Parrish and Wheeler 1983) to 162 Ma (Galena Bay, Parrish and Armstrong 1987). Several of these plutons are intruded along the suture between Quesnellia and the Paleozoic Kootenay metasediments (Fig. 1).

The youngest magmatic episode in the Mesozoic in SEBC (Armstrong 1988) occurred in the mid-Cretaceous, although there is only one reliable crystallization age (i.e. U-Pb zircon, Rb-Sr whole rock isochron, or K-Ar hornblende ages) from plutons representing this episode (115 Ma, Rb-Sr whole rock isochron from White Creek, Wanless et al. 1968a), and therefore its duration in this region is poorly constrained. These plutons intruded into Proterozoic Purcell-Windermere and Paleozoic Kootenay metasediments (Fig. 1). Within the southern Cordillera, a mid-Cretaceous episode from 130 to 84 Ma produced the bulk of the Coast Plutonic Complex in southern British Columbia (Armstrong 1988). Also, the Spences Bridge Group residing within Quesnellia has an Albian age (~110 Ma). These volcanic rocks may have been part of a volcanic arc formed when Terrane II moved toward Terrane I (Thorkelson and Smith 1989).

Analytical Techniques

Rb and Sr abundances on whole rock powders were obtained by XRF at Washington State University using techniques described by Hooper and Johnson (1987). Experimental precision was determined by replicate analysis of USGS standards BCR-1 and AGV-1, with 2σ standard deviation for Rb ranging from +/- 3.60% to 2.38% and for Sr ranging from 0.84% to 0.54% (Table 2, Brandon 1989). Apatite and whole rock powders were dissolved in dilute HNO₃ and concentrated HF, respectively. Rb and Sr were separated using standard

cation exchange chromatographic procedures. Rb and Sr abundances of spiked aliquots of apatite separates were determined by isotope dilution on a VG MM30 mass spectrometer at the University of Alberta. $^{87}\text{Sr}/^{86}\text{Sr}$ ratios were also measured on the VG MM30 mass spectrometer using the methodology reported in Trønnes and Brandon (1992). Replicate analysis of NBS 987 Sr standard yielded $^{87}\text{Sr}/^{86}\text{Sr} = 0.710249 \pm 88$ (2σ , $n = 6$). Rb and Sr abundances and isotopic compositions are reported in Table 2.1. Regressions were calculated according to the method of York (1969), with 2σ uncertainties in $^{87}\text{Rb}/^{86}\text{Sr}$ at $\pm 4\%$ and 2σ in $^{87}\text{Sr}/^{86}\text{Sr}$ of ± 0.00016 on the measured ratio. These uncertainties reflect the long-term reproducibility of the standards run for XRF and mass spectrometry using NBS 987.

Results

Figures 2.2-2.7 display whole rock-apatite Rb-Sr age relations. For two reasons, apatite was found to be valuable in constraining the initial $^{87}\text{Sr}/^{86}\text{Sr}$ ratio as well as reducing age uncertainties of isochrons for several of the plutons. First, apatite has negligible Rb contents and high Sr abundances and consequently $^{87}\text{Rb}/^{86}\text{Sr}$ ratios approaching zero. Second, apatite is considerably more resistant to post-crystallization modification of its $^{87}\text{Sr}/^{86}\text{Sr}$ ratio than either feldspars or micas, and this ratio in apatite is likely to reflect that of the magma from which the apatite crystallized (Creaser and Gray 1992). Therefore, in situations where other minerals in granitoids may reflect post-crystallization overprinting and yield younger isochrons, apatite is useful in constraining Rb-Sr ages by pinning the near-zero $^{87}\text{Rb}/^{86}\text{Sr}$ side of the whole rock isochrons.

Figure 2.2 shows Rb-Sr whole rock age relations for the Raft batholith. The samples analyzed from the Raft batholith range from quartz diorite to

granite and aplite in composition. Initial Sr, Nd, and Pb isotope ratios for the Raft samples have a restricted range and have been interpreted by Brandon et al. (1992) to reflect crystallization from one parent magma. These samples yield an age of 164.0 ± 4.4 Ma (2σ). This age is within error of a U-Pb zircon age for Raft of $168 \pm 14/-12$ Ma reported by Calderwood et al. (1990), and confirms a Middle Jurassic crystallization age for Raft. A whole rock-mineral Rb-Sr isochron of 104.3 ± 3.3 Ma was also obtained by Calderwood et al. (1990) which is discordant with both our whole rock Rb-Sr isochron and the U-Pb zircon age. The younger whole rock-mineral isochron age is interpreted by Calderwood et al. (1990) to represent resetting of minerals for the Rb-Sr system by selective loss of ^{87}Sr .

Figures 2.3-2.5 show whole rock-apatite Rb-Sr age relations for the Bugaboo, Fry Creek, and Horsethief Creek plutons. The whole rock samples for these plutons are hornblende and biotite granites, except that one sample from Fry Creek (Fry-4), and one sample from Bugaboo (Bug-7) are aplite veins that crosscut these granites. One sample (Hor-6) from Horsethief Creek is a cognate xenolith of quartz diorite interpreted to be a cumulate from the Horsethief Creek magma (Brandon and Lambert 1992a). All three plutons have mid-Cretaceous ages. The Bugaboo batholith has a whole rock age of 107.0 ± 0.8 Ma (2σ) with a mean squared weighted deviation (MSWD) of 2.92. Adding apatite to the regression gives an age of 107.0 ± 0.8 Ma (2σ) with an MSWD of 2.62. Fry Creek gives a whole rock age of 115 ± 8 Ma (2σ) with an MSWD of 0.55. Including apatite gives 115.4 ± 7 Ma (2σ) and an MSWD of 0.39 for Fry Creek. The Horsethief Creek whole rock samples produce a scatterchron of 127 ± 35 Ma (2σ) with an MSWD of 3.01. Adding apatite to the regression greatly improves the Horsethief Creek age uncertainties to 109.5 ± 14 Ma (2σ) with an MSWD of 2.56. The calculated initial $^{87}\text{Sr}/^{86}\text{Sr}$ ratios for all three plutons

are similar, from 0.70773 ± 12 to 0.70831 ± 20 (2σ). These results suggest that all three plutons are similar isotopically.

Rb-Sr age relations for the White Creek batholith are shown in Figures 2.6 and 2.7. The White Creek batholith is a composite intrusion that ranges in composition from quartz monzodiorite along the rim of the batholith, and grades into granodiorite then into porphyritic granodiorite (with centimeter size alkali feldspar phenocrysts) towards the center of the batholith. Within the core of the White Creek batholith, a unit of peraluminous biotite-muscovite granite has intruded the earlier units. Trace element and isotopic data for the White Creek batholith indicates that there were three separate batches of magma including, 1), the rim quartz monzodiorite and adjoining granodiorite, 2), the porphyritic granodiorite, and 3) the core two-mica granite (Brandon and Lambert 1992b).

Wanless et al. (1968a) obtained a Rb-Sr whole rock isochron of 115 ± 5 Ma for the core two-mica granite (Fig. 2.6). Our results (which include aplite samples 5, 6, 24, and 25, Table 2.1) do not correspond to an isochron but scatter around the isochron obtained by Wanless et al. (1968a) suggesting either initial isotopic inhomogeneity or Rb-Sr resetting by later thermal episodes. $\delta^{18}\text{O}$ compositions for whole rock-quartz pairs for three of these samples (4, 8, and 26), may reflect the influx of fluid with a different $\delta^{18}\text{O}$ composition than the host magma during hydrothermal alteration, which could have also affected the Rb-Sr system in this zone (Brandon and Lambert 1992b). A Rb-Sr whole rock isochron of 106.1 ± 1.2 Ma (2σ) with MSWD of 2.12, and a whole rock-apatite isochron of 105.9 ± 0.6 Ma (2σ) with MSWD of 2.30 was obtained for the porphyritic granodiorite which included one pegmatite sample (WC-9, found within the porphyritic granodiorite) and is displayed in Figure 2.7. The samples from the exterior unit of quartz monzodiorite and granodiorite do not

yield an isochron because of their narrow range in Rb/Sr ratios (Fig. 2.7). However, the samples from this unit correspond well to a 105.9 Ma reference line with a $^{87}\text{Sr}/^{86}\text{Sr}$ initial ratio of 0.707260 ± 60 (2σ , for the measured ratio for apatite from sample WC-18). Our results, combined with the results from Wanless et al. (1968a) suggest that although the White Creek batholith is composite in nature, the separate units crystallized within the period between 105 to 115 Ma. These ages correlate with those of Fry Creek, Horsethief Creek, and Bugaboo plutons, and the similar initial $^{87}\text{Sr}/^{86}\text{Sr}$ ratios for these three plutons and the rim unit of White Creek suggest similar production mechanisms for all plutons.

Discussion and Conclusions

The comparison of whole rock ages and whole rock-apatite ages illustrate apatite's utility for constraining ages of granitoid rocks that have a restricted range in whole rock Rb/Sr ratios. The apatites analyzed from the mid-Cretaceous plutons plot at or near the initial $^{87}\text{Sr}/^{86}\text{Sr}$ ratios obtained from the regressions for each set of samples, and therefore pinpoint the y-intercept value for these regressions. When apatite is used in conjunction with whole rock data in the regressions, the age and MSWD uncertainties for the most part decrease significantly. This is particularly true in the case of Horsethief Creek where the addition of apatite data greatly reduces the uncertainty of this scatterchron, and produces an age that falls in the range for the rest of the mid-Cretaceous plutons in SEBC. These results confirm the conclusions of Creaser and Gray (1992) concerning the advantages of using apatite to constrain initial $^{87}\text{Sr}/^{86}\text{Sr}$ ratios and ages from granites that would otherwise be difficult to assess with the Rb-Sr isotopic system.

Table 2.2 summarizes crystallization age relations for these Mesozoic granitoids shown in Figure 2.1. Rb-Sr whole rock ages are generally concordant with U-Pb zircon ages when both are available for any given pluton. Rb-Sr whole rock-mineral ages are slightly younger for the Galena Bay and Baldy plutons, but in most instances the mineral systems have been reset and are therefore recording younger thermal events (i.e., data from Wanless et al. 1968a; Archibald et al. 1983; Archibald et al. 1984 which are not shown). Most of the K-Ar and $^{40}\text{Ar}/^{39}\text{Ar}$ ages also appear to represent post-crystallization ages (not shown), although K-Ar ages for both the Nelson and Mt. Toby intrusions are within the range for Middle Jurassic U-Pb zircon and Rb-Sr whole rock ages that are interpreted as crystallization ages (Table 2.2).

In conclusion, from the compilation of ages from this study and earlier age determinations, it is apparent that most granitoids in this region during the Mesozoic were primarily produced in two pulses. The first pulse lasted 10 to 15 m.y. during the Middle Jurassic from about 175 to 162 Ma.

The U-Pb zircon and Rb-Sr whole rock-apatite dates (i.e., crystallization ages) for the mid-Cretaceous granitoids range from about 115 Ma to 106 Ma for all plutons investigated. This second pulse of granitoid magma generation was also about 10 m.y. in duration within the late Aptian to early Albian times. The 77 Ma U-Pb zircon age from Whatshan may indicate that this magmatic event was substantially longer. However, within the present geochronological database for plutons in Figure 2.1, this age is not comparable to that of any other Mesozoic intrusion of large volume (Table 2.2). Therefore Whatshan may represent a distinct "small volume" pulse of granitoid magmatism near the end of the Mesozoic, unrelated to Albian magmatism in the southern Canadian Cordillera.

Acknowledgements. This research was funded by NSERC operating and Lithoprobe grants to R.StJ. Lambert (1988-1991). We thank Rob Creaser for providing us with a copy of his apatite paper prior to publication. Reviews by Rob Creaser, Gordon Goles, Tom Chacko, Jonathan Patchett, George Cumming, Bob Luth, and D. Archibald substantially improved this paper. This paper is dedicated to the memory of R.L. Armstrong for his open cooperation and helpful advice he was always willing to give to his colleagues

Table 2.1. Rb-Sr isotopic results for whole rock powders and apatite separates from Bugaboo, Fry Creek, Horsethief Creek, White Creek, and Raft intrusions.

Type	Sample	Rb	Sr	$^{87}\text{Rb}/^{86}\text{Sr}$	$^{86}\text{Sr}/^{87}\text{Sr}_0$	$^{86}\text{Sr}/^{87}\text{Sr}_T$	$\epsilon_{\text{Sr}T}$
Bugaboo							
BtGr	Bug-1a	243	381	1.846	0.710566(16)	0.70776	+44.1
BtGr	Bug-2	242	248	2.825	0.711458(22)	0.70715	+35.7
Apatite	Bug-2	0.98	166.0	0.017	0.707821(50)	0.70778	+44.6
BtGr	Bug-6	274	395	2.004	0.711118(40)	0.70806	+48.5
Aplite	Bug-7	339	46	21.40	0.740287(81)	0.70776	+44.1
BtGr	Bug-10	210	434	1.401	0.710027(44)	0.70789	+46.1
BtGr	Bug-12	223	342	1.888	0.710592(36)	0.70772	+43.6
Fry Creek							
Aplite	Fry-4	220	220	2.896	0.712525(34)	0.70779	+44.7
HbBtGr	Fry-8	150	1618	0.2683	0.708176(34)	0.70774	+44.0
Apatite	Fry-8	0.68	1095	0.0018	0.707774(60)	0.70777	+44.0
HbBtGr	Fry-10	155	1513	0.2965	0.708314(36)	0.70783	+45.3
Horsethief Creek							
BtGr	Hor-1	253	655	1.118	0.710241(46)	0.70849	+54.7
BtGr	Hor-3	246	637	1.118	0.710325(18)	0.70859	+55.9
Xeno	Hor-6	291	571	1.475	0.710447(34)	0.70814	+49.7
BtGr	Hor-8	198	707	0.8107	0.709211(30)	0.70794	+46.9
Apatite	Hor-8	1.31	479.5	0.0079	0.708355(36)	0.70834	+52.5
White Creek							
2MGr	WC-4	410	52	22.93	0.756822(0)	0.72237	+251
Aplite	WC-5	333	128	7.545	0.728260(62)	0.71691	+174
Aplite	WC-6	294	168	5.078	0.734517(66)	0.72688	+315
2MGr	WC-8	324	89	10.58	0.745207(50)	0.72929	+350
Aplite	WC-24	308	86	10.41	0.747189(32)	0.73153	+381
Aplite	WC-25	425	91	13.58	0.755838(48)	0.73540	+436
2MGr	WC-26	398	96	12.04	0.747116(70)	0.72904	+346
PGd	WC-2	184	570	0.935	0.711534(14)	0.71013	+77.7
Peg	WC-9	532	103	14.99	0.732756(30)	0.71020	+78.7
PGd	WC-11	210	517	1.178	0.711852(18)	0.71008	+77.0
PGd	WC-14	268	607	1.278	0.712032(18)	0.71011	+77.4
PGd	WC-15	229	625	1.061	0.711903(52)	0.71031	+80.2
Apatite	WC-15	1.05	317.4	0.0096	0.710754(36)	0.71074	+86.4
PGd	WC-23	224	505	1.284	0.712495(18)	0.71056	+83.9
PGd	WC-28	182	565	0.934	0.711230(84)	0.70982	+73.4
	WC28rpt	181	564				
HbBtGd	WC-17	154	948	0.470	0.707899(34)	0.70719	+36.0
HbBtGd	WC-18	141	957	0.426	0.707966(56)	0.70732	+37.9
Apatite	WC-18	0.48	585.0	0.0024	0.707260(60)	0.70726	+37.0
QMD	WC-19	142	1225	0.335	0.707417(36)	0.70691	+32.1
HbBtGd	WC-21	154	801	0.555	0.708037(26)	0.70720	+36.2

Raft							
Gr	8131	135	391	0.999	0.70770(2)	0.70537	+11.1
Gr	17.4	166	333	1.443	0.707839(18)	0.70447	-1.59
Gd	64.9	99	573	0.500	0.706287(44)	0.70512	+7.58
Gr	ERa-2	209	169	3.581	0.713064(50)	0.70471	+1.81
QMD	ERa-4	59	875	0.195	0.705928(62)	0.70547	+12.6
QD	ERa-6	47	1260	0.108	0.704906(28)	0.70465	+1.00
Ton	ERa-18	72	736	0.283	0.705744(20)	0.70508	+7.05
Gd	ERa-20	114	827	0.399	0.705990(18)	0.70506	+6.71
Aplite	ERa-21	200	169	3.424	0.713509(38)	0.70553	+13.3

Type abbreviations: 2MGr - 2-mica granite, HbBtGr - hornblende-biotite granite, BtGr - biotite granite, Gr - granite, PGd - porphyritic granodiorite, Gd - granodiorite HbBtGd - hornblende-biotite granodiorite, QMD - quartz monzodiorite, QD - quartz diorite, Peg - pegmatite, and Xeno - quartz diorite xenolith. Sample mineralogical descriptions and locales are given in the Appendix. Rb and Sr abundances are in ppm. $^{86}\text{Sr}/^{87}\text{Sr}_0$ is the present day measured ratio. All ratios and ϵ values relative to $^{86}\text{Sr}/^{88}\text{Sr} = 0.1194$; $^{87}\text{Rb}/^{86}\text{Sr}_{\text{UR}} = 0.0827$; $\lambda^{87}\text{Rb} = 1.42 \cdot 10^{-11}/\text{yr}$; and $^{87}\text{Sr}/^{86}\text{Sr}_{\text{UR}} \text{ at } 0 = 0.70478$. Precisions in the last place for measured $^{87}\text{Sr}/^{86}\text{Sr}$ ratios are shown in parentheses (2σ). ϵ values and $^{87}\text{Sr}/^{86}\text{Sr}_T$ are calculated at T for Bugaboo for 107 Ma, for Fry Creek at 115 Ma, for Horsethief Creek at 110 Ma, for White Creek at 106 Ma, and for Raft at 164 Ma.

Table 2.2. Crystallization age determinations for Mesozoic granitoids in the southern Canadian Cordillera.

Intrusion	K-Ar	U-Pb	Rb-Sr
Galena Bay		161.6 +/- 0.5	156.7 +/- 2.4
Kuskanax		173 +/- 5	
Mine Stock		171	
Mount Toby	166		
Nelson	165-174	164 +/- 2	
Raft		168 +/- 14/-12	164.0 +/- 4.4
Spruce Grove		174.8 +/- 0.8	
Baldy		115.9 +/- 4.6	98.5 +/- 2.2
Bugaboo			107.0 +/- 0.8
Fry Creek			115.4 +/- 7
Horsethief Creek			109.5 +/- 14
Salmo			115
Wallack Creek			115
White Creek			115 +/- 5
			105.9 +/- 1.2
Whatshan		77.0 +/- 0.5	

The data are in Ma and compiled from Parrish and Wheeler (1983), Kuskanax; Calderwood et al. (1990) U-Pb for Raft; Parrish and Armstrong (1987), Galena Bay; Nguyen et al. (1968) and Wanless et al. (1968b), K-Ar for Nelson; Ghosh and Lambert unpublished data, U-Pb for Nelson; Wanless et al. (1968a), Mt. Toby; Carr (1991a, 1991b), Whatshan; Archibald et al. (1983), Mine Stock; Carr (1991b) Spruce Grove; Calderwood et al. (1990), Baldy; Einarsen (1991) and Einarsen (personal communication 1991) for Salmo and Wallack Creek; and Wanless et al. (1968a) for 115 Ma on White Creek. All other determinations are from this study. Rb-Sr isochron ages for Galena Bay and Baldy are whole rock-mineral isochrons and most likely do not represent crystallization ages (see text).

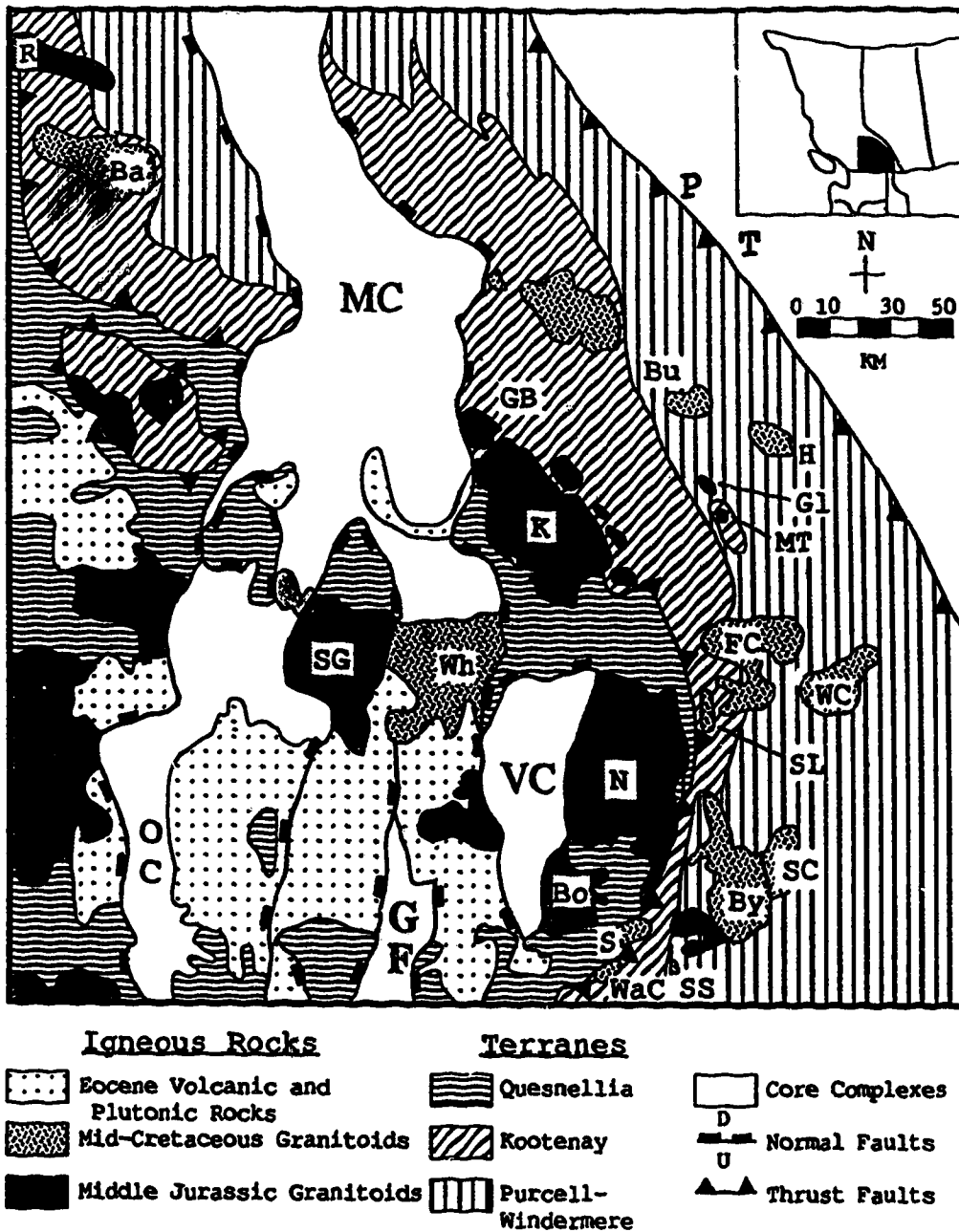


Figure 2.1. Tectono-magmatic map of the southern Omineca Crystalline Belt (modified from Parrish et al. 1988, Lambert and Chamberlain 1988, and Monger and Berg 1987). Metamorphic core complexes shown include GF - Kettle-Grand Forks complex, MC - Monashee complex, OC - Okanagan complex, and VC - Valhalla complex. The plutons include Ba - Mt. Baldy, Bo - Bonnington, Bu - Bugaboo, By - Bayonne, FC - Fry Creek, GB - Galena Bay, Gl - Glacier Stock, H - Horsethief Creek, K - Kuskanax, MT - Mt. Toby, N - Nelson, R - Raft, S - Salmo, SC - Skelly Creek, SL - Shore Line Stock, SS - Summit Stock, WaC - Wallack Creek, WC - White Creek, and Wh - Whatshan. The Purcell Thrust is labelled PT.

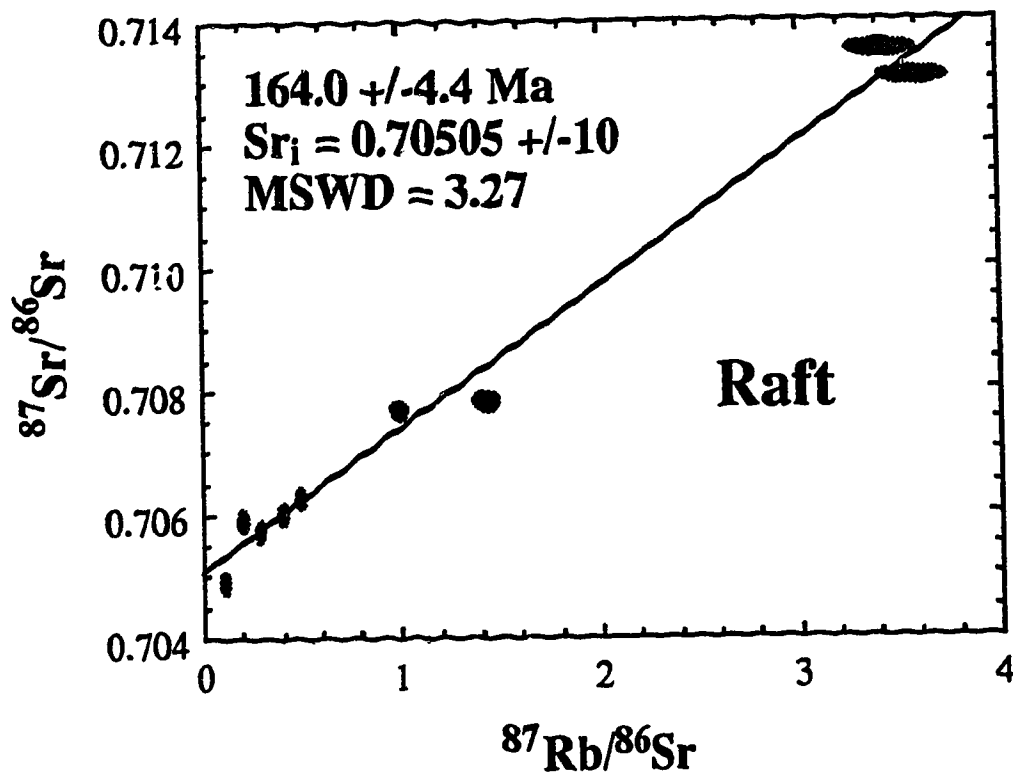


Figure 2.2. Rb-Sr age relations for the Raft batholith. Sr_i is the calculated initial $^{86}Sr/^{87}Sr$ ratio for the isochron (both 2σ). The data points are plotted as ellipses with 2σ uncertainties.

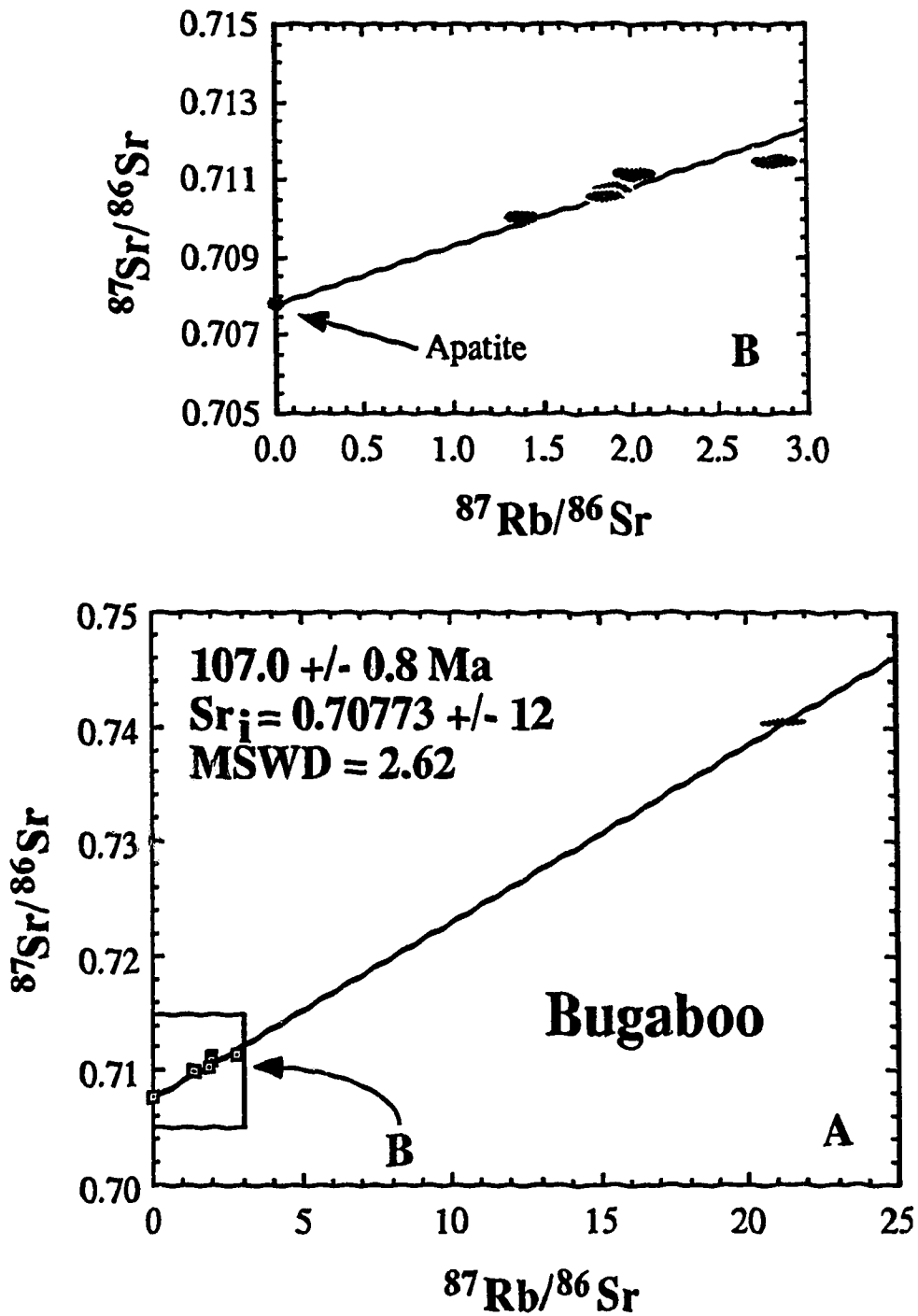


Figure 2.3. Rb-Sr age relations Bugaboo batholith with symbols and abbreviations as in Figure 2.2. The $^{87}\text{Rb}/^{86}\text{Sr}$ error for the apatite is larger than measured. B. is an expanded view from A.

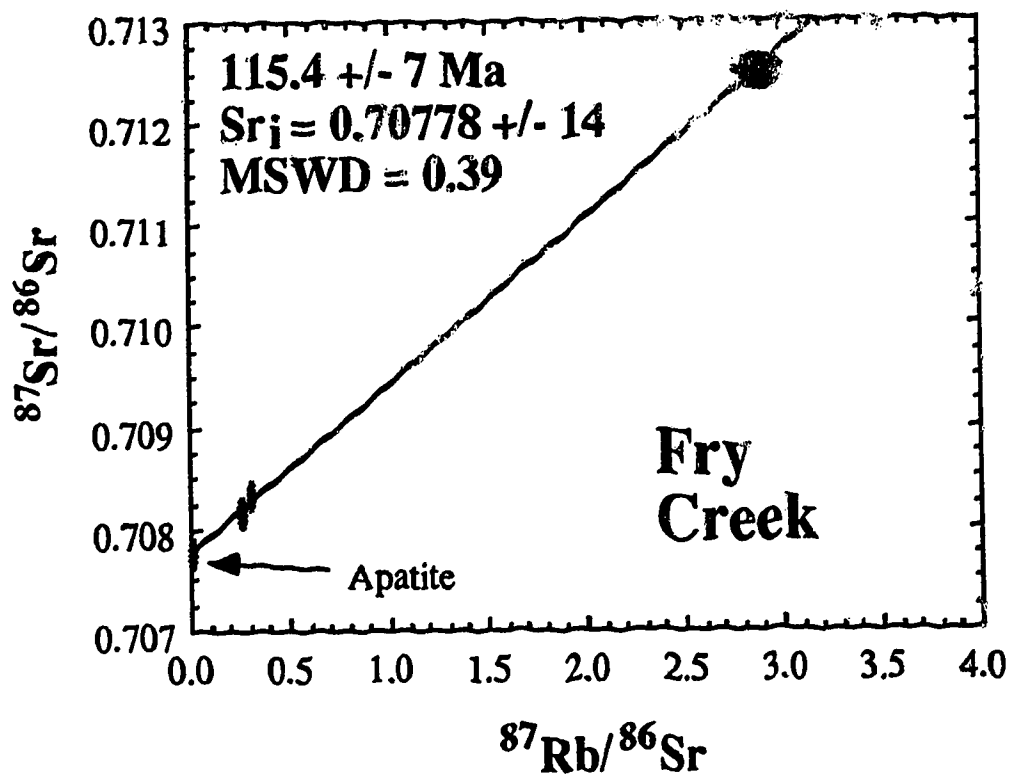


Figure 2.4. Rb-Sr age relations for the Fry Creek batholith with symbols as in Figures 2.2 and 2.3.

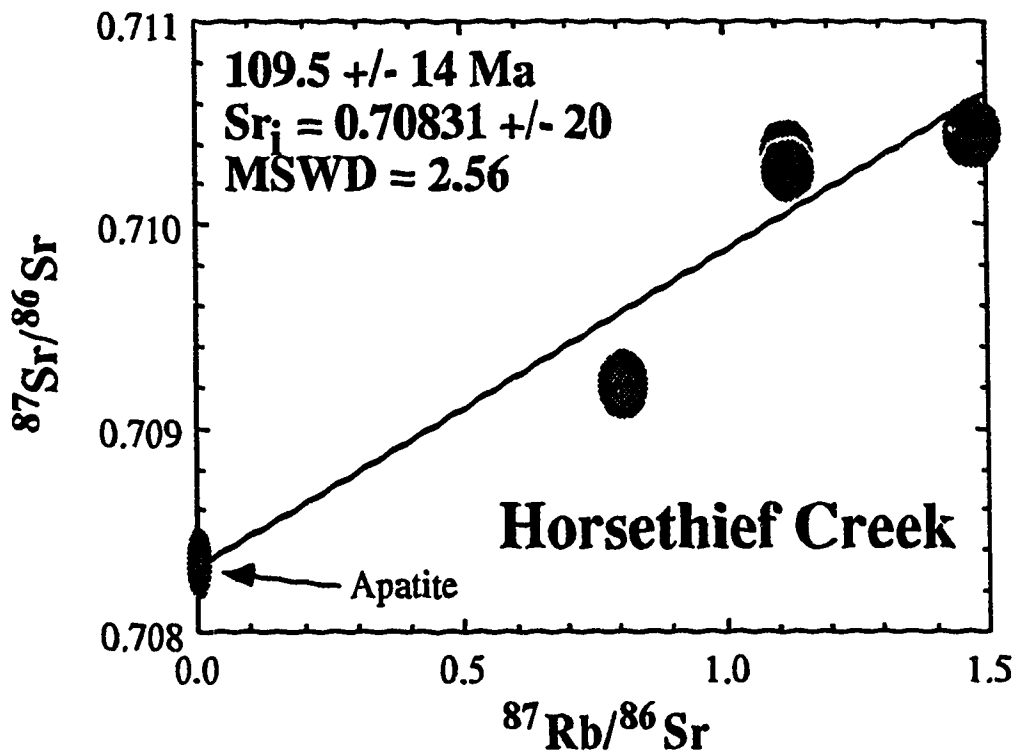


Figure 2.5. Rb-Sr age relations for the Horsethief Creek batholith with symbols as in Figures 2.2 and 2.3.

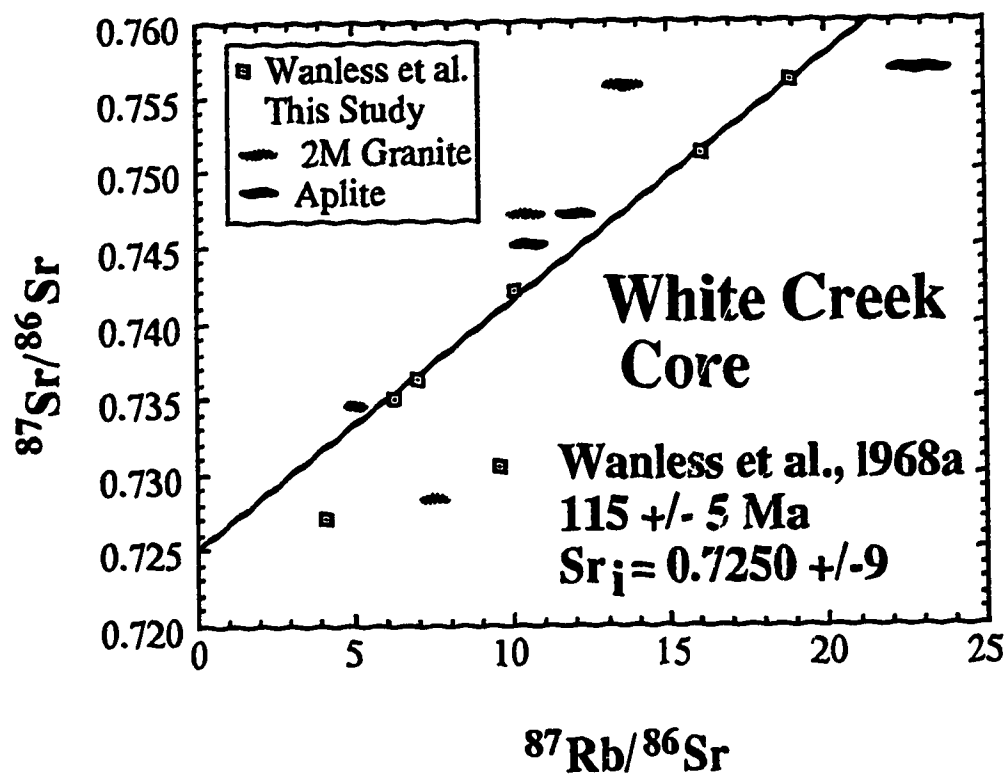


Figure 2.6. Rb-Sr age relations for the White Creek batholith core with symbols as in Figures 2.2 and 2.3.

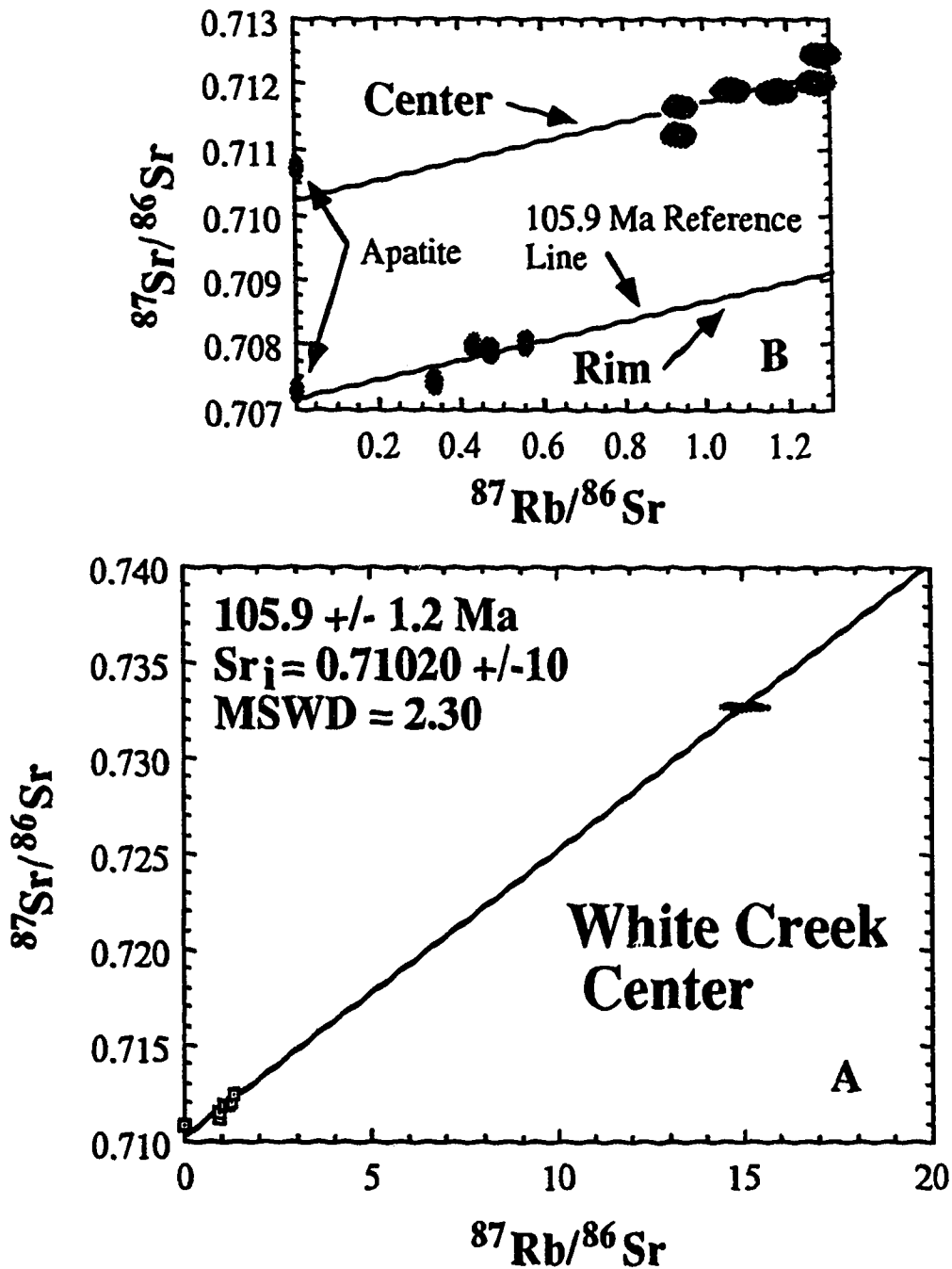


Figure 2.7. Rb-Sr age relations for the White Creek batholith rim and center with symbols as in Figures 2.2 and 2.3. A. Rb-Sr isochron for the porphyritic granodiorite from the center zone. B. An expanded view which includes the Rb-Sr data for the rim zone, and corresponding 105.9 Ma reference line.

Appendix 2.1

Sample Lithologies and Locations.

1. **Bugaboo.** The Bugaboo samples are biotite granite with alkali feldspar phenocrysts collected from the following locales: Bug-1a - 50°44'10"N Lat., 116°46'55"W Long.; Bug-2 - 50°44'30"N Lat., 116°45'30"W Long.; Bug-6 - 50°44'10"N Lat., 116°46'55"W Long.; Bug-10 - 50°44'10"N Lat., 116°46'54"W Long.; and Bug-12 - 50°45'45"N Lat., 116°46'12"W Long. One sample (Bug-7) is an aplite from 50°44'10"N Lat., 116°46'55"W Long.

2. **Fry Creek.** Samples Fry-8 and Fry-10 are leucocratic granites with sphene, hornblende, and biotite from the following locations: Fry-8 - 50°05'04"N Lat., 116°27'50"W Long.; and Fry-10 - 49°59'23"N Lat., 116°35'35"W Long. Sample Fry-4 is an aplite from 50°03'47"N Lat., 116°49'25"W Long.

3. **Horsethief Creek.** Hor-1, Hor-3, and Hor-8 are porphyritic granite with hornblende, biotite, and sphene. The phenocrysts are alkali feldspar. Hor-6 is a cognate xenolith of quartz diorite with biotite, sphene, and less than 1% muscovite. The locales for the Horsethief Creek suite are: Hor-1 - 50°35'40"N Lat., 116°29'0"W Long.; Hor-3 and Hor-6 - 50°37'43"N Lat., 116°29'50"W Long.; and Hor-8 - 50°38'15"N Lat., 116°31'35"W Long.

4. **White Creek.** WC-4, WC-8, and WC-26 are two-mica granites with muscovite predominant over biotite. WC-5, WC-6, WC-24, and WC-25 are aplites with 5 and 24 containing muscovite, and 6 and 25 having biotite predominant over muscovite. WC-9 is a muscovite pegmatite of granitic composition. WC-2, WC-11, WC-14, WC-15, WC-23, and WC 28 are porphyritic granodiorites with alkali feldspar phenocrysts and biotite as the only mafic phase present. WC-17, WC-18, and WC-21 are hornblende-biotite granodiorites with muscovite and epidote. WC-19 is a quartz monzodiorite with biotite, hornblende, epidote, and sphene. Samples locales: WC-2 - 49°50'30"N Lat., 116°15'55"W Long.; WC-4-9 -

49°51'47"N Lat., 116°13'55"W Long.; WC-11 - 49°51'39"N Lat., 116°13'47"W Long.; WC-14 - 49°51'31"N Lat., 116°13'46"W Long.; WC-15 - 49°51'21"N Lat., 116°13'48"W Long.; WC-17 - 49°50'08"N Lat., 116°14'37"W Long.; WC-18 - 49°49'54"N Lat., 116°13'10"W Long.; WC-19 - 49°49'16"N Lat., 116°12'48"W Long.; WC-21 - 49°49'49"N Lat., 116°14'16"W Long.; WC-23 and WC-24 - 49°51'32"N Lat., 116°15'20"W Long.; WC-25 and 26 - 49°52'24"N Lat., 116°16'14"W Long.; and WC-28 - 49°54'48"N Lat., 116°16'52"W Long.

5. Raft. The ERa samples are from the eastern side and the rest of the samples are from the west side of the intrusion. ERa-2 and ERa-21 are aplites with biotite and muscovite. ERa-4 is a quartz diorite, ERa 6 is a diorite, ERa-18 and 64.9 are tonalites, and ERa-20 is a granodiorite, all with hornblende, biotite and sphene as mafic phases. 8131 and 17.4 are granites with biotite as the primary mafic phase. Locales are: ERa-2, ERa-4 - 51°41'41"N Lat., 119°56'18"W Long.; ERa-6 - 51°41'45"N Lat., 119°52'57"W Long.; ERa-18, ERa-20 - 51°41'18"N Lat., 119°54'40"W Long.; and ERa-21 - 51°40'24"N Lat., 119°52'03"W Long.

References

- Archibald, D.A., Glover, J.K., Price, R.A. Farrar, E., and Carmichael, D.M., 1983. Geochronology and tectonic implications of magmatism and metamorphism, southern Kootenay Arc and neighboring regions, southeastern British Columbia. Part I: Jurassic to Mid-Cretaceous. *Canadian Journal of Earth Sciences*, **20**, 1891-1913.
- Archibald, D.A., Krogh, T.E., Armstrong, R.L., and Farrar, E., 1984. Geochronology and tectonic implications of magmatism and metamorphism, southern Kootenay Arc and neighboring regions, southeastern British Columbia. Part II: Mid-Cretaceous to Eocene. *Canadian Journal of Earth Sciences*, **21**, 567-583.
- Armstrong, R.L., 1988. Mesozoic and Early Cenozoic magmatic evolution of the Canadian Cordillera. *In Processes In Continental Lithospheric Deformation*, Edited by S.P. Clark, B.C. Burchfiel, and J. Suppe. Geological Society of America, Special Paper 218, 55-91.
- Brandon, A.D., 1989. Constraints on magma genesis behind the Neogene Cascade arc: Evidence from major and trace element variation of high-alumina and tholeiitic volcanics of the Bear Creek area. *Journal of Geophysical Research*, **94**, 7775-7798.
- Brandon, A.D., and Lambert, R.StJ., 1992a. Geochemical characterization of mid-Cretaceous granitoids in the Kootenay Arc in the southern Canadian Cordillera. *Canadian Journal of Earth Sciences*, submitted.
- Brandon, A.D., and Lambert, R.StJ. Lambert, 1992b. Crustal melting in the Cordilleran interior: The mid-Cretaceous White Creek batholith in the southern Canadian Cordillera. *Journal of Petrology*, submitted.
- Brandon, A.D., Smith, A.D., and Lambert, R.StJ., 1992. Mesozoic granitoid magmatism in the Omineca Belt of southeast British Columbia:

- Implications for the generation of silicic magmas in the North American Cordillera. *Journal of Geophysical Research*, submitted.
- Calderwood, A.R., van der Heyden, P., and Armstrong, R.L., 1990. Geochronometry of the Thuya, Takomkane, Raft, and Baldy batholiths, south-central British Columbia. *Geological Association of Canada, Program with Abstracts*, 15, p.A19.
- Carr, S.D., 1991a. Tectonic evolution of the Thor-Odin - Pinnacles area, southern Omineca Belt, British Columbia. *Proceedings of the Lithoprobe Cordilleran Workshop, University of Calgary Publ.*, 61-75.
- Carr, S.D., 1991b. U-Pb zircon and titanite ages for three Mesozoic igneous rocks south of the Thor-Odin - Pinnacles area, southern Omineca Belt, British Columbia. *Canadian Journal of Earth Sciences*, 28, 1877-1882.
- Creaser, R.A., and Gray, C.M., 1992. Preserved initial $^{87}\text{Sr}/^{86}\text{Sr}$ in apatite from altered igneous rocks: A case study from the Middle Proterozoic of South Australia. *Geochimica et Cosmochimica Acta*, 56, 2789-2795.
- Einarsen, J.M., 1990. Structural setting and geochemistry of granitic stocks in the Quesnellia-North America boundary of southeastern B.C. *Geological Society of America, Abstracts with Programs*, 22, no.3, p.20-21.
- Hooper, P.R., and Johnson, D., 1987. Major and trace element analyses of rocks and minerals by automated X-ray spectrometry. In house report, Department of Geology, Washington State University, Pullman.
- Lambert, R.StJ., and Chamberlain, V.E., 1988. Cordillera revisited, with a three-dimensional model for Cretaceous tectonics in British Columbia. *Journal of Geology*, 96, 47-60.
- Monger, J.W.H., and Berg, H.C., 1987. Lithotectonic terranes of Western Canada and Southeastern Alaska. Map MF-1874B, United States Geological Survey, 1-12.

- Monger, J.W.H., Price, R.A., and Templeman-Kluit, D.J. 1982. Tectonic accretion and the origin of the two major metamorphic and plutonic belts in the Canadian Cordillera. *Geology*, 10, 70-75.
- Nguyen, K.K., Sinclair, A.J., and Libby, W.G., 1968. Age of the northern part of the Nelson batholith. *Canadian Journal of Earth Sciences*, 5, 955-957.
- Parrish, R.R., and Armstrong, R.L., 1987. The ca. 162 Ma Galena Bay stock and its relationship to the Columbia River fault zone, southeast British Columbia. *In Radiogenic Age and Isotopic Studies. Report 1, Geological Survey of Canada, Paper 87-2, 25-32.*
- Parrish, R.R., and Wheeler, J.O., 1983. A U-Pb zircon age from the Kuskanax batholith, southeastern British Columbia. *Canadian Journal of Earth Sciences*, 20, 1751-1756.
- Parrish, R.R., Carr, S.D., and Parkinson, D.L., 1988. Eocene extensional tectonics and geochronology of the southern Omineca Belt, British Columbia and Washington. *Tectonics*, 7, 181-212.
- Tipper, H.W. 1984. The age of the Jurassic Rossland Group of southeastern British Columbia. *Geological Survey of Canada, Paper 84-1A, 631-632.*
- Thorkelson, D.J., and Smith, A.D. 1989. Arc and intraplate volcanism in the Spences Bridge Group: Implications for Cretaceous tectonics in the Canadian Cordillera. *Geology*, 17, 1093-1096.
- Trønnes, R.G., and Brandon, A.D., 1992. Mildly peraluminous high-silica granites in a continental rift: the Drammen and Finnemarka batholiths, Oslo Rift, Norway. *Contributions to Mineralogy and Petrology*, 109, 275-294.
- Wanless, R.K., Loveridge, W.D., and Mursky, G., 1968a. A geochronological study of the White Creek batholith, southeastern British Columbia. *Canadian Journal of Earth Sciences*, 5, 375-386.

- Wanless, R.K. Stevens, R.D., Lachance, G.R., and Edmonds, C.M., 1968b. Age determinations and geological studies, K-Ar isotopic ages. Report 8: Geological Survey of Canada, Paper 67-2A, p.1-53.
- York, D., 1969. Least squares fitting of a straight line with correlated errors. Earth and Planetary Science Letters, 5, 320-324.

Chapter 3

Geochemical Characterization of Mid-Cretaceous Granitoids of the Kootenay Arc in the Southern Canadian Cordillera

Alan D. Brandon* and Richard StJ. Lambert
Department of Geology, University of Alberta
Edmonton, Alberta CANADA T6G 2E3

* - Present Address:
Department of Earth, Atmospheric,
and Planetary Sciences
Massachusetts Institute of Technology
Cambridge, MA, USA 02139-4307

Submitted to Canadian Journal of Earth Sciences (8/20/92)

Introduction

During the Mesozoic, the continental margin of western North America grew by accretion of allochthonous terranes to the North American plate (Monger 1977, Monger and Price 1979, Monger and Irving 1980, Coney et al. 1980, Monger et al. 1982). At present, the timing and mechanisms of terrane accretion in the Canadian Cordillera remain controversial and have led to several models, including those advocating collision by a sequence of terranes in the Late Mesozoic to Early Cenozoic (i.e. the Baja BC model of Umhoefer 1987, and Umhoefer et al. 1989), and those favoring a collision of a single superterrane (i.e. the Cordillera model of Chamberlain and Lambert 1985 and Lambert and Chamberlain 1988).

Common to all the models is the intimate association of Mesozoic plutonic rocks with tectonic processes. Petrogeneses of Mesozoic rocks of the Coast Plutonic Complex in Canada and southeast Alaska have been studied in some detail (Barker et al. 1986, Arth et al. 1989, Barker 1990, Samson et al. 1991).

Within the Canadian Cordilleran interior, information on Mesozoic plutons is restricted to geochronological studies to constrain crystallization, emplacement, and cooling ages, and paleomagnetic studies to investigate latitudinal displacement of the plutons and their host terranes since crystallization (Monger and Irving 1980, Irving and Archibald 1990). Their petrogeneses are poorly understood and remain under-utilized in the overall understanding of terrane accretion and lithospheric tectonics within this region. No comprehensive geochemical work has yet been published on the major, trace element, and Sr, Nd, and Pb isotopic compositions of Mesozoic plutonic rocks in the Canadian Cordilleran interior. In conjunction with the Lithoprobe Southern Cordilleran Transect project, we have undertaken a study on the geochemistry of three batholiths in southeastern British Columbia (SEBC) within the Kootenay Arc, namely the Bugaboo, Fry Creek, and Horsethief Creek (BFH) batholiths. These batholiths were intruded in the mid-Cretaceous and are some of the eastern-most Mesozoic plutons in the Canadian Cordillera. The petrological and geochemical features described here are consistent with an origin by partial melting of the underlying crust, with a minimal chemical contribution from a juvenile mantle component. Tectonic models for the amalgamation of SEBC in the Mesozoic must take into account mechanisms for partial melting of the crust with little or no contemporaneous input of mantle-derived magma, at least during the mid-Cretaceous. An alternative model is one where parental basic magmas from the mantle have had their isotopic signatures largely diluted by the highly radiogenic crust. However, the absence of mafic igneous rocks in the Early Cretaceous in SEBC does not support the latter model, unless the crust acting as a very effective density filter, prevented the rise of these magmas into the middle and lower crust.

Geology

Figure 3.1 displays the major geological units within southeastern British Columbia. The Bugaboo, Fry Creek, and Horsethief Creek batholiths are located east of the suture between Quesnellia (as part of Terrane I of Monger et al. 1982) and the Paleozoic Kootenay metasediments. This suture and the Paleozoic rocks on either side form the Kootenay Arc in SEBC. The BFH plutons intruded into the Kootenay and Proterozoic Purcell-Windermere metasediments.

Armstrong (1988) recognizes as many as seven magmatic episodes within the Canadian Cordillera during the Mesozoic and early Cenozoic, ranging from Late Triassic to Middle Eocene. The plutonic rocks in Figure 3.1 belong to two of these episodes that are prevalent throughout the Canadian Cordillera. The Nelson and Kuskanax batholiths, and the Mt. Toby stock are part of the Mid-Jurassic episode which lasted from ~175 Ma to ~162 Ma in SEBC. U-Pb zircon ages for the Nelson and Kuskanax batholiths are 164 +/- 2 Ma and 173 +/- 5 Ma, respectively (Ghosh 1986, Parrish and Wheeler 1983). These batholiths intruded along the suture between Quesnellia and the Kootenay metasediments. The Mt Toby stock has a K-Ar age of 166 Ma (Wanless et al 1968, date recalculated by Archibald et al. 1983 using new constants) and is emplaced east of the suture within the Kootenay metasediments.

The Bugaboo, Fry Creek, and Horsethief Creek batholiths belong to a mid-Cretaceous magmatic episode that also includes the Battle Range and White Creek batholiths in Figure 3.1. This magmatic episode is constrained by Rb-Sr isochron ages of 107.0 +/- 0.8 Ma, 115.4 +/- 7 Ma, 109.5 +/- 14 Ma, and 105.9 +/- 1.2 Ma (2σ) for the Bugaboo, Fry Creek, Horsethief Creek, and White Creek batholiths, respectively (Brandon and Lambert 1992a).

Earlier reconnaissance studies have shown that two granitoid types are present within the BFH batholiths (Reesor 1973). Muscovite-biotite granites occur in the eastern half of the Bugaboo and the northwest, northeast, and southwest quadrants of the Fry Creek, whereas the western half of Bugaboo (not sampled in this study) and Horsethief Creek contain hornblende-biotite granite and granodiorite (Fig. 3 of Archibald et al. 1983). The southeast quadrant of the Fry Creek batholith was not examined in earlier investigations. Archibald et al. (1983) used the mineral assemblages of the contact aureoles of the Bugaboo, Fry Creek, and Horsethief Creek batholiths to constrain their emplacement levels. The contact aureoles for the BFH batholiths have mineral assemblages including garnet, sillimanite, staurolite, and biotite (Reesor 1973) and lie within bathozones 2 and 3 (following Glover 1978), suggesting an emplacement level of 2.3 to 3.8 kbar (7 to 11 km depth). The BFH granites are post-kinematic with respect to the penetrative deformation observed within the Kootenay and Purcell-Windermere rocks (Reesor 1973). However, the BFH batholiths have discordant biotite and muscovite K-Ar ages (relative to their Rb-Sr whole rock-apatite ages) ranging from ~95 to ~50 Ma (Geological Survey of Canada data compiled by Archibald et al. 1984). These ages have been interpreted by Archibald et al. (1984) to represent resetting during late Cretaceous compression and thrusting along the Purcell thrust (Fig. 3.1), followed by Eocene extension.

Petrography

Samples were collected from as many locales within these batholiths as possible, in order to study a representative selection of petrographic and lithologic types (Appendix 3.1). Petrographic features described below are based on observations made in the present study, and those made by Reesor

(1973) from correlative locations in all three batholiths. Granitoid rocks from the Bugaboo, Fry Creek, and Horsethief Creek batholiths display hypidiomorphic granular textures. No corroded or partly resorbed crystals, reverse zoning in plagioclase, or crystals with reaction rims were observed.

The eastern part of the Bugaboo pluton is composed of porphyritic biotite granite. This granite has 5 to 10 modal % biotite with trace amounts (< 1 modal %) of euhedral allanite, sphene, magnetite, apatite, and zircon. Perthitic microcline is commonly 2 cm in size, giving the granite a porphyritic texture. Plagioclase is albite to oligoclase in composition and shows normal oscillatory zoning. Muscovite is present in trace amounts, but generally as irregular grains in altered plagioclase, or in association with chlorite replacing biotite. It probably not a primary igneous phase. Therefore, these conclusions differ slightly from the earlier reconnaissance studies (Reesor 1973) in that we identify the eastern part of the Bugaboo granite to be a biotite granite rather than a two-mica granite, because the muscovite is secondary. Aplitic granite veins from Bugaboo are primarily equigranular microcline (non-perthitic), albitic plagioclase, and primary muscovite. The aplites show a trace of biotite. One metapelite xenolith from Bugaboo (Bug-8) was examined in this study. It has an equigranular texture of equal proportions of biotite, muscovite, and microcline, several modal % quartz, and with trace amounts of fluorite, epidote, and albite. This xenolith is most likely a piece of Precambrian basement underlying the Purcell Mountains, based on isotopic constraints (see below).

The Horsethief Creek porphyritic granite is similar to the Bugaboo granite with similar textures and mineral assemblage, although allanite is more abundant (up to 3 modal %). The aplites also display the same mineralogical features as those in Bugaboo. One Horsethief Creek xenolith

(Hor-6) was analyzed in this study and is classified as a quartz diorite in the IUGS classification (Streckeisen 1973). This xenolith contains all of the phases in the granites mentioned above, as well as trace amounts of epidote. Epidote was observed from Hor-6 with rims of biotite, and was irregular in habit, suggesting a reaction relationship with the biotite during decompression (Zen and Hammarstrom 1984). All of the rest of the epidote in Hor-6 displayed subhedral habit with no rims. In all of the rocks observed in this study, this relationship between epidote and biotite was the only petrographic feature inconsistent with equilibrium crystallization from a silicic melt. This quartz diorite may represent the cumulate phases crystallizing from the Horsethief magma, as suggested by its geochemistry (see below).

The Fry Creek batholith contains two granitoid lithologies. Two-mica granites were collected from locales along Fry Creek. These granites have 2 to 7 modal % muscovite and 0 to 2 modal % biotite. The muscovite occurs as subhedral crystals in a hypidiomorphic texture, and does not appear to be secondary replacement of primary minerals. The plagioclase is albite to oligoclase, and the microcline is not perthitic. Aplites from Fry Creek are similar to those in the other two batholiths. Two pegmatites were also collected (Fry-7 and Fry-99). One of the pegmatites from a locale along Fry Creek (Fry-7) in association with two-mica granite, consists of garnet, tourmaline, albite, muscovite, and microcline perthite. The other pegmatite (Fry-9) has biotite, albite, magnetite, and microcline perthite, and was collected within the hornblende-biotite granite zone near Mt. Findlay. Biotite granites collected in the southeastern quadrant of Fry Creek are non-porphyritic, and are composed of quartz, albitic plagioclase, microcline, and several modal percent each of allanite and biotite, with trace amounts of sphene and muscovite. The microcline in this granite is perthitic.

In summary, two petrographic types of granite are found within these three batholiths. One type found in all three is a biotite granite. The second is a two-mica granite, which was collected from a restricted part of the Fry Creek batholith.

Analytical Methods

Five to 15 kilograms samples of the granites were collected. Aplite and mafic xenolith samples were 1 to 2 kilograms. Samples were first crushed in steel jaw crushers to centimeter-size pieces. These pieces were inspected for metal from the steel jaws, and the contaminated pieces were removed. The samples were then ground to 10 to 50 mesh size in a mullite disc grinder. Finally, 200 gram aliquants of these powders were ground in an agate mortar into <200 mesh powders. In every stage of the grinding, acetone and ultrapure-deionized water were used to clean the surfaces of the grinders. In the agate mortar stage, an initial 100 gram cut of the same powder was ground to coat the agate surfaces. This first powder was discarded. The agate surfaces were then cleaned, and another aliquot of the same powder was ground and kept for chemical analysis.

Whole rock X-ray fluorescence (XRF) data were obtained from the XRF lab at Washington State University. Precision and accuracy for the XRF analyses are reported in Hooper and Johnson (1987) and Brandon (1989). Whole rock instrumental neutron activation analysis (INAA) data were obtained at the University of Oregon INAA lab of Gordon G. Goles. The methods used for INAA follow Gordon et al. (1968). Estimates of 2σ imprecision values for INAA analyses are as follows: +/-3% - Th, Ta, Sc, Ce, Sm; +/-4% - Hf; +/-5% - La, Eu, Tb, Lu; and +/-6% - U, Cr, Co, Nd, and Yb. Major and trace element analyses are

reported in Table 3.1, except for Rb and Sr which are listed in Table 3.3, and U, Th, and Pb in Table 3.4.

Sr and Pb isotope ratios were obtained on a VG MM30 mass spectrometer maintained by the Departments of Physics and Geology at the University of Alberta (UA). Nd isotope ratios were obtained on a VG 354 five-collector mass spectrometer at UA. Details of the chemical and mass spectrometric procedures for isotopic analysis are listed in Appendix 3.2. Replicate isotopic analysis for Sr, Nd, and Pb isotopic standards are reported in Table 3.2.

Results

Major and trace element geochemistry

The granite samples collected from the BFH batholiths range from approximately 72 to 76 wt.% SiO₂. All of the rocks (excluding the Fry Creek biotite pegmatite) are peraluminous with alumina saturation indices (ASI, molar proportions of Al₂O₃/[Na₂O + K₂O + CaO] corrected for apatite, Shand 1949, Zen 1986) larger than 1 (Fig. 3.2). The BFH biotite granites have ASI's from ~1.0 to ~1.13 and are weakly to moderately peraluminous (wP), and the Fry Creek two-mica granites have ASI's of > 1.1 and are strongly peraluminous (sP) according to the definition of Miller and Barton (1990). In Figure 3.2, the biotite granites from all three plutons cluster together and are distinct from the two-mica granites, which have higher Fe ratios (wt.% FeO*/[FeO* + MgO]) and ASI's. Fractionation vectors for removal of alkali feldspar, albite, hornblende, muscovite, and biotite, which may control the observed compositional variation of the granites, are also shown. Zen (1986) noted that the generation of strongly peraluminous plutons by fractional crystallization from metaluminous (ASI < 1) and weakly peraluminous magmas is an inefficient process. Large amounts of subaluminous crystals (such as Al-poor

hornblende) must be subtracted before a magma can show significant changes in ASI. For instance, Zen (1986) notes that the Grayling Lake pluton in Montana has residual pockets of peraluminous granite, but these represent about 0.001 of the areal extent of the pluton. Given the relative volumes required to generate peraluminous granites from wP magmas, it is unlikely that the wP hornblende-biotite granites are strictly comagmatic with the Fry Creek two-mica granites. The wP granites from all three plutons, on the other hand, appear to represent granitic magmas with similar characteristics and possibly related petrogeneses.

In Figure 3.3, the same distinctions and relations between the two granite types are demonstrated in ASI and Fe ratio versus SiO₂. In general, increasing SiO₂ has no effect on ASI or Fe ratio within the wP granites. For a given SiO₂ abundance, the two-mica granites of Fry Creek have higher Fe ratio and ASI and are distinct from the wP granites. The sP granites from Fry Creek have SiO₂ abundances overlapping the Bugaboo granites and are distinct in Fe ratios and ASI's.

In both Figures 3.2 and 3.3, the aplites and the pegmatites plot in distinct fields from the granites, and exhibit chemical characteristics (i.e. high Fe ratios and SiO₂ contents), of small volume, residual or partial melts left after removal of mafic minerals or with these minerals left behind in the granite restite. Because these rocks are found crosscutting both types of granite and have isotopic compositions overlapping both the wP and sP granites (see below), these data do not resolve which of the processes generated these rocks.

The quartz diorite xenolith (Hor-6) from Horsethief Creek may be related to its host granite as a cumulate, or may be a piece of basement picked up by the granite magma. For Hor-6 to be related as a cumulate, minerals observed in this rock must be removed from the original Horsethief Creek

magma and result in an AKN (molar $\text{Al}_2\text{O}_3/[\text{Na}_2\text{O} + \text{K}_2\text{O}]$) change from ≈ 1.25 (host granite) to 1.56 (xenolith) while remaining unchanged in the Fe ratio (Fig. 3.2). The large amounts of biotite in Hor-6 are consistent with this relationship between the magma and cumulate. Whether this origin is possible will depend on the composition of the biotite being removed. The biotite must have a non-stoichiometric excess in aluminum to give an AKN ratio of > 1 . Biotite compositions in silicic magmas commonly have an ASI of as much as 1.3 to 1.5 (Zen 1986) and a corresponding AKN ratio of 1.3 to 1.5. In order to keep the ASI ratio of Hor-6 unchanged, hornblende and/or albitic plagioclase, which are both observed in this rock, must also be removed from the original magma, and the required proportions will depend on the original position of the granitic/granodioritic magma in AKN-ASI space.

The trace element abundances of the BFH plutons are listed in Table 3.1. Figure 3.4 shows trace element normalized diagrams (normalized relative to ocean ridge granite following Pearce et al. 1984) for the different granites and xenoliths. The Fry Creek two-mica granites have lower abundances of Ba to Sm and higher abundances of K_2O , Rb, Y, and Yb relative to the BFH biotite granites. They overlap in composition with granites from post-collision tectonic settings (Fig. 3.4). The lower normalized abundance of Ba relative to Rb and Th, and the lack of a strong depletion (resulting in a negative anomaly) of Ta and Nb relative to Th and Ce in the patterns for the hornblende-biotite granites are characteristic of within-plate granites, but the steeply declining normalized abundances from Th to Yb are more similar to those of post-collision granites (Fig. 3.4). The quartz diorite xenolith from Horsethief Creek, and the metapelite xenolith from Bugaboo (Fig. 3.4) also show the same general patterns as do the granitoids. If these xenoliths are representative of basement rocks in SEBC, the similarity between their trace

element patterns and those for the granites suggests that such rocks may be in part sources for the granites.

The two granite types are distinguished by Rb versus Nb + Y, and Nb versus Y. The two-mica granites have lower Nb + Y for a given Rb abundance and lower Nb for a given Y abundance relative to the hornblende-biotite granites (Fig. 3.5). All of the granites plot in the within-plate granite field of Pearce et al (1984) in both diagrams. The quartz diorite xenolith from Horsethief Creek plots at larger Nb, Y, and Rb than does its host granite (Fig. 3.5). High concentrations of biotite, hornblende, and accessory phases (observed in this xenolith) could have resulted in its elevated Rb, Nb, and Y abundances relative to the host rock.

In summary, major and trace element characteristics of the BFH granites indicate that there are two lithologic types, two-mica granites from Fry Creek, and biotite granites from all three batholiths. The strongly-peraluminous two-mica granites can be distinguished from the biotite granites petrographically, as well as by their contrasting major and trace element compositions. All of the granite types have trace element characteristics primarily of within-plate granites (Pearce et al. 1984). The major and trace element characteristics of the Horsethief Creek quartz diorite xenolith are consistent with derivation by accumulation of mafic phases from a more silicic magma, probably one parental to the host granite. However, an origin as an exotic inclusion derived from the basement lithologies cannot be ruled out. The metapelite xenolith has generally large abundances of incompatible trace elements and may in part reflect the compositional characteristics of lower and mid-crustal basement rocks within the present-day Purcell Mountains.

Isotope geochemistry

Rb-Sr and Sm-Nd isotopic relations for the Bugaboo, Fry Creek, and Horsethief batholiths, are listed in Table 3.3. Rb-Sr isochron ages of 107 Ma, 115 Ma, and 110 Ma for the Bugaboo, Fry Creek, and Horsethief Creek batholiths, respectively (Brandon and Lambert 1992a), were used to calculate the initial ϵ_{Sr} and ϵ_{Nd} (following Jacobsen and Wasserburg 1984, and Allegre and Ben Othman 1980), and initial Pb isotopic ratios. Nd model ages (TDM) are calculated relative to the depleted mantle curve from DePaolo (1981a). All three batholiths show a wide range in ϵ_{Sr} and ϵ_{Nd} , but their diversities depend on the granite type. The Bugaboo biotite granites have ϵ_{Sr} from +35.7 to +44.1 and ϵ_{Nd} from -4.8 to -5.3, whereas the Fry Creek biotite granites have ϵ_{Sr} from +44.0 to +45.3 and ϵ_{Nd} from -8.7 to -9.4, and the Horsethief Creek granites have ϵ_{Sr} from +46.9 to +78.7 and ϵ_{Nd} from -5.7 to -7.5. The two-mica granites from Fry Creek have much higher ϵ_{Sr} with a wide range from +173 to +467 and much lower ϵ_{Nd} with a wide range from -14.8 to -20.8, and are isotopically distinct from the biotite granites from all three batholiths. Aplites and pegmatites from all three plutons show ϵ_{Sr} and ϵ_{Nd} isotopic diversity that spans the complete range of the BFH granites.

The quartz diorite xenolith (Hor-6) from Horsethief Creek has ϵ_{Sr} of +49.7 and ϵ_{Nd} of -6.5, overlapping with its host granite. The metapelite xenolith (Bug-8) from Bugaboo has ϵ_{Sr} +237 and a very low ϵ_{Nd} of -23.8 consistent with a Precambrian age for this rock.

Figure 3.6 displays ϵ_{Sr} and ϵ_{Nd} for the BFH rocks, Proterozoic metasediments, and Precambrian basement gneisses from SEBC and northern Idaho. The isotopic composition of the BFH suite completely overlap those of the crustal rocks found in this region. This concordance suggests that the magmas of the BFH batholiths were primarily derived from crustal sources,

without geochemical involvement of juvenile mantle components. The Fry Creek two-mica granites plot on a trend leading away from the biotite granites in the upper left part of the diagram towards higher ϵ_{Sr} and lower ϵ_{Nd} indicative of crustal sources with high time-integrated Rb/Sr and low Sm/Nd. The Bugaboo and Horsethief Creek granites plot as a distinct trend above the Fry Creek trend in the diagram. All of the data for the rocks converge towards ϵ_{Sr} of $\sim +25$ and ϵ_{Nd} of ~ -4.0 , which may be one end-member isotopic composition, while the other end-member may be towards very high ϵ_{Sr} and lower ϵ_{Nd} if a simple two source mixing model is appropriate for all three batholiths. In such a case, the differences observed in the two trends would arise because of differences in Sr/Nd ratios in the mineral/melt mixtures as melting proceeded within the source lithologies.

Neodymium model ages (TDM) of granitic rocks are unusable in absolute terms in defining the age (i.e. crustal residence age) of possible crustal source lithologies because of potential changes in Sm/Nd ratios during partial melting and post-extraction differentiation processes, and when there are multiple sources for the igneous melts (Arndt and Goldstein 1987, Patchett 1991). In many instances, model ages can be used to constrain qualitatively the ages of the source material, provided such material was originally extracted from a depleted mantle reservoir. For most of Earth history since the Archean, this assumption is valid. However, the aplites clearly give reset TDM (i.e. Bug-7, TDM = 29.5 Ga, and Hor-2, TDM = 4.9 Ga) and cannot be used. The biotite granites have a range of TDM from ~ 830 to ~ 1130 Ma consistent with a Proterozoic average age for their source material. The Fry Creek two-mica granites yield higher TDM of 1903 Ma to 2822 Ma, and for both types of granites, these model ages correlate roughly with their respective ϵ_{Nd} values (Table 3.3). These correlations suggest that the isotopic differences observed

within the BFH granites may be related in part to the age(s) of their source materials.

The metapelite xenolith has $T_{DM-Nd} = 3.19$ Ga, and $T_{DM-Sr} = 3.16$ Ga. The concordance of these model ages is consistent with the interpretation that this rock was unaffected by interaction with its host magma and that this metapelite reflects a protolith of at least 3.2 Ga.

U, Th, and Pb abundances and isotopic ratios are listed in Table 3.4. Initial Pb ratios for the BFH suite are plotted in Figure 3.7. All of the Pb ratios for the BFH rocks plot in a band above the line for northern hemisphere oceanic basalts (NHRL) and, in $^{207}Pb/^{204}Pb$ versus $^{206}Pb/^{204}Pb$ space, to the right of the 110 Ma geochron. Sparse Pb data for the basement rocks in the Purcell Mountains, as represented by Proterozoic metasediments in Figure 3.1 (Ghosh 1986), plot along the same band as the plutonic rocks in both Pb plots. The metapelite xenolith from Bugaboo also plots within this band. The biotite granites plot at lower values of $^{206}Pb/^{204}Pb$ for a given $^{207}Pb/^{204}Pb$ and $^{208}Pb/^{204}Pb$ than do the two-mica granites, and therefore these two granite types are also distinct in their Pb isotopic compositions.

In summary, the Bugaboo, Fry Creek, and Horsethief Creek granitoid rocks have Sr, Nd, and Pb isotopic compositions overlapping known compositions for the basement rocks in the Purcell Mountains, and are consistent with the interpretation that these granites are crustal melts with little or no juvenile mantle component. These inferences will be further considered in the next section.

Sources for the BFH granites

Isotopic constraints

Isotopic data for the BFH granitoids are consistent with a petrogenesis wherein two-member source mixing produces the observed range in compositions. One end-member (M1) is constrained by the biotite granites with higher abundances in incompatible trace elements, less-radiogenic Pb and Sr isotopic compositions, and more-radiogenic Nd isotopic compositions. The other end-member (M2) is constrained by the strongly peraluminous two-mica granite from Fry Creek, and produces melts generally with lower abundances of incompatible trace elements (Figs. 3.4 and 3.5), more radiogenic Pb and Sr isotopic compositions, and less radiogenic Nd isotopic compositions. Melts representing the M1 isotopic composition can be either a mantle source contaminated by Precambrian crust, or wholly Proterozoic crust (as qualitatively implied by TDM ages). Figure 3.8 displays ϵ_{Nd} versus $^{147}Sm/^{144}Nd$ systematics for the mid-Cretaceous granites and Precambrian crust in SEBC. The BFH biotite granites completely overlap the ϵ_{Nd} compositions for the basement rocks and plot at lower $^{147}Sm/^{144}Nd$. These circumstances are consistent with the biotite granites being derived directly as partial melts from the crust, or by fractional crystallization from partial melts of SEBC crustal rocks, because Sm/Nd ratios decrease during both of these processes (DePaolo 1981b). Alternatively, mixtures of mantle-derived melts contaminated with more negative ϵ_{Nd} material (i.e., Archean crust) followed by fractionation could produce the same results. About 20% contamination of a mantle-derived magma by this crust could result in the Nd isotopic systematics of the BFH biotite granites (Fig. 3.8). However, in light of: (a) the within-plate granite trace element characteristics, and in particular low Ba, and high Rb and Nb + Y abundances, which are inconsistent with granitoids derived

through differentiation of mantle-derived magmas (Pearce et al. 1984); (b) Pb isotope compositions which completely overlap SEBC crustal compositions and which do not appear to trend towards a possible mantle end-member (i.e. NHRL, Fig. 3.7); (c) crustal oxygen isotopic compositions for similar granitoids in the White Creek batholith shown in Figure 3.1 (Brandon and Lambert, 1992b); and (d) the lack of any field evidence for Early Cretaceous basalts anywhere in the area of Figure 3.1, it is unlikely that these granitoids are differentiates of mantle-derived magmas. Given these constraints, M1 melts appear to be derived from crustal lithologies.

The two-mica granites from Fry Creek completely fall within the range of SEBC crustal lithologies in Figure 3.8, and require 80 to 100% of the average SEBC crustal component ($\epsilon_{Nd} = -20$) to produce their Nd isotopic compositions. This mass balance suggests that the two-mica granites from Fry Creek are most likely crustal melts, and that these M2 melts represent a different crustal lithology than do M1 melts.

Given the above trace element and isotopic evidence, all of the BFH granites were probably produced by melting and subsequent mixing of a minimum of two crustal end-members. In $\epsilon_{Nd} - \epsilon_{Sr}$ space (Fig. 3.6), these end-members must lie at opposite ends of the band of BFH granites. The Fry Creek granites plot on a different trend than those for Bugaboo and Horsethief Creek, but both trends converge towards the M1 crust with $\epsilon_{Nd} = \sim -3.5$ to -5 and $\epsilon_{Sr} = \sim +20$. These different trends are most likely the result of different Sr/Nd ratios in the sources, reflecting local variations in the composition of the basement. Using a Sr abundance of 1500 ppm for M1 melts (similar to the Fry Creek biotite granites) for mixing with M2 melts, produces the Fry Creek trend. A Sr abundance of 600 ppm for M1 melts (similar to the Horsethief Creek granites) with the same Nd abundances used in the mixing calculations for the

Fry Creek trend, and the same parameters for M2 melts, produces the Bugaboo - Horsethief Creek trend. Resulting Sr/Nd ratios for the M1 melts for the two trends are 25 and 10, respectively. Such values of Sr and Sr/Nd are not found in basalts derived directly from the mantle, thus reinforcing a crustal melt hypothesis.

In order to match both trends with melts produced by mixing of M1 - M2 melts, an abundance of 30 ppm for Nd is required for M2. The Sr and Nd abundances used for M1 and M2 melts which produce the two trends are within the ranges for those abundances in the granitoids plotting near the end-members (Fig. 3.6), except for the Nd abundance of M2. The two-mica granites of Fry Creek have Nd abundances from 7.9 to 17.2 ppm. These values are considerably less (by 2 to 4 times) than the abundance of 30 ppm predicted by the mixing calculations. They coincide with overall low LREE contents for these granites (Table 3.1, Fig. 3.4). Experimental and geochemical studies on solubility and fractionation of accessory phases (i.e. zircon and monazite) in strongly peraluminous granites, suggest that much less than 1% removal of such phases during late stage crystallization can decrease the REE abundances of these granites by substantial amounts (Miller and Mittlefehldt 1982, Watson and Harrison 1983, Mittlefehldt and Miller 1983, Gromet and Silver 1983, Watson and Harrison 1984, Rapp and Watson 1986). Removal of accessory phases, and in particular LREE-rich monazite, is consistent with the observed low Nd and LREE abundances of the Fry Creek two-mica granites relative to the predicted Nd abundances in our M1 - M2 melt mixing calculations.

Phase equilibrium constraints on crustal melting

The most fertile crustal lithologies that produce felsic magmas in equilibrium with hornblende and biotite are quartzofeldspathic rocks.

containing hydrous phases, such as amphibolites and tonalites (Miller et al. 1988). Under vapor absent conditions and lower crustal pressures, liquids with SiO₂ contents from 70 to 77 wt.% can be generated by partial melting of amphibolite at ~900 - 1000 °C, leaving garnet and amphibole in the residue (Rapp et al. 1991, Beard and Lofgren 1990, 1991, Rushmer 1991, Wolff and Wyllie 1991). The Bugaboo hornblende-biotite granodiorite in the western part of the batholith, and magmatic hornblende observed in several samples from the Fry Creek batholith (Reesor 1973), require an amphibole-bearing protolith in order to derive these granitoids by crustal anatexis. The major element abundances of the BFH biotite granites fall within the range for those of the experimental melts generated in these studies except for K₂O contents in the BFH granites, which are at least 2 times greater. The starting materials in the experiments were poor in K₂O (all < 1 wt.% and most < 0.5 wt.%). Amphibolite gneisses from the basement Malton gneiss block near Valemount just north of Figure 3.1 (Chamberlain et al. 1988) have major element compositions which overlap those for the amphibolites used in the melting experiments of Rapp et al. (1991) and Beard and Lofgren (1991) except for K₂O contents from 3 to 5 wt.%. These higher K₂O contents must result in higher K₂O contents in silicic melts which these gneisses could produce, because K₂O in the melt is proportional to its source (Thy et al. 1990) and because no K-bearing minerals are residual during partial melting. Therefore, these basement gneisses are favorable candidates for sources of the BFH biotite granites.

Vapor-absent melting of tonalitic gneiss has been recently investigated (Rutter and Wyllie 1988, Skjerlie and Johnston 1992). During melting of a tonalitic gneiss at 10 kbar, Skjerlie and Johnston (1992) showed that at temperatures of 950 to 975 °C, biotite and amphibole break down to produce granitic melts with a garnet, orthopyroxene, and titanomagnetite residue.

Chamberlain et al. (1988) showed that the Malton gneiss, the only exposed and proven pre-Purcell basement in the area under consideration, is composed of four main rock types, tonalite gneiss interlayered with mildly alkaline amphibolite gneiss, with subordinate volumes of granodiorite augen gneiss and Late Proterozoic peralkaline granite sills. Merging the experimental studies cited above suggests that melting of a gneiss complex consisting of alternating sheets of tonalite and amphibolite would yield a melt which was derived from both of these lithologies, a possible M1 composition in both chemical and Sr-Nd compositional terms.

Fluid-absent melting of metapelitic rocks has been examined recently by Vielzeuf and Holloway (1988) and Patiño Douce and Johnston (1991). At 7 to 10 kbar, strongly peraluminous granitic liquids are produced at temperatures of ~850 to 1000 °C, with compositions overlapping the Fry Creek two-mica granites, by the breakdown of biotite and muscovite leaving a residue primarily of garnet and aluminosilicate.

In conclusion, we favor a model where the BFH biotite granites and the Fry Creek two-mica granites are derived by partial melting of amphibolitic/tonalitic and pelitic crustal lithologies, respectively. Because the Sr, Nd, and Pb isotopic compositions are consistent with mixing between two crustal end-member compositions, it is likely that these isotopic end-members are represented by amphibolitic/tonalitic basement gneisses (M1) and pelitic rocks (M2). Melting of mixed crustal lithologies is only now beginning to be investigated experimentally, and only preliminary results are available, but such melting appears to replicate natural granitic compositions (Patiño Douce et al. 1991). During the large degrees of melting required to produce separation of granitoid melts from their source region (ca. 30-40%, Wickham 1987), mixed lithology melting should be favored in complicated lower crustal

metamorphic sequences. Besides the Malton gneiss example mentioned above, Late Proterozoic amphibolites are complexly interlayered with metapelites in the Monashee Mountains (Ghent et al. 1977, Sevigny 1988), and therefore the spatial association required to produce the mixed lithology melting we favor here is present in the SEBC basement. Without further comprehensive geochemical characterization of basement rocks in SEBC, however, we cannot test this model, and only support it on a qualitative basis until further information is available.

Conclusions

The Bugaboo, Fry Creek, and Horsethief Creek batholiths have lithological, petrographic, and geochemical characteristics of granitoid rocks that can be modelled by melting of crustal protoliths. The Sr, Nd, and Pb isotopic compositions of these granites are most easily reconciled by simple mixing between two crustal end-members. In Sr - Nd isotope space (Fig. 3.6), the Sr and Nd abundances for the granites are also predicted by mixing of melts derived from the two crust end-members, designated M1 and M2 here. Phase equilibrium considerations suggest that M1 was an amphibolite or a mixed amphibolite-tonalite lithology. M1 has isotopic compositions and Nd model ages consistent with a Late Proterozoic age. Similar-age amphibolites exposed in the Malton gneiss to the north and in the Monashee Mountains to the west may reflect analogous rocks underlying the Purcell Mountains, and therefore represent in part the source for the biotite granites. M2 crust was likely pelitic in nature. Proterozoic metapelites in the Purcell Mountains have isotopic compositions overlapping the Fry Creek two-mica granites. A mixed lithology anatexis model most readily explains the isotopic mixing relations between M1 and M2. The early-Proterozoic to late-Archean Nd model ages for

these granitoids would therefore reflect the average crustal residence age of the protolith of the pelitic metasediments, provided no Sm/Nd fractionation occurred within these granites. However, the significantly lower Nd abundances in the two-mica granites than predicted by the M1-M2 isotopic mixing calculations suggests that these granitoids have undergone accessory phase fractionation depleting the magma in LREE (common in strongly peraluminous granites, Mittlefehldt and Miller 1983), which would change the Sm/Nd ratios and modify the Nd model ages in these granitoids.

The absence of Early Cretaceous mafic magmas, representing a mantle heat source causing crustal anatexis, requires consideration of an alternative mechanism to produce anatexis during terrane accretion in this region and time period. Detailed modelling of crustal thickening has demonstrated that downwarping of medium grade metamorphic rocks containing hydrous mineral phases into a higher temperature regime in the lower crust promotes the generation of granitic melts by fluid-absent anatexis and produces regional granulite facies metamorphism (Patiño Douce et al. 1990). Recent seismic refraction studies across SEBC in Figure 3.1 shows evidence for a 10 km step-down in the Moho between the Slocan Lake fault (along which the movement occurred near the left edge of Fig. 3.1) and the crest of the Purcell Mountains (White et al 1992). It is not clear when the onset of thickening occurred, but the last movement of the Slocan Lake fault was in the Eocene and places a minimum age for thickening in this region. Unless a mantle heat source can be shown to exist from other lines of evidence, a model of crustal anatexis in the mid-Cretaceous in SEBC by crustal thickening is favored.

Acknowledgements. This research was supported from NSERC operating and Lithoprobe grants to R.StJ. Lambert (1988-1991). Reviews from Gordon

Goles, Rob Creaser, Tom Chacko, George Cumming, Jonathan Patchett, and Bob Luth greatly improved this paper.

Table 3.1. Major and trace element abundances of the Bugaboo, Fry Creek, and Horsethief Creek batholiths.

Sample Type	Bugaboo								
	Bug-1a BtGr	Bug-1a Rpt	Bug-1b Aplite	Bug-1b Rpt	Bug-2 BtGr	Bug-6 BtGr	Bug-6 Rpt	Bug-7 Aplite	Bug-8 MXen
SiO ₂	73.78	74.02	75.18	75.35	75.88	73.65	73.51	75.11	54.10
TiO ₂	0.248	0.247	0.049	0.046	0.193	0.210	0.207	0.058	0.908
Al ₂ O ₃	14.20	14.05	14.38	14.31	13.07	14.23	14.33	14.25	22.60
FeO*	1.34	1.37	0.12	0.12	1.25	1.29	1.28	0.44	6.85
MnO	0.042	0.042	0.009	0.010	0.049	0.044	0.044	0.036	0.196
MgO	0.58	0.43	0.10	0.01	0.32	0.26	0.28	0.04	2.53
CaO	1.48	1.47	0.99	0.99	1.06	1.44	1.42	0.58	2.86
Na ₂ O	3.82	3.80	4.51	4.45	3.54	3.65	3.71	4.86	4.78
K ₂ O	4.40	4.45	4.61	4.64	4.57	5.13	5.13	4.53	5.08
P ₂ O ₅	0.114	0.117	0.065	0.065	0.069	0.081	0.079	0.101	0.099
TTL	100.00	100.00	100.01	99.99	100.00	99.99	99.99	100.00	100.00
Ni	14	14	13	9	14	14	14	13	71
Ba	604	609	138	155	431	834	839	79	631
Y	24	24	15	14	24	24	24	28	38
Zr	143	142	36	36	116	121	122	45	225
Nb	104	106	36	37	130	102	105	36	34
Hf	4.34		1.35		4.23	3.79		2.24	6.44
Ta	7.94		4.94		10.24	8.19		5.16	1.52
Cr	5.5		BD		5.2	4.9		BD	BD
Co	1.69		BD		1.47	1.59		BD	15.9
Sc	3.86		2.25		2.49	2.92		4.00	18.3
La	65.1		5.57		59.5	59.5		6.41	54.6
Ce	111.6		10.52		102.6	99.4		14.81	98.5
Nd	40.1		4.06		38.4	38.1		5.72	41.9
Sm	5.65		0.95		5.10	5.45		2.05	8.98
Eu	0.98		0.31		0.77	0.98		0.14	1.65
Tb	0.47		0.14		0.41	0.41		0.39	1.00
Yb	2.65		1.42		2.41	2.36		3.01	2.83
Lu	0.47		0.21		0.47	0.43		0.44	0.46

Sample	Bugaboc				Fry Creek				
	Bug-10	Bug-11	Bug-12	Bug-13	Fry-1	Fry-1 Rpt	Fry-2	Fry-3	Fry-4
Type	BtGr	Aplite	BtGr	BtGr	2MGr		2MGr	2MGr	Aplite
SiO ₂	75.01	75.31	74.26	75.74	74.65	74.67	74.80	74.87	76.83
TiO ₂	0.140	0.083	0.273	0.231	0.069	0.072	0.092	0.074	0.059
Al ₂ O ₃	13.88	13.94	13.61	12.92	14.79	14.74	14.51	14.79	13.66
FeO*	0.88	0.56	1.72	1.44	0.50	0.52	0.67	0.50	0.36
MnO	0.027	0.027	0.052	0.043	0.023	0.022	0.034	0.020	0.015
MgO	0.15	0.00	0.57	0.39	0.09	0.02	0.05	0.01	0.00
CaO	1.33	0.82	1.49	1.26	0.81	0.84	0.90	0.84	0.60
Na ₂ O	3.55	3.99	3.37	3.28	3.94	3.97	4.14	3.86	4.08
K ₂ O	4.98	5.23	4.54	4.61	5.04	5.06	4.71	4.94	4.37
P ₂ O ₅	0.053	0.052	0.111	0.094	0.080	0.083	0.094	0.100	0.031
TTL	100.00	100.01	100.00	100.01	99.99	100.00	100.00	100.00	100.00
Ni	11	14	13	14	13	14	14	13	11
Ba	985	280	743	709	283	285	429	287	332
Y	14	26	23	22	16	15	21	17	11
Zr	83	60	139	131	43	43	68	41	20
Nb	62	48	113	101	35	34	25	28	50
Hf	2.25		4.02		1.37		2.32	1.39	0.24
Ta	4.50		8.19		2.41		2.23	2.61	2.91
Cr	2.6		6.1		BD		BD	BD	BD
Co	1.15		2.16		BD		BD	BD	BD
Sc	1.85		3.60		2.48		2.24	2.12	5.20
La	47.1		81.2		9.53		19.9	7.9	4.10
Ce	74.7		129.2		22.0		41.7	19.5	8.63
Nd	25.2		45.2		9.7		17.2	7.9	2.74
Sm	3.15		6.25		1.85		3.38	1.79	0.60
Eu	0.81		0.97		0.58		0.67	0.68	0.41
Tb	0.20		0.51		0.32		0.40	0.27	0.17
Yb	1.42		2.41		1.43		1.79	1.41	1.29
Lu	0.27		0.45		0.21		0.24	0.19	0.19

Sample Type	Fry Creek						Horsethief Creek		
	Fry-5 2MGr	Fry-6 2MGr	Fry-7 TmPg	Fry-8 BtGr	Fry-9 BtPg	Fry-10 BtGr	8641a BtGr	8641b BtGr	Hor-1 BtGr
SiO ₂	75.30	74.21	77.31	72.14	76.53	72.12	71.38	72.51	71.72
TiO ₂	0.103	0.099	0.041	0.294	0.024	0.270	0.285	0.264	0.280
Al ₂ O ₃	14.24	14.94	13.31	14.96	13.37	15.15	15.25	14.72	14.99
FeO*	0.76	0.66	0.40	1.74	0.25	1.59	1.75	1.66	1.76
MnO	0.035	0.022	0.088	0.041	0.010	0.038	0.033	0.031	0.055
MgO	0.00	0.08	0.00	0.31	0.00	0.24	0.68	0.48	0.61
CaO	0.70	0.86	0.46	1.58	0.68	1.71	1.78	1.64	1.78
Na ₂ O	4.02	3.68	4.08	4.53	4.29	4.71	4.01	3.83	3.79
K ₂ O	4.78	5.34	4.24	4.29	4.84	4.09	4.68	4.71	4.87
P ₂ O ₅	0.061	0.092	0.068	0.100	0.006	0.086	0.161	0.150	0.148
TTL	100.00	99.98	100.00	99.99	100.00	100.00	100.01	100.00	100.00
Ni	14	13	13	13	11	13	10	11	13
Ba	381	418	120	2302	190	1592	1145	858	1004
Y	22	21	14	13	4	12	21	20	19
Zr	74	59	23	262	36	243	160	138	144
Nb	59	31	57	51	37	55	75	94	109
Hf		1.99		6.38	1.06		4.36		4.32
Ta		1.78		2.90	1.78		5.86		7.48
Cr		BD		BD	BD		7.5		7.1
Co		BD		1.61	BD		BD		2.36
Sc		2.91		2.09	0.43		3.37		3.49
La		16.4		131.5	1.2		83.8		66.6
Ce		35.9		220.9	3.1		140.4		116.8
Nd		16.3		77.5	1.5		52.1		43.4
Sm		3.20		9.43	0.15		7.06		6.13
Eu		0.86		1.68	0.34		1.39		1.31
Tb		0.39		0.39	0.03		0.52		0.53
Yb		1.71		1.16	0.26		1.86		1.93
Lu		0.23		0.14	0.07		0.28		0.36

Horsethief Creek						
Sample Type	Hor-2 Aplite	Hor-3 BtGr	Hor-4 Aplite	Hor-6 DXen	Hor-7 BtGr	Hor-8 BtGr
SiO ₂	74.96	72.26	76.84	62.52	72.39	72.56
TiO ₂	0.042	0.298	0.052	0.808	0.279	0.315
Al ₂ O ₃	14.49	14.50	13.32	16.76	14.76	14.06
FeO*	0.15	1.89	0.07	5.45	1.76	2.19
MnO	0.011	0.051	0.007	0.139	0.043	0.052
MgO	0.03	0.71	0.00	2.47	0.58	0.85
CaO	0.80	1.85	0.49	3.89	1.80	2.02
Na ₂ O	4.35	3.77	3.77	5.05	3.83	3.82
K ₂ O	5.05	4.52	5.39	2.25	4.40	3.97
P ₂ O ₅	0.111	0.158	0.052	0.660	0.146	0.159
TTL	99.99	100.01	99.99	100.00	99.99	100.00
Ni	14	14	14	21	17	15
Ba	169	956	132	510	927	916
Y	15	17	18	43	19	19
Zr	37	155	36	260	142	161
Nb	21	95	72	150	101	105
Hf	1.19	4.00	1.48	6.97		4.22
Ta	2.76	5.42	8.94	5.08		6.88
Cr	BD	7.2	BD	21.1		10.0
Co	BD	3.2	BD	9.4		3.7
Sc	1.05	4.09	1.83	11.52		3.85
La	4.1	64.1	5.2	75.6		97.8
Ce	7.4	111.2	9.2	138.3		158.3
Nd	3.8	43.8	4.4	59.3		60.3
Sm	1.16	5.33	0.84	10.97		7.60
Eu	0.34	1.17	0.25	1.69		1.39
Tb	0.21	0.36	0.17	1.11		0.52
Yb	1.42	1.56	2.41	3.80		1.94
Lu	0.23	0.30	0.37	0.62		0.32

Major element analyses are normalized on a volatile-free basis. Ni, Ba, Y, Zr, and Nb were analyzed by XRF, and the rest of the trace elements were analyzed by INAA. Rock types: BtGr - biotite granite; MXen - metapelite xenolith; 2MGr - two-mica granite; BtGr - biotite granite; TmPg - garnet-tourmaline pegmatite; BtPg - biotite pegmatite; and DXen - quartz diorite xenolith. Repeat analyses are labeled Rpt. Below detection limit is BD.

Table 3.2. Isotopic standard data analyzed during this study.

NBS-SRM 987 $^{87}\text{Sr}/^{86}\text{Sr}$	La Jolla $^{143}\text{Nd}/^{144}\text{Nd}$	$^{206}\text{Pb}/^{204}\text{Pb}$	NBS 981 $^{207}\text{Pb}/^{204}\text{Pb}$	$^{208}\text{Pb}/^{204}\text{Pb}$
0.710286(30)	0.511817(9)	16.9312(30)	15.4841(10)	36.6984(28)
0.710256(22)	0.511810(6)	16.9342(18)	15.4912(32)	36.7053(104)
0.710240(54)	0.511826(6)	16.9626(44)	15.4991(44)	36.7579(102)
0.710250(50)	0.511823(6)	16.9436(28)	15.4940(34)	36.7317(180)
0.710246(50)	0.511809(6)	16.9474(26)	15.4994(60)	36.7382(178)
0.710219(38)				

Run precision (2σ) in the last place for the listed ratios is in parentheses.

Table 3.3. Rb-Sr and Sm-Nd isotopic relations for the Bugaboo, Fry Creek, and Horsethief Creek batholiths.

Type	Sample	Rb	Sr	$^{87}\text{Rb}/^{86}\text{Sr}$	$^{86}\text{Sr}/^{87}\text{Sr}_0$	$^{86}\text{Sr}/^{87}\text{Sr}_T$	$\epsilon_{\text{Sr}T}$
Bugaboo							
BtGr	Bug 1a	243	381	1.846	0.710566(16)	0.70776	+44.1
Aplite	Bug 1b	257	97	7.685	0.729479(34)	0.71780	+187
BtGr	Bug 2	242	248	2.825	0.711458(22)	0.70715	+35.7
BtGr	Bug 6	274	395	2.004	0.711118(40)	0.70806	+48.5
Aplite	Bug 7	339	46	21.40	0.740287(82)	0.70776	+44.1
MXeno	Bug 8	652	275	6.879	0.731785(32)	0.72133	+237
BtGr	Bug 10	210	434	1.401	0.710027(44)	0.70789	+46.1
BtGr	Bug 12	223	342	1.888	0.710592(36)	0.70772	+43.6
Fry Creek							
2MGr	Fry 1	227	181	3.626	0.725733(18)	0.71981	+215
		227	182				
2MGr	Fry 2	228	223	2.963	0.721739(42)	0.71690	+173
2MGr	Fry 3	216	147	4.268	0.743319(30)	0.73634	+450
Aplite	Fry 4	220	220	2.896	0.712525(34)	0.70779	+44.7
2MGr	Fry 6	205	184	3.236	0.742827(38)	0.73754	+467
TmPg	Fry-7	213	121	5.103	0.724758(60)	0.71642	+167
HBGr	Fry 8	150	1618	0.2683	0.708176(34)	0.70774	+44.0
BtPg	Fry 9	236	366	1.867	0.709529(22)	0.70648	+26.1
HBGr	Fry 10	155	1513	0.2965	0.708314(36)	0.70783	+45.3
Horsethief Creek							
BtGr	8641A	237	633	1.090	0.71189(2)	0.71019	+78.7
					0.711886(66)		
BtGr	Hor-1	253	655	1.118	0.710241(46)	0.70849	+54.7
Aplite	Hor-2	254	227	3.242	0.718279(36)	0.71321	+122
BtGr	Hor-3	246	637	1.118	0.710325(18)	0.70859	+55.9
Aplite	Hor-4	272	122	6.461	0.720530(360)	0.71015	+78.2
Xeno	Hor-6	291	571	1.475	0.710447(34)	0.70814	+49.7
BtGr	Hor-8	198	707	0.8107	0.709211(30)	0.70794	+46.9

Sample	Sm	Nd	$^{147}\text{Sm}/^{144}\text{Nd}$	$^{143}\text{Nd}/^{144}\text{Nd}_0$	$^{143}\text{Nd}/^{144}\text{Nd}_T$	$\epsilon_{\text{Nd}T}$	TDM
Bugaboo							
Bug 1a	5.65	40.1	0.0852	0.512319(4) 0.512302(5)	0.512251	-4.9	896
Bug 1b	0.95	4.06	0.1416	0.512191(13)	0.512092	-8.0	1745
Bug 2	5.10	38.4	0.0803	0.512320(11)	0.512254	-4.8	854
Bug 6	5.45	38.1	0.0865	0.512290(4)	0.512229	-5.3	927
Bug 7	2.05	5.72	0.2168	0.512008(8)	0.511856	-12.6	29.5G
Bug 8	8.98	41.9	0.1397	0.511382(5) 0.511377(7)	0.511282	-23.8	3184
Bug 10	3.15	25.2	0.0756	0.512302(5)	0.512249	-4.9	834
Bug 12	6.25	45.2	0.0837	0.512302(6)	0.512243	-5.0	845
Fry Creek							
Fry 1	1.85	9.7	0.1154	0.511757(10)	0.511670	-16.0	1934
Fry 2	3.38	17.2	0.1187	0.511817(8) 0.511823(27)	0.511731	-14.8	1903
Fry 3	1.79	7.9	0.1371	0.511532(9) 0.511533(10)	0.511429	-20.7	2822
Fry 4	0.60	2.74	0.1325	0.512072(29)	0.511972	-10.1	1769
Fry 6	3.20	16.3	0.1188	0.511514(14)	0.511425	-20.8	2352
Fry 8	9.43	77.5	0.0736	0.512106(5) 0.512106(6)	0.512044	-8.7	1041
Fry 9	0.15	1.5	0.0605	0.512210(64)	0.512165	-6.4	853
Fry 10	7.61		0.075*	0.512064(9)	0.512008	-9.4	1088
Horsethief Creek							
8641A	7.06	52.1	0.0819	0.512168(8) 0.512189(20)	0.512109	-7.5	1029
Hor-1	6.13	43.4	0.0854	0.512243(4) 0.512234(10)	0.512178	-6.2	972
Hor-2	1.16	3.8	0.1846	0.511890(11)	0.511757	-14.4	4924
Hor-3	5.33	43.8	0.0736	0.512223(9)	0.512170	-6.4	915
Hor-4	0.84	4.42	0.1149	0.512166(9)	0.512083	-8.1	1311
Hor-6	11.0	59.3	0.1119	0.512244(5)	0.512163	-6.5	1203
Hor 8	7.60	60.3	0.0762	0.512261(8)	0.512206	-5.7	892

Rb and Sr abundances by XRF, and Sm and Nd abundances by INAA; *, assumed value; all ratios and ϵ values relative to $^{86}\text{Sr}/^{88}\text{Sr} = 0.1194$ and $^{144}\text{Nd}/^{146}\text{Nd} = 0.7219$; $^{87}\text{Rb}/^{86}\text{Sr}_{\text{UR}} = 0.0827$; $\lambda^{87}\text{Rb} = 1.42 \cdot 10^{-11}/\text{yr}$; $^{87}\text{Sr}/^{86}\text{Sr}_{\text{UR}}$ at 0 = 0.70478; $\lambda^{147}\text{Sm} = 6.54 \cdot 10^{-12}/\text{yr}$; $^{147}\text{Sm}/^{144}\text{Nd}_{\text{CHUR}} = 0.1967$; $^{143}\text{Nd}/^{144}\text{Nd}_{\text{CHUR}}$ at 0 = 0.512638; TDM after the depleted mantle growth curve of DePaolo (1981a) and are in Ma except for Bug 7 in Ga. The 2σ precision in the last listed place for each measured isotopic ratio are shown in parentheses. The ϵ values and ratios calculated at T for Bugaboo for 107 Ma, for Fry Creek for 115 Ma, and for Horsethief Creek for 110 Ma.

Table 3.4. U-Th-Pb isotopic relations for Bugaboo, Horsethief Creek, and Fry Creek samples.

Sample	U	Th	Pb	$^{238}\text{U}/^{204}\text{Pb}$	$^{232}\text{Th}/^{238}\text{U}$	$^{206}\text{Pb}/^{204}\text{Pb}$	$^{207}\text{Pb}/^{204}\text{Pb}$	$^{208}\text{Pb}/^{204}\text{Pb}$
Bugaboo								
Bug-1a	22.6	49.3	26	56.35	2.26	20.227	15.780	39.967
			21					
Bug-1b	6.34	3.12	49	8.39	0.51	19.294	15.710	39.146
Bug-2	27.0	55.0	18	97.24	2.11	20.792	15.757	40.332
Bug-6	17.9	45.7	22	53.97	2.64	20.113	15.728	39.874
Bug-7	11.1	4.25	31	23.13	0.40	19.391	15.730	39.176
Bug-8	5.56	18.5	48	7.51	3.44	19.260	15.692	39.329
Bug-10	17.6	26.5	17	64.9	1.61	19.875	15.706	39.528
Bug-12	28.8	42.4	16	116.7	1.52	20.465	15.733	39.874
						20.463	15.738	39.867
Fry Creek								
Fry-1	14.3	5.09	44	21.8	0.37	20.075	15.778	39.753
			41			20.073	15.761	39.708
Fry-2	4.20	11.1	41	6.64	2.72	19.502	15.719	39.720
Fry-3	12.1	4.33	51	15.38	0.37	19.677	15.748	39.944
						19.679	15.760	39.957
Fry-4	4.20	3.80	32	8.51	0.94	19.048	15.654	39.425
Fry-6	4.17	8.22	59	4.58	2.04	19.617	15.754	39.905
Fry-8	6.68	34.1	19	22.79	5.29	18.865	15.620	39.643
Fry-9	22.1	7.67	33	43.42	0.36	19.419	15.651	39.319
Fry-10	4.53	27.9	23	12.77	6.38	19.004	15.626	39.511
Horsethief Creek								
8641A	7.56	29.4	31	15.81	4.03	19.523	15.692	40.002
						19.540	15.693	40.209
Hor-1	20.4	40.3	19	69.60	2.05	19.992	15.704	40.118
Hor-2	13.9	2.43	38	23.63	0.18	19.512	15.730	39.747
Hor-3	14.7	32.3	20	47.65	2.28	19.869	15.701	40.099
Hor-4	22.7	4.35	36	40.88	0.20	19.848	15.721	39.713
Hor-6	5.0	20.1	16	20.26	4.16	19.279	15.663	39.940
Hor-8	16.0	36.9	15	69.19	2.39	20.063	15.697	40.267

U and Th abundances by INAA, and Pb abundances by XRF; Radiogenic Pb ratios listed are the present day measured ratios and have 2σ precision of 0.05%.

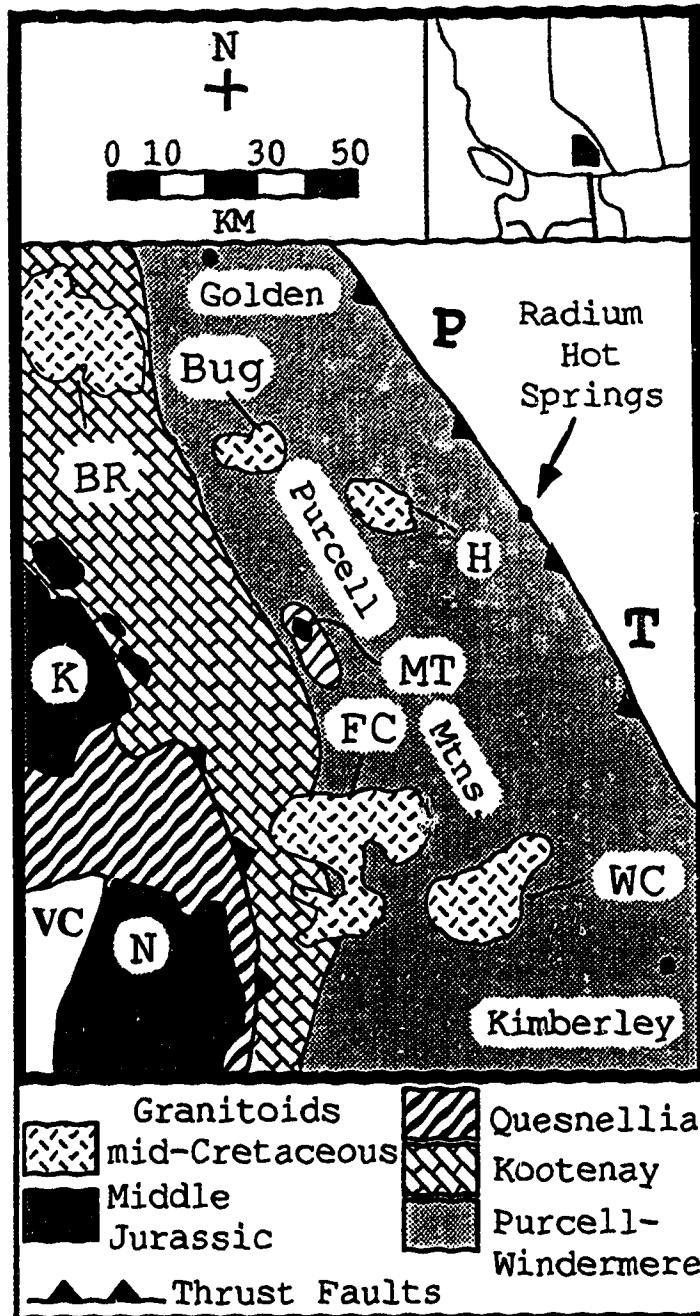


Figure 3.1. Generalized geologic map for southeast British Columbia along the Kootenay arc (modified after Monger and Berg 1987, Lambert and Chamberlain 1988, and Parrish et al. 1988). Abbreviations for the plutons are as follows: K - Kuskanax, MT - Mount Toby, N - Nelson, BR - Battle Range, Bug - Bugaboo, H - Horsethief Creek, FC - Fry Creek, and WC - White Creek. The Valhalla metamorphic core complex (VC) is shown in white in the southwest corner. The Purcell Thrust is labelled PT.

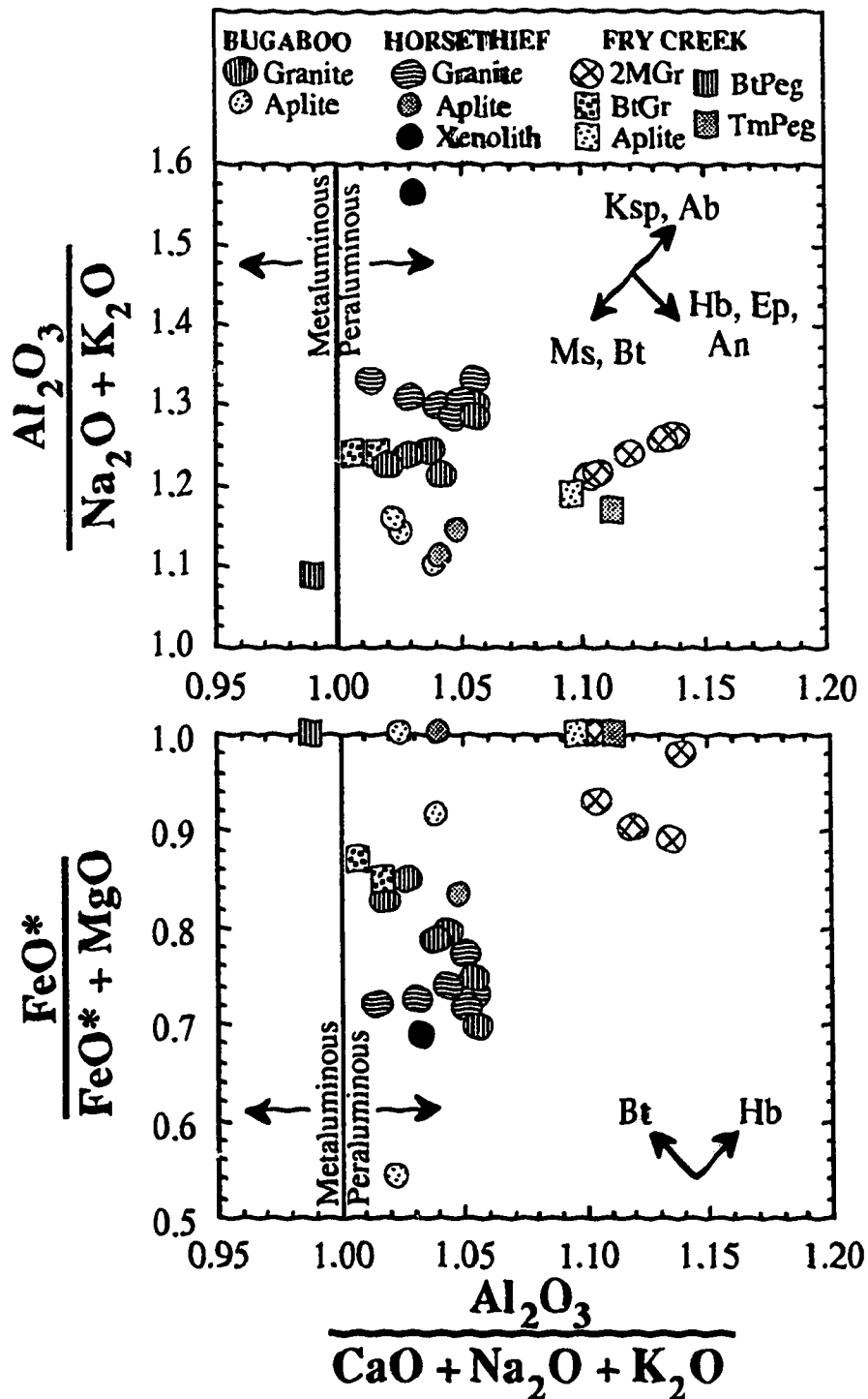


Figure 3.2. Alumina-saturation index versus Fe ratio and AKN for the BFH granites, associated aplites and pegmatites, and the Horsethief Creek quartz diorite xenolith. Abbreviations for the Fry Creek samples are for two-mica granite (2MGr), biotite granite (BtGr), biotite pegmatite (BtPeg), and tourmaline pegmatite (TmPeg). Also shown are qualitative fractionation trends for major mineral phases which may control these ratios in the granites. Ksp - alkali feldspar, Ab - albite, An - anorthite, Hb - hornblende, Ep - epidote, Ms - muscovite, and Bt - biotite. The mineral ASIs and AKNs are from Table 1 of Zen (1986). Fe ratios of 0.5 are assumed for Bt and Hb.

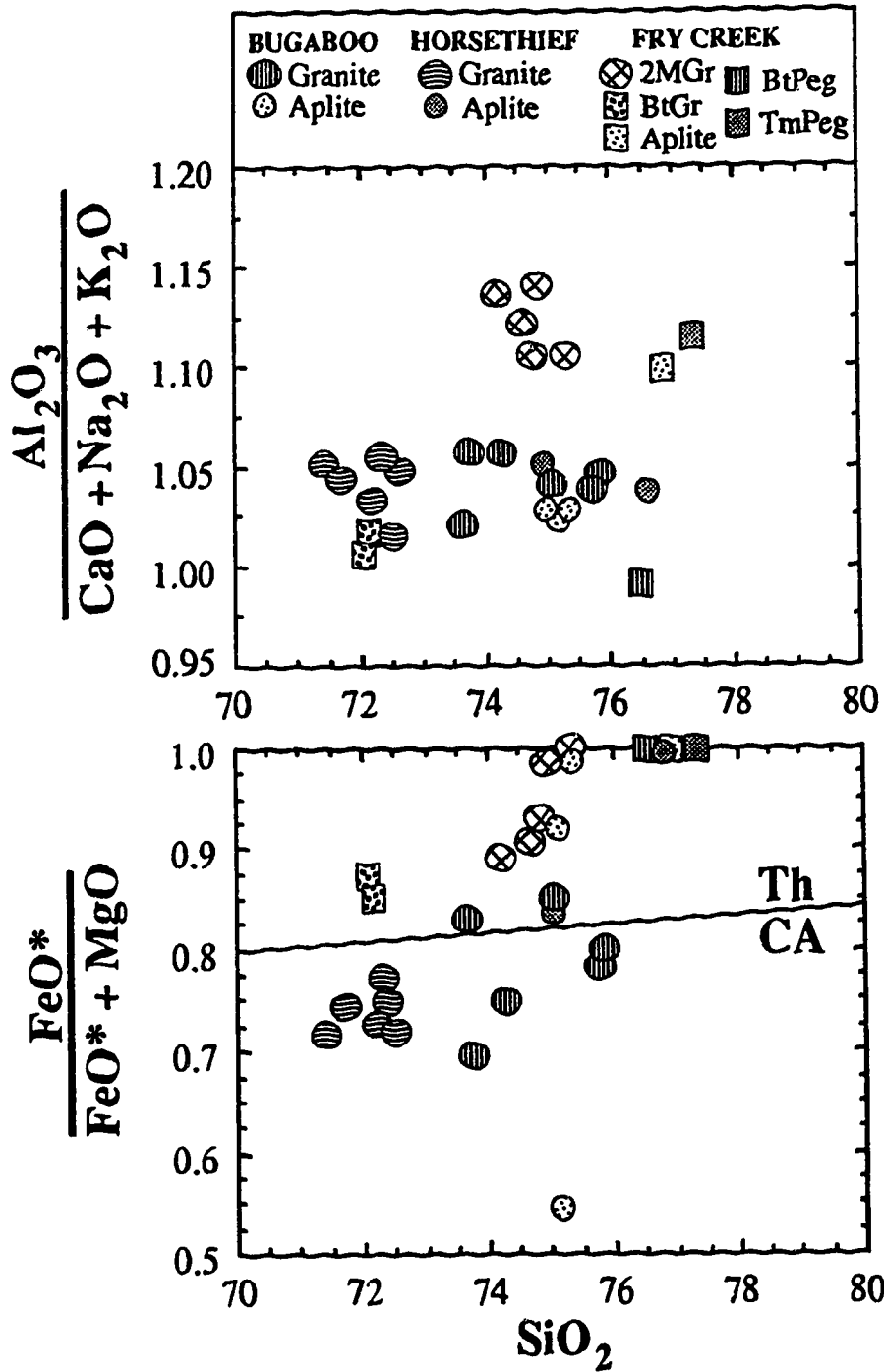


Figure 3.3. SiO_2 versus ASI and Fe ratios for the same BFH samples in Figure 3.2. Th is for the tholeiitic, and CA is for the calc-alkaline compositional fields.

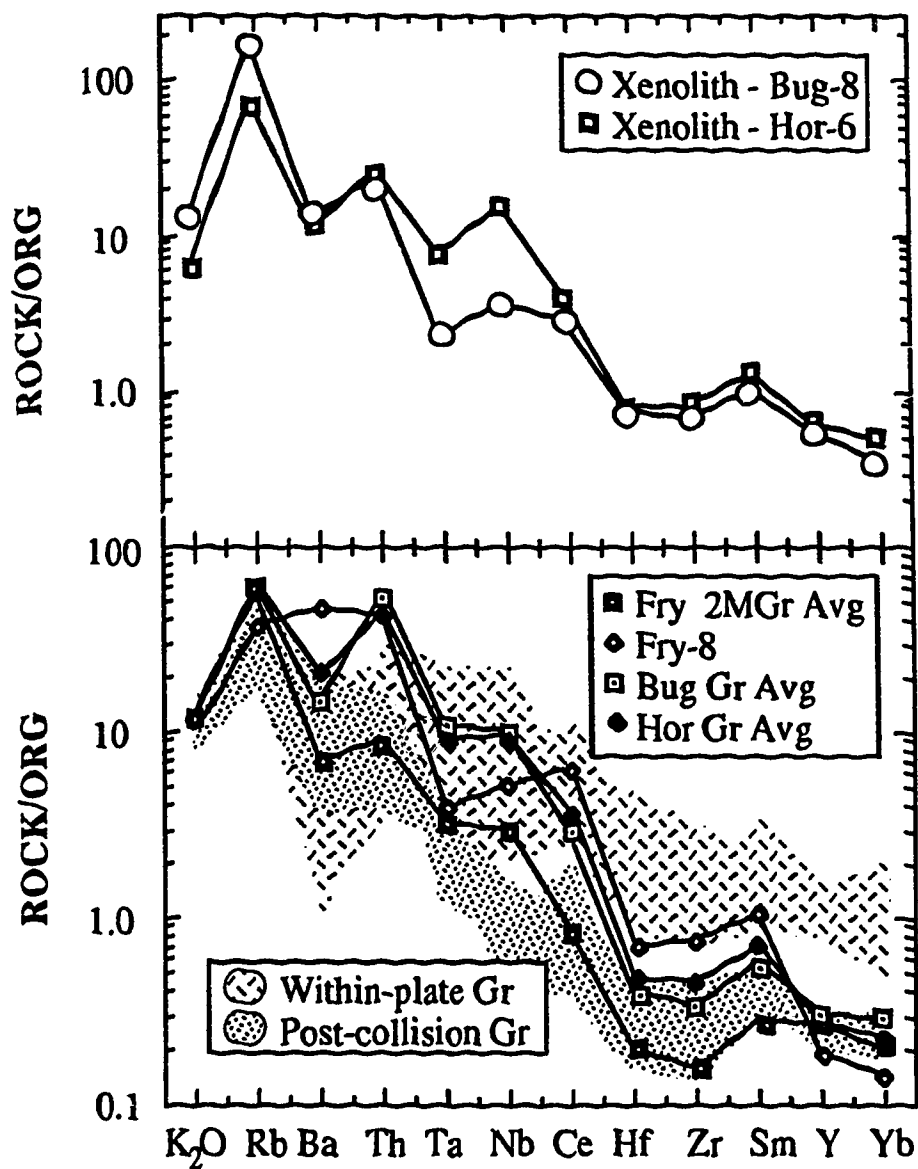


Figure 3.4. Trace element normalized diagrams for selected BFH samples. The trace element abundances are normalized relative to ocean-ridge granite following Pearce et al. (1984). Shown are the averaged abundances of the different granite types including the Fry Creek two-mica granite (Fry 2MGr Avg), the Bugaboo biotite granite (Bug Gr Avg), and the Horsethief Creek biotite granite (Hor Gr Avg). Only one sample of the Fry Creek biotite granite has a complete set of trace element abundances (Fry-8). The fields shown for within-plate and post-collision granites are from Pearce et al. (1984). Also shown are the metapelite xenolith (Bug-8) and the quartz diorite xenolith (Hor-6).

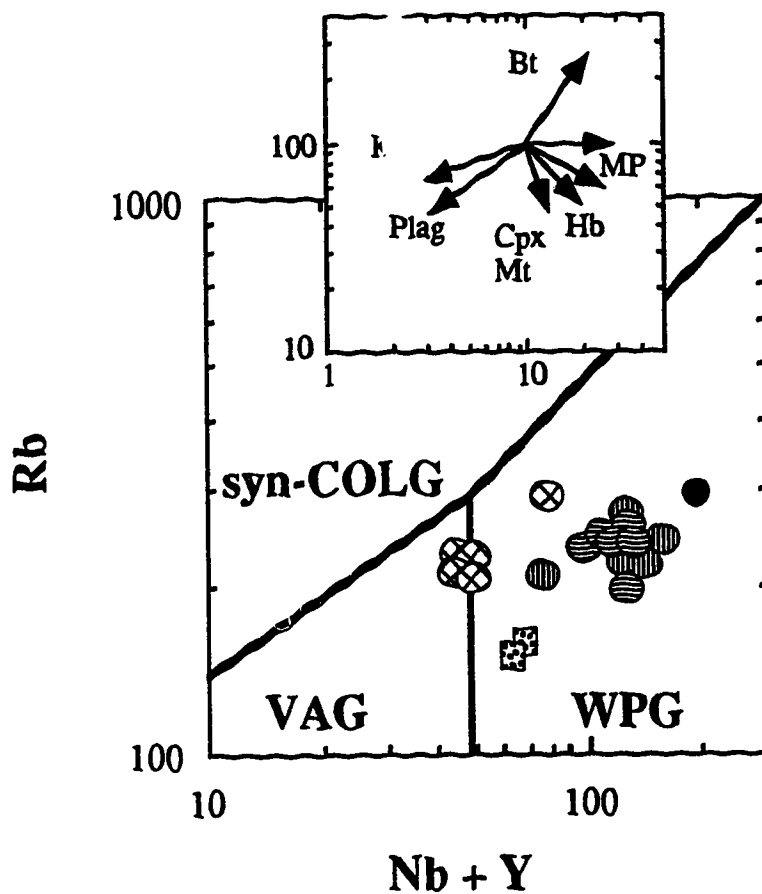


Figure 3.5A. Nb + Y versus Rb tectonic discrimination diagram plotting the BFH granites with symbols as in Figure 3.2 (after Pearce et al. 1984). The different granitoid fields are: VAG - volcanic arc granites, syn-COLG - syn-collision granites, and WPG - within plate granites. Accumulation trends for addition of 50% of the cumulate mineral, alkali feldspar (Ksp), biotite (Bt), minor phases (MP), hornblende (Hb), magnetite (Mt), clinopyroxene (Cpx), and plagioclase (Pl), are adapted from Pearce et al. (1984).

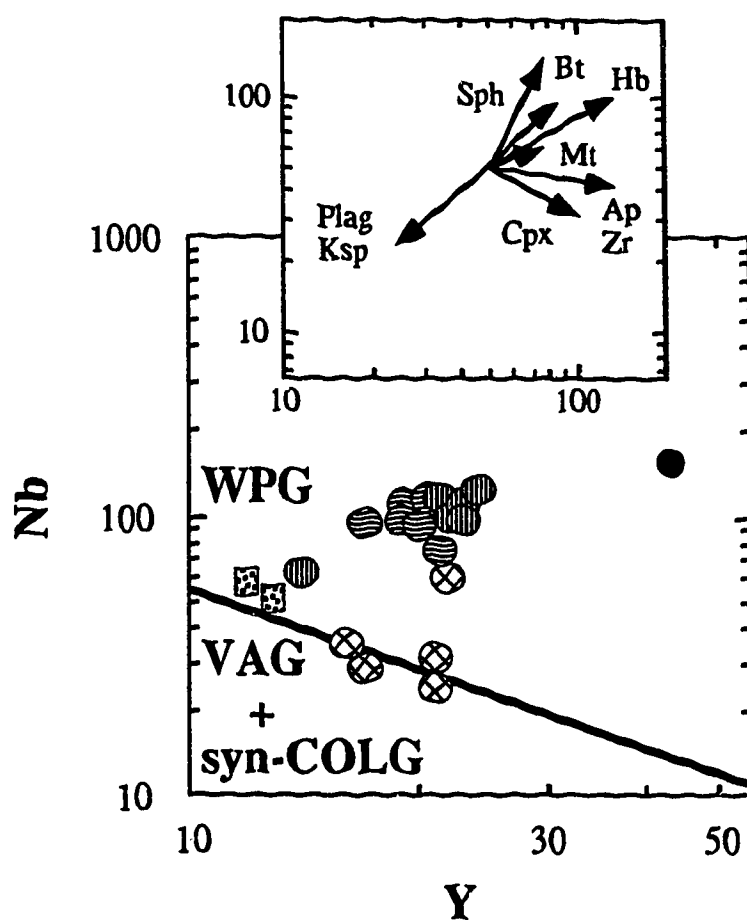


Figure 3.5B. Y versus Nb tectonic discrimination diagram plotting the BFH granites with symbols as in Figure 3.2 (after Pearce et al. 1984). The different granitoid fields are: VAG - volcanic arc granites, syn-COLG - syn-collision granites, and WPG - within plate granites. Accumulation trends for addition of 50% of the cumulate mineral, alkali feldspar (Ksp), biotite (Bt), magnetite (Mt), hornblende (Hb), clinopyroxene (Cpx), plagioclase (Pl), sphene (Sph), apatite (Ap), and zircon (Zr), are adapted from Pearce et al. (1984).

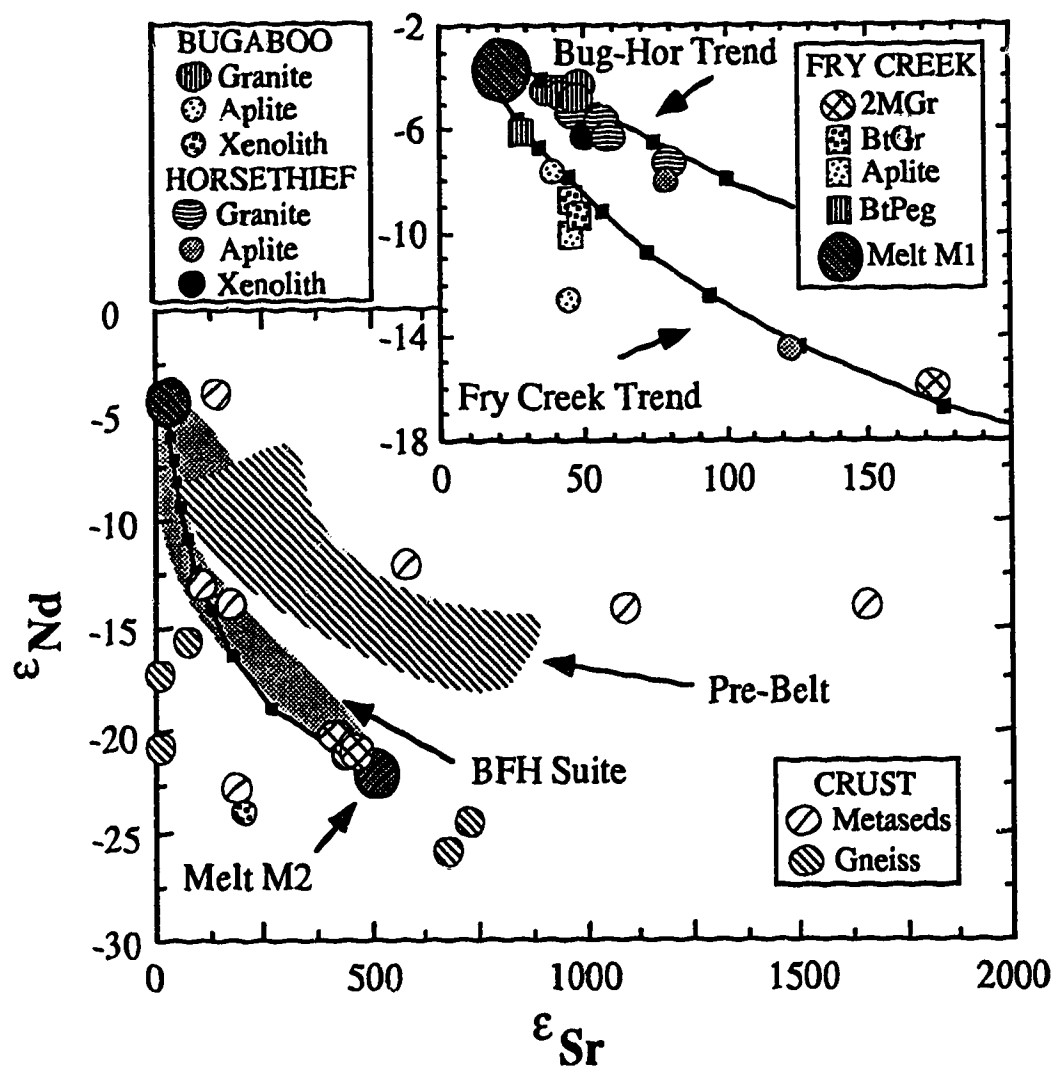


Figure 3.6. Initial ϵ_{Sr} versus ϵ_{Nd} diagram for crustal rocks and Mesozoic granites from SEBC. The basement gneiss compositions are from Lambert and Chamberlain (1990). The Pre-Belt gneisses are from northern Idaho 100 to 250 Km south of Kimberley and underlying Belt-Purcell metasediments. The metasediments (Metaseds) are for the Proterozoic metasediments in Figure 3.1 from Ghosh and Lambert (1989). Mixing lines that coincide to the Fry Creek and Bugaboo-Horsthief Creek (Bug-Hor) trends by hypothetical melts produced by crustal compositions M1 and M2 are shown with 10% increments (black squares) for the mixes. The mixing parameters are as follows: M2 - $\epsilon_{Sr} = +500$, Sr = 180 ppm, $\epsilon_{Nd} = -22$, and Nd = 30 ppm; for the Fry Creek mixing line, M1 - $\epsilon_{Sr} = +20$, Sr = 1500 ppm, $\epsilon_{Nd} = -5.0$, and Nd = 60 ppm; and for the Bug-Hor mixing line, M1 - $\epsilon_{Sr} = +20$, Sr = 600 ppm, $\epsilon_{Nd} = -3.0$, and Nd = 60 ppm.

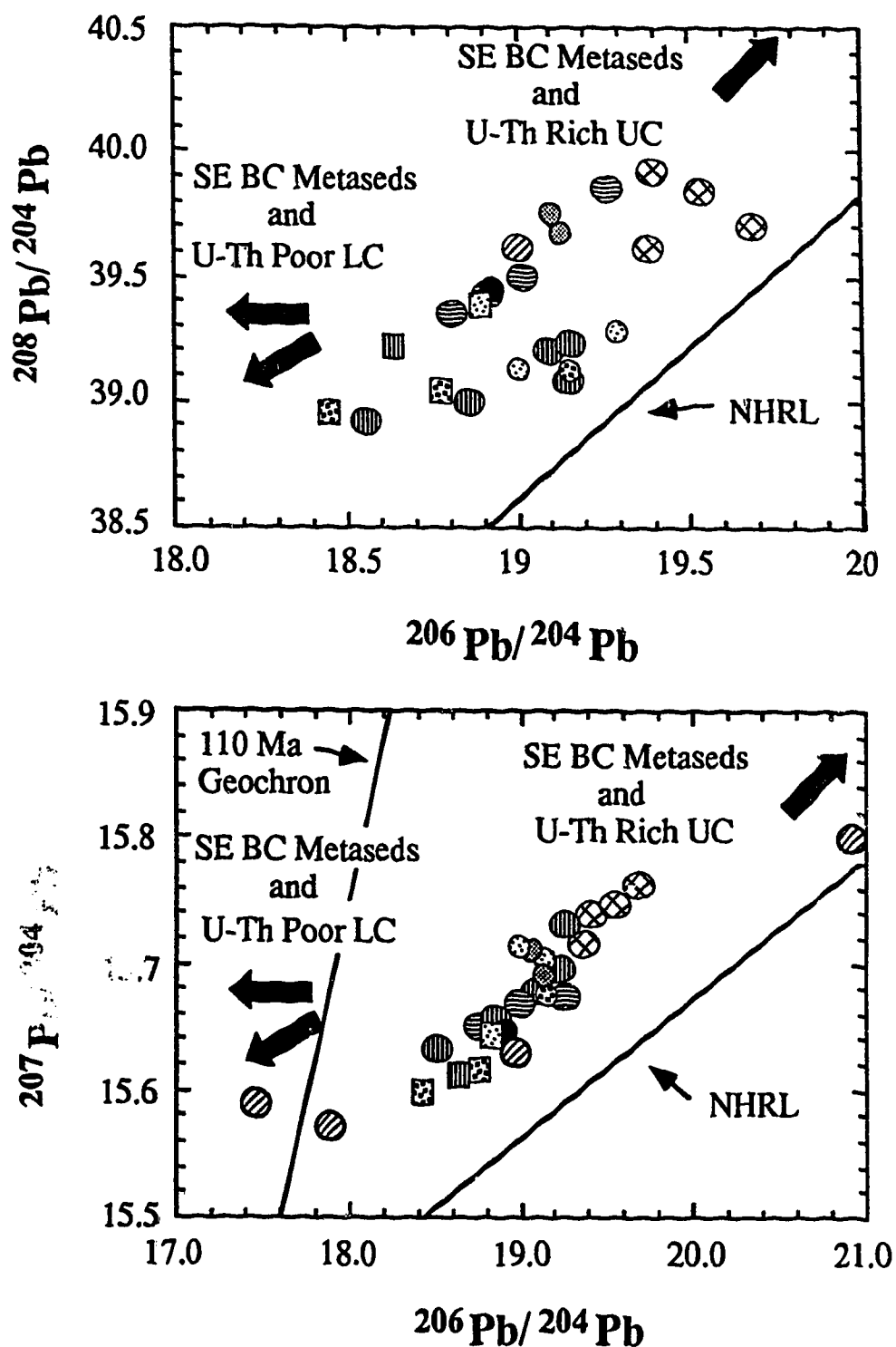


Figure 3.7. Initial $^{206}\text{Pb}/^{204}\text{Pb}$ versus $^{208}\text{Pb}/^{204}\text{Pb}$ and $^{207}\text{Pb}/^{204}\text{Pb}$ for the BFH samples (this study) and SEBC metasediments (from Ghosh 1986), with patterns and symbols as in Figure 3.6. LC and UC are for lower and upper crust, respectively. The northern hemisphere regression lines (NHRL) are the oceanic basalt array for the northern hemisphere from Hart (1984).

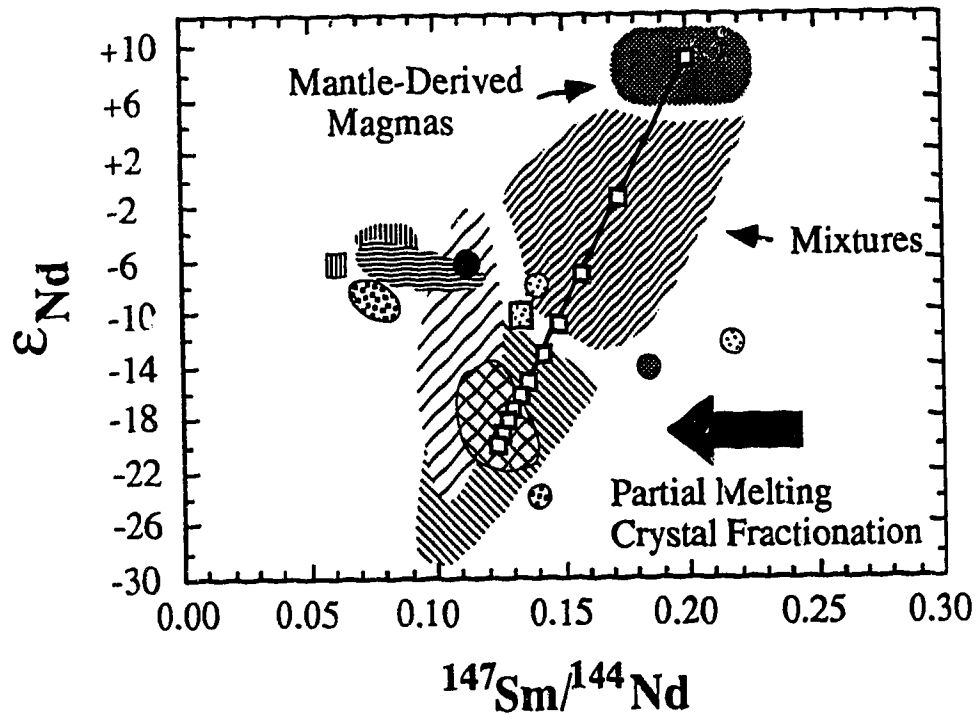


Figure 3.8. $^{147}\text{Sm}/^{144}\text{Nd}$ versus ϵNd (after DePaolo 1981b) for the BFH samples (this study) and SEBC basement rocks (from Ghosh and Lambert 1989, Frost and O'Nions 1984, and Lambert and Chamberlain 1990) with patterns and symbols as in Figure 3.6. A mixing line between mantle-derived magmas with $\epsilon\text{Nd} = +9$, $^{147}\text{Sm}/^{144}\text{Nd} = 0.2$, and Nd = 10 ppm, and crust with $\epsilon\text{Nd} = -20$, $^{147}\text{Sm}/^{144}\text{Nd} = 0.125$, and Nd = 50 ppm is illustrated with open boxes representing 10% increments for the mix. Partial melting of crust, and crystal fractionation within the granite system generally increases the Sm/Nd ratio and moves melt compositions toward the left in this diagram.

Appendix 3.1

Sample locales, rock types, and estimated modal proportions (%) of mineralogy.

Sample	Latitude	Longitude	Type	Pl	Ksp	Qtz	Bt	All	Ep	Ms	Acs
Bugaboo											
Bug-1a	50°44'10"N	116°46'55"W	BtGr	35	29	28	5		X	X	X
Bug-1b	"	"	Apl	31	38	31	X			X	
Bug-2	50°44'30"N	116°45'30"W	BtGr	30	38	28	4	X		X	X
Bug-6	50°44'10"N	116°46'55"W	BtGr	32	34	30	4	X	X	X	X
Bug-7	"	"	Apl	28	40	32	X			X	
Bug-8	"	"	MXen	6	20	22	30		4	18	X
Bug-10	50°44'30"N	116°46'54"W	BtGr	22	39	33	6	X	X		X
Bug-11	"	"	Apl	27	40	33	X			X	
Bug-12	50°45'45"N	116°46'10"W	BtGr	33	33	28	5	X			X
Bug-13	50°45'05"N	116°46'12"W	BtGr	30	35	29	6	X	X	X	X
Fry Creek											
Fry-1	50°04'35"N	116°47'30"W	2MGr	38	28	30	X			4	
Fry-2	50°04'25"N	116°47'50"W	2MGr	34	30	31	X			5	
Fry-3	50°04'10"N	116°48'35"W	2MGr	33	31	29				6	
Fry-4	50°03'47"N	116°49'25"W	Apl	29	33	32				6	
Fry-5	50°03'30"N	116°50'30"W	2MGr	32	31	30	X			7	
Fry-6	50°03'05"N	116°51'50"W	2MGr	28	34	31	2			6	X
Fry-7	50°03'47"N	116°49'25"W	TmPg	10	45	36	Gnt	Tm		3	
							2	4			
Fry-8	50°05'04"N	116°27'50"W	BtGr	36	34	25	3	2		X	X
Fry-9	49°59'23"N	116°35'35"W	BtPg	31	37	29	3				X
Fry-10	"	"	BtGr	38	24	30	6	1		X	1
Horsethief Creek											
8641A	50°48'45"N	116°27'30"W	BtGr	37	30	26	5	X		2	X
8641B	"	"	BtGr								
Hor-1	50°48'45"N	116°27'30"W	BtGr	27	36	30	7	X		X	
Hor-2	"	"	Apl	28	40	32				X	
Hor-3	50°37'43"N	116°29'50"W	BtGr	23	35	30	8	3	1	X	X
Hor-4	"	"	Apl	26	36	33				1	
Hor-6	"	"	DXen	65		8	22	X	X	3	X
Hor-7	"	"	BtGr	30	33	28	9		X	X	X
Hor-8	50°38'15"N	116°31'35"W	BtGr	28	36	30	6			X	X

The Accessory phases (Acs) are zircon, apatite, and magnetite. Sphenc was always found in the rocks with allanite (All). Abbreviations: BtGr - biotite granite; 2MGr - two-mica granite; Apl - aplite; TmPg - tourmaline pegmatite; BtPg - biotite pegmatite; MXen - metapelite xenolith; DXen - quartz diorite xenolith; Pl - plagioclase; Ksp - alkali feldspar; Qtz - quartz; Bt - biotite; Ep - epidote; Ms - muscovite; Gnt - garnet; Tm - tourmaline. X denotes present in 1% or less.

Appendix 3.2

Chemical and mass spectrometric procedures for isotopic analysis.

Samples for isotope analysis were dissolved in a 10:1 solution of concentrated HF and HNO₃, followed by decomposition in concentrated HNO₃, and finally by 6M HCl. Sr and Nd were purified using cation exchange procedures. Sr and rare earth elements (REE) were separated from Rb, Ba, and Ca in a 15X1 centimeter column with Dowex AG 50W-X8 cation exchange resin using 2.5M and 6M HCl elutions. Sr was further purified in successive elutions in a scaled down version of the first cation column. Nd was separated from other REE by eluting 0.25M HCl in a column with HDEHP (Bis (2-ethylhexyl) hydrogen phosphate) absorbed on teflon powder, a method modified from Smith et al. (1990). Pb was purified by using 0.7M HBr in an anion exchange column and collected in 6N HCl or ultrapure water. The procedural blanks were 1 ng for Sr and Nd. Two separate blanks were analyzed for the Pb using HBr with 6N HCl. These blanks were 1070 and 800 pg. Blanks for Pb extracted in water were 250 pg. In both cases, at least 10 µgm of Pb was loaded onto the column so that the blanks were negligible.

Samples for Sr isotope analysis were loaded in pure H₂O onto Re or Ta side filaments and were ionized by Re center filaments. ⁸⁷Sr/⁸⁶Sr ratios during the runs were corrected for fractionation using ⁸⁶Sr/⁸⁸Sr equal to 0.1194. Individual runs on the NBS 987 Sr standard analyzed on the same turrets as the samples in this study by one of us (ADB) are reported in Table 3.2. The average for replicate runs on the NBS 987 standard measured during this study for ⁸⁷Sr/⁸⁶Sr was equal to 0.710249 +/- 44 (2σ). Samples Nd isotope analysis were loaded in pure dilute nitric acid onto Re or Ta side filaments, and the samples were ionized by Re center filaments. ¹⁴³Nd/¹⁴⁴Nd ratios were corrected for fractionation relative to ¹⁴⁶Nd/¹⁴⁴Nd equal to 0.7219. The

average for replicate runs on the LaJolla Nd standard measured during this study for $^{143}\text{Nd}/^{144}\text{Nd}$ was equal to 0.511817 ± 12 (2σ). Individual runs of LaJolla on the same turret as the samples in this study by one of us (ADB) are reported in Table 3.2. Nd isotope ratios were corrected to $^{143}\text{Nd}/^{144}\text{Nd}$ for La Jolla equal to 0.511855.

The samples for Pb isotope analysis were loaded onto Re center filaments in ultrapure H_2O and then treated with silica gel - phosphoric acid mixture. The samples were ionized at a temperature of 1250°C and empirically-derived correction factors for mass fractionation were applied to obtain final results. Analytical uncertainties, based on reproducibility of results on NBS 981 Pb standard by the UA isotope group are 0.05% (2σ) for the ratios cited (Deb et al. 1989). Individual runs on NBS 981 during this study are in Table 3.2. The accepted values for NBS 981 used by the University of Alberta isotope group are 16.9371 for $^{206}\text{Pb}/^{204}\text{Pb}$, 15.4913 for $^{207}\text{Pb}/^{204}\text{Pb}$, and 36.7213 for $^{208}\text{Pb}/^{204}\text{Pb}$. The unweighted average for the NBS 981 values in Table 3.2 are 16.9417, 15.4909, and 36.7263 for the ratios cited.

References

- Allegre, C.J., Hart, S.R., and Minster, J.F., 1983. Chemical structure and evolution of the mantle and continents determined by inversion of Nd and Sr isotopic data. II. Numerical experiments and discussion. *Earth and Planetary Science Letters*, **37**, 191-213.
- Archibald, D.A., Glover, J.K., Price, R.A. Farrar, E., and Carmichael, D.M., 1983. Geochronology and tectonic implications of magmatism and metamorphism, southern Kootenay Arc and neighboring regions, southeastern British Columbia. Part I: Jurassic to Mid-Cretaceous. *Canadian Journal of Earth Sciences*, **20**, 1891-1913.
- Archibald, D.A., Krogh, T.E., Armstrong, R.L., and Farrar, E., 1984. Geochronology and tectonic implications of magmatism and metamorphism, southern Kootenay Arc and neighboring regions, southeastern British Columbia. Part II: Mid-Cretaceous to Eocene. *Canadian Journal of Earth Sciences*, **21**, 567-583.
- Armstrong, R.L., 1988. Mesozoic and Early Cenozoic magmatic evolution of the Canadian Cordillera. *In Processes In Continental Lithospheric Deformation*, Edited by S.P. Clark, B.C. Burchfiel, and J. Suppe. Geological Society of America, Special Paper 218, 55-91.
- Arndt, N.T., Goldstein, S.L., 1987. Use and abuse of crust-formation ages. *Geology*, **15**, 893-895.
- Arth, J.G., Barker, F., and Stern, T.W., 1988. Coast Batholith and Taku plutons near Ketchikan, Alaska: Petrography, geochronology, geochemistry, and isotopic character. *American Journal of Science*, **288A**, 461-489.
- Barker, F., 1990. Two traverses across the Coast batholith, southeastern Alaska. *In The nature and origin of Cordilleran magmatism*, Edited by J.L. Anderson. Geological Society of America, Memoir 174, 395-405.

- Barker, F., Arth, J.G., and Stern, T.W., 1986. Evolution of the Coast batholith along the Skagway Traverse, Alaska and British Columbia. *American Mineralogist*, **71**, 632-643.
- Beard, J.S., and Lofgren, G.E., 1989. Effect of water on the composition of partial melts of greenstone and amphibolite. *Science*, **244**, 195-197.
- Beard, J.S., and Lofgren, G.E., 1991. Dehydration melting and water-saturated melting of basaltic and andesitic greenstones and amphibolites at 1, 3, and 6.9 kbar. *Journal of Petrology*, **32**, 365-401.
- Brandon, A.D., 1989. Constraints on magma genesis behind the Neogene Cascade arc: Evidence from major and trace element variation of high-alumina and tholeiitic volcanics of the Bear Creek area. *Journal of Geophysical Research*, **94**, 7775-7798.
- Brandon, A.D., and Lambert, R.StJ., 1992a. Rb-Sr geochronology of Mesozoic granitoids to the southern Canadian Cordillera. *Canadian Journal of Earth Science*, submitted.
- Brandon, A.D., and Lambert, R.StJ., 1992b. Crustal melting in the Cordilleran interior: The mid-Cretaceous White Creek batholith in the southern Canadian Cordillera. *Journal of Petrology*, submitted.
- Chamberlain, V.E., and Lambert, R.StJ., 1985. Cordillera, a newly defined Canadian microcontinent. *Nature*, **314**, 707-713.
- Chamberlain, V.E., Lambert, R.StJ., and Holland, J.G., 1988. Geochemistry of the gneissic basement complex near Valemount, British Columbia: further evidence for a varied origin. *Canadian Journal of Earth Sciences*, **25**, 1725-1739.
- Coney, P.J., Jones, D.L., and Monger, J.W.H., 1980. Cordilleran suspect terranes. *Nature*, **288**, 329-333.
- Deb M., Thorpe, R.I., Cumming, G.L., and Wagner, P.A., 1989. Age, source, and

- stratigraphic implications of Pb isotopic data for conformable, sediment hosted base metal deposits in the Proterozoic Aravalli-Dehli orogenic belt northwestern India. *Precambrian Research*, 43, 1-22.
- DePaolo, D.J., 1981a. Neodymium isotopes in the Colorado Front Range and the crust-mantle evolution in the Proterozoic. *Nature*, 291, 193-196.
- DePaolo, D.J. 1981b. A neodymium and strontium isotope study of the Mesozoic calc-alkaline granitic batholiths of the Sierra Nevada and Peninsular Ranges, California. *Journal of Geophysical Research*, 86, 10470-10488.
- Frost, C.D., and O'Nions, R.K., 1984. Nd evidence for Proterozoic crustal development in the Belt-Purcell Supergroup. *Nature*, 312, 53-56.
- Ghent, E.D., Nicholls, J. Stout, M.Z., and Rottenfusser, B., 1977. Clinopyroxene amphibolite boudins from Three Valley Gap, British Columbia. *Canadian Mineralogist*, 15, 269-282.
- Ghosh, D.K., 1986. Geochemistry of the Nelson-Rossland area, B.C. Ph.D. Thesis, University of Alberta, Edmonton.
- Ghosh, D.K. and Lambert, R.StJ., 1989. Nd-Sr isotope study of Proterozoic to Triassic sediments from southeastern British Columbia. *Earth and Planetary Science Letters*, 94, 29-44.
- Glover, J.K., 1978. Geology of the Summit Creek map-area, southern Kootenay Arc, British Columbia. Ph.D. Thesis, Queen's University, Kingston, Ontario.
- Gordon, G.E., Randle, K., Goles, G.G., Corliss, J.B., and Beeson, M.H., 1968. Instrumental activation analysis of standard rocks with high-resolution gamma-ray detectors. *Geochimica et Cosmochimica Acta*, 32, 369-396.
- Gromet, L.P., and Silver, L.T., 1983. Rare earth element distributions among minerals in a granodiorite and their petrogenetic implications. *Geochimica et Cosmochimica Acta*, 47, 925-939.

- Hart, S.R., 1984. A large-scale isotope anomaly in the Southern Hemisphere mantle. *Nature*, **309**, 753-757.
- Hooper, P.R., and Johnson, D., 1987. Major and trace element analyses of rocks and minerals by automated X-ray spectrometry. In house report, Department of Geology, Washington State University, Pullman.
- Irving, E., and Archibald, D.A., 1990. Bathozonal tilt corrections to paleomagnetic data from mid-Cretaceous plutonic rocks: Examples from the Omineca Belt, British Columbia. *Journal of Geophysical Research*, **95**, 4579-4585.
- Jacobsen, S.B., and Wasserburg, G.J., 1984. Sm-Nd isotopic evolution of chondrites and achondrites, 2. *Earth and Planetary Science Letters*, **67**, 137-150.
- Lambert, R.StJ., and Chamberlain, V.E., 1988. Cordillera revisited, with a three-dimensional model for Cretaceous tectonics in British Columbia. *Journal of Geology*, **96**, 47-60.
- Lambert, R.StJ., and Chamberlain, V.E., 1990. Isotopic studies on Mesozoic and Tertiary granitoids and their Precambrian basement, BC, Washington, and Idaho. *Proceedings of the 1990 Lithoprobe Cordilleran Workshop*, University of Calgary, 91-98.
- Miller, C.F., and Barton, M.D., 1990. Phanerozoic plutonism in the Cordilleran Interior, USA. *In Plutonism from Antarctica to Alaska, Edited by S.M. Kay and C.W. Rapela*. Geological Society of America, Special Paper 241, 213-231.
- Miller, C.F., and Mittlefehldt, D.W., 1982. Depletion of light rare-earth elements in felsic magmas. *Geology*, **10**, 129-133.
- Miller, C.F., Watson, E.B., and Harrison, T.M., 1988. Perspectives on the source, segregation and transport of granitoid magmas. *Transactions of the*

- Royal Society of Edinburgh , Earth Sciences, 79, 135-156.
- Mittlefehldt, D.W. and Miller, C.F., 1983. Geochemistry of the Sweetwater Wash pluton, California: Implications for "anomalous" trace element behavior during differentiation of felsic magmas. *Geochimica et Cosmochimica Acta*, 47, 109-124.
- Monger, J.W.H., 1977. Upper Paleozoic rocks of the western Canadian Cordillera and their bearing on Cordillera evolution. *Canadian Journal of Earth Sciences*, 14, 1832-1859.
- Monger, J.W.H., and Berg, H.C., 1987. Lithotectonic terranes of Western Canada and Southeastern Alaska. Map MF-1874B, United States Geological Survey, pp. 1-12
- Monger, J.W.H., and Irving, E., 1980. Northward displacement of north-central British Columbia. *Nature*, 285, 289-293.
- Monger, J.W.H., and Price, R.A., 1979. Geodynamic evolution of the Canadian Cordillera - progress and problems. *Canadian Journal of Earth Sciences*, 16, 770-791.
- Monger, J.W.H., Price, R.A., and Templeman-Kluit, D.J. 1982. Tectonic accretion and the origin of the two major metamorphic and plutonic belts in the Canadian Cordillera. *Geology*, 10, 70-75.
- Parrish, R.R., and Wheeler, J.O., 1983. A U-Pb zircon age from the Kuskanax batholith, southeastern British Columbia. *Canadian Journal of Earth Sciences*, 20, 1751-1756.
- Parrish, R.R., Carr, S.D., and Parkinson, D.L., 1988. Eocene extensional tectonics and geochronology of the southern Omineca Belt, British Columbia and Washington. *Tectonics*, 7, 181-212.
- Fatchett, P.J., 1991. Isotope geochemistry and chemical evolution of the mantle and crust. *Reviews of Geophysics*, 29, Supplement, 457-470.

- Patiño Douce, A.E. and Johnston, A.D., 1991. Phase equilibria and melt productivity in the pelitic system: Implications for the origin of peraluminous granitoids and aluminous granulites. *Contributions to Mineralogy and Petrology*, **107**, 202-218.
- Patiño Douce, A.E., Humphreys, E.D., and Johnston, A.D., 1990. Anatexis and metamorphism in tectonically thickened continental crust exemplified by the Sevier hinterland, western North America. *Earth and Planetary Science Letters*, **97**, 290-315.
- Patiño Douce, A.E., Skjerlie, Draper, D.S., and Johnston, A.D., 1991. Partial melting of mixed lithology crustal protoliths: Preliminary experimental results. *Transactions of the American Geophysical Union*, **72**, p.542.
- Pearce, J.A., Harris, N.B.W., and Tindle, A.G., 1984. Trace element discrimination diagrams for the tectonic interpretation of granitic rocks. *Journal of Petrology*, **25**, 956-983.
- Rapp, R.P., and Watson, E.B., 1986. Monazite stability and dissolution kinetics: implications for the thorium and light rare earth chemistry of felsic magmas. *Contributions to Mineralogy and Petrology*, **94**, 304-316.
- Rapp, R.P., Watson, E.B., and Miller, C.F., 1991. Partial melting of amphibolite/eclogite and the origin of Archean trondhjemites and tonalites. *Precambrian Research*, **51**, 1-25.
- Reesor, J.E., 1973. Geology of the Lardeau map-area, east half, British Columbia. Geological Survey of Canada, Memoir 369.
- Rushmer, T., 1991. Partial melting of two amphibolites: Contrasting experimental results under fluid-absent conditions. *Contributions to Mineralogy and Petrology*, **107**, 41-59.
- Rutter, J.M., and Wyllie, P., 1988. Melting of vapour-absent tonalite at 10 kbar to simulate dehydration-melting in the deep crust. *Nature* **331**, 159-160.

- Samson, S.D., Patchett, P.J., McClelland, W.C., and Gehrels, G.E., 1991. Nd and Sr isotopic constraints on the petrogenesis of the west side of the northern Coast Mountains batholith, Alaskan and Canadian Cordillera. *Canadian Journal of Earth Sciences*, 28, 939-946.
- Sevigny, J., 1988. Geochemistry of Late-Proterozoic amphibolites and ultramafic rocks, southeastern Canadian Cordillera. *Canadian Journal of Earth Sciences*, 25, 1323-1337.
- Shand, S.J., 1949. *Eruptive Rocks*. John Wiley and Sons, New York.
- Skjerlie, K.P., and Johnston, A.D., 1992. Vapor-absent melting at 10 kbar of a biotite- and amphibole-bearing tonalitic gneiss: Implications for the generation of A-type granites. *Geology*, 20, 263-266.
- Smith, A.D., Gillis, K.M., and Ludden, J.N., 1990. A Pre-irradiation group separation (PIGS) technique for the analysis of rare-earth elements during Nd-isotopic analysis of geological samples. *Chemical Geology*, 81, 17-22.
- Streckeisen, A.L., 1973. Plutonic rocks: Classification and nomenclature recommended by the IUGS Subcommittee on the Systematics of Igneous Rocks. *Geotimes*, 18, 26-30.
- Thy, P., Beard, J.S., and Lofgren, G.E., 1990. Experimental constraints on the origin of Icelandic rhyolites. *Journal of Geology*, 98, 417-421.
- Umhoefer, P.J., 1987. Northward translation of "Baja British Columbia" along the late Cretaceous to Paleogene margin of western North America. *Tectonics*, 6, 377-394.
- Umhoefer, P.J., Dragovich, J., Cary, J., and Engebretson, D.C., 1989. Refinements of the "Baja British Columbia" plate-tectonic model for northward translation along the margin of western North America. *In Deep Structure and Past Kinematics of Accreted Terranes*, Edited by J.W.

- Hillhouse, Geophysical Monograph 50, American Geophysical Union, 101-112.
- Vielzeuf, D., and Holloway, J.R., 1988. Experimental determination of the fluid-absent melting relations in the pelitic system. *Contributions to Mineralogy and Petrology*, **98**, 257-276.
- Wanless, R.K., Loveridge, W.D., and Mursky, G., 1968a. A geochronological study of the White Creek batholith, southeastern British Columbia. *Canadian Journal of Earth Sciences*, **5**, 375-386.
- Watson, E.B., and Harrison, T.M., 1983. Zircon saturation revisited: Temperature and composition effects in a variety of crustal magma types. *Earth and Planetary Science Letters*, **64**, 295-304.
- Watson, E.B., and Harrison, T.M., 1984. Accessory minerals and the geochemical evolution of crustal magmatic systems: A summary and prospectus of experimental approaches. *Physics of the Earth and Planetary Interiors*, **35**, 19-30.
- Wickham, S.M., 1987. The segregation and emplacement of granitic magmas. *Journal of the Geological Society of London*, **144**, 281-297.
- White, D., Asudeh, I., and Zelt, C., 1992. Crustal thickening beneath the Canadian Eastern Cordillera. *Proceedings of the 1992 Lithoprobe Cordilleran Workshop*, University of Alberta, p.131.
- Wolff, M.B., and Wyllie, P.J., 1991. Dehydration-melting of solid amphibolite at 10 kbar: Textural development, liquid interconnectivity and applications to the segregation of magmas. *Mineralogy and Petrology*, **44**, 151-179.
- Zen, E.A., 1986. Aluminum enrichment in silicate melts by fractional crystallization: Some mineralogic and petrographic constraints. *Journal of Petrology*, **27**, 1095-1117.

Zen, E.A., 1984, and Hammarstrom, J.M., 1984. Magmatic epidote and its petrologic significance. *Geology*, 12, 515-518.

Chapter 4

Crustal Melting in the Cordilleran Interior: The Mid-Cretaceous White Creek Batholith in the Southern Canadian Cordillera

Alan D. Brandon* and Richard StJ. Lambert
Department of Geology, University of Alberta
Edmonton, Alberta CANADA T6G 2E3

* - Present Address:
Department of Earth, Atmospheric,
and Planetary Sciences
Massachusetts Institute of Technology
Cambridge, MA, USA 02139-4307

Submitted to Journal of Petrology (8/25/92)

Introduction

Granitoid magmatism was widespread in western North America during the Mesozoic. Batholiths several hundreds of kilometers long were emplaced along the continental margins and were associated with magmatic arc formation and subduction. These batholiths include the Peninsular Ranges batholith in southern California and in Baja California, Mexico, the Sierra Nevada batholith in California, and the Coast Ranges batholith in British Columbia, the Yukon, and Alaska (Gromet and Silver 1987). These batholiths are composed primarily of low-K₂O granodiorites and tonalites. In petrogenetic models for arc-related granitoids, the contribution of basalt, as parental magma to many of the granitoids, or as a heat source for crustal anatexis, is certain (e.g. DiPaolo 1981a, Gromet and Silver 1987). Much emphasis has been given to the mechanisms producing granitoids in the large, arc-related batholiths on the continental margin to the production of granitoids within the interior regions of the North American continent.

Within the Cordilleran interior, the batholiths have much smaller volumes, and are not directly associated with subduction and arc formation (Miller and Barton 1990). These plutonic rocks range from gabbro to strongly-peraluminous granite, and are dominated by high-K₂O granodiorite and granite. Tonalitic compositions typical of arcs are minor or nonexistent. Mechanisms for producing these granitoid suites, either by crustal anatexis, or through basalt differentiation and crustal contamination, remain unresolved.

Within southeast British Columbia, mid-Cretaceous plutons are exposed in the Omineca Belt, a N-S trending metamorphic and plutonic region which formed as the result of compressional tectonics in the Mesozoic during terrane accretion (Monger and Price 1979, Monger et al. 1982, Lambert and Chamberlain 1988), and extensional tectonics in the Paleocene and Eocene (Armstrong 1982, Parrish et al. 1988). The mid-Cretaceous White Creek batholith (WCB) is one of a set of batholiths which intrudes the lower metamorphic grade margin of the region, east of a high-grade zone. It is a post-kinematic, zoned pluton with concentric rings from quartz monzodiorite on the rim to 2-mica granite in the interior (Reesor 1958), which is similar to the range of lithologies displayed by other calc-alkaline granitoids within the Cordilleran interior. Rb-Sr isotopic data from the WCB show that the different lithologic zones have different initial $^{87}\text{Sr}/^{86}\text{Sr}$ isotopic compositions, and that these zones were not produced by inward fractional crystallization during cooling of the intrusion but had a more complex petrogenetic history (Wanless et al. 1968). The lithologic and geochemical zoning observed within the WCB provides an opportunity to assess the mechanisms for producing granitoid magmatism on the continental side of the western margin of North America during the Mesozoic.

This paper reports major, trace element, and Sr, Nd, Pb, and O isotopic data for the WCB. The distinctions defined by Sr isotopes for the lithologic zones reported by Wanless et al. (1968) are confirmed by corresponding variation in most other chemical parameters. Model calculations favor anatexis of crustal sources for the generation of all WCB granitoids. The geochemical influence of mantle-derived magma on the WCB compositions appears to be minimal. A scenario where a melt zone migrated upwards in the crust beneath the intrusion level of the Cretaceous batholiths, likely as the result of dehydration melting in response to crustal thickening, is preferred to explain the relationship between source rocks for the WCB and the timing of intrusion of the different zones within the batholith. These results for the WCB suggest that intra-crustal melting was the primary mechanism for generating granitoid magmas in the Cordilleran interior during the Mesozoic, likely in response to terrane accretion and collision.

Geology

Figure 4.1 displays the major geological units within southeastern British Columbia. The White Creek batholith is part of a group of mid-Cretaceous plutons that includes the Bugaboo, Fry Creek, and Horsethief Creek, and Battle Range. These batholiths reside east of the suture along which Quesnellia (as part of Terrane I of Monger et al. 1982) and the Paleozoic Kootenay metasediments are joined. The WCB intruded the Late Proterozoic Purcell metasediments, the exposed samples of which are in the biotite zone of a Barrovian series of regional metamorphism (Archibald et al. 1984).

The mid-Cretaceous magmatic episode in southeast British Columbia (SEBC) is constrained by Rb-Sr whole rock-apatite isochron ages of *ca.* 105 to 115 Ma, including 105.9 \pm 1.2 Ma (2σ) on the porphyritic granite lithologic

zone (Fig. 4.2) for the White Creek batholith (Brandon and Lambert 1992a). A Rb/Sr isochron age of 115 Ma was previously obtained on the interior 2-mica granite phase of the WCB (Wanless et al. 1968).

The WCB is post-kinematic with respect to the penetrative deformation observed within the Kootenay and Purcell-Windermere rocks (Reesor 1973). The WCB has discordant biotite and muscovite K-Ar ages (relative to their Rb-Sr whole rock-apatite ages) ranging from ~89 to ~19 Ma (Geological Survey of Canada data compiled by Archibald et al. 1984). These ages have been interpreted by Archibald et al. (1984) to represent resetting during late Cretaceous compression and thrusting along the Purcell thrust (Fig. 4.1), followed by Eocene extension.

Detailed mapping by Reesor (1958) on the WCB documents that it is a zoned intrusion with 5 major lithologic units present (Fig. 4.2). The western rim of the batholith is composed of quartz monzodiorite (QMD; using modal mineral abundances in the classification scheme of Streckeisen 1973). QMD grades into a hornblende-biotite granodiorite (HbBtGd), which grades further into a porphyritic granodiorite-granite (PGd) containing up to 40 modal % microcline phenocrysts (Reesor 1958). PGd has the largest areal exposure, and extends to the northeast beyond the other lithologic zones. The interior of the batholith is composed of a 2-mica granite (2MGr) which has both intrusive and gradational contacts with the other lithologies. A later phase of 2-mica granite-granodiorite intrudes HbBtGd in the northwest corner of the batholith. Pegmatites and aplites are found within all of the units in the WCB and extend into the surrounding country rock (Reesor 1958). On an outcrop scale, the WCB granitoid rocks are generally uniform in texture. However, local textural variations do occur. For instance, large microcline phenocrysts within QMD, HbBtGd, and PGd vary in modal abundance from 10 to 40%, but can

be concentrated to 90% locally (Reesor 1958). Similar lithologic characteristics have been observed within the other Cretaceous batholiths in Figure 4.1, except for the concentric zoning, which is unique to the WCB (Archibald et al. 1983, Brandon and Lambert 1992b).

Planar orientation of platy minerals was observed by Reesor (1958), primarily along contacts between the different lithologies and along the margin of the intrusion in contact with the Purcell country rocks. Abundant, oriented mafic inclusions were observed within the first few meters along the edge of the intrusion within QMD, and sparse oriented mafic inclusions were noted by Reesor (1958) to occur tens of meters inward from the intrusion contact in several locations in the WCB. Contacts of the WCB with the Purcell country rock observed in this study and by Reesor (1958) were sharp.

Archibald et al. (1984) used the mineral assemblages of the contact aureole of the WCB to constrain its emplacement level. The contact aureole has an assemblage containing quartz, muscovite, sillimanite, and staurolite (Reesor 1958) and lies within bathozones 2 and 3 (following Glover 1978), suggesting an emplacement level of 2.3 to 3.8 kbar (7 to 11 km depth) and therefore at upper-crustal levels.

Petrography

Detailed petrographic studies on the WCB were carried out by Reesor (1958) and Wanless et al. (1968). Ranges of modal mineralogical proportions for the different units of the WCB from these studies, and for the samples collected in this study, are listed in Table 4.1. Modal proportions for each sample collected for this study are listed in Appendix 4.1. QMD and HbBtGd have similar minerals, and the textural relationships between these minerals are also similar in both units. Plagioclase (oligoclase-andesine, An₂₅ to An₄₀) is

normal-oscillatory zoned and subhedral, and has no overgrowths indicative of distinct crystallization periods. The alkali feldspar is microcline, and phenocrysts thereof contain abundant perthite as blebs and stringers. Groundmass microcline occurs in both lithologies but is not perthitic. Mafic mineral phases in these lithologies include biotite, hornblende, and epidote. These minerals generally occur in clots between the felsic phases. Both biotite and hornblende are subhedral, and show brown to green pleochroism. Epidote and allanite occur as subhedral to euhedral prismatic crystals. Several epidote crystals were observed as rims on dark brown, euhedral allanite. Biotite was commonly observed enclosing epidote. These features are consistent with a magmatic origin for the epidote, with a change in phase stability from allanite to epidote to biotite during decompression and/or cooling (Zen and Hammarstrom 1984, Dawes and Evans 1991). Accessory phases include subhedral muscovite, subhedral to euhedral sphene, and euhedral apatite, magnetite, and zircon.

The porphyritic granodiorite contains most of the same mineral phases as QMD and HbBtGd, but different proportions of minerals (Table 4.1). The plagioclase in PGd ranges from An₂₃ to An₂₉ (oligoclase). The microcline phenocrysts are larger than in the earlier intrusive phases (ranging to 5 cm), have only minor perthitic stringers, and are poikilitic. The biotite is much browner than in QMD and HbBtGd. Only a few crystals (i.e., ranging to 1 modal %) each of muscovite, allanite, and epidote were observed in all of the sections of PGd studied.

The last intrusive phases are 2-mica granites. Plagioclase in 2MGr has an anorthite content of An₂₀ to An₂₃. This rock type contains microcline of similar textural occurrence as in PGd, subhedral muscovite, and subhedral biotite with red-brown pleochroism. The only accessory phase observed was

zircon, which is found primarily within biotite. Aplite and pegmatite samples collected for this study have similar textural and mineralogical relationships as the 2MGr samples and differ primarily in their grain size, which defines each rock type, and their occurrence as veins and dikes within the WCB.

Petrographic examination of all the major rock types in the WCB showed no obvious examples of textural disequilibrium between mineral phases. The exception to this generalization is the occurrence of epidote as rims around allanite suggesting a reaction relationship between these two minerals.

Analytical Methods

X-ray fluorescence (XRF) data on whole rock powders were obtained from the XRF lab at Washington State University. Details of precision are reported in Hooper and Johnson (1987) and Brandon (1989). The major element analyses are reported on a volatile free basis and normalized to 100%. Instrumental neutron activation analysis (INAA) was performed on whole rock powders at the University of Oregon INAA lab using the methodology of Gordon et al. (1968). Reproducibilities of values for whole rock standards used for INAA are reported in Brandon and Lambert (1992b). Reproducibilities (2σ) for the trace element analyses by INAA are as follows: $\pm 3\%$ - Th, Ta, Sc, Ce, Sm; $\pm 4\%$ - Hf; 5% - La, Eu, Tb, Lu; and $\pm 6\%$ - U, Cr, Co, Nd, and Yb. Major and trace element analyses are reported in Table 4.2, except for U, Th (by INAA) and Pb (by XRF) which are listed in Table 4.4.

Dissolution and chemical separation techniques, and mass spectrometer procedures for whole rock Sr, Nd, and Pb isotope analysis are reported in Trønnes and Brandon (1992) and Brandon and Lambert (1992b). In addition to whole rock analysis, Pb isotope analysis on alkali feldspar separates was carried out for selected samples. The feldspars were first leached in a

concentrated solution of HNO₃ at 200°C. The solution, potentially containing radiogenic Pb owing to post-crystallization addition of U and Th, was discarded. The leached residue was then put through the standard dissolution and chemical separation procedures for Pb reported in Brandon and Lambert (1992b). The Pb isotopic composition of the residue approaches the initial common Pb composition of the magma because there is little or no U and Th in alkali feldspar.

Sr isotopic results were obtained on a VG MM30 single collector mass spectrometer maintained by the Departments of Physics and Geology at the University of Alberta (UA). ⁸⁷Sr/⁸⁶Sr ratios during the runs were corrected for fractionation using ⁸⁶Sr/⁸⁸Sr = 0.1194. ⁸⁷Sr/⁸⁶Sr ratios reported in Table 4.3 are relative to ⁸⁷Sr/⁸⁶Sr = 0.710249 +/- 44 (2σ) for NBS 987. Nd isotope ratios were obtained on a VG 354 5 collector mass spectrometer at UA. ¹⁴³Nd/¹⁴⁴Nd ratios were corrected for fractionation relative to ¹⁴⁶Nd/¹⁴⁴Nd = 0.7219. Replicate runs for the LaJolla Nd standard gave ¹⁴³Nd/¹⁴⁴Nd = 0.511817 +/- 12 (2σ). ¹⁴³Nd/¹⁴⁴Nd ratios in Table 4.3 were normalized relative to ¹⁴³Nd/¹⁴⁴Nd = 0.511853, which matches the accepted value for the LaJolla Nd standard when analyzed at LaJolla (Carlson, 1980). Age corrected ⁸⁷Sr/⁸⁶Sr and ¹⁴³Nd/¹⁴⁴Nd ratios are reported using ε notation (DePaolo, 1988). 2σ errors at 106 Ma for ε_{Sr} are +/-11.84 for the sample with the highest Rb/Sr (WC-9) and +/-0.74 for the sample with the lowest Rb/Sr (WC-2) and typical for most of the White Creek samples. 2σ errors at 106 Ma for ε_{Nd} are typically equal to +/-0.29. These uncertainties in ε were calculated using 2σ errors for Rb/Sr, Sm/Nd, and for the measured ratios of the Sr and Nd isotopic standards. Pb isotope ratios were obtained on the VG Micromass 30 mass spectrometer, and are reproducible to 0.05% (2σ). The accepted values for NBS 981 used by the University of Alberta

isotope group are $^{206}\text{Pb}/^{204}\text{Pb} = 16.9371$, $^{207}\text{Pb}/^{204}\text{Pb} = 15.4913$, and $^{208}\text{Pb}/^{204}\text{Pb} = 36.7213$.

Oxygen isotopic compositions were determined for whole rock powders and quartz separates (Table 4.5). Oxygen was purified and extracted using the standard BrF_5 technique of Clayton and Mayeda (1963). The oxygen isotopic compositions were obtained using a gas emission mass spectrometer at the University of Alberta (Rob King, analyst). The ratios are reported as units of per mil (‰) deviation from SMOW which correspond to the δ notation listed in Table 4.5. Replicate analyses of standards indicate reproducibility of ± 0.2 ‰ (2σ) on $\delta^{18}\text{O}$, and replicate analyses listed in Table 4.5 fall within this range. The $\delta^{18}\text{O}$ value used for the NBS-28 quartz standard was 9.6 during the course of this study.

Results

Major and trace element geochemistry

Major element compositions of the WCB samples are listed in Table 4.2. The SiO_2 content ranges from ~61 wt.% for QMD samples to a maximum of ~78 wt.% in the 2MGr samples. Major element abundances plotted against SiO_2 are shown in Figure 4.3. There is a definite clustering for each rock type into distinct fields, which indicates a correlation between rock type and composition, and location within each zone of the intrusion. A general systematic decrease in all elements except K_2O is observed with increasing SiO_2 towards the interior of the batholith, and these chemical relationships confirm the systematic variation observed lithologically and petrographically by Reesor (1958) and in this study. When the averages of QMD, HbBtGd, PGd, and 2MGr (in order to average out sampling bias) are fitted to regression lines, correlation coefficients of greater than 0.9 are achieved for all elements

versus SiO_2 except for K_2O and Na_2O . The correlation coefficients for K_2O and Na_2O may be lower because of a feldspar control on these elements; variable modal alkali feldspar and plagioclase (in particular microcline phenocrysts) in these samples would produce such scatter and low correlation. Alternatively, the lower correlations may arise because these two elements show much less variation against SiO_2 than do the other six major elements, or because linear variation may not be applicable. In the latter case, crystallization of new phases results in changes in the slopes of the curves in Harker plots, during cooling and differentiation by a single magma. This scenario cannot be evaluated on the basis of whole rock major element analyses alone, and will be considered further below.

The alumina saturation index (ASI; molecular ratio of $\text{Al}_2\text{O}_3/(\text{K}_2\text{O} + \text{Na}_2\text{O} + \text{CaO})$ where CaO is corrected for apatite following Shand 1949, and Zen 1986) varies from ~0.98 in QMD and HbBtGd, to 1.023-1.13 in PGd, to 1.13 to 1.28 in 2MGr (Table 4.3) reflecting a change from metaluminous, to weakly peraluminous, to strongly peraluminous compositions with increasing SiO_2 towards the center of the batholith. Coupled with these changes in ASI, AKN (molar $\text{Al}_2\text{O}_3/(\text{K}_2\text{O} + \text{Na}_2\text{O})$) decreases from about 1.55 in QMD to 1.1 to 1.3 in the SiO_2 -rich samples, and the Fe ratio (wt.% $\text{FeO}/(\text{FeO} + \text{MgO})$), changes from ~0.65 in QMD to as much as 1.0 in the SiO_2 -rich samples. Although a notable scatter occurs for samples from each zone, these variations across the lithologic zones are consistent with early fractionation of biotite, hornblende, and epidote during differentiation of granodioritic to granitic melts (Zen 1986) as shown in Figure 4.4 for ASI vs. AKN. As will be discussed below, however, isotopic data for the WCB are inconsistent with fractionation of these minerals from a single magma to explain the observed compositional zoning.

Trace element analyses for the WCB are listed in Table 4.2. In Figure 4.5, Ba, Sr, Rb, Nb, Zr, Y, and Ce are plotted versus SiO₂. With increasing SiO₂ content, Ba, Sr, Nb, Zr, Y, and Ce all decrease, while Rb increases in abundance. When the averages of each lithologic unit are taken for each trace element, the calculated regression lines yield correlation coefficients better than 0.9, except for Nb which has a correlation coefficient versus SiO₂ of slightly less than 0.9 (Fig. 4.5). Therefore, a majority of both major elements, and trace elements representing several chemical groups, all have strong correlations with SiO₂, and with the different lithological zones in the WCB when the bulk or average compositions are used.

Chondrite-normalized rare earth element plots for WCB samples are shown in Figure 4.6. All of the patterns show strong light rare earth element (LREE) enrichment, with a general flattening out in the heavy rare earth elements (HREEs). Most of the samples have a negative Eu anomaly, and Eu/Eu* ranges from a minimum of 0.19 in one of the 2MGr samples to a maximum of 0.97 in one of the pegmatites (Table 4.2). The moderate Eu/Eu* ratios of around 0.8 in the QMD and HbBtGd rocks are inconsistent with fractional crystallization from basalt parents where plagioclase was a fractionating phase. Fractionation of basaltic melts dominated by plagioclase, pyroxene, and olivine in the lower to middle crust, would produce more-silicic magmas with very large negative Eu anomalies develop (Cullers and Graf 1984). When the fractionation from basalt includes hornblende in the assemblage, large negative Eu anomalies would also develop unless more than 50% of the fractionating assemblage is hornblende (Gromet and Silver 1987). In the latter case, the HREE have concave-up patterns which are not seen in the QMD and HbBtGd rocks of the WCB. The Ce/Yb ratios are, for the most part, higher in QMD, HbBtGd, and PGd, relative to 2MGr, aplites, and pegmatites (Table 4.2).

Ce/Yb does not correlate strongly with SiO₂, or with Eu/Eu* (Fig. 4.7A), suggesting that these two ratios are controlled by independent mechanisms. A strong correlation of Eu and Sr (Fig. 4.7B) and SiO₂ and Eu, suggests that Eu/Eu* is controlled by Sr and Eu⁺² compatible phases, i.e., primarily plagioclase in calc-alkaline magmas. Enrichment in LREE is controlled by a different process, and will be evaluated further below.

Isotope geochemistry

Table 4.3 lists Rb-Sr and Sm-Nd isotopic data for the White Creek batholith. A wide range in both initial ϵ_{Sr} and ϵ_{Nd} (corrected to 105.9 Ma) is observed and correlated with rock type. Samples from QMD and HbBtGd have ϵ_{Sr} from +32.1 to +37.9 and ϵ_{Nd} from -5.4 to -6.2. PGd, including a pegmatite collected within this unit (WC-9), has higher ϵ_{Sr} from +70.8 to 83.9, and lower ϵ_{Nd} , from -9.1 to -10.9, than does QMD and HbBtGd. The interior 2MGr and all of the aplites analyzed for isotopes show another jump to higher ϵ_{Sr} and lower ϵ_{Nd} , and show a greater range of ϵ values than do the outer lithologic units of the WCB. ϵ_{Sr} for these rock types ranges from +174 to +436, and ϵ_{Nd} ranges from -12.1 to -16.0. Coupled with these initial isotopic ratio jumps inward through the lithologic zones are jumps in $^{87}\text{Rb}/^{86}\text{Sr}$ and $^{147}\text{Sm}/^{144}\text{Nd}$. $^{87}\text{Rb}/^{86}\text{Sr}$ increases systematically from low values in QMD-HbBtGd to moderate values in PGd (except WC-9), to higher values in 2MGr and the aplites. Although not as distinct, the 3 isotopic groupings observable in Table 4.3 are also weakly confirmed in the $^{147}\text{Sm}/^{144}\text{Nd}$ ratios. QMD and HbBtGd overlap and have an average $^{147}\text{Sm}/^{144}\text{Nd}$ of 0.083, and PGd has a slightly lower average of 0.080, but is essentially the same as in the outer 2 lithologic zones. The 2MGr and aplites have higher and overlapping $^{147}\text{Sm}/^{144}\text{Nd}$ ratios with an average of 0.103, which is distinct from those of the outer zones.

Depleted mantle model ages for Nd (following the depleted mantle growth curve of DePaolo 1981b) also show distinct jumps within the lithologic zones. QMD and HbBtGd have T_{DM} from 910 to 960 Ma, PGd from 1070 to 1150 Ma, and the 2MGr have T_{DM} from 1475 to 1530 Ma. The change of T_{DM} from Late Proterozoic ages in the outer lithologic zones to Middle Proterozoic in the inner 2MGr zone correlates well with the changes in Rb-Sr and other Sm-Nd isotopic changes within the WCB. Because Sm/Nd ratios mostly decrease during post-extraction differentiation, these model ages represent minimum ages for the source material. Also, a juvenile mantle component mixed with older crustal material could produce the isotopic changes observed from the more mafic and isotopically primitive-younger T_{DM} zones, to the more silicic and isotopically evolved-older T_{DM} zones of the batholith. However, given all of the assumptions built into the model age concept (see Arndt and Goldstein 1987, Patchett 1991, DePaolo et al. 1992) these ages can only be evaluated on a strictly qualitative basis, and other petrological and geochemical parameters need to be considered to understand these isotopic changes within the WCB.

Figure 4.8 displays $\epsilon_{Sr}-\epsilon_{Nd}$ relations for the WCB, Proterozoic metasediments from SEBC (Ghosh and Lambert 1989), and Precambrian basement gneisses exposed in SEBC and northern Idaho (Lambert and Chamberlain 1990). The distinct jumps in ϵ_{Sr} and ϵ_{Nd} from the outer lithologic zones to the inner 2MGr zone are readily observable. All of the WCB samples plot entirely within the range of ϵ_{Sr} and ϵ_{Nd} for the Precambrian crustal rocks.

The observed changes in Rb-Sr and Sm-Nd isotopic abundances between lithologic zones in the WCB are also evident in the initial ratios of Pb isotopes for whole rock and leached alkali feldspar residues shown in Table 4.4. The initial ratios of $^{206}Pb/^{204}Pb$, $^{207}Pb/^{204}Pb$, and $^{208}Pb/^{204}Pb$ all increase

toward the inner zones of the batholith (Fig. 4.9). The alkali feldspar data show less within-zone variation than do the whole rock data, which probably reflect larger uncertainties resulting from: 1) inhomogeneity for U, Th, and Pb in the aliquants of the powders used for analyses by XRF, INAA, and mass spectrometry; 2) U, Th, and Pb loss and addition during a post-crystallization hydrothermal stage in the batholith; or 3) because these ratios were corrected to initial values using U and Th abundances (by INAA) and Pb abundances (by XRF). 2σ uncertainties are $\pm 7.8\%$ and $\pm 5.8\%$ for the U/Pb and Th/Pb ratios, respectively. Age corrected ratios using these uncertainties and those for the reproducibility of $^{206}\text{Pb}/^{204}\text{Pb}$, $^{207}\text{Pb}/^{204}\text{Pb}$, and $^{208}\text{Pb}/^{204}\text{Pb}$ for the measured present-day ratios on the mass spectrometer ($\pm 0.05\%$) yield uncertainties in the corrected ratios of up to $\pm 0.30\%$, 0.067% , and 0.31% for the age corrected ratios respectively, and suggests the latter case produces the observed scatter. The first two cases cannot be ruled out within the constraints of this study. However, it is apparent that the alkali feldspar Pb isotope data more accurately represent the initial Pb isotopic compositions than do the whole rock data. Note that the Pb isotopic abundances in the alkali feldspar show distinct jumps in composition, as opposed to the transitional changes in the whole rock Pb isotope data (Fig. 4.9). Regression lines fitted to the feldspar Pb isotopic compositions in Figure 4.9 yield correlation coefficients of 0.963 and 0.978 in $^{207}\text{Pb}/^{204}\text{Pb}$ and $^{208}\text{Pb}/^{204}\text{Pb}$ versus $^{206}\text{Pb}/^{204}\text{Pb}$, respectively. These strong correlations are consistent with a linear control of the Pb isotopes of the WCB, as when secondary Pb isochrons are produced by rocks derived from a source with Pb homogenized at a given time but with variable $^{238}\text{U}/^{204}\text{Pb}$. Alternatively, simple, 2 end-member mixing can produce these linear patterns.

The initial Pb isotope data for the WCB plot in arrays which are parallel to the available Pb isotopic data for SEBC Proterozoic metasediments (Fig. 4.9). No Pb isotopic data are available for the Precambrian basement gneisses, and their relationship to the WCB and Proterozoic metasediments in Pb isotopic space is therefore uncertain.

Figure 4.10 shows $^{207}\text{Pb}/^{204}\text{Pb}$ versus ϵ_{Nd} for the WCB. The distinct isotopic compositions of the lithologic zones for Pb correlate with those for ϵ_{Nd} (and thus for ϵ_{Sr}). A regression line using the feldspar Pb ratios with their respective whole rock ϵ_{Nd} yields a correlation coefficient of 0.943 (Fig. 4.10).

Oxygen isotopic data for whole rock and quartz separates are listed in Table 4.5. The $\delta^{18}\text{O}$ values for whole rocks are +7.1 in QMD, and range from +6.8 to +8.2 in HbBtGd, from +8.0 to +8.5 in PGd, and from +9.1 to +10.3 in 2MGr. $\delta^{18}\text{O}$ -quartz ranges from +10.1 to +10.3 in QMD, HbBtGd and PGd, and is higher in 2MGr with values ranging from +10.3 to +11.2. In general, quartz is enriched in $\delta^{18}\text{O}$ relative to the melt it is crystallizing from, and results in a fractionation $\delta^{18}\text{O}$ between quartz and melt of < 1.5 ‰ (Garlick 1966, Taylor 1968, Taylor and Sheppard 1986). Late-stage hydrothermal fluids may change the $\delta^{18}\text{O}$ of crystallized magmas, so that whole rock values may not represent the $\delta^{18}\text{O}$ of the original magma in such cases. The $\delta^{18}\text{O}$ of quartz is less affected by such processes (Taylor and Sheppard 1986). The consistency in $\delta^{18}\text{O}$ -quartz and the relative scatter of $\delta^{18}\text{O}$ for the whole rocks (Table 4.5) is consistent with post-crystallization alteration having affected the whole rock samples analyzed, even though every attempt was made to take only fresh samples. Mildly altered feldspars observed in some of the rocks are consistent with such alteration. Alternatively, because the feldspar + biotite : quartz ratio changes from ~4 in QMD to < 2 in 2MGr (Table 4.1, Appendix 4.1) during closed system re-equilibration of the different phases in the batholith, the

quartz in QMD undergoes a larger increase in $\delta^{18}\text{O}$ values than does the quartz in 2MGr (Gilletti 1986, Jenkin et al. 1991). This in turn results in larger differences between whole rock and quartz $\delta^{18}\text{O}$ values in QMD. Magaritz and Taylor (1986) have used an extrapolation technique to estimate the whole rock $\delta^{18}\text{O}$ on altered samples by using $\delta^{18}\text{O}$ of feldspar and quartz for granitoids in southern British Columbia, including the Nelson batholith in Figure 4.1. For all of the granitoid rocks studied, their estimate of whole rock $\delta^{18}\text{O}$ was 0 to 2 ‰ less than the respective $\delta^{18}\text{O}$ -quartz for the same samples. In most cases, their estimate was 1 ‰ or less than the whole rock. If granitoids in the WCB have been altered by late stage fluids as is the case for most of the Mesozoic granitoids in southern British Columbia studied by Magaritz and Taylor (1986), then an average 1 ‰ fractionation between quartz and whole rock would result in QMD, HbBtGd, and PGd rocks all having similar $\delta^{18}\text{O}$ values, ranging from +9.0 to +9.3, which are higher than the observed values (Fig. 4.11). The 2MGr rocks would have whole rock $\delta^{18}\text{O}$ values from +9.3 to +10.2. Two of the measured whole rock $\delta^{18}\text{O}$ values for the 2MGr samples fall within this range while one sample has a slightly lesser value of +9.1. Without further analyses of WCB minerals for oxygen and deuterium, it cannot be determined whether the $\delta^{18}\text{O}$ values for the WCB have been affected by late stage fluids.

A weak correlation between $\delta^{18}\text{O}$ and Sr, Nd, and Pb also occurs within the samples analyzed from the WCB. With an increasing ϵ_{Sr} from +32 in QMD to up to +350 in 2MGr, the whole rock $\delta^{18}\text{O}$ values increase from +6.8 to +10.3 using the measured values, and from +9.0 to as high as 10.2 using an inferred 1 ‰ fractionation between quartz and whole, respectively (Fig. 4.11)

In summary, the major, trace element, and isotopic compositions of the lithologic zones within the WCB show systematic changes and confirm those inferences made from petrography and the observed lithologies by Reesor

(1958) and in this study. In the next section, possible processes which result in such variation will be evaluated.

Constraints on WCB source materials

Isotopic constraints

The primarily gradational contacts observed between QMD, HbBtGd, PGd, and in part 2MGr suggest that the units were emplaced together or before earlier intrusions had completely crystallized. Reesor (1958) notes the significance of a "roughly systematic and gradational changes" in petrographic and lithologic features from the exterior QMD to the interior 2MGr, and argues that this evidence is consistent for cooling from a single magma, not the result of multiple intrusion of magmas from different sources. Rb-Sr isotopic ages also suggest similar emplacement times; The PGd age of 105.9 +/- 0.6 (Brandon and Lambert 1992a), the 2MGr age of 115 Ma (Wanless et al. 1968), and the QMD and HbBtGd Rb-Sr isotopic compositions conform to a 105.9 Ma reference (Brandon and Lambert 1992a), supports this view. However, the changing isotopic compositions (Figs. 4.8 and 4.9) do not support a scenario of a single magma cooling towards the interior. At least 3 pulses of isotopically and chemically distinct magma were present. The clustering observed within the Harker variation diagrams (Figs. 4.3 and 4.5) is consistent with this view.

The Sr-Nd-Pb isotopic relations shown in Figures 4.8-4.10 are consistent with the WCB granitoids being derived wholly from crustal lithologies. Mixing lines between mantle-derived melts and crustal rocks could also produce the observed trends in the isotopic diagrams. If a mantle component (i.e. basalt) was parental to granitoids in the WCB, it would be at positive ϵ_{Nd} and negative ϵ_{Sr} and would lie within the field for the oceanic mantle array in $\epsilon_{Nd}-\epsilon_{Sr}$

space, and have a Pb isotopic composition approaching the lower end of the NHRL in Figure 4.9. The lower whole rock $\delta^{18}\text{O}$ for the more basic lithologies relative to more felsic lithologies in the WCB is also consistent with a contribution of a mantle-derived magma, if these $\delta^{18}\text{O}$ values are interpreted as magmatic.

In order to constrain the possible contribution of a mantle component in the WCB, assimilation and fractional crystallization (AFC) and mixing calculations were carried out using O and Sr isotopes and Sr abundances using the equations of Taylor (1980) and DePaolo (1981c). AFC and mixing calculations using these chemical parameters produce realistic constraints on possible petrogenetic scenarios because O and Sr isotopic compositions of potential mantle and crust end-members can be determined, and the Sr bulk distribution coefficient is controlled by one mineral phase during differentiation from mafic to intermediate compositions - plagioclase. In calc-alkaline melts, the amount of plagioclase in the fractionating assemblage can be predicted by the pressure, temperature and compositional parameters used. The amount of plagioclase removed during AFC was constrained following model calculations for producing andesite from basalt by assimilation of rhyolite (Table 8, column 2, Brandon 1989), using thermodynamically derived solution models to predict mineral phases in equilibrium with magma compositions (using the program SILMIN, Ghiorso 1985).

The results are shown in Figure 4.12. Both AFC and mixing using mantle-derived basalt and 2MGr as end-members (representing 100% crustal melt) can produce the observed trends in $\delta^{18}\text{O}$ versus ϵ_{Sr} in the WCB (Fig. 4.12). The O-Sr isotopic composition of QMD can be produced by a 60-40 mix of basalt and 2MGr, respectively. Alternatively, mixing between basalt and a high Sr-low ϵ_{Sr} granite similar to those observed in the adjacent mid-Cretaceous Fry

Creek batholith (samples Fry 8 and Fry 10 of Brandon and Lambert 1992b) can also produce QMD by a 50-50 mix of these two components. Using high Sr-low ϵ_{Sr} granite and basalt with an R of 3 (R is the ratio of the mass crystallized to mass assimilated) in the AFC calculations can reduce the amount of crust required to about 20%, but 70% of the basalt must be removed as cumulate. All of these calculations assume that measured whole rock $\delta^{18}O$ values for the WCB represent magmatic O compositions. If a 1 ‰ fractionation between quartz and host magma to WCB lithologies is assumed, then the amount of crust mixed with basalt will be higher, and the amount of basalt crystallized during AFC will also be higher.

Figure 4.12 also shows AFC and mixing relations for $1/Sr$ versus ϵ_{Sr} . The calculations show that AFC and mixing with 2MGr and basalt end-members cannot produce the compositions of QMD/HbBtGd. High-Sr and low- ϵ_{Sr} granite must be used to produce QMD/HbBtGd by AFC and mixing with a basalt, and require the same amounts of the crust end-member and basalt cumulates as in the $\delta^{18}O$ - ϵ_{Sr} calculations. Mixing between QMD/HbBtGd and 2MGr can produce intermediate values close to those of PGd compositions for both $\delta^{18}O$ and $1/Sr$ versus ϵ_{Sr} (Fig. 4.12).

The relations in Figure 4.12 show that there are at least two possible ways to generate the observed isotopic variations in the WCB with well-constrained end-member components. Using a mantle-derived basalt requires a minimum of 3 end-members mixed together in two stages; basalt mixed with high Sr-low ϵ_{Sr} granite to produce QMD/HbBtGd that in turn mixes with 2MGr melts to produce the range of isotopic compositions in the WCB. This model requires large amounts of crustal melts for the case of simple mixing with basalt, and therefore large sums of excess heat to melt the crust. In AFC, large amounts of mafic cumulates (providing latent heat of crystallization), and

hence large amounts of basalt are required to produce batholith size bodies of the most isotopically primitive granitoids observed in the WCB. As there are no primitive mafic igneous rocks in spatial and temporal association with this batholith, it is unlikely that mantle-derived basalt was an important source contribution to the WCB, unless the lower to middle crust behaved as a very effective density filter, and all of the basalt and intermediate magmas remained at deep levels. Also, if the $\delta^{18}\text{O}$ compositions of the WCB are altered, as most of the granitoids analyzed by Magaritz and Taylor (1986) from southern British Columbia are, then the actual magmatic compositions approach +9 ‰, and having one mixing end-member as a mantle component is even less likely. Furthermore, the range of $\delta^{18}\text{O}$ for the nearest Precambrian basement mafic gneisses in SE British Columbia is from +4.8 to +5.3 ‰ while more silicic gneisses have $\delta^{18}\text{O}$ as much as +10.1 ‰ (Chamberlain 1983). If these $\delta^{18}\text{O}$ compositions are representative of the basement gneisses during the mid-Cretaceous, then the range of $\delta^{18}\text{O}$ in the WCB quartz monzodiorites and granodiorites can simply be explained by partial melting of these basement rocks, as is the case for Sr, Nd, and Pb isotopes. Such inferences are supported by trace elements and phase equilibrium constraints as discussed in the next section.

Mixing between melts representative of QMD/HbBtGd and 2MGr can produce the majority of chemical variation. This variation could be produced by mixing melts derived from two different crustal reservoirs, which would both be Precambrian in age according to Nd and Sr isotopic compositions and Nd model ages of the WCB lithologies. Further tests are required to constrain the possible basement lithologies in SE British Columbia that may have been sources for the WCB granitoids.

Trace element and phase equilibrium constraints on crustal melting

Figures 4.13 and 4.14 illustrate calculations using REE to test whether different Precambrian basement lithologies exposed in SE British Columbia can produce melt compositions similar to granitoid rocks within the WCB. The batch partial melting equation of Shaw (1970) was used for the calculations and the degree of melting (F) ranged from 0.3 to 0.5 in all but one case. This range for F approximates the critical melt fraction needed for granitic melts to separate from their source regions and into discrete magma bodies (ca. 30-40%, Wickham 1987). Partition coefficients (Kds) used for the calculations are reported in Appendix 4.2.

Peraluminous granitic melts have been produced experimentally by fluid-absent melting of pelitic rocks by the breakdown of biotite and muscovite leaving a residue containing garnet (Vielzeuf and Holloway 1988, and Patiño Douce and Johnston 1991). Petrologic, trace element, and isotopic evidence are consistent with the derivation of late-Cretaceous peraluminous two-mica granites exposed in the Monashee Mountains just north of Figure 4.1, derived from metapelites exposed in SE British Columbia (Sevigny et al. 1989). Proterozoic metapelites from SE BC have Sr, Nd, and Pb isotopic compositions at 106 Ma similar to the WCB 2MGr samples (Figs. 4.9 and 4.10). The WCB 2MGr samples were used as melt compositions for calculating model REE patterns for their sources assuming a residual mineralogy produced by pelite melting.

Successful models in the pelite melting calculations required a residual mineralogy including 0.1% monazite, 10 to 12% garnet, and 50% total feldspar to match the REE patterns and abundances of plausible source pelites in Figure 4.13A (Pelite Source 2 and 3). High Kds for LREE in monazite are the primary control of these elements in peraluminous granitic melts (Miller and Mittlefehldt 1982, Mittlefehldt and Miller 1983, Rapp and Watson 1986).

Calculations using no residual accessory phases (Pelite Source 1) require a pelitic source for the WCB 2MGr much lower in LREE abundances than those samples shown (Figs. 4.13A and 4.13B). High Kds for HREE in garnet control these elements in the patterns. The amount of monazite and garnet predicted as residue by these calculations fall within the range for those of a metapelite considered as residue from partial melting by Sevigny et al. (1989). 30% plagioclase and 20% alkali feldspar was necessary in the pelite residue to match the Eu abundances of SE BC pelites (Pelite Source 3, Fig. 4.13A). This represents a slightly higher amount of plagioclase (1.36 times), and a 4 times higher amount of alkali feldspar than observed in the Sevigny et al. (1989) residual metapelite, and is only a minimum amount for alkali feldspar, as a high Kd was used for Eu (9.06, Appendix 4.2, versus 5.83 by Sevigny et al. 1989). This high-feldspar residue result from the negative Eu anomalies in the 2MGr patterns (Eu/Eu^* from 0.19 to 0.75, Table 4.2). The Sr content of peraluminous granite melts are lowered by fractional crystallization of feldspars because of their high Kds for Sr (e.g. the models of Sevigny et al. 1989). The correlation of Sr and Eu in the WCB granitoids (Fig. 4.7B) are consistent with a feldspar control for both elements within the source and during fractionation. It is plausible that fractional crystallization of feldspar could have enhanced the negative Eu anomalies in the 2MGr melts which in turn would reduce the amount of feldspar required in the pelite residue. In either case, the REE profiles in WCB 2MGr samples can be generated by melting models of Proterozoic pelitic rocks in SE British Columbia. The similar Sr, Nd, and Pb isotopic compositions for the Proterozoic metapelites and the 2MGr samples corroborates this source to melt relationship for these rocks.

The most fertile crustal lithologies that produce intermediate to felsic magmas in equilibrium with hornblende and biotite are quartzofeldspathic

rocks containing hydrous phases, such as amphibolites and tonalites (Clemens and Vielzeuf 1987, Miller et al. 1988). Amphibolite melting has been investigated experimentally most recently by Beard and Lofgren (1989, 1991), Rapp et al. (1991), Rushmer (1991), and Wolff and Wyllie (1991). Under-vapor absent conditions and lower crustal pressures, liquids with SiO₂ contents from <60 to 77 wt.% can be generated by partial melting of amphibolite at ~900 - 1000 °C, leaving garnet and amphibole in the residue (Rapp et al. 1991, Beard and Lofgren 1991). The major element abundances of the QMD and granodiorite samples fall within the range for those of the experimental melts generated in these studies except for K₂O contents of the WCB rocks, which are at least 2 times greater (Fig. 4.15). The starting materials in the amphibolite melting experiments (Table 4.6) were low in K₂O (<1 wt.%), and produced tonalitic melts. Table 4.6 compares major element compositions of mafic basement lithologies within SE British Columbia with starting materials used by Beard and Lofgren (1991) and Rapp et al. (1991). Late Proterozoic amphibolites from the Monashee Mountains (Sevigny, 1988) completely overlap with amphibolites used in the experiments except for higher TiO₂ and slightly lower Na₂O. All the other amphibolites (not shown) reported by Sevigny (1988) have generally lower TiO₂ and higher Na₂O similar to those used in the experiments. Archean to Early Proterozoic mafic gneisses from the Malton gneiss complex in the Valemount area of SE British Columbia (about 100 km north of Fig. 4.1) also have major element abundances generally falling within the range of those amphibolites used in the experiments, except for K₂O which is 3 to 6 times higher in the gneisses. These gneisses are composed of oligoclase, hornblende, green biotite and quartz (in decreasing abundance), with accessory sphene, apatite, garnet, and epidote (Chamberlain 1983), and this mineralogy is generally equivalent to the mineralogy of the starting

materials for amphibolite melting reported by Beard and Lofgren (1991), except for the latter having no biotite and garnet. These gneisses have experienced amphibolite metamorphism with retrograde greenschist metamorphism (Chamberlain 1983). The higher K₂O contents in the mafic gneisses relative to the Beard and Lofgren (1991) amphibolites is probably contained in biotite. The effect biotite would have on melt compositions has not been investigated when melting amphibolite. Biotite begins to disappear early during dehydration melting of tonalite (875°C, 10 kbar, Skjerlie and Johnston 1992). If biotite melts early in more mafic material, a higher K₂O content would be expected than in the melts produced by Beard and Lofgren (1991) and Rapp et al. (1991). In addition, experimental data for melting of mafic compositions producing dacitic to rhyolitic melts indicate that the K₂O content of these melts is dependent upon the K₂O content of the source material (Thy et al. 1990). Given these constraints, melting of Malton mafic gneisses may be a plausible mechanism to produce WCB quartz-monzodiorites and granodiorites.

Partial melting producing QMD and HbBtGd melt compositions leaving residues of mafic granulite, amphibolite, and gabbro residues require source REE compositions similar to both Late Proterozoic amphibolites and Malton mafic gneisses (Figs. 4.13C and 4.13D). The Ce/Sm and Ce/Yb ratios of these source rocks are most similar to those required by melting producing amphibolite residues (Fig. 4.14). The Ce/Sm ratios for a source leaving a granulite residue are higher than required, but 10% garnet was used in this calculation. A smaller amount of garnet residue (ca. 2%), or a change in K_ds used for garnet, reduce the Ce/Sm ratios required for the source for a model leaving a granulite residue, and would not affect the amphibolite residue calculations. Therefore, the accessory (<1%) amounts of garnet found within the Malton mafic gneisses would not have an affect on the REE patterns and

ratios if left in the residue. Furthermore, garnet in granulite residues was only observed at pressures of 16 kbar or greater during amphibolite melting experiments of Rapp et al. (1991). Granulite residues lacking garnet were generated by Beard and Lofgren (1991) at temperatures $> 900^{\circ}\text{C}$ and 6.9 kbar, and also predict no garnet control during melting at mid- to lower-crustal pressures. Consequently, models of amphibolite melting, producing granulite or amphibolite residues may both be consistent with the REE abundances and patterns for Malton mafic gneisses. A similar case may be made for the Late Proterozoic amphibolites, but their low K_2O contents preclude them as a primary source for the granitoids. Also, these amphibolites occur as sporadic, tens of meter size boudins within associated metasediments (Ghent et al. 1977), and their volume may not be large enough to yield batholith-sized granitoid melts.

Tonalite, containing hornblende, biotite, and epidote at crustal pressures produces granodiorite liquids by dehydration melting (Rutter and Wyllie 1988, Skjerlie and Johnston 1992). During melting of a tonalitic gneiss at 10 kbar and 950 to 975 $^{\circ}\text{C}$, biotite and amphibole break down to produce felsic melts with plagioclase, quartz, garnet, orthopyroxene, titanomagnetite, and +/- biotite residues (Skjerlie and Johnston 1992). The WCB porphyritic granodiorites at ~70 wt.% SiO_2 have major element compositions similar to granodioritic melts produced by Skjerlie and Johnston (1992) as shown in Figure 4.15 for Al_2O_3 , FeO^* , and K_2O . Archean to Early Proterozoic tonalitic gneisses compose a major portion of the lithologies found within the Malton gneiss complex (Chamberlain et al. 1988). In Table 4.6, the tonalite gneiss used by Skjerlie and Johnston (SJ, 1992) and averages for tonalitic grey gneiss and felsic gneisses from the Malton gneiss compare well. The only significant discrepancy between the SJ tonalite gneiss and the Malton gneiss is for K_2O ,

which is about 2 times higher in the Malton gneisses. The mineralogy of the SJ tonalite gneiss consists of biotite, plagioclase, and quartz, with minor and trace quantities of amphibole, epidote, apatite, and zircon. The Malton grey gneisses have similar mineralogy with the addition of microcline (Chamberlain 1983), presumably reflected in the higher K₂O contents of these gneisses. As discussed above, the K₂O content of melt compositions is proportional to the K₂O content in the source rock, and partial melting of Malton gneiss would probably produce melts higher in K₂O than the SJ tonalite gneiss.

REE model calculations for tonalite melting were carried out approximating the phase and melt proportions produced in the experiments of Skjerlie and Johnston (1992), and assuming that melts similar to average PGd were produced. The results in Figures 4.13E and 4.13F show that tonalite sources similar to tonalite gneisses from the Malton gneiss complex can produce melts with REE contents similar to PGd rocks from the WCB.

Discussion

Evolution of the White Creek magmatic system

Isotopic, REE modelling, along with phase equilibrium considerations demonstrate that all of the WCB granitoids may be produced by melting of several crustal lithologies found within the Precambrian basement complexes in SE British Columbia. In addition, Eu/Eu* ratios (as discussed above), and Cr and Ni abundances for QMD and HbBtGd are hard to reconcile by fractionation from basaltic parents, and add credence to a crustal melting hypothesis to generate the WCB. The QMD and HbBtGd rocks have overlapping isotopic compositions. QMD rocks are probably cumulates from this granodiorite magma. The extremely low Cr (16.7 ppm) and Ni (11 ppm) contents for these

rocks similar to their contents in HbBtGd (Table 4.2) suggest that they were derived from a magma already devoid in these elements (such as a granodiorite liquid), and are unlikely to represent an evolved liquid derived from a more mafic parent. Cr contents for granitoids from arc-related batholiths are much greater. For instance, the Peninsular Ranges batholith have average Cr contents of 69 to 74 ppm for quartz diorites and tonalites with similar SiO₂ contents (61 to 65 wt.%) to QMD and HbBtGd rocks from the WCB (Table 4.2, Silver and Chappell 1988).

Field relations show that the compositions of melts intruded within the White Creek magma chamber changed from the metaluminous, less felsic QMD/HbBtGd, to weakly peraluminous PGd, to more felsic, strongly peraluminous 2-mica granites (Fig. 4.2). These lithologic zones within the WCB probably represent 3 pulses of magma.

The origin of apparently linear variation on Harker plots for the WCB samples may be the result of several processes; restite unmixing, mixing within the magma chamber, mixing of melts below the intrusion level, or an artifact of melting processes occurring within the source region(s) and hence coincidental to linear variation. Linear variation in Harker plots has been attributed to variable mixtures of melt and its residue after melting (White and Chappell 1977, Wyborn and Chappell 1986, Chappell et al. 1987). The WCB chemical variation is not likely the result of this process because of the difference in isotopic compositions of the likely residue-rich compositions (QMD/HbBtGd) and the melt-rich compositions (2MGr), and the lack of petrographic evidence for non-magmatic, residual assemblages within the WCB such as reversely zoned plagioclase, highly corroded mineral phases, and high pressure, high temperature, and anhydrous minerals such as

clinopyroxene, orthopyroxene, garnet, sillimanite, etc. (Wall et al. 1987, Clemens 1989), none of which are found in the WCB.

Mixing of end-member melts within the magma chamber and between the intrusion level and the source region are also unlikely because of the 3 distinct jumps in isotopic compositions and correlative major and trace element jumps which are delineated within the boundaries of the lithologic zones of the WCB (Figs. 4.3-4.10.). Binary mixing of melts should produce smooth chemical trends without gaps and jumps. Rather, the WCB chemical variation appears to represent at least 3 distinct pulses of magma. These distinct jumps in melt compositions most likely reflect different physical and chemical conditions for melting in the lower to middle crust.

A model for crustal melting

The spatial relationships between source rocks for the WCB granitoids can constrain the physical models for crustal melting in the mid-Cretaceous in SE British Columbia. As discussed in the preceding sections, the most likely source materials for QMD and the granodiorite units are mafic and tonalitic gneisses comprising the majority of lithologies of the Precambrian gneissic basement complexes exposed in SE British Columbia. The favorable source for the strongly peraluminous granites are Mid to Late Proterozoic metapelites of the Purcell and Windermere Supergroups that directly overlie basement gneisses (Chamberlain et al. 1988).

These source stratigraphic relationships combined with the spatial arrangement of granitoids within the WCB (Fig. 4.2), suggest that melt generation proceeded upward through the crustal column. Two different mechanisms can lead to an increasing progression in temperature and resultant melting upwards. Underplating of basaltic magma at the Moho and

intrusion of basalt into the lower crust have been advocated for supplying heat for crustal anatexis (Fountain 1989, Bergantz 1989, Hyndman and Foster 1988). These mechanisms would result in heat transfer from the mantle to the lower crust promoting melting. Migration of melts upwards would result in heating of crust above the initial melting regions, and ultimately lead to melting at higher levels. The importance of basaltic magma providing a heat source for crustal anatexis has been demonstrated in tectonic settings where large amounts of mafic magmas are observed such as volcanic arcs (Hyndman and Foster 1988) and extensional terranes (Fountain 1989, Bergantz 1989). The absence of mafic igneous rocks in the early to mid-Cretaceous within the Omineca Belt, is not in accordance with this mechanism inducing crustal anatexis in the Cretaceous in SE British Columbia, unless the lower crust acted as a density filter for basaltic magmas, and the latter are thus not exposed at higher levels.

Crustal thickening could also produce anatexis moving upwards within the crust. In crustal thickening models, dehydration melting of fertile lithologies generate large degrees of melting and mobile magmas by 10 to 40 m.y. after maximum thickening (Zen 1988, Patiño Douce et al. 1990). In most instances, crustal thickening induced anatexis results in post-kinematic granites, as is the case for the WCB and related mid-Cretaceous granitoids (Reesor 1973). Crustal thickening occurred by thrusting within the Sevier Belt of the Cordilleran interior in the United States during the mid- to late-Cretaceous including the southern Omineca Belt (Coney and Harms 1984, Parrish et al. 1988). A belt of granitoid magmatism from 110 to 60 Ma in age occurs through Arizona, Nevada, Idaho, and extending into the southern Omineca Belt and in part may be the result of anatexis associated with the thrusting in the Sevier hinterland (Patiño Douce et al. 1990). Maximum crustal

thicknesses during this orogeny were on the order of 60 km. Thickened crust with a minimum Eocene age has been identified seismically within the southern Omineca Belt (White et al. 1992). Crustal thickening, which induced an upward progression of melting, is favored as a mechanism producing the compositional and spatial variation preserved in the WCB. An added complication to this scenario is the high temperatures required for hornblende melting in the source for the WCB hornblende-bearing lithologies. The crustal thickening models of Patiño Douce et al. (1990) reach temperatures in the lower crust high enough to generate biotite dehydration melting, but not the higher temperatures of hornblende dehydration melting (850 to 920°C at 10 kbar, Clemens and Vielzeuf 1987, Wolff and Wyllie 1991). A hotter crust, either by an initial higher geotherm from higher heat production within the SEBC crust, previous thermal preconditioning, or by contemporaneous basaltic underplating is required. None of these conditions can be ruled out or favored within the present understanding of the events which affected the crust in SEBC. Brandon et al. (1992) favor thermal preconditioning by basaltic underplating which was most likely associated with volcanic arc formation in the Middle Jurassic in SEBC. Intrusion of up to several km thick basaltic sills into the lower crust can raise the ambient temperatures up to 300°C, depending on the cooling rates of the magma (Lambert 1983).

The apparent mixing lines in the chemical variation diagrams reflect the various proportions of different source materials contributing to the WCB magmas. The Malton mafic and tonalitic gneisses show complex layering and crosscutting relationships (Chamberlain 1983, Chamberlain et al. 1988, McDonough and Parrish 1991). Melting in these source rocks would result in geochemical signatures reflecting the mixed lithologies present, which is

consistent with the chemical variation observed in the quartz monzodiorites and granodiorites from the WCB. As the crust thickened and the overlying pelites were raised above their solidus temperatures, they would contribute melts, and if homogenization occurred within the melt zones and before emplacement into the magma chamber, these melts would be intermediate between the early melts and the final melts produced primarily by pelite melting. These final melts, the 2MGr units within the WCB, would be the last to intrude and reflect melting after the mafic and tonalitic gneiss source region had been exhausted of fertile components. Mixed lithology melting is only beginning to be investigated experimentally (Patiño Douce et al., 1991), but the model presented here suggests that such melting is a more realistic condition in the lithologically diverse terranes that exist on the continents.

Conclusions

The lithologic and chemical characteristics of the White Creek batholith constrain the process of crustal melting during the mid-Cretaceous in the southern Canadian Cordillera. Variation in trace element abundances and Sr., Nd, Pb, and O isotopes are most easily reconciled by derivation of the WCB granitoids through crustal anatexis. The change from early quartz monzodiorite and hornblende-biotite granodiorite, followed by intermediate porphyritic granodiorite and finally strongly peraluminous two-mica granites in the WCB can be modeled successfully as melting of mafic and tonalitic gneiss followed by melting of overlying metapelites. A migrating melt zone proceeded upward in the crust most likely in response to continued crustal thickening, with possibly an additional heat source via basaltic underplating, either from earlier magmatic events in SEBC, or contemporaneous to mid-Cretaceous magmatism. These inferences are consistent with evidence for

Cretaceous compressional tectonics resulting from terrane accretion along the western continental margin of British Columbia.

Acknowledgements. This research was supported from NSERC operating and Lithoprobe grants to R.StJ. Lambert (1988-1991). Reviews from Gordon Goles, Rob Creaser, Tom Chacko, Jonathan Patchett, George Cumming, and Bob Luth greatly improved this paper. We thank Gordon Goles for allowing one of us (ADB) to use his INAA facilities.

Table 4.1. Modal mineralogical proportions (%) of the main lithologic zones of the White Creek batholith (Fig. 4.2), including samples studied by Reesor (1958), Wanless et al. (1968), and in this study.

Mineral	Quartz Monzodiorite	HbBt Granodiorite	Porphyritic Granodiorite	2 Mica Granite
Plagioclase	35 - 46	40 - 45	36 - 40	25 - 36
Microcline	15 - 17	15	15 - 21	20 - 32
Quartz	13 - 19	20 - 28	20 - 28	30 - 36
Biotite	15 - 20	15 - 18	12 - 16	0 - 4
Hornblende	2 - 6	0 - 7	<1	
Muscovite	0 - 2	0 - 2	<1	1 - 10
Epidote	2 - 4	0 - 1	<1	
Accessories*	~2	~2	1 - 2	~1

*Accessories include magnetite, sphene, zircon, and apatite.

Table 4.2. Major and trace element abundances of the White Creek batholith.

Sample Type	WC-1 PGd	WC-2 PGd	WC-4 2MGr	WC-5 Aplite	WC-6 Aplite	WC-7 PGd	WC-8 2MGr	WC-9 Peg	WC-11 PGd
SiO ₂	67.73	70.16	77.71	76.36	74.00	69.74	74.77	75.10	70.27
TiO ₂	0.597	0.440	0.080	0.067	0.116	0.472	0.178	0.036	0.512
Al ₂ O ₃	15.29	15.29	13.64	13.97	14.54	15.54	14.47	14.34	14.82
FeO*	3.38	2.48	0.26	0.28	0.78	2.70	1.18	0.23	2.96
MnO	0.076	0.053	0.018	0.013	0.029	0.070	0.043	0.013	0.069
MgO	1.66	0.98	0.02	0.02	0.23	1.10	0.24	0.00	1.19
CaO	3.06	2.70	0.31	0.61	0.98	2.39	0.96	0.44	2.66
Na ₂ O	3.48	3.59	3.40	3.96	3.49	3.70	3.21	3.62	3.48
K ₂ O	4.30	4.06	4.43	4.64	5.77	4.02	4.82	5.96	3.72
P ₂ O ₅	0.423	0.236	0.127	0.070	0.074	0.260	0.118	0.251	0.326
TTL	100.00	99.99	100.00	99.99	100.01	99.99	99.99	99.99	100.01
ASI	1.023	1.043	1.281	1.119	1.069	1.097	1.209	1.137	1.072
AKN	1.473	1.484	1.313	1.211	1.212	1.489	1.378	1.156	1.520
FeRatio	0.671	0.717	0.929	0.933	0.772	0.711	0.831	1.000	0.713
XRF									
Ni	17	15	14	13	15	18	13	12	16
Rb	200	184	410	333	294	234	324	532	210
Sr	705	570	52	128	168	543	89	103	517
Ba	1277	1049	173	211	403	1296	237	225	886
Y	22	16	15	12	21	21	20	10	24
Zr	217	190	48	41	56	188	73	30	208
Nb	67.1	46.9	37.6	30.6	29.8	53.9	42.3	46.6	58.2
Ce	130	111	27	26	38	125	47	29	132
INAA									
Hf		5.58	1.66	1.22	2.21		2.57	1.37	5.83
Ta		2.95	5.81	5.05	3.87		3.87	11.74	3.81
Cr		14.4	10.0	BD	BD		BD	BD	17.9
Co		5.13	BD	BD	BD		BD	BD	6.1
Sc		5.91	1.55	2.59	2.15		3.01	0.58	7.1
La		65.2	10.28	5.55	15.45		28.72	1.12	70.8
Ce		122.6	21.07	13.49	33.8		61.7	2.58	136.0
Nd		51.2	8.81	6.1	16.0		26.4	1.54	52.2
Sm		6.27	1.59	0.94	2.88		4.13	0.48	7.47
Eu		1.49	0.24	0.29	0.62		0.54	0.15	1.42
Tb		0.46	0.11	0.21	0.40		0.38	0.07	0.69
Yb		1.16	1.02	1.14	1.60		1.49	0.43	1.93
Lu		0.228	0.155	0.204	0.295		0.254	0.084	0.345
Ce/Yb		105.7	20.66	11.83	21.13		41.41	6.06	70.47
Eu/Eu*		0.822	0.750	0.848	0.667		0.434	0.968	0.636

Sample Type	WC-13 PGd	WC-14 PGd	WC-15 PGd	WC-16 Peg	WC-17 HbBtGd	WC-18 HbBtGd	WC-19 QMD	WC-20 QMD	WC-20 Rpt
SiO ₂	69.08	68.82	61.75	68.22	64.48	64.60	61.05	61.62	61.57
TiO ₂	0.528	0.398	0.865	0.160	0.721	0.716	0.846	0.663	0.662
Al ₂ O ₃	15.47	16.20	18.07	17.39	16.30	16.10	16.89	18.02	18.07
FeO*	2.96	2.13	5.21	0.87	3.88	4.02	5.38	4.20	4.08
MnO	0.061	0.056	0.100	0.022	0.078	0.080	0.108	0.089	0.088
MgO	1.25	0.93	2.01	0.21	2.10	2.22	2.63	2.06	2.09
CaO	2.71	2.01	3.81	0.89	4.05	3.88	4.41	4.21	4.20
Na ₂ O	3.47	3.09	4.58	2.84	3.86	3.56	3.79	4.27	4.39
K ₂ O	4.17	6.16	3.16	9.33	4.00	4.32	4.22	4.42	4.41
P ₂ O ₅	0.307	0.203	0.446	0.067	0.546	0.497	0.667	0.448	0.447
TTL	100.01	100.00	100.00	100.00	100.01	100.00	99.99	100.00	100.01
ASI	1.072	1.085	1.073	1.071	0.973	0.981	0.980	0.975	
AKN	1.513	1.378	1.649	1.177	1.526	1.528	1.563	1.516	
FeRatio	0.703	0.696	0.722	0.806	0.649	0.644	0.671	0.666	
XRF									
Ni	15	13	17	13	17	18	11	14	13
Rb	199	268	229	280	154	141	142	128	124
Sr	604	607	625	674	948	957	1225	1456	1448
Ba	1215	2159	556	3180	1621	1903	2490	3058	3082
Y	21	17	33	12	20	25	28	21	21
Zr	206	168	332	96	245	224	304	210	207
Nb	57.7	46.2	91.3	22.6	63.3	63.2	66.7	54.8	56.7
Ce	116	53	374	30	130	142	172	113	124
INAA									
Hf		4.75	11.16		5.41	4.91	8.11		
Ta		3.35	6.04		3.80	4.17	3.27		
Cr		13.1	32.3		24.0	28.1	16.7		
Co		4.25	10.2		9.8	9.7	12.38		
Sc		5.02	11.43		8.54	8.95	10.68		
La		37.7	234.1		77.8	78.4	109.9		
Ce		73.3	427.0		144.2	149.6	198.9		
Nd		30.7	148.0		60.8	62.3	74.2		
Sm		4.26	18.32		7.85	8.33	10.26		
Eu		1.19	2.42		1.88	1.91	2.47		
Tb		0.44	0.96		0.78	0.56	0.76		
Yb		1.25	2.66		1.57	1.96	2.36		
Lu		0.212	0.482		0.293	0.321	0.383		
Ce/Yb		58.64	160.53		91.85	76.40	84.28		
Eu/Eu*		0.919	0.475		0.791	0.802	0.832		

Sample Type	WC-21 HbBtGd	WC-22 Aplite	WC-23 PGd	WC-24 Aplite	WC-25 Aplite	WC-26 2MGr	WC-27 Aplite	WC-28 PGd	WC-28 Rpt
SiO ₂	66.90	73.48	70.22	76.04	73.87	74.32	74.38	70.25	70.16
TiO ₂	0.634	0.286	0.489	0.055	0.212	0.087	0.102	0.426	0.422
Al ₂ O ₃	15.12	13.90	15.23	14.43	15.05	14.96	14.60	15.12	15.20
FeO*	3.74	1.48	2.84	0.34	1.27	0.51	0.77	2.55	2.54
MnO	0.074	0.024	0.057	0.012	0.048	0.030	0.028	0.054	0.054
MgO	1.90	0.48	1.19	0.04	0.29	0.10	0.10	1.00	1.07
CaO	3.49	1.74	2.30	0.40	1.23	0.88	1.11	2.35	2.37
Na ₂ O	3.36	3.19	3.43	3.72	3.33	3.82	3.95	3.53	3.47
K ₂ O	4.32	5.21	3.95	4.85	4.58	5.19	4.87	4.48	4.47
P ₂ O ₅	0.460	0.214	0.281	0.105	0.130	0.107	0.092	0.245	0.245
TTL	100.00	100.00	99.99	99.99	100.01	100.00	100.00	100.01	100.00
ASI	0.978	1.026	1.133	1.269	1.217	1.130	1.076	1.059	
AKN	1.482	1.276	1.535	1.325	1.442	1.257	1.240	1.430	
FeRatio	0.663	0.755	0.705	0.895	0.814	0.836	0.885	0.711	
XRF									
Ni	16	13	15	14	16	15	14	16	16
Rb	154	149	224	308	425	398	253	206	206
Sr	801	656	505	86	91	96	131	565	564
Ba	1425	1504	1052	191	393	305	277	1111	1131
Y	19	9	19	14	14	15	22	16	16
Zr	196	131	191	36	103	56	61	182	181
Nb	60.7	31.0	54.7	26.4	26.4	22.3	27.2	49.3	49.3
Ce	124	111	101	22	78	55	38	109	108
INAA									
Hf	4.93		5.24	1.16	3.52	1.80		4.40	
Ta	3.71		3.71	5.35	4.59	3.97		2.94	
Cr	21.7		16.3	BD	BD	BD		14.3	
Co	8.78		5.75	BD	BD	BD		5.12	
Sc	8.28		6.43	1.83	2.75	1.19		5.20	
La	66.5		60.4	7.13	42.6	18.76		69.7	
Ce	122.6		112.7	15.19	84.9	36.9		122.0	
Nd	47.4		45.9	6.1	36.9	15.74		47.5	
Sm	6.92		6.09	1.27	5.58	2.54		6.13	
Eu	1.59		1.31	0.31	0.64	0.17		1.29	
Tb	0.59		0.48	0.18	0.30	0.51		0.46	
Yb	1.37		1.49	1.15	0.63	1.09		1.36	
Lu	0.276		0.280	0.174	0.119	0.156		0.234	
Ce/Yb	89.49		75.64	13.21	135.41	33.85		89.71	
Eu/Eu*	0.777		0.738	0.760	0.469	0.192		0.726	

Major element analyses are normalized on a volatile-free basis. All Fe expressed as Fe⁺² (FeO*). Ni, Rb, Sr, Ba, Y, Zr, Nb, and Ce were analyzed by XRF, and Hf, Ta, Cr, Co, Sc, La, Ce, Nd, Sm, Eu, Tb, Yb, and Lu were analyzed by INAA, and are in parts per million (ppm). Repeat analyses are designated Rpt.

Table 4.3. Rb-Sr and Sm-Nd isotopic relations for the White Creek batholith.

Type	Sample	Rb	Sr	$^{87}\text{Rb}/^{86}\text{Sr}$	$^{86}\text{Sr}/^{87}\text{Sr}_0$	$^{86}\text{Sr}/^{87}\text{Sr}_T$	ϵ_{SrT}
PGd	WC-2	184	570	0.935	0.711534(14)	0.71013	+77.7
2MGr	WC-4	410	52	22.93	0.756882(0)	0.72237	+251
Aplite	WC-5	333	128	7.545	0.728260(62)	0.71691	+174
Aplite	WC-6	294	168	5.078	0.734517(66)	0.72688	+315
2MGr	WC-8	324	89	10.58	0.745207(59)	0.72920	+350
Peg	WC-9	532	103	14.99	0.732756(39)	0.71019	+77.7
PGd	WC-11	210	517	1.178	0.711852(18)	0.71098	+78.7
PGd	WC-14	268	607	1.278	0.712032(17)	0.71031	+77.4
PGd	WC-15	229	625	1.061	0.711903(52)	0.71031	+80.2
HbBtGd	WC-17	154	948	0.470	0.707899(34)	0.70729	+36.0
HbBtGd	WC-18	141	957	0.426	0.707966(56)	0.70732	+37.9
QMD	WC-19	142	1225	0.335	0.707417(36)	0.70691	+32.1
HbBtGd	WC-21	154	801	0.555	0.708037(26)	0.70720	+36.2
PGd	WC-23	224	505	1.284	0.712495(18)	0.71056	+53.9
Aplite	WC-24	308	86	10.41	0.747189(32)	0.73153	+381
Aplite	WC-25	425	91	13.58	0.755838(48)	0.73540	+436
2MGr	WC-26	398	96	12.04	0.74716(70)	0.72940	+346
PGd	WC-28	206	565	1.035	0.711230(84)	0.70964	+70.8
		206	564				

Sample	Sm	Nd	$^{147}\text{Sm}/^{144}\text{Nd}$	$^{143}\text{Nd}/^{144}\text{Nd}_0$	$^{143}\text{Nd}/^{144}\text{Nd}_T$	ϵ_{Nd_T}	TDM
WC-2	6.27	51.2	0.0741	0.512060(11)	0.512009	-9.6	1085
WC-4	1.59	8.81	0.1092	0.511936(11)	0.511860	-12.5	1588
WC-5	0.94	6.1	0.0932	0.511947(8)	0.511882	-12.1	1379
WC-6	2.88	16.0	0.1089	0.511902(21)	0.511827	-13.2	1630
WC-8	4.13	26.4	0.0946	0.511881(11)	0.511815	-13.4	1473
WC-9	0.48	1.54	0.1886	0.512072(25)	0.511941	-10.9	4697
WC-11	7.47	52.2	0.0866	0.512094(7)	0.512034	-9.1	1148
WC-14	4.26	30.7	0.0839	0.512096(5)	0.512038	-9.1	1123
WC-15	18.32	148.0	0.0749	0.512072(7)	0.512020	-9.4	1079
WC-17	7.85	60.8	0.0781	0.512236(8)	0.512182	-6.2	930
WC-18	8.33	62.3	0.0809	0.512270(6)	0.512216	-5.6	910
				0.512278(15)			
WC-19	10.26	74.2	0.0837	0.512285(12)	0.512227	-5.4	914
WC-21	6.92	47.4	0.0883	0.512273(8)	0.512212	-5.7	959
WC-23	6.09	45.9	0.0803	0.512042(7)	0.511986	-10.1	1152
WC-24	1.27	6.1	0.1260	0.511897(13)	0.511810	-13.5	1926
WC-25	5.58	36.9	0.0915	0.511745(11)	0.511682	-16.0	1596
WC-26	2.54	15.7	0.0976	0.511861(11)	0.511793	-13.8	1532
WC-28	6.13	47.5	0.0781	0.512105(6)	0.512039	-9.0	1081

Rb and Sr abundances by XRF, and Sm and Nd abundances by INAA and are in ppm; Rb-Sr data are from Brandon and Lambert (1992a); all ratios and ϵ values relative to $^{86}\text{Sr}/^{88}\text{Sr} = 0.1194$ and $^{144}\text{Nd}/^{146}\text{Nd} = 0.7219$; $^{87}\text{Rb}/^{86}\text{Sr}_{\text{UR}} = 0.0827$; $\lambda^{87}\text{Rb} = 1.42 \cdot 10^{-11}/\text{yr}$; $^{87}\text{Sr}/^{86}\text{Sr}_{\text{UR}} \text{ at } 0 = 0.70478$; $\lambda^{147}\text{Sm} = 6.54 \cdot 10^{-12}/\text{yr}$; $^{147}\text{Sm}/^{144}\text{Nd}_{\text{CHUR}} = 0.1967$; $^{143}\text{Nd}/^{144}\text{Nd}_{\text{CHUR}} \text{ at } 0 = 0.512638$; TDM after the depleted mantle growth curve from DePaolo (1981b) and are in Ma. The 2σ precision in the last listed place for each measured isotopic ratio is listed in parentheses. ϵ_{Sr} , ϵ_{Nd} , and initial Sr and Nd ratios calculated at $T = 105.9$ Ma, using the chondritic uniform reservoir ratios listed above (UR, Allegre and Ben Othman 1980, CHUR, Jacobsen and Wasserburg 1984).

Table 4.4. U-Th-Pb isotopic compositions for the White Creek samples.

Sample	U	Th	Pb	$^{238}\text{U}/^{204}\text{Pb}$	$^{206}\text{Pb}/^{204}\text{Pb}$ Meas	$^{206}\text{Pb}/^{204}\text{Pb}$ Init	$^{207}\text{Pb}/^{204}\text{Pb}$ Meas	$^{207}\text{Pb}/^{204}\text{Pb}$ Init	$^{208}\text{Pb}/^{204}\text{Pb}$ Meas	$^{208}\text{Pb}/^{204}\text{Pb}$ Init
WC-2	5.76	29.2	23	16.20	18.915	18.647	15.638	15.625	39.403	38.955
WC-4	4.35	8.72	24	11.75	19.232	19.037	15.679	15.669	39.721	39.607
Ksp					18.970		15.690		39.529	
WC-5	5.82	6.2	36	10.48	19.303	19.129	15.700	15.692	39.208	39.148
WC-6	8.80	9.90	55	10.37	18.980	18.808	15.663	15.655	38.952	38.888
WC-8	6.29	18.02	34	11.99	19.500	19.302	15.705	15.695	39.661	39.474
Ksp					19.011		15.720		39.668	
WC-9	9.52	0.78	23	26.83	19.179	18.735	15.673	15.652	39.264	39.252
WC-11	11.57	33.9	23	32.61	19.084	18.544	15.650	15.624	39.353	38.833
Ksp					18.649		15.635		39.073	
WC-14	3.73	15.08	34	7.11	18.854	18.736	15.637	15.631	39.178	39.022
WC-15	10.03	82.2	17	38.25	19.223	18.589	15.678	15.648	40.239	38.533
Ksp					18.627		15.635		39.089	
WC-17	6.89	31.2	22	20.30	18.744	18.408	15.594	15.577	39.013	38.513
WC-18	6.01	39.56	21	18.55	18.749	18.442	15.610	15.595	39.169	38.504
Ksp					18.427		15.592		38.586	
WC-19	4.97	23.4	17	18.95	18.592	18.279	15.596	15.581	38.793	38.308
Ksp					18.333		15.598		38.405	
WC-21	8.67	27.0	20	28.10	18.757	18.291	15.612	15.590	39.013	38.537
Ksp					18.455		15.602		38.643	
WC-23	7.14	26.2	24	19.37	19.505	18.684	15.669	15.654	39.261	38.876
WC-24	6.04	5.73	40	9.79	19.186	19.024	15.701	15.693	38.971	38.921
WC-25	5.27	26.8	29	11.78	19.242	19.047	15.666	15.657	40.364	40.038
WC-26	4.97	11.14	33	9.76	19.083	18.922	15.656	15.648	39.555	39.434
Rpt					19.118	18.956	15.660	15.652	39.553	39.432
Ksp					18.881		15.689		39.568	
WC-28	9.6	29.5	27	23.05	18.891	18.510	15.635	15.616	39.293	38.907

U and Th abundances by INAA, and Pb abundances by XRF and are in ppm; Alkali feldspar analyses are listed as Ksp. Rpt are repeat analyses. Meas Pb ratios listed are the present day measured ratios which have a precision of 0.05% (2σ) for each ratio. Init Pb ratios are the initial ratios corrected to 105.9 Ma using the following decay constants: $\lambda^{238}\text{U} = 1.55125 \times 10^{-10}$; $\lambda^{235}\text{U} = 9.8485 \times 10^{-10}$; and $\lambda^{232}\text{Th} = 4.9475 \times 10^{-11}$.

Table 4.5. Whole rock (WR) and quartz (Qtz) oxygen isotope compositions for selected White Creek samples. Values are in parts per thousand (‰) relative to SMOW = 0 ‰.

Rock Type	Sample	$\delta^{18}\text{O}$ - WR	$\delta^{18}\text{O}$ - Qtz
2MGr	WC-4	9.1	11.0
	Rpt		11.2
2MGr	WC-8	10.2	10.3
PGd	WC-11	8.5	10.1
PGd	WC-15	8.1	10.1
	Rpt	8.1	10.1
HbBtGd	WC-18	6.8	10.0
	Rpt	6.8	
QMD	WC-19	7.1	10.2
HbBtGd	WC-21	8.2	
	Rpt	8.1	
2MGr	WC-26	10.3	10.9

Table 4.6. A comparison between amphibolite and tonalite starting material in melting experiments with mafic and felsic Precambrian basement rocks in SE British Columbia.

	1	2	3	4	5	6	7	8	9
SiO ₂	49.48-57.02	47.6-51.19	46.96	49.33	44.80	51.10	68.26	68.54	70.02
TiO ₂	0.6-1.74	0.72-2.06	3.66	1.72	1.16	2.67	0.52	0.55	0.45
Al ₂ O ₃	14.94-17.76	14.18-17.03	15.19	14.07	15.40	11.30	14.89	14.31	14.34
FeO*	8.01-12.49	10.69-13.77	11.17				4.67		
Fe ₂ O ₃			0.99	13.66	14.20	16.20		4.48	3.94
MnO	0.17-0.26	0.19-0.23	0.33	0.20	0.20	0.21	0.06	0.07	0.08
MgO	4.01-5.52	6.07-8.40	6.34	7.20	11.10	5.60	1.73	1.60	1.05
CaO	6.07-10.9	5.49-12.60	11.61	8.45	8.20	6.70	2.93	2.85	1.93
Na ₂ O	1.96-3.30	2.27-4.33	1.52	2.61	2.20	0.30	4.47	3.61	4.14
K ₂ O	0.03-0.44	0.19-0.82	0.27	2.37	2.67	4.60	2.05	4.05	4.10
P ₂ O ₅	0.21-1.56	0.70-1.65	<u>0.62</u>	<u>0.48</u>	<u>0.22</u>	<u>0.01</u>	<u>0.19</u>	<u>0.16</u>	<u>0.10</u>
Total			98.48	100.09	100.10	98.69	99.70	100.2	100.15

1. The range of starting compositions for amphibolite melting by Beard and Lofgren (1991).
2. The range of starting compositions for amphibolite melting by Rapp et al. (1991).
3. Late Proterozoic amphibolite sample D091 from the Monashee Mountains in SE British Columbia (Sevigny 1988).
4. Average Precambrian mafic gneiss (n = 59) from the Malton gneiss complex exposed near Valemount, SE British Columbia (Chamberlain et al. 1988).
5. Malton mafic gneiss sample 5819.02 (Chamberlain et al. 1988).
6. Malton mafic gneiss sample 5831.05 (Chamberlain et al. 1988).
7. Archean tonalite gneiss starting composition for tonalite melting by Skjerlie and Johnston (1992).
8. Average Malton tonalitic grey gneiss (n=33) from the Malton Range (Chamberlain et al. 1988).
9. Average of all felsic gneisses (n=174) from the Malton gneiss complex (Chamberlain et al. 1988).

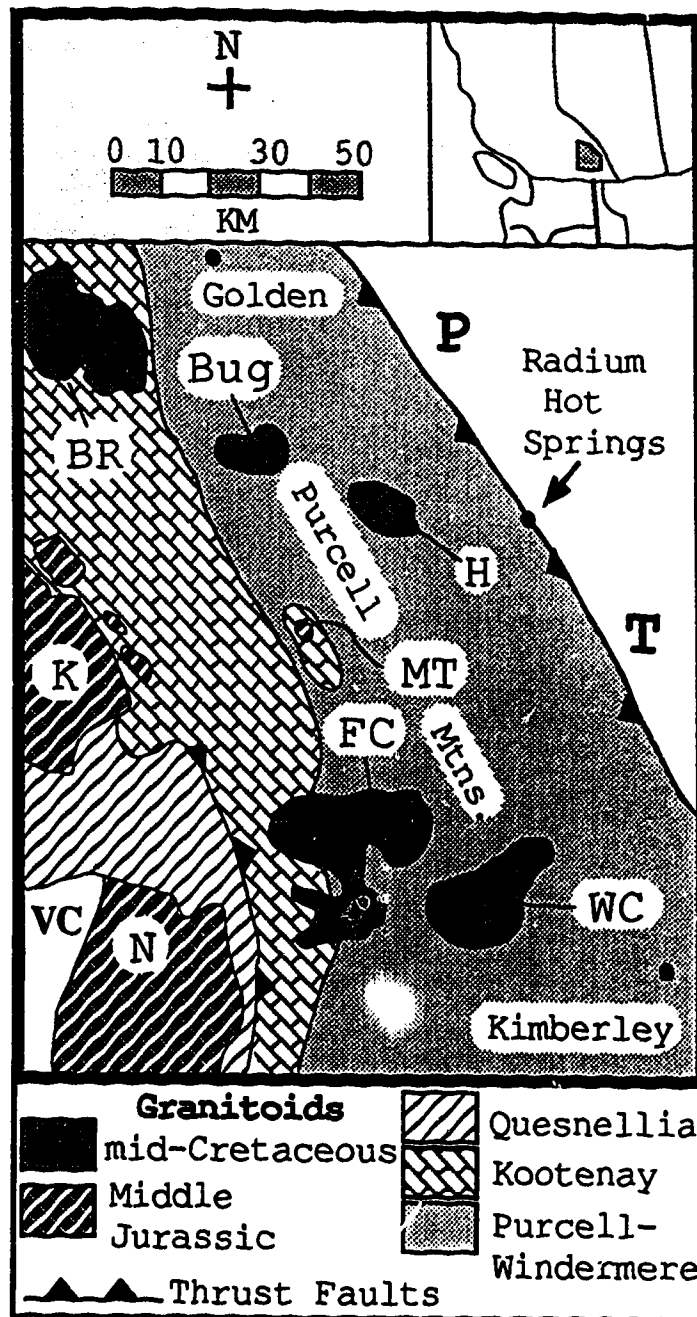


Figure 4.1. Generalized geologic map for southeast British Columbia emphasizing Mesozoic granitoids and large-scale lithologic units (modified from Monger and Berg 1987, Lambert and Chamberlain 1988, and Parrish et al. 1988). Quesnellia is part of Terrane I of Monger et al. (1982). The Kootenay metasediments are Paleozoic in age, and the Purcell-Windermere metasediments are Late Proterozoic. Symbols for the Mesozoic plutons include: K - Kuskanax, MT - Mt. Toby, N - Nelson, BR - Battle Range, Bug - Bugaboo, H - Horsethief Creek, FC - Fry Creek, and WC - White Creek. VC is for the Valhalla metamorphic core complex. The Purcell thrust fault is also shown (PT).

Figure 4.2. Lithologic map for the White Creek batholith (after Reesor 1958, and Wanless et al. 1968). Lithologic units are : 2MGr₂ - 2-mica granite no.2, 2MGr₁ - 2-mica granite no.1, PGd - porphyritic granodiorite, HbBtGd hornblende-biotite granodiorite, and QMD - quartz monzodiorite. Sample locations are circled and given in the Appendix 4.1.

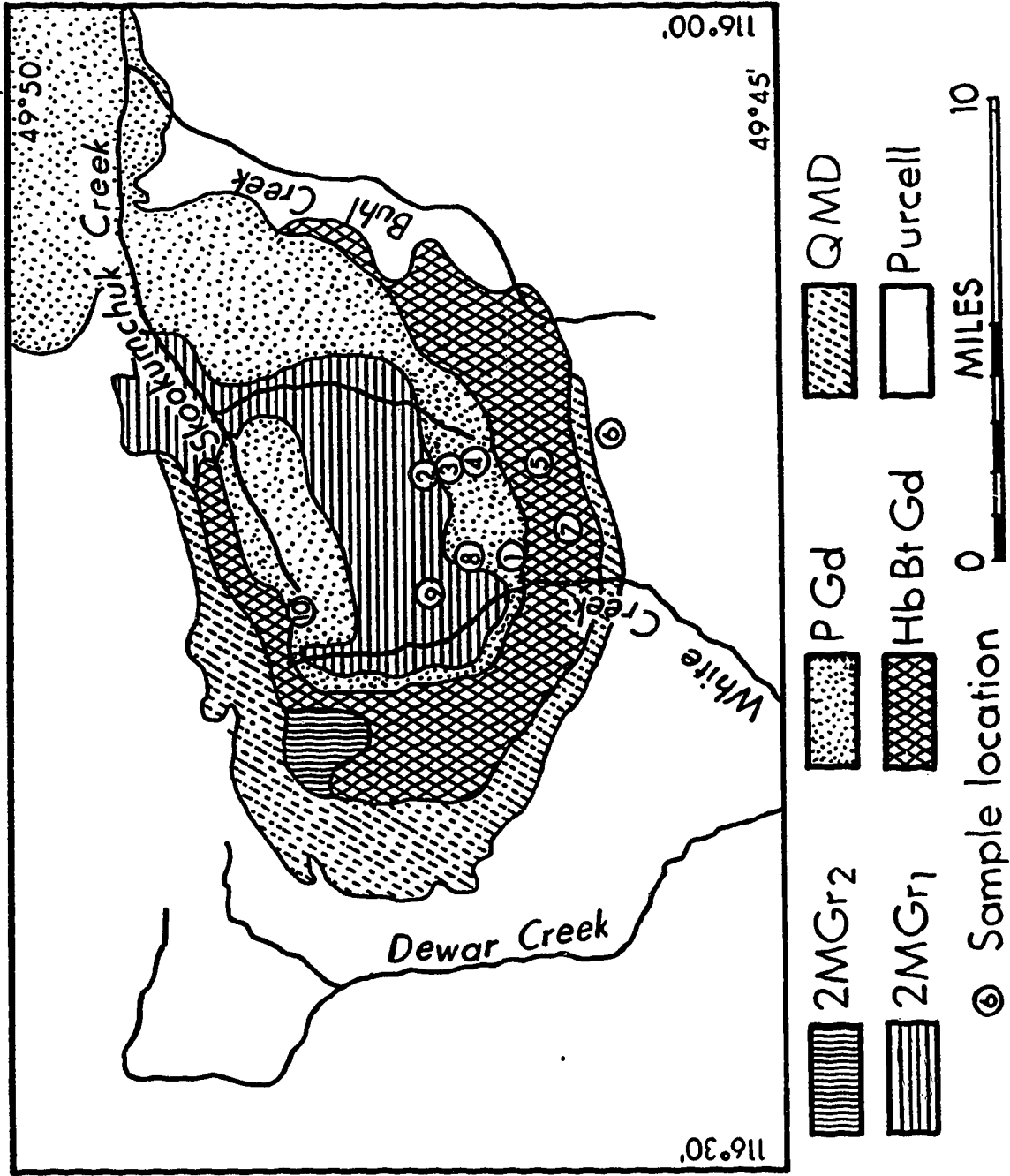
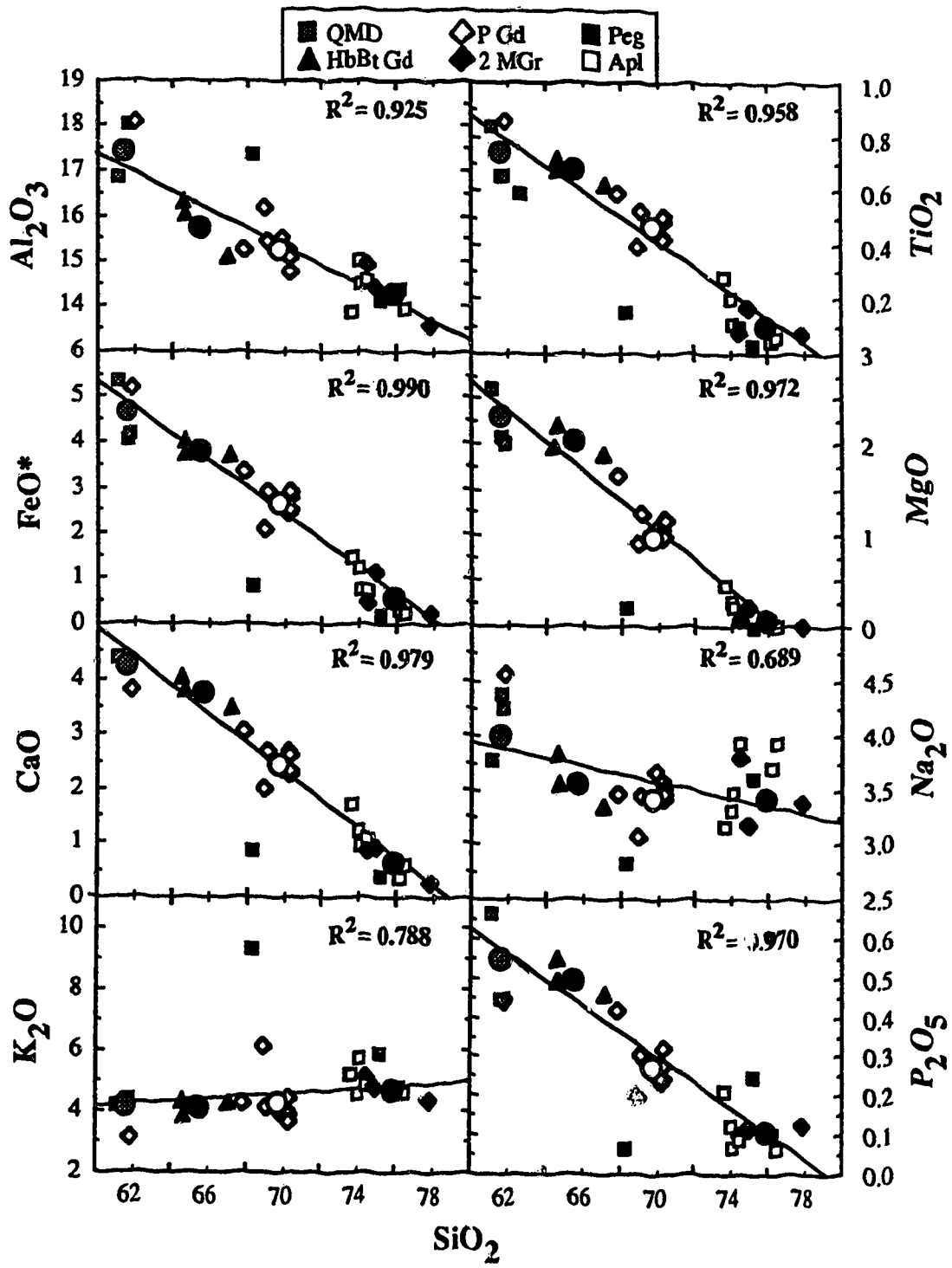


Figure 4.3. Harker variation diagrams for major element compositions of samples from the WCB. The circles are averages for the analyses from each respective lithologic unit. For PGd, WC-15 was excluded from the average because this rock is not representative of this unit owing to a much larger mafic mineral content than the rest of the samples from PGd. Regression lines are shown for the trends for the averaged points, with R^2 being the correlation coefficients at 2σ . Regression using the raw data instead of averages produces similar lines with with the same to slightly lower R^2 values.



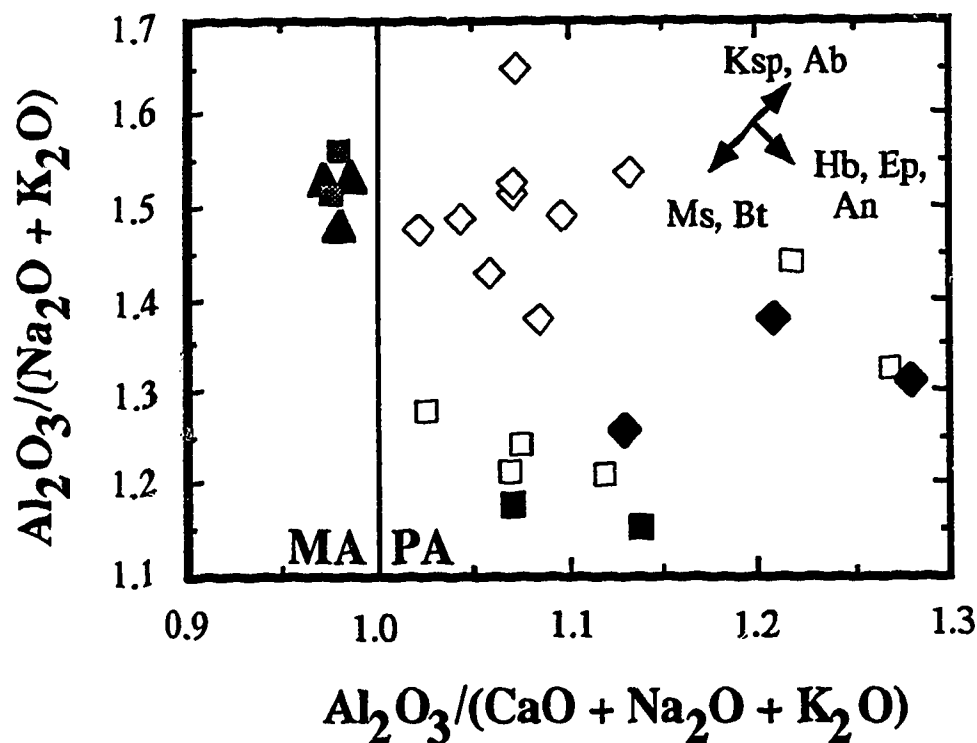
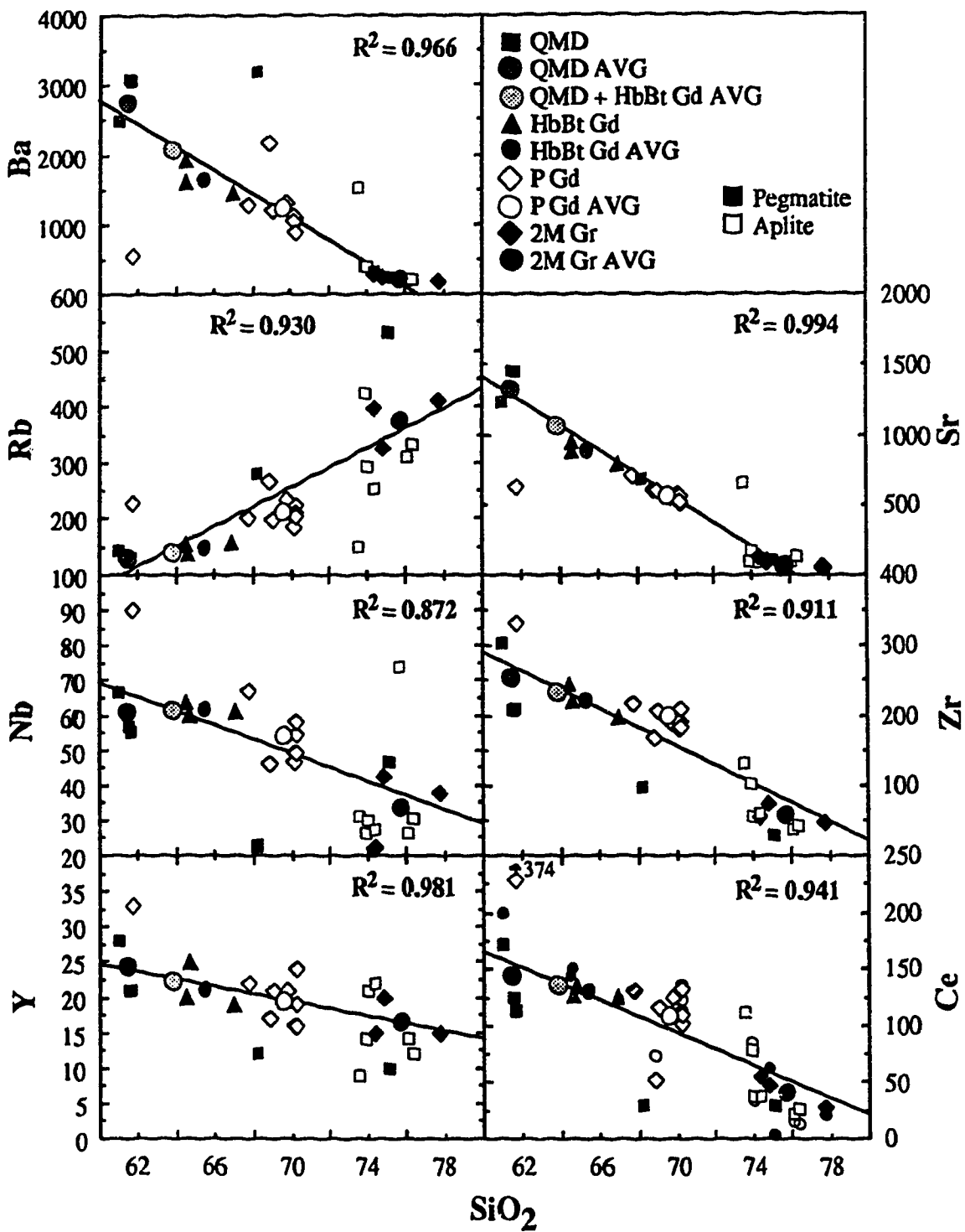


Figure 4.4. Alumina-saturation index (ASI - molar $\text{Al}_2\text{O}_3/[\text{CaO} + \text{K}_2\text{O} + \text{Na}_2\text{O}]$ corrected for apatite) versus AKN (molar $\text{Al}_2\text{O}_3/[\text{K}_2\text{O} + \text{Na}_2\text{O}]$) for the WCB samples with symbols as in Figure 4.3. The fields for metaluminous (MA) and peraluminous (PA) are shown. Qualitative fractionation trends for mineral phases which may control these ratios in granitoids are shown and the values chosen are those from Table 1 of Zen (1986). The mineral symbols are: Ab - albite, An - Anorthite, Bt - biotite, Ep - epidote, Hb - hornblende, Ksp - alkali feldspar, and Ms - muscovite.

Figure 4.5. Harker variation diagrams for selected trace elements for WCB samples. Regression lines follow those in Figure 4.3, except the average of QMD+HbBtGd is included in the regression.



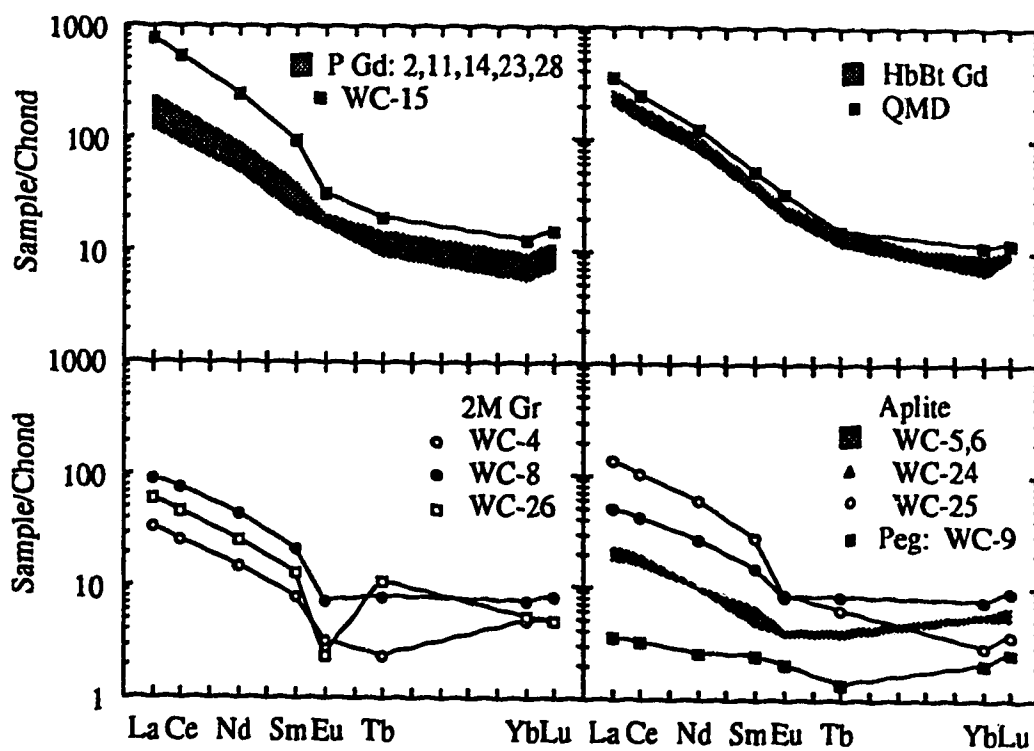


Figure 4.6. Rare earth element compositions of the WCB samples normalized to recommended chondritic values from Table 3.3 of Boynton (1983). Shaded regions are for composite compositions of the lithologic units listed.

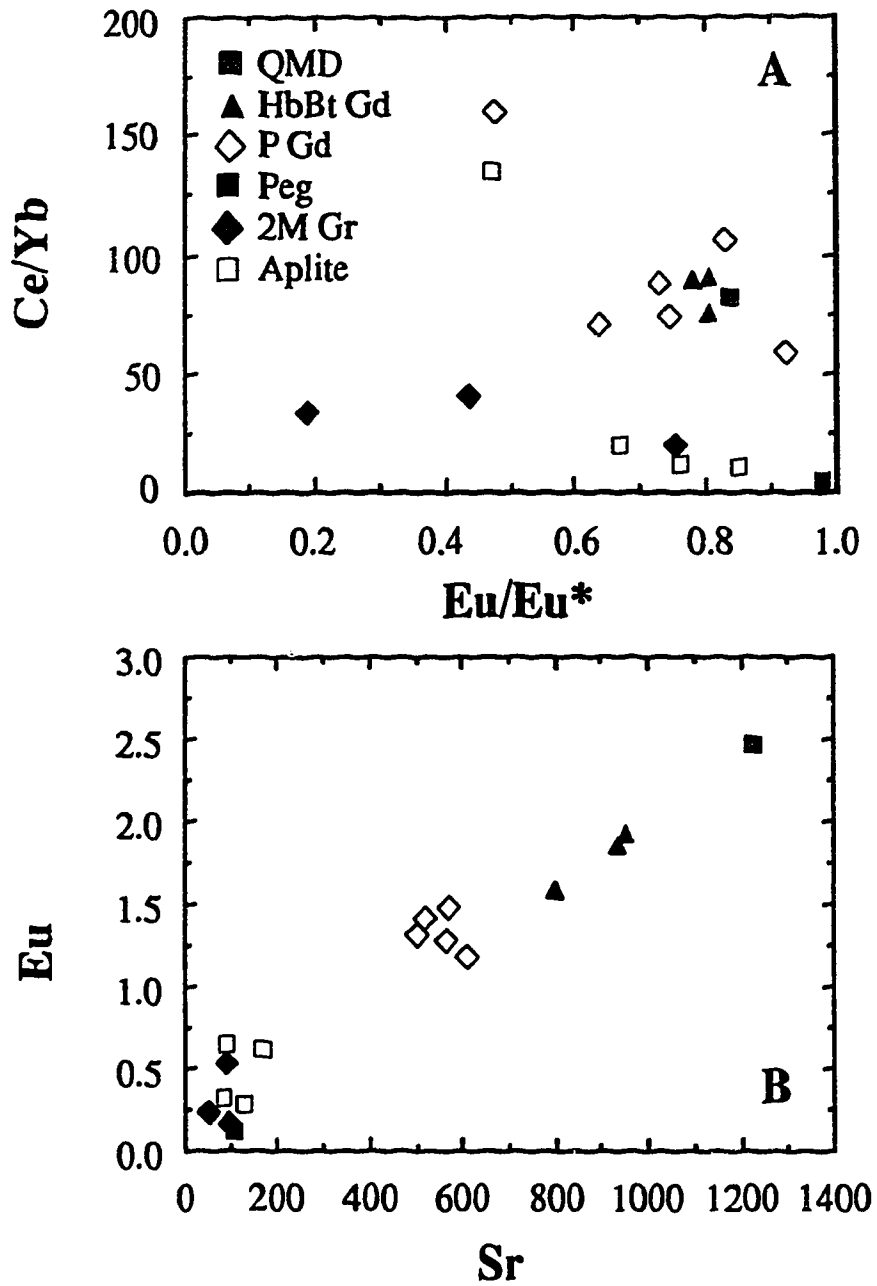


Figure 4.7. A) Ce/Yb versus Eu/Eu* for the WCB samples. Eu* is calculated assuming the expected Eu value by extrapolating between Sm and Tb. B) Eu versus Sr for the WCB samples.

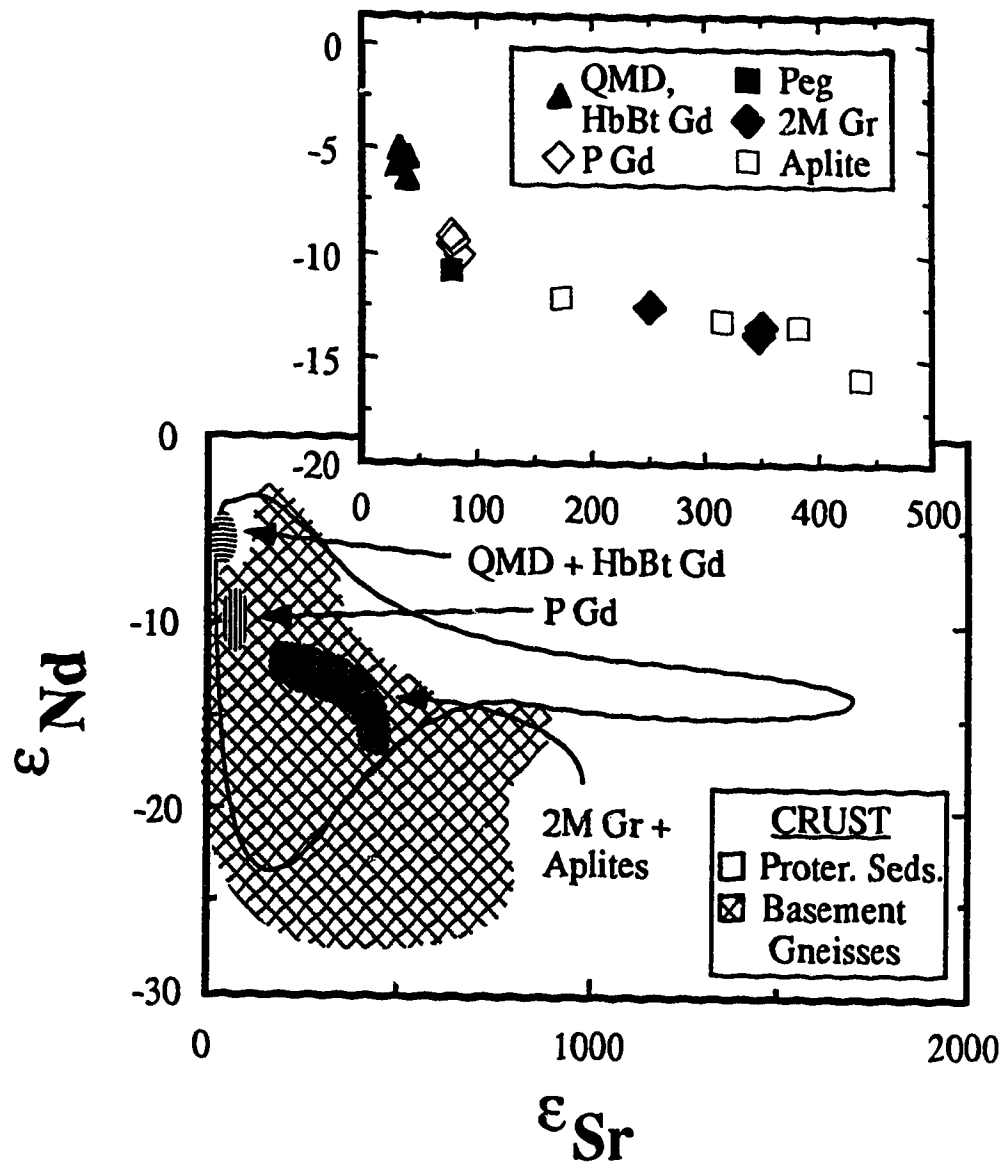
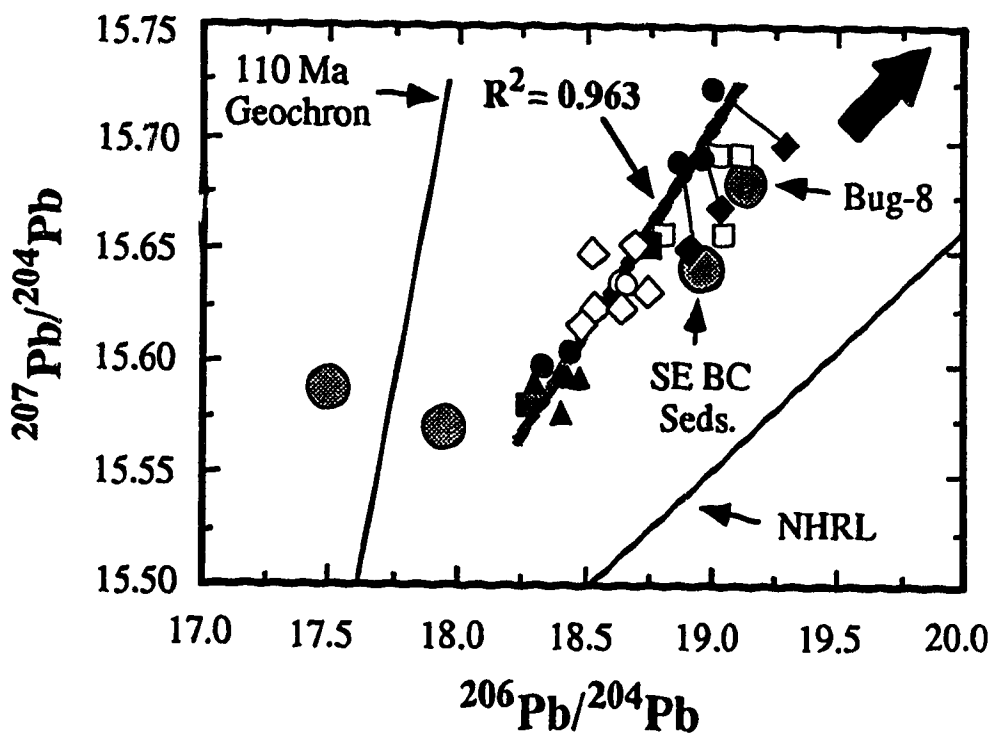
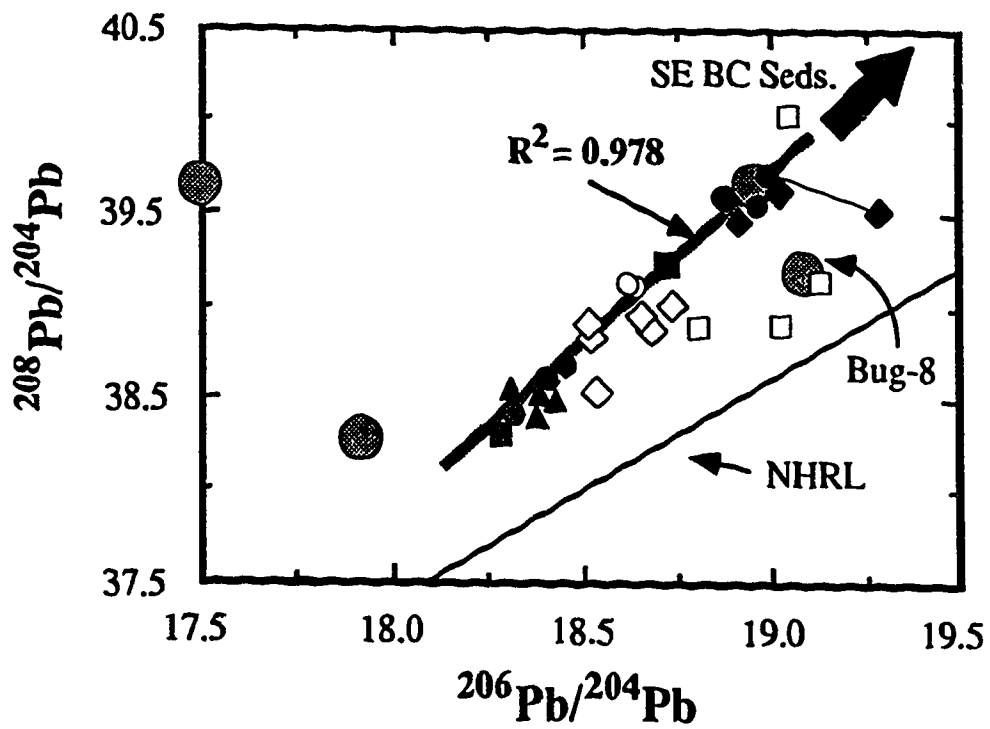


Figure 4.8. Initial ϵ_{Sr} versus ϵ_{Nd} diagram for the WCB granitoid and Precambrian crustal rocks from SE British Columbia. The main diagram shows the fields of the three lithologic groups of WCB samples and the inset shows the compositions of individual samples. The basement gneiss compositions are from Lambert and Chamberlain (1990). These include the Pre-Belt gneisses from northern Idaho 100 to 250 km south of Kimberley and underlying Belt-Purcell metasediments, and those from the Malton Gneiss complex in the Valemont are of British Columbia about 100 km north of Figure 4.1. The Proterozoic metasediments (Proter. Seds.) are for the Proterozoic metasediments in Figure 4.1 from Ghosh and Lambert (1989) that are exposed within Figure 4.1.

Figure 4.9. Initial $^{206}\text{Pb}/^{204}\text{Pb}$ versus $^{208}\text{Pb}/^{204}\text{Pb}$ and $^{207}\text{Pb}/^{204}\text{Pb}$ for the WCB granitoid whole rock samples with patterns and symbols as in Figure 4.8, and alkali feldspars (small circles). SEBC metasediments are shown as large circles (from Ghosh 1986). For the 2MGr samples, tie lines are drawn between whole rock and feldspar compositions. The large arrow in the upper right corner of both diagrams point toward additional SEBC metasediment compositions reported by Ghosh (1986) at much higher Pb isotopic compositions. A metapelite xenolith from the Bugaboo pluton is shown (Bug-8, Brandon and Lambert 1992b). The northern hemisphere regression line (NHRL) is the oceanic basalt array for the northern hemisphere from Hart (1984). Regression lines using the alkali feldspar compositions are shown with respective R^2 values.



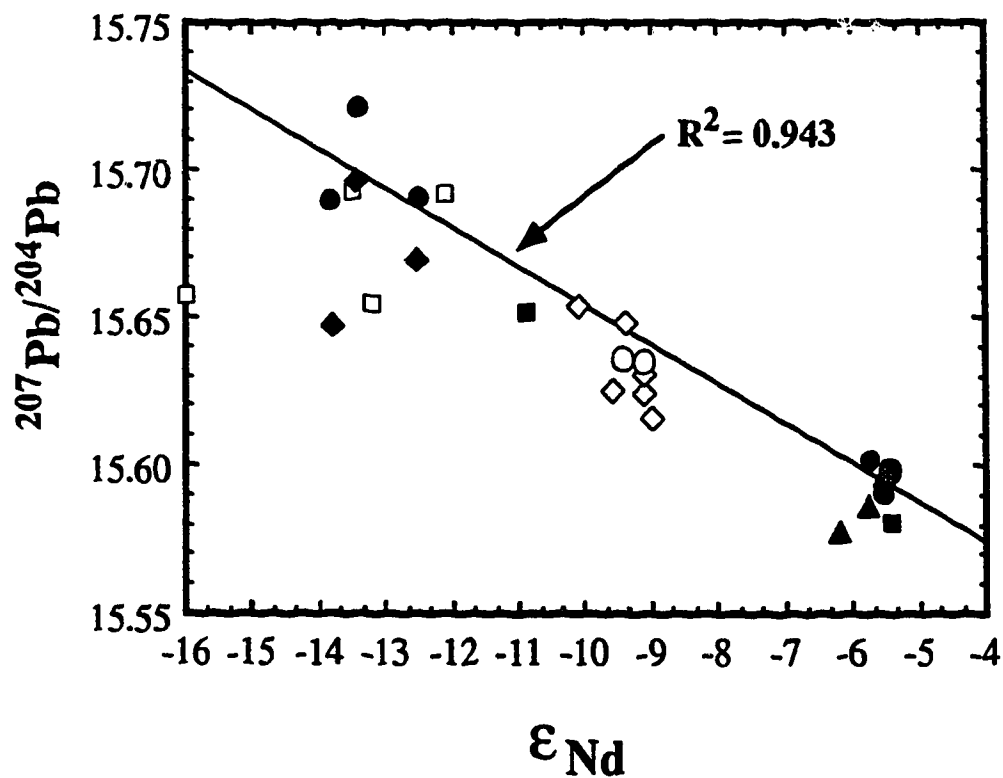


Figure 4.10. Initial $^{206}\text{Pb}/^{204}\text{Pb}$ versus ϵ_{Nd} for the WCB samples with symbols as in Figures 4.8 and 4.9. A regression line and its R^2 is shown for the feldspar-Pb compositions with ϵ_{Nd} used for the whole rocks of the same samples.

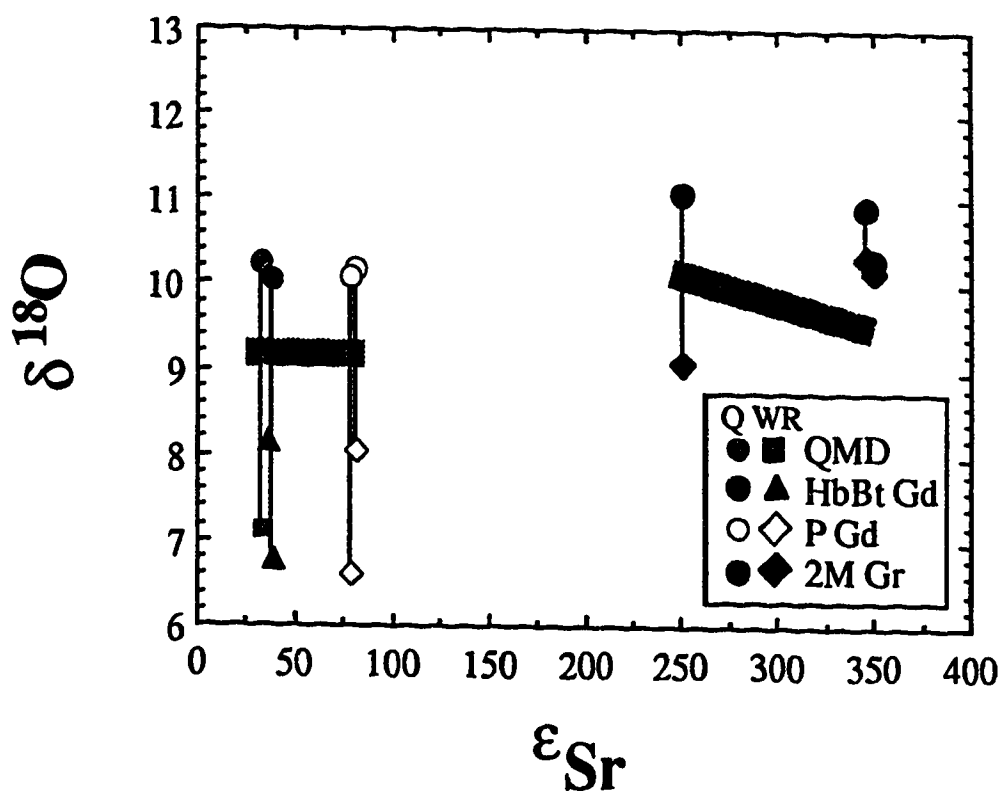


Figure 4.11. $\delta^{18}\text{O}$ versus ϵ_{Sr} for the WCB samples including oxygen analyses of quartz (Q) and whole rocks (WR). The shaded rectangles are for the $\delta^{18}\text{O}$ values estimated for the whole rocks assuming a 1‰ fractionation between quartz and respective magma.

Figure 4.12. AFC and mixing calculated models for $\delta^{18}\text{O}$ and $1/\text{Sr}$ versus ϵ_{Sr} using various end-member compositions. Shown are the $\delta^{18}\text{O}$ analyses for quartz, whole rock, and estimated whole rock (shaded rectangles) from Figure 4.11. Each symbol for the calculated trends in the AFC models represent 0.1 increments in F (the fraction of melt remaining) except for the last two increments towards the crustal end-members which are for F equal to 0.05 and 0.005. The symbols for the mixing trends represent 10% increments between basalt and crustal end-member mixes. The basalt composition used assumed a moderately evolved Sr abundance of 500 ppm (as opposed to a lower Sr abundance for more primitive, high-Mg basalt) to more easily attempt to produce the most mafic WCB granitoid compositions (QMD and HbBtGd), with $\delta^{18}\text{O}$ of +5.7 and ϵ_{Sr} of -25. The two crustal end-members used were approximating average WCB 2MGr with Sr equal to 75 ppm, ϵ_{Sr} of +300, and $\delta^{18}\text{O}$ of +10, and a Hi Sr Gr (high Sr, low ϵ_{Sr} granite) with Sr equal to 1500, ϵ_{Sr} of +60, and $\delta^{18}\text{O}$ of +10. In the AFC calculations, R is the ratio of mass of basalt crystallized to the mass of crust assimilated at each increment. The bulk partition coefficient (Kd) used for Sr in the AFC calculations was 0.9 and hence slightly incompatible in order to increase the Sr content in the evolved melt and approach the Sr composition of QMD/HbBtGd with a lower degree of fractionation and assimilation than with a higher partition coefficient. As plagioclase controls the Sr Kd, and using an averaged Kd of 1.8 for an andesitic magma (range of 1.3 to 3.2, Table 6.3, Gill 1981), the cumulate assemblage has about 40% plagioclase and is similar to the amount of plagioclase calculated for producing andesite in AFC with basalt assimilating rhyolite (Table 8, column 2, Brandon 1989) using thermodynamically derived solution models to predict mineral phases in equilibrium with magma compositions (using the program SILMIN, Ghiorso 1985).

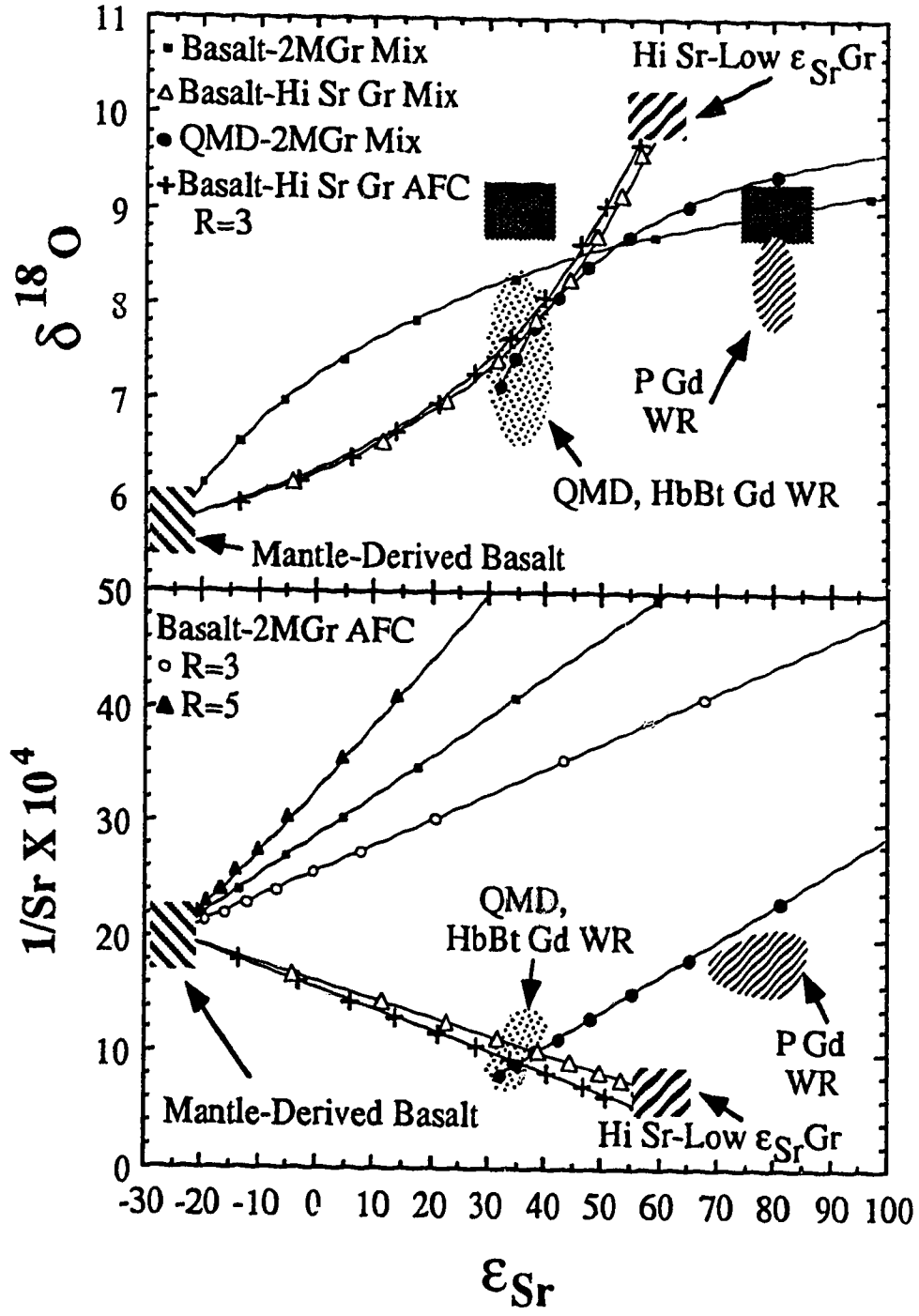
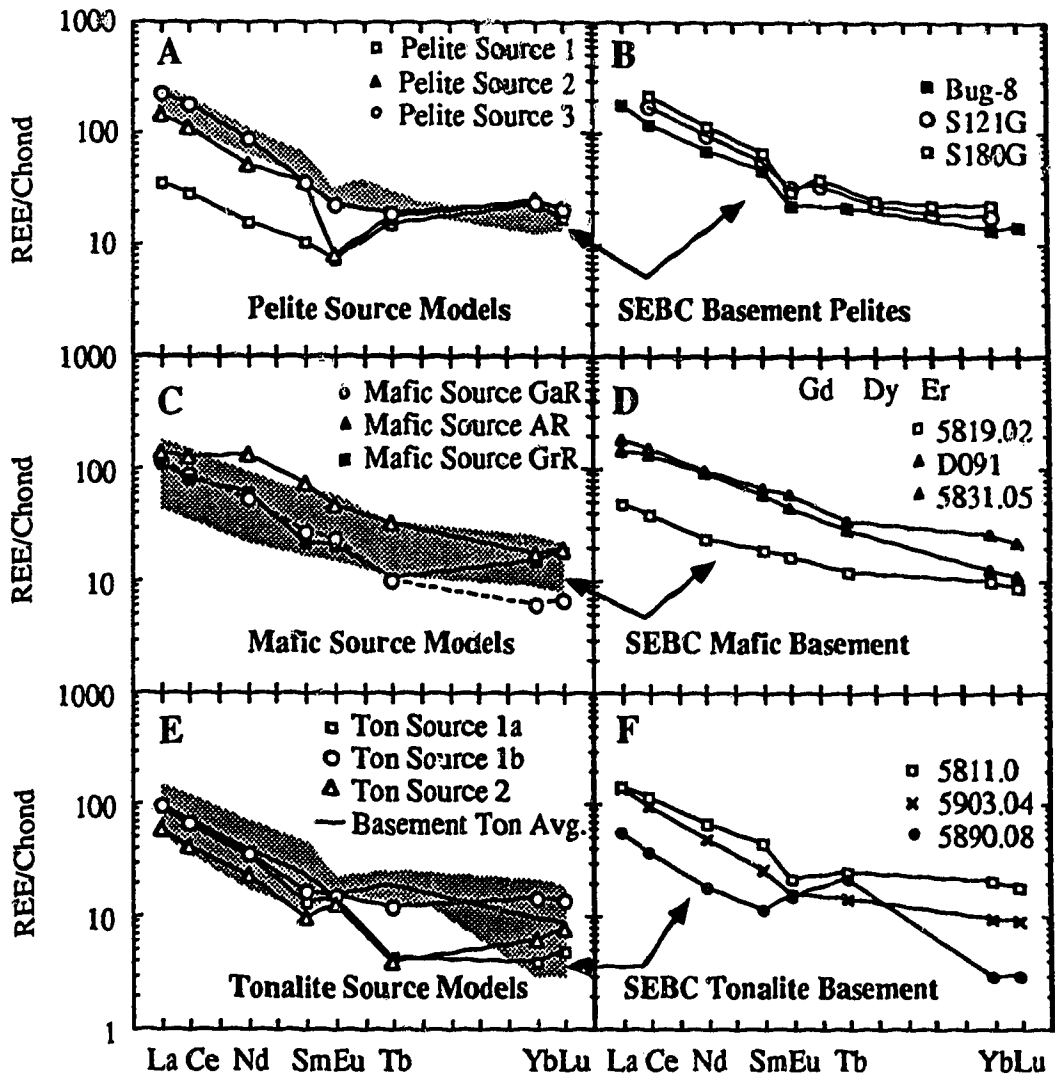


Figure 4.13. Calculated REE compositions of source materials for the WCB and SE British Columbia (SEBC) basement rocks. (A) Calculated source REE patterns for pelite melting assuming 2MGr melts (average of WC-4, 8, and 26) at 30% batch partial melting, and using the felsic partition coefficients in Appendix 4.2. Pelite Source 1 is for a residue of 12.2% garnet (gnt), 22% plagioclase (pl), 5% alkali feldspar (ksp), 25% biotite (bt), and the remainder being quartz (qtz) and sillimanite (sill) with Kds equal to zero. Pelite Source 2 assumes a melt composition of WC-8, and an additional 0.1% of apatite, zircon, and monazite as residue. Pelite Source 3 has a residue with 30% pl, 20% ksp, 10% gnt, 20% bt, 0.1% monazite, 0.4% apatite, and the remainder as qtz and sill, with WC-8 as the melt composition. (B) Late Proterozoic metapelites from SEBC. Bug-8 is from Brandon and Lambert (1992b), and S121G and S180B is from Sevigny et al. (1989). (C) Calculated source REE patterns for amphibolite melting assuming QMD/HbBtGd melts (average of WC-17, 18, 19, and 21) at 30% batch partial melting and using the intermediate Kds in Appendix 4.2. Mafic Source GaR is a source leaving a gabbroic residue 40% pl and 60% clinopyroxene (cpx); Mafic Source AR is a source leaving 30% pl, 25% cpx, and 45% hornblende (hb); and Mafic Source Gr leaves a granulite residue with 40% pl, 30% cpx, 10% gnt, 10% orthopyroxene (opx), and 10% qtz. (D) Mafic gneisses from the Malton gneiss complex (samples 5819.02 and 5831.05, Chamberlain et al. 1988), and a Late Proterozoic amphibolite from the Monashee Mountains (sample D091, Sevigny 1988.). (E) Calculated source REE patterns for partial melting of tonalite assuming PGd melts (average of samples WC-11, 14, 23, and 28), using the intermediate Kds from Appendix 4.2 except gnt where the silicic Kds were used. Ton Source 1a is for 28% melting leaving a residue of 53% pl, 5.2% bt, 3.9% opx, 27.8% qtz, and 0.05% apatite and zircon; Ton Source 1b adds 5% gnt and subtracts 5% qtz from the residue relative to 1a; and Ton Source 2 is for 10% melting leaving a residue of 45% pl, 17.7% bt, 4.8% opx, 2.4% gnt, 28.8% qtz, 1.2% hb, and 0.05% apatite and zircon. (F) Tonalitic gneisses from the Malton complex (Chamberlain et al. 1988).



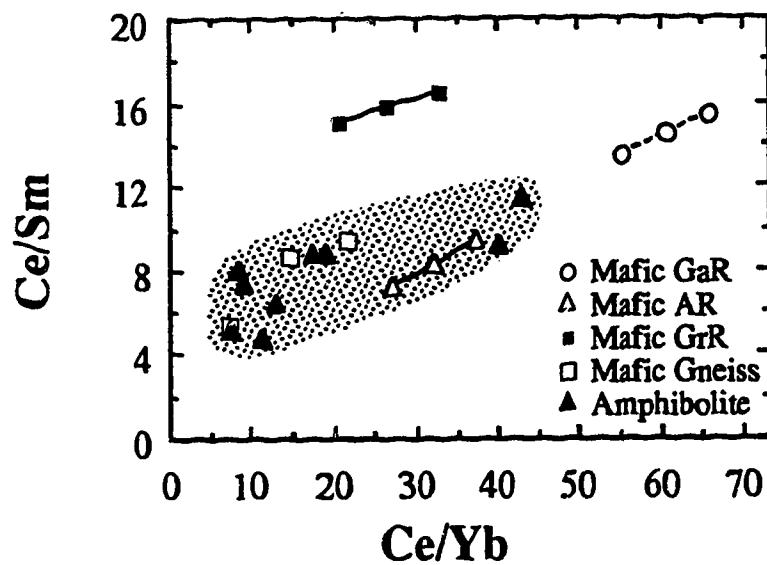


Figure 4.14. Ce/Sm versus Ce/Yb ratios for mafic sources calculated for 30, 40, and 50% melting of amphibolite leaving residues as in Figure 4.13. 10% increments in melting increase upwards and to the right. Mafic gneiss compositions are from the Malton gneiss complex (Chamberlain et al. 1988) and Late Proterozoic amphibolites are from the Monashee Mountains (Sevigny 1988). The shaded area represents the region for all of the data for Precambrian rocks from SE British Columbia presently available.

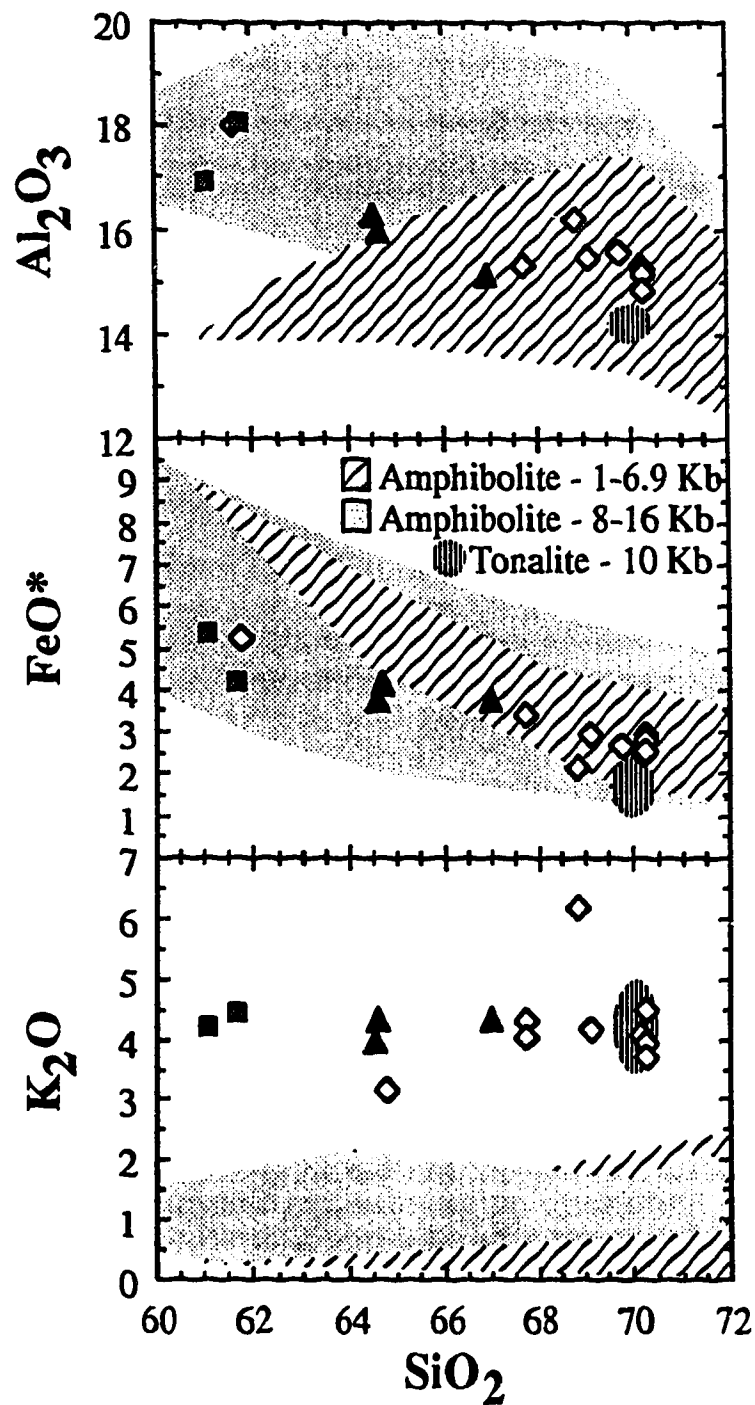


Figure 4.15. Harker variation diagrams for compositions produced by amphibolite melting at 1-6.9 kbar (Beard and Lofgren 1991), and 8 and 16 kbar (Rapp et al. 1991), and tonalite melting at 10 kbar (Skjerlie and Johnston 1992), with White Creek samples (symbols as in Fig. 4.3) plotted for comparison.

Appendix 4.1

Sample localities, rock types, and estimated modal proportions (%) of mineralogy.

Sample	Lc	Latitude	Longitude	Type	Pl	Ksp	Qtz	Bt	Hb	Ep	Ms	Ac
WC-1	1	49°50'30"N	116°15'55"W	PGd	40	18	26	13	1	X		2
WC-2		"	"	PGd	36	21	28	15		X	X	1
WC-4	2	49°59'47"N	116°13'55"W	2MGr	34	25	33				8	X
WC-5		"	"	Aplite	26	35	32	1			6	X
WC-6		"	"	Aplite	24	40	29	6			1	X
WC-7		"	"	PGd	37	20	27	15		X	X	1
WC-8		"	"	2MGr	25	30	32	4			9	X
WC-9		"	"	Peg	22	30	25				23	
WC-11	3	49°51'39"N	116°13'47"W	PGd	37	21	26	15		X		1
WC-13	4	49°51'31"N	116°13'46"W	PGd	40	19	25	16		X	X	X
WC-14		"	"	PGd	38	22	25	14		X	X	1
WC-15	4	49°51'21"N	116°13'48"W	PGd	37	27	20	15		X		1
WC-16		"	"	Peg	5	70	20	3			2	X
WC-17	4	49°50'08"N	116°14'37"W	HbBtGd	41	15	19	16	6	1		2
WC-18	5	49°49'54"N	116°13'10"W	HbBtGd	40	15	21	18	4	X		2
WC-19	6	49°49'16"N	116°12'48"W	QMD	40	15	16	20	4	3		2
WC-20		"	"	QMD	45	17	13	15	6	2		2
WC-21	7	49°49'49"N	116°14'16"W	HbBtGd	41	15	20	16	7	X		2
WC-22		"	"	Aplite	33	36	25	5		X	X	1
WC-23	8	49°51'32"N	116°15'20"W	PGd	40	18	28	14			X	X
WC-24		"	"	Aplite	30	28	34				8	
WC-25	9	49°52'24"N	116°16'14"W	Aplite	15	40	35	4			6	X
WC-26		"	"	2MGr	28	32	30	4			6	X
WC-27	10	49°54'48"N	116°16'52"W	Aplite	17	41	32	3	Tm		3	X
									3			
WC-28		"	"	PGd	30	21	27	12		X	X	2

Estimated modal percentages are based on hand sample and thin section determinations. Locations (Lc) are on Figure 4.2. The Accessory phases (A) are zircon, apatite, and magnetite. Spene was always found in the rocks with hornblende. Abbreviations: 2MGr - two-mica granite; HbBtGd - hornblende-biotite granodiorite; PGd - porphyritic granodiorite; QMD - quartz monzodiorite; Peg - pegmatite; Pl - plagioclase; Ksp - alkali feldspar; Qtz - quartz; Bt - biotite; Hb - hornblende; Ep - epidote + allanite; Ms - muscovite; and Tm - tourmaline. X denotes present in less than 1%.

Appendix 4.2

Partition coefficients used in trace element modelling.

-----Intermediate-----						
	Cpx	Hb	Gnt	Opx	Bt	Plag
La	0.30	0.100	0.440	0.020	0.025	0.033
Ce	0.24	0.208	0.889	0.039	0.031	0.037
Nd	0.17	0.427	2.80	0.094	0.034	0.044
Sm	0.13	0.681	3.99	0.395	0.047	0.053
Eu	1.1	0.635	3.44	0.610	0.060	0.145
Tb	0.088	0.930	5.84	2.98	0.094	0.090
Yb	0.077	0.896	4.89	16.60	0.244	0.179
Lu	0.070	0.880	4.50	18.50	0.303	0.190

-----Felsic-----							
	Plag	Ksp	Gnt	Bt	Ap	Zr	Mon
La	0.40	0.129	0.20	1.02	47.0	16.9	2494
Ce	0.35	0.065	0.35	1.03	69.4	16.8	2279
Nd	0.30	0.054	0.53	0.99	114.0	13.3	1620
Sm	0.20	0.026	2.66	1.03	126.0	14.4	866.5
Eu	5.4	9.06	1.50	0.68	60.8	16.0	111
Tb	0.21	0.018	19.5	0.99	107.0	37	273
Yb	0.145	0.015	38.9	0.71	48.0	527	30.8
Lu	0.125	0.012	29.6	0.73	35.0	641.5	33

The intermediate partition coefficients are from intermediate igneous rocks modified from the compilation of Gromet and Silver (1987) with La, Tb and Lu added for Pl (plagioclase), Cpx (clinopyroxene), Gnt (garnet), and Hb (hornblende), and all REE added for Bt (orthopyroxene) and Opx (biotite). The sources of data used by Gromet and Silver (1987) and here are: Pl from Arth (1976) with Eu from Gromet and Silver (1987); Cpx from Schnetzler and Philpotts (1970); Hb from Arth (1976); Gnt following the calculation by Gromet and Silver (1987); Opx from Schnetzler and Philpotts (1970); and Bt. from Arth and Hanson (1975). The felsic partition coefficients are from felsic igneous rocks modified from the compilation of Sevigny et al. (1989) with La, Tb, and Lu added, and a different set of coefficients for Ksp(alkali feldspar). The data sources for the felsic partition coefficients are: Pl from Hildreth (1977); Ksp from Leeman and Phelps (1981); Gnt from Philpotts and Schnetzler (1970); Bt from Nash and Crecraft (1985); Ap (apatite) following the calculation of Sevigny et al. (1989) using data from Nagasawa and Schnetzler (1971) and Mahood and Hildreth (1983); Zr (zircon) from Mahood and Hildreth (1983); and Mon (monazite) using allanite partition coefficients from Mahood and Hildreth (1983) following the assumptions of Sevigny et al. (1989). In some cases, La, Tb, and Lu coefficients were not available and were obtained by interpolation from the REE pattern.

References

- Allegre, C.J., and Ben Othman, D., 1980. Nd-Sr isotopic relationships in granitoid rocks and continental crust development: A chemical approach to orogenesis. *Nature*, 286, 335-342.
- Archibald, D.A., Glover, J.K., Price, R.A. Farrar, E., and Carmichael, D.M., 1983. Geochronology and tectonic implications of magmatism and metamorphism, southern Kootenay Arc and neighboring regions, southeastern British Columbia. Part I: Jurassic to Mid-Cretaceous. *Canadian Journal of Earth Sciences*, 20, 1891-1913.
- Archibald, D.A., Krogh, T.E., Armstrong, R.L., and Farrar, E., 1984. Geochronology and tectonic implications of magmatism and metamorphism, southern Kootenay Arc and neighboring regions, southeastern British Columbia. Part II: Mid-Cretaceous to Eocene. *Canadian Journal of Earth Sciences*, 21, 567-583.
- Armstrong, R.L., 1982. Cordilleran metamorphic core complexes. *Annual Reviews of Earth and Planetary Sciences*, 10, 129-154.
- Arndt, N.T., and Goldstein, S.L., 1987. Use and abuse of crust-formation ages. *Geology*, 15, 893-895.
- Arth, J.G., 1976. Behavior of trace elements during magmatic processes - a summary of theoretical models and their applications. *United States Geological Survey, Journal of Research*, 4, 41-47.
- Arth, J.G., and Hanson, G.N., 1975. Geochemistry and origin of the early Precambrian crust of northeastern Minnesota. *Geochimica et Cosmochimica Acta*, 39, 325-362.
- Beard, J.S., and Lofgren, G.E., 1989. Effect of water on the composition of partial melts of greenstone and amphibolite. *Science*, 244, 195-197.
- Beard, J.S., and Lofgren, G.E., 1991. Dehydration melting and water-saturated

- melting of basaltic and andesitic greenstones and amphibolites at 1, 3, and 6.9 kb. *Journal of Petrology*, **32**, 365-401.
- Bergantz, G.W., 1989. Underplating and partial melting: Implications for melt generation and extraction. *Science*, **245**, 1093-1095
- Boynton, W.V., 1983. Cosmochemistry of the rare earth elements: Meteorite studies. *In Rare Earth Element Geochemistry. Developments in Geochemistry 2, Edited by P. Henderson, Elsevier, Amsterdam*, 63-114
- Brandon, A.D., 1989. Constraints on magma genesis behind the Neogene Cascade arc: Evidence from major and trace element variation of high-alumina and tholeiitic volcanics of the Bear Creek area. *Journal of Geophysical Research*, **94**, 7775-7798.
- Brandon, A.D., and Lambert, R.StJ., 1992a. Rb-Sr geochronology of Mesozoic granitoids in the southern Canadian Cordillera. *Canadian Journal of Earth Sciences*, submitted.
- Brandon, A.D., and Lambert, R.StJ., 1992b. Geochemical characterization of mid-Cretaceous granitoids of the Kootenay arc in the southern Canadian Cordillera. *Canadian Journal of Earth Sciences*, submitted.
- Carlson, R.W., 1980. Crust-mantle differentiation of the Earth and Moon: Evidence from isotopic studies for contrasting mechanisms and duration. Ph.D. Thesis, University of California at San Diego, San Diego.
- Chamberlain, V.E., 1983. The Malton gneiss complex, Valemount, B.C. Ph.D. Thesis, The University of Alberta, Edmonton.
- Chamberlain, V.E., Lambert, R.StJ., and Holland, J.G., 1988. Geochemistry of the gneissic basement complex near Valemount, British Columbia: Further evidence for a varied origin. *Canadian Journal of Earth Sciences*, **25**, 1725-1739.
- Chappell, B.W., White, A.J.R., and Wyborn, D., 1987. The importance of residual

- source material (restite) in granite petrogenesis. *Journal of Petrology*, **28**, 287-306.
- Clayton, R.N., and Mayeda, T.K., 1963. The use of bromide pentafluoride in the extraction of oxygen from oxides and silicates for isotopic analysis. *Geochimica et Cosmochimica Acta*, **27**, 43-52.
- Clemens, J.D., 1989. The importance of residual source material (restite) in granite petrogenesis: A comment. *Journal of Petrology*, **30**, 1313-1316.
- Clemens, J.D., and Vielzeuf, D., 1987. Constraints on melting and magma production in the crust. *Earth and Planetary Science Letters*, **86**, 287-306.
- Coney, P.J., and Harms, T., 1984. Cordilleran metamorphic core complexes: Cenozoic extensional relics of Mesozoic compression. *Geology*, **12**, 550-554.
- Cullers, R.L., and Graf, J.L., 1984. Rare earth elements in igneous rocks of the continental crust: Predominantly basic and ultrabasic rocks. *In Rare Earth Element Geochemistry, Edited by P. Henderson. Elsevier, Amsterdam, 235-274.*
- Dawes, R.L., and Evans, B.W., 1991. Mineralogy and geothermobarometry of magmatic epidote-bearing dikes, Front Range, Colorado. *Geological Society of America Bulletin*, **103**, 1017-1031.
- DePaolo, D.J., 1981a. A neodymium and strontium isotopic study of the Mesozoic calc-alkaline granitic batholiths of the Sierra Nevada and Peninsular Ranges, California. *Journal of Geophysical Research*, **86**, 10470-10488.
- DePaolo, D.J., 1981b. Neodymium isotopes in the Colorado Front Range and the crust-mantle evolution in the Proterozoic. *Nature*, **291**, 193-196.
- DePaolo, D.J. 1981c. Trace element and isotopic effects on combined wallrock assimilation and fractional crystallization. *Earth and Planetary Science*

- Letters, 53, 189-202.
- DePaolo, D.J., 1988. Neodymium Isotope Geochemistry. An Introduction. Springer-Verlag, Berlin.
- DePaolo, D.J., Linn, A.M., and Schubert, G., 1991. The continental crustal age distribution: Methods of determining mantle separation ages from Sm-Nd isotopic data and application to the southwestern United States. *Journal of Geophysical Research*, 96, 2071-2088.
- Fountain, D.M., 1989. Growth and modification of lower continental crust in extended terrains: The role of extension and magmatic underplating. *In Properties and Processes in Earth's Lower Crust*, Edited by R.F. Mero, R.F., S. Mueller, and M.F. Fountain, American Geophysical Union, Geophysical Monograph Series, 51, 287-299.
- Garlick, G.D., 1966. Oxygen isotope fractionation in igneous rocks. *Earth and Planetary Science Letters*, 1, 361-368.
- Ghent, E.D., Nicholls, J. Stout, M.Z., and Rottenfusser, B., 1977. Clinopyroxene amphibolite boudins from Three Valley Gap, British Columbia. *Canadian Mineralogist*, 15, 269-282.
- Ghiorso, M.S., 1985. Chemical mass transfer in magmatic processes, I, Thermodynamic relations and numerical algorithms. *Contributions to Mineralogy and Petrology*, 90, 107-120.
- Ghosh, D.K., 1986. Geochemistry of the Nelson-Rossland area, B.C. Ph.D. Thesis, University of Alberta, Edmonton.
- Ghosh, D.K. and Lambert, R.St.J., 1989. Nd-Sr isotope study of Proterozoic to Triassic sediments from southeastern British Columbia. *Earth and Planetary Science Letters*, 94, 29-44.
- Giletti, B.J., 1986. Diffusion effects on oxygen isotope temperatures of slowly cooled igneous and metamorphic rocks. *Earth and Planetary Science*

- Letters, 77, 218-228.
- Gill, J., 1981. *Orogenic Andesites and Plate Tectonics*, Springer-Verlag, Berlin.
- Glover, J.K., 1978. *Geology of the Summit Creek map-area, southern Kootenay Arc, British Columbia*. Ph.D. thesis, Queen's University, Kingston, Ontario.
- Gordon, G.E., Randle, K., Goles, G.G., Corliss, J.B., and Beeson, M.H., 1968. Instrumental activation analysis of standard rocks with high-resolution gamma-ray detectors. *Geochimica et Cosmochimica Acta*, 32, 369-396.
- Gromet, L.P., and Silver, L.T., 1987. REE variations across the Peninsular Ranges batholith: Implications for batholithic petrogenesis and crustal growth in magmatic arcs. *Journal of Petrology*, 28, 75-125.
- Hart, S.R., 1984. A large-scale isotope anomaly in the Southern Hemisphere mantle. *Nature*, 309, 753-757.
- Hildreth, W., 1977. *The magma chamber of the Bishop Tuff: Gradients in pressure, temperature, and composition*. Ph.D. Thesis, University of California, Berkeley.
- Hooper, P.R., and Johnson, D., 1987. Major and trace element analyses of rocks and minerals by automated X-ray spectrometry. In house report, Department of Geology, Washington State University, Pullman.
- Hyndman, D.W., and Foster, D.A., 1988. The role of tonalites and mafic dikes in the generation of the Idaho batholith. *Journal of Geology*, 25, 894-928.
- Jacobsen, S.B., and Wasserburg, G.J., 1984. Sm-Nd isotopic evolution of chondrites and achondrites, 2. *Earth and Planetary Science Letters*, 67, 137-150.
- Jenkin, G.R.T., Linklater, C., and Fallick, A.E., 1991. Modeling of mineral $\delta^{18}\text{O}$ values in an igneous aureole: Closed-system model predicts apparent open-system $\delta^{18}\text{O}$ values. *Geology*, 19, 1185-1188.

- Lambert, R.StJ., 1983. Metamorphism and thermal gradients in the Proterozoic continental crust. *In* Proterozoic Geology: Selected Papers from an International Symposium, *Edited by* L.G. Medaris, C.W. Byers, D.M. Mickelson, and W.C.Shanks. Geological Society of America, Memoir 161, 155-165.
- Lambert, R.StJ., and Chamberlain, V.E., 1988. Cordillera revisited, with a three-dimensional model for Cretaceous tectonics in British Columbia. *Journal of Geology*, 96, 47-60.
- Lambert, R.StJ., and Chamberlain, V.E., 1990. Isotopic studies on Mesozoic and Tertiary granitoids and their Precambrian basement, BC, Washington, and Idaho. *Proceedings of the 1990 Lithoprobe Cordilleran Workshop*, University of Calgary, 91-98.
- Leeman, W.P.,and Phelps, D.W., 1981. Partitioning of rare earths and other trace elements between sanidine and coexisting glass. *Journal of Geophysical Research*, 86, 10193-10199.
- Mahood, G., and Hildreth, W., 1983. Large partition coefficients for trace elements in high-silica rhyolites. *Geochimica et Cosmochimica Acta*, 47, 11-30.
- Magaritz, M., and Taylor, H.P., 1986. Oxygen 18/Oxygen 16 and D/H studies of plutonic granitic and metamorphic rocks across the Cordilleran batholiths of southern British Columbia. *Journal of Geophysical Research*, 91, 2193-2217.
- McDonough, M.R., and Parrish, R.R., 1991. Proterozoic gneisses of the Malton complex near Valemount, British Columbia: U-Pb ages and Nd isotopic signatures. *Canadian Journal of Earth Sciences*, 28, 1202-1216.
- Miller, C.F., and Barton, M.D., 1990. Phanerozoic plutonism in the Cordilleran Interior, USA. *In* Plutonism from Antarctica to Alaska, *Edited by* S.M.

- Kay, and C.W. Rapela. Geological Society of America, Special Paper 241, 213-231.
- Miller, C.F., and Mittlefehldt, D.W., 1982. Depletion of light rare-earth elements in felsic magmas. *Geology*, **10**, 129-133.
- Miller, C.F., Watson, E.B., and Harrison, T.M., 1988. Perspectives on the source, segregation and transport of granitoid magmas. *Transactions of the Royal Society of Edinburgh, Earth Sciences*, **79**, 135-156.
- Mittlefehldt, D.W. and Miller, C.F., 1983. Geochemistry of the Sweetwater Wash pluton, California: Implications for "anomalous" trace element behavior during differentiation of felsic magmas. *Geochimica et Cosmochimica Acta*, **47**, 109-124.
- Monger, J.W.H., and Berg, H.C., 1987. Lithotectonic terranes of Western Canada and Southeastern Alaska. Map MF-1874B, United States Geological Survey, 1-12.
- Monger, J.W.H., and Price, R.A., 1979. Geodynamic evolution of the Canadian Cordillera - progress and problems. *Canadian Journal of Earth Sciences*, **16**, 770-791.
- Monger, J.W.H., Price, R.A., and Templeman-Kluit, D.J. 1982. Tectonic accretion and the origin of the two major metamorphic and plutonic belts in the Canadian Cordillera. *Geology*, **10**, 70-75.
- Nagasawa, H., and Schnetzler, C.C., 1971. Partitioning of rare earth, alkali and alkaline earth elements between phenocrysts and acidic igneous magma. *Geochimica et Cosmochimica Acta*, **35**, 953-968.
- Nash, W.P., and Crecraft, H.R., 1985. Partition coefficients for trace element in silicic magmas. *Geochimica et Cosmochimica Acta*, **49**, 2309-2322.
- Parrish, R.R., Carr, S.D., and Parkinson, D.L., 1988. Eocene extensional tectonics and geochronology of the southern Omineca Belt, British Columbia and

- Washington. *Tectonics*, 7, 181-212.
- Patchett, P.J., 1991. Isotope geochemistry and chemical evolution of the mantle and crust. *Reviews of Geophysics*, 29, Supplement, 457-470.
- Patiño Douce, A.E. and Johnston, A.D., 1991. Phase equilibria and melt productivity in the pelitic system: Implications for the origin of peraluminous granitoids and aluminous granulites. *Contributions to Mineralogy and Petrology*, 107, 202-218.
- Patiño Douce, A.E., Humphreys, E.D., and Johnston, A.D., 1990. Anatexis and metamorphism in tectonically thickened continental crust exemplified by the Sevier hinterland, western North America. *Earth and Planetary Science Letters*, 97, 290-315.
- Patiño Douce, A.E., Skjerlie, Draper, D.S., and Johnston, A.D., 1991. Partial melting of mixed lithology crustal protoliths: Preliminary experimental results. *Transactions of the American Geophysical Union*, 72, p.542.
- Rapp, R.P., and Watson, E.B., 1986. Monazite stability and dissolution kinetics: implications for the thorium and light rare earth chemistry of felsic magmas. *Contributions to Mineralogy and Petrology*, 94, 304-316.
- Rapp, R.P., Watson, E.B., and Miller, C.F., 1991. Partial melting of amphibolite/eclogite and the origin of Archean trondhjemites and tonalites. *Precambrian Research*, 51, 1-25.
- Reesor, J.E., 1958. Dewar Creek map-area with special emphasis on the White Creek batholith, British Columbia. *Geological Survey of Canada, Memoir* 292.
- Reesor, J.E., 1973. Geology of the Lardeau map-area, east half, British Columbia. *Geological Survey of Canada, Memoir* 369.
- Rushmer, T., 1991. Partial melting of two amphibolites: Contrasting experimental results under fluid-absent conditions. *Contributions to*

- Mineralogy and Petrology, 107, 41-59.
- Rutter, J.M., and Wyllie, P., 1988. Melting of vapour-absent tonalite at 10 kbar to simulate dehydration-melting in the deep crust. *Nature*, 331, 159-160.
- Schnetzler, C.C., and Philpotts, J.A., 1970. Partition coefficients of rare-earth elements between igneous matrix material and rock-forming mineral phenocrysts - II. *Geochimica et Cosmochimica Acta*, 34, 331-340.
- Sevigny, J.H., 1988. Geochemistry of Late-Proterozoic amphibolites and ultramafic rocks, southeastern Canadian Cordillera. *Canadian Journal of Earth Sciences*, 25, 1323-1337.
- Sevigny, J.H., Parrish, R.R., and Ghent, E.D., 1989. Petrogenesis of peraluminous granites, Monashee Mountains, southeastern Canadian Cordillera. *Journal of Petrology*, 30, 557-581.
- Shand, S.J., 1949. *Eruptive Rocks*. John Wiley and Sons, New York.
- Shaw, D.M., 1970. Trace element fractionation during anatexis, *Geochimica et Cosmochimica Acta*, 34, 237-242.
- Silver, L.T., and Chappell, B.W., 1988. The Peninsular Ranges batholith: An insight into the evolution of the Cordilleran batholiths of southwestern North America. *Transactions of the Royal Society of Edinburgh, Earth Sciences*, 79, 105-122.
- Skjerlie, K.P., and Johnston, A.D., 1992. Vapor-absent melting at 10 kbar of a biotite- and amphibole-bearing tonalitic gneiss: Implications for the generation of A-type granites. *Geology*, 20, 263-266.
- Streckeisen, A.L., 1973. Plutonic rocks: Classification and nomenclature recommended by the IUGS Subcommittee on the Systematics of Igneous Rocks. *Geotimes*, 18, 26-30.
- Taylor, H.P., 1968. The oxygen isotope geochemistry of igneous rocks. *Contributions to Mineralogy and Petrology*, 19, 1-71.

- Taylor, H.P., 1980. The effects of assimilation of country rock by magmas on $^{18}\text{O}/^{16}\text{O}$ and $^{87}\text{Sr}/^{86}\text{Sr}$ systematics in igneous rocks. *Earth and Planetary Science Letters*, **47**, 243-254.
- Taylor, H.P., and Sheppard, S.M.F., 1986. Igneous rocks I: Processes of isotopic fractionation and isotope systematics. *In Stable Isotopes in High Temperatures Geological Processes*, Edited by J.W. Valley, H.P. Taylor, and J. O'Neil, *Reviews in Mineralogy* 21, Mineralogical Society of America, Chelsea, 227-271.
- Thy, P., Beard, J.S., and Lofgren, G.E., 1990. Experimental constraints on the origin of Icelandic rhyolites. *Journal of Geology*, **98**, 417-421.
- Trønnes, R.G., and Brandon, A.D., 1992. Mildly peraluminous high-silica granites in a continental rift: the Drammen and Finnemarka batholiths, Oslo Rift, Norway. *Contributions to Mineralogy and Petrology*, **109**, 275-294.
- Vielzeuf, D., and Holloway, J.R., 1988. Experimental determination of the fluid-absent melting relations in the pelitic system. *Contributions to Mineralogy and Petrology*, **98**, 257-276.
- Wall, V.J., Clemens, J.D., and Clarke, D.B., 1987. Models for granitoid evolution and source compositions. *Journal of Geology*, **95**, 731-749.
- Wanless, R.K., Loveridge, W.D., and Mursky, G., 1968a. A geochronological study of the White Creek batholith, southeastern British Columbia. *Canadian Journal of Earth Sciences*, **5**, 375-386.
- White, A.J.R., and Chappell, B.W., 1977. Ultrametamorphism and granitoid genesis. *Tectonophysics*, **43**, 7-22.
- White, D., Asudeh, I., and Zelt, C., 1992. Crustal thickening beneath the Canadian Eastern Cordillera. *Proceedings of the 1992 Lithoprobe Cordilleran Workshop*, University of Alberta, p.131.

- Wickham, S.M., 1987. The segregation and emplacement of granitic magmas. *Journal of the Geological Society of London*, 144, 281-297.
- Wolff, M.B., and Wyllie, P.J., 1991. Dehydration-melting of solid amphibolite at 10 kbar: Textural development, liquid interconnectivity and applications to the segregation of magmas. *Mineralogy and Petrology*, 44, 151-179.
- Wyborn, C., and Chappell, B.W., 1986. The petrogenetic significance of chemically related plutonic and volcanic rocks. *Geological Magazine*, 123, 619-628.
- Zen, E.A., 1986. Aluminum enrichment in silicate melts by fractional crystallization: Some mineralogic and petrographic constraints. *Journal of Petrology*, 27, 1095-1117.
- Zen, E.A., 1988. Thermal modelling of stepwise anatexis in a thrust-thickened sialic crust, *Transactions of the Royal Society of Edinburgh, Earth Sciences*, 79, 223-35.
- Zen, E.A., and Hammarstrom, J.M., 1984. Magmatic epidote and its petrologic significance. *Geology*, 12, 515-518.

Chapter 5

Mesozoic Granitoid Magmatism in the Omineca Belt of Southeast British Columbia: Implications for the Generation of Silicic Magmas in the North American Cordillera

Alan D. Brandon¹, Alan D. Smith², and Richard StJ. Lambert
Department of Geology
University of Alberta
Edmonton, Alberta T6G 2E3
Canada

1 - Present Address:
Department of Earth, Atmospheric,
and Planetary Sciences
Massachusetts Institute of Technology
Cambridge, MA, USA 02139-4307

2 - Present Address:
Department of Earth Sciences
Cheng Kung National University
1 Tahseu Road
Tainan, Taiwan 700, R.O.C.

Submitted to Journal of Geophysical Research

Introduction

The relationship between Phanerozoic granitoids and the orogenic belts in which they reside in western North America has been the focus of numerous studies. In many of these orogenic belts, especially within the western United States, models for the petrogenesis of granitoids, and factors controlling the timing of magmatism have been addressed in some detail. Until recently, few studies have been directed toward understanding the petrogenesis of granitoids found within the Omineca Belt in southeast British Columbia (SEBC). Large volumes of granitoid rocks are exposed with ages from Middle Jurassic to Eocene in SEBC, northern Idaho, and northern Washington (Fig. 5.1). These magmas were emplaced in a region undergoing a series of

tectonic changes, from terrane accretion and compressional tectonics in the Mesozoic (Monger et al. 1982, Lambert and Chamberlain 1988) to extensional tectonics and core complex formation in the late-Cretaceous to Eocene (Armstrong 1982, Parrish et al. 1988). Within this changing tectonic framework, the compositions of the granitoids also changed with time. In the Middle Jurassic, a N-S trending belt dominated by low-K₂O granodiorites and tonalites with rock types ranging from diorite to granite were emplaced in SEBC (Fig. 5.2). In the mid-Cretaceous, a group of high-K₂O granodiorite and granite plutons formed, which was followed by magmatism in the late-Cretaceous to Eocene that included syenites and granites, and Eocene volcanic rocks (Fig. 5.2).

In this paper, major, trace element, and Sr, Nd, Pb isotopic data for the Middle Jurassic Raft, Galena Bay, and Mt. Toby plutons in the Omineca Belt are presented. These data, combined with compositional data from plutons in the Omineca Belt presented here help determine the tectonic settings, constrain the factors contributing to granitoid petrogenesis in SEBC and the development of the Omineca Belt during the Middle Jurassic to mid-Cretaceous. These results indicate that the Middle Jurassic plutons have petrological and geochemical characteristics that are best explained by basalt-crust interaction in the lower crust prior to emplacement in the middle to upper crust. Granitoids from the SEBC Middle Jurassic suite have compositional and lithological characteristics similar to Mesozoic granitoid suites found along the margins of western North America in large batholiths, such as the Peninsular Ranges, Sierra Nevada, and Idaho batholiths, and suggest that the former were emplaced in association with a volcanic arc and subduction. The mid-Cretaceous granitoids have chemical characteristics that are consistent with derivation from crustal sources by anatexis, in response to crustal thickening

and possibly basalt underplating. The SEBC mid-Cretaceous suite have similar characteristics to Mesozoic plutons in the Cordilleran interior within the western United States. The factors controlling the change in character of the Mesozoic granitoids in SEBC may have also played a role in the generation of their analogous rocks in the western United States.

Geology

The Omineca Belt is a plutonic and metamorphic belt in the Canadian Cordillera that separates Proterozoic and Paleozoic continental sediments of the Rocky Mountain Belt from Paleozoic and Mesozoic accreted terranes of probable oceanic origin (Monger and Price 1979, Monger et al. 1982). Throughout much of the Cordillera, the Omineca Belt comprises the Paleozoic Barkerville and Kootenay terranes, and Proterozoic metasediments of the Windermere and Purcell Groups (Fig. 5.1). The Barkerville and Kootenay terranes have been interpreted as allochthonous slivers of sedimentary rocks detached from the continental margin (Monger and Berg 1987). A similar origin has also been suggested for the Windermere and Purcell Groups, which along with the Kootenay and Barkerville terranes may comprise a single superterrane (Terrane III, Chamberlain and Lambert 1985). In southeast British Columbia (SEBC) the Omineca Belt also includes several Eocene metamorphic core complexes and associated igneous rocks (Armstrong 1982, Parrish et al. 1988). The Okanagan complex contains reworked strata of the Quesnel Terrane, part of the microcontinent Terrane I (Monger et al. 1982) which was accreted to the Barkerville and Kootenay Terranes in the Early to Middle Jurassic. Terrane II, another microcontinent composed of the Wrangell and Alexander terranes, accreted to Terrane I in the Cretaceous (Monger et al. 1982, Thorkelson and Smith 1989).

Two phases of plutonism make up the extensive magmatic features of the southern Omineca Belt during the Mesozoic (Armstrong 1988). Early to Middle Jurassic plutons intrude both Terrane I and the Barkerville, Kootenay and Windermere-Purcell terranes (Figs. 1 and 2). Zircons have yielded U-Pb ages of 162-175 Ma for the Nelson, Galena Bay, Raft, Kuskanax, and Spruce Grove plutons (Ghosh 1986, Parrish and Armstrong 1987, Calderwood et al. 1990, Parrish and Wheeler 1983, Carr 1991a, 1991b), and a K-Ar hornblende age of 166 Ma was derived for the Mt. Toby stock (Wanless et al. 1968, date recalculated by Archibald et al. 1983, using new constants).

The Early to Late Cretaceous plutons (Bayonne, Skelly Creek, Fry Creek, White Creek, Horsethief Creek, Bugaboo, and several others, Fig. 5.2) mainly occur east of the Middle Jurassic plutons and in the Kootenay terrane and in the Windermere and Purcell groups, except for the Salmo and Wallack Creek plutons which intruded along the suture of the Quesnel and the Kootenay terranes. The timing of a mid-Cretaceous event is partly constrained by Rb-Sr isochrons of approximately 98 to 115 Ma obtained on the White Creek pluton (Wanless et al. 1968, Brandon and Lambert 1992a), the Wallack Creek and Salmo plutons (Einarsen 1990, Einarsen personal comm.), the Mt. Baldy batholith (Calderwood et al. 1990), and the Bugaboo, Horsethief Creek, and Fry Creek plutons (Brandon and Lambert 1992a). K-Ar ages for muscovite and biotite of 102 Ma were obtained for the Summit Stock (Archibald et al. 1983). U-Pb zircon ages of 77 Ma for the Whatshan batholith which intruded into Quesnellia (Fig. 5.2) suggests that magmatism in the OCB extended to the Late Cretaceous (Carr 1991a, 1991b).

Geophysical and geochemical evidence suggest that the crust during Mesozoic plutonism consisted of the same units presently extending from the Rocky Mountain Trench west to the western edge of the Nelson batholith (Cook

et al. 1988, Cook et al 1990, Carr and Brown 1990, Ghosh 1990, Ghosh 1991). The basement consisted of the Quesnellia terrane rocks which are underlain by units in the Kootenay and Purcell-Windermere terranes interleaved by a complex series of west-dipping thrust faults, and the older (early Proterozoic) North American cratonic basement that extended west to the western edge of the Omineca Belt during the Early Jurassic (Ghosh 1991). This basement package in its present position has been traced from between 47° to 53° N (Armstrong et al. 1989, Armstrong et al. 1991).

Sampling, lithologies, and petrography

Locations, rock types, and estimated mineral abundances for the Raft, Galena Bay, and Mt. Toby plutons are listed in Appendix 5.1. Granitoid lithologies occurring within these plutons span the range from diorite to tonalite to granite reported for other Middle Jurassic plutons within the Omineca Belt in SEBC, including the Nelson and Bonnington plutons (Little 1960, Ghosh 1986) and the Glacier Stock (Reesor 1973). The Raft batholith has lithologies ranging from quartz diorite to tonalite to granite. The quartz diorites are primarily composed of euhedral to subhedral plagioclase, hornblende, and biotite, with minor amounts of alkali feldspar, quartz, and epidote. The tonalites differ from the quartz diorites in having larger amounts of quartz and generally less hornblende. The granodiorites contain hornblende and biotite as the primary mafic phases, while the granites contain biotite and in some cases muscovite. Microcline is observed as a subhedral groundmass phase in most of the lithologies, and as perthitic phenocrysts in the granodiorites and granites. In the samples studied, the minerals showed euhedral to subhedral habit and no indications of

disequilibrium such as corroded crystals, resorbed rims, or rims enclosing minerals of different compositions.

The Galena Bay stock consists of a 2-mica granite with minor amounts of subhedral to euhedral biotite and muscovite. Euhedral garnet is found as a minor phase in the granites and aplites within Galena Bay. The Mt. Toby stock has lithologies ranging from quartz monzodiorite to granite (Reesor 1973). The samples collected for this study were a quartz monzodiorite and a granodiorite, both containing euhedral to subhedral epidote. The quartz monzodiorite contains orthopyroxene and clinopyroxene both in various stages of corrosion enclosed by green amphibole rims. Several epidote crystals were observed with rims of brown amphibole. In both Raft and Mt. Toby, the subhedral to euhedral character of epidote, its tendency to cluster with magmatic hornblende and biotite, and its occasional core/rim relationship with hornblende, are all consistent with a magmatic origin for this mineral phase (Zen and Hammarstrom 1984).

Analytical techniques

X-ray fluorescence (XRF) data on whole rock powders were obtained from the XRF lab at Washington State University. Precision and accuracy are reported in Hooper and Johnson (1987) and Brandon (1989). Instrumental neutron activation analysis (INAA) data were obtained on whole rock powders at the University of Oregon INAA lab using the methodology of Gordon et al. (1968). Reproducibility of whole rock standards used for INAA are reported in Brandon (1989). Estimates of precision (2σ) for the trace element analyses by INAA are as follows: +/- 3% - Th, Ta, Sc, Ce, Sm; 4% - Hf; 5% - La, Eu, Tb, Lu; and 6% - U, Cr, Co, Nd, and Yb. Major and trace element analyses are reported

in Table 5.1, except for U, Th (by INAA) and Pb (by XRF) which are listed in Table 5.3.

Dissolution and chemical separation techniques, and mass spectrometer procedures for whole rock Sr, Nd, and Pb isotope analysis are reported in Trønnes and Brandon (1992) and Brandon and Lambert (1992b). Sr and Pb isotopic results were obtained on a VG MM30 single collector mass spectrometer at the University of Alberta. $^{87}\text{Sr}/^{86}\text{Sr}$ ratios during the runs were corrected for fractionation using $^{86}\text{Sr}/^{88}\text{Sr}$ equal to 0.1194. Replicate runs for the NBS 987 Sr standard gave $^{87}\text{Sr}/^{86}\text{Sr} = 0.710249 \pm 44$ (2σ). Values for NBS 981 Pb standard used by the University of Alberta isotope group are $^{206}\text{Pb}/^{204}\text{Pb} = 16.9371$, $^{207}\text{Pb}/^{204}\text{Pb} = 15.4913$, and $^{208}\text{Pb}/^{204}\text{Pb} = 36.7213$. Nd isotope ratios were obtained on a VG 354 5 collector mass spectrometer. $^{143}\text{Nd}/^{144}\text{Nd}$ ratios were corrected for fractionation relative to $^{146}\text{Nd}/^{144}\text{Nd}$ equal to 0.7219. Replicate runs for the LaJolla Nd standard gave $^{143}\text{Nd}/^{144}\text{Nd} = 0.511817 \pm 12$ (2σ). $^{143}\text{Nd}/^{144}\text{Nd}$ ratios in Table 5.2 were normalized relative to $^{143}\text{Nd}/^{144}\text{Nd} = 0.511855$ for the LaJolla Nd standard. Age corrected $^{87}\text{Sr}/^{86}\text{Sr}$ and $^{143}\text{Nd}/^{144}\text{Nd}$ ratios are reported using ϵ notation (DePaolo 1988). The 2σ errors for initial ϵ_{Sr} are from ± 0.76 to 5.0 with increasing Rb/Sr, and ϵ_{Nd} at 165 Ma are from ± 0.34 to 0.46 with increasing Sm/Nd, using the 2σ errors on Rb, Sr, Sm, and Nd abundances, and errors for the reproducibility of isotopic ratios measured on the standards.

Compositional features of the SEBC granitoids

Major and trace element compositions

Major and trace element abundances for the Raft, Galena Bay, and Mt. Toby plutons are listed in Table 5.1. Tonalites are prevalent in the Middle Jurassic suite, but have not been observed in the mid-Cretaceous plutons in the

southern Omineca Belt. SiO_2 versus $\text{FeO}^*/(\text{FeO}^*+\text{MgO})$ distinguishes subalkaline igneous rocks as calc-alkaline or tholeiitic (Fig. 5.3). The most primitive quartz diorites and diorites are calc-alkaline, and the granitoids remain in the calc-alkaline field until higher SiO_2 contents where the band crosses into the tholeiitic field. There is no discernable difference in the trends for the Middle Jurassic and mid-Cretaceous granitoids except the Middle Jurassic suite extends to lower SiO_2 contents to 51 wt.% in the Nelson and Bonnington samples. The tonalites from Raft fall within the band for all of the samples. Both suites represent typical calc-alkaline magmatic trends.

The alumina saturation index (ASI = mole % $\text{Al}_2\text{O}_3/(\text{CaO}+\text{Na}_2\text{O}+\text{K}_2\text{O})$ corrected for apatite following Shand 1949, and Zen 1986) increases from 0.5 in the quartz diorites and diorites to ca. 0.9 to 1.06 for the granodiorites and biotite granites (Fig. 5.4) indicating metaluminous (M) to weakly peraluminous chemistry (wP). High-silica two-mica granites, located within the mid-Cretaceous White Creek and Fry Creek batholiths, have larger ASI's (> 1.1, Brandon and Lambert 1992b, 1992c) and are strongly peraluminous (sP). These compositional relationships fall into the categories for granitoids within the Cordilleran interior defined by Miller and Barton (1990), where alumina saturation is related to primary mineralogy. Granitoids containing 1 - hornblende +/- biotite and clinopyroxene, or 2 - biotite only, or 3 - containing muscovite, cordierite, or Ca-poor garnet, were classified as M, wP, and sP, respectively. Although granites in the Galena Bay stock have ASI's lower than 1.1 (Table 5.1 and Fig. 5.4), the primary garnet in this pluton is an sP granite in this classification scheme.

Trace element normalized plots (spidergrams) of granitoid samples characteristic of the compositional types of each suite are shown in Figure 5.5. The mid-Cretaceous granitoids show enrichments in Rb, Th, Ta, Nb, and Ce, and

less in Ba, with steeply declining abundances from Th to Yb compared with oceanic ridge granites (Pearce et al. 1984). The enrichments in Nb and Ta are typical of granitoids found in within-plate tectonic settings, while the rest of the trace element abundances for these granitoids show characteristics of both within-plate and collisional granites. The sP granites have lower abundances for most trace elements than the M-wP granitoids, but have Nb and Ta concentrations and overall similar shaped patterns to the other mid-Cretaceous granitoids (Fig. 5.5). The Middle Jurassic granitoids have lower Rb, Th, Ta, and Nb and generally higher Ce to Yb abundances than the mid-Cretaceous granitoids with a resulting hump in the patterns over the large ion lithophile elements (K₂O, Rb, Ba, and Th) and a flattening out of the patterns from Ta to Yb. These trace element characteristics are indistinguishable from those of calc-alkaline granites found in volcanic arc settings (Fig. 5.5), including the relative larger Ba and smaller Ta and Nb abundances which characterize calc-alkaline arc magmas. As with the mid-Cretaceous sP granites, the Galena Bay sP granite has generally lower abundances in trace elements but an overall similar pattern compared to the other Middle Jurassic granitoid types.

The distinct trace element features between the Middle Jurassic and mid-Cretaceous granitoids can be illustrated using tectonic discrimination diagrams. In the Rb versus Nb + Y and Nb versus Y diagrams (Pearce et al. 1984) shown in Figures 5.6 and 5.7, the majority of Middle Jurassic granites and granodiorites plot in the volcanic arc granites (VAG) field, with only minor overlap into the within-plate granites (WPG) field. Granitoids from volcanic arcs have chemical compositions which are derived in part by fractional crystallization from primitive (mantle-derived mafic) arc magmas with contamination from crustal sources (Pearce et al. 1984). The mid-Cretaceous

granites and granodiorites plot primarily within the WPG field in both diagrams. The mid-Cretaceous sP granites cluster around the juncture of the WPG, VAG, and syn-collision (syn-COLG fields) in Figure 5.6, and across the WPG - VAG+syn-COLG boundary in Figure 5.7, and are distinct from the rest of the mid-Cretaceous suite. In Figure 5.7, the granitoids from both the Middle Jurassic and mid-Cretaceous groups have similar abundances in Y and are distinguished primarily in Nb contents for both diagrams. Fractional crystallization from mantle-derived basaltic magmas cannot alone account for the trace element enrichments in WPG granites, and a major contribution of a crustal component is required to explain the high abundances of Rb, Th, and LREE (Pearce et al. 1984). By analogy, the generally greater Rb and Nb abundances in the mid-Cretaceous granitoids could reflect a larger contribution of a crustal component than in the Middle Jurassic granitoids. However, either some mantle component such as ancient subcontinental lithosphere identified under the Columbia River Province in Washington (Smith 1992) or a high Nb crustal component such as found in the Malton gneiss complex, a package of Precambrian basement exposed in SEBC (Chamberlain et al. 1988), is required to account for the enrichments in Nb, as suggested by Brandon and Lambert (1990) based on isotopic constraints on the White Creek batholith.

An alternative mechanism to produce the distinctions in Rb and Nb between the granitoids from the two age groups is by accumulation or fractionation of mineral phases found within both groups. In Figures 5.6 and 5.7, accumulation trends for the addition of 50% cumulate material for the major mineral phases, and qualitative trends for accessory phases are illustrated. All of the minerals except for clinopyroxene are found within both sets of granitoids, and clinopyroxene is found only within more mafic

compositions within the Middle Jurassic suites (Ghosh 1986, Reesor 1973, and this study). Petrographic data for granitoids from both suites (Brandon and Lambert 1992b, 1992c, and this study) indicates that the proportions of mineral phases in similar lithologies from each suite are found in similar amounts. Furthermore, isotopic distinctions (see below) between the suites cannot be accounted for by mineral fractionation or accumulation. It is therefore unlikely that the trace element distinctions between the mid-Cretaceous and Middle Jurassic granitoids can be completely accounted for by mineral accumulation or fractionation differences during differentiation.

A plot of Ce/Nb versus Ba/Nb further distinguishes the Middle Jurassic and mid-Cretaceous granitoids (Fig. 5.8). This diagram illustrates the relationship during petrogenetic processes for three different groups of trace elements, large-ion lithophile elements (Ba), high field strength elements (Nb), and light rare earth elements (Ce). The range of compositions for volcanic arc magmas reflects mixing between subduction-derived fluids with very high Ce/Nb (> 12) as Nb is severely depleted in these fluids (Hawkesworth 1979, Tatsumi et al. 1986, Brandon and Goles 1988, Brandon 1989, Smith 1992), and peridotitic mantle with much lower Ce/Nb (1 to 2) and Ba/Nb of 5 to 20 (EMORB and OIB source mantle, Saunders et al. 1988, Smith 1992).

Arc magmas which have interacted with young oceanic crust in the Pacific Northwest including SEBC should have Ce/Nb and Ba/Nb ratios plotting within the field of the Cascade arc in Figure 5.8, because the mantle domains developed during the Phanerozoic in this region reflect oceanic OIB source mantle, combined with MORB mantle and subduction derived fluids (Menzies 1989, Smith 1992). The Late Cretaceous Idaho Batholith represents an arc tectonic setting where ancient continental crust and and/or associated enriched mantle lithosphere (EM1 and EM2 domains, Menzies 1989) are possible

sources, as it formed within Precambrian continental crust in the Pacific Northwest (Hyndman and Foster 1988). Sr and Nd isotopic compositions for the range in magmas types within the Idaho Batholith suggests mixing between mafic arc-mantle melts and silicic melts from Proterozoic orthogneisses and metasediments (i.e., initial $\epsilon_{Nd} = +3$ to $+7.6$ and $\epsilon_{Nd} = -7.4$ to -15.7 , respectively, Fleck 1990). The larger Ba/Nb ratios for the Idaho batholith compared to the Cascade arc probably signals interaction with Proterozoic crust (Figure 5.8). Similar Proterozoic Belt-Purcell Supergroup metasediments and basement gneisses underlie Washington, Idaho, and SEBC (Fig. 5.1, Armstrong et al. 1991, Lambert and Chamberlain 1990). The Middle Jurassic granitoids of SEBC for the most part overlap the compositions of the Idaho batholith (Fig. 5.8); they may have had a similar origin, including contamination of mantle-derived magmas by Proterozoic crust.

The mid-Cretaceous granitoids only partially overlap with the Middle Jurassic and the Idaho batholith rocks (Fig. 5.8). Both Ba/Nb and Ce/Nb for the most part decrease from intermediate to felsic lithologies in the mid-Cretaceous suite, which is the opposite case for the Idaho batholith suite. The Middle Jurassic granitoids show no correlation of rock type with Ba/Nb and Ce/Nb ratios. As shown in the spidergrams in Figure 5.5 and for Nb versus Y (Fig. 5.7) the mid-Cretaceous granitoids have larger Nb and smaller Ba abundances which would in part account for the smaller Ce/Nb and Ba/Nb ratios in these rocks. If no arc mantle component (mantle-derived magmas composed of various proportions of OIB, MORB, and subduction-derived fluid sources as discussed above) is involved in the petrogenesis of these rocks, then the Ba and Nb distinctions in the mid-Cretaceous suite should reflect the source(s) of the granitoids, being primarily crustal in origin for the mid-Cretaceous magmas. Isotopic evidence discussed in the next section suggests

that the compositional distinctions of the mid-Cretaceous granitoids most likely reflects a crustal source, with little or no contribution from a mantle-derived magma, which is consistent with the inferences from trace elements.

Isotopic compositions

The Rb-Sr and Sm-Nd isotopic compositions for samples from the Raft, Galena Bay, and Mt. Toby plutons are listed in Table 5.2. The Raft samples have initial ϵ_{Sr} ranging from -27.4 to +12.8 and initial ϵ_{Nd} from +0.1 to -6.8. The one Galena Bay sP granite sample has ϵ_{Sr} of +13.1 and ϵ_{Nd} of -6.1 and falls within the range of variation for the Raft samples. The Mt. Toby samples extend to higher ϵ_{Sr} of up to +32.9, but have ϵ_{Nd} values falling within the range of the Raft and Galena Bay samples. In Figure 5.9, available data for Middle Jurassic and mid-Cretaceous granitoids, Precambrian basement gneisses, and Proterozoic metasediments from the southern Omineca Belt are plotted for ϵ_{Sr} versus ϵ_{Nd} (data from Ghosh 1986, Ghosh and Lambert 1989, Lambert and ~~Crook~~ ^{Crook} 1990, Armstrong et al. 1991, Brandon and Lambert 1992b, 1992c). The Raft, Galena Bay, and Mt. Toby samples mostly plot within the field for Middle Jurassic granitoids, with some of the Raft samples plotting to slightly higher ϵ_{Nd} and lower ϵ_{Sr} . These granitoids have Sr-Nd compositions similar to the granitoids within the Sierra Nevada and Peninsular Ranges batholiths formed in volcanic arcs (Fig. 5.9) The field for the Middle Jurassic granitoids partly overlaps the field for the mid-Cretaceous suite at its lower ϵ_{Nd} and higher ϵ_{Sr} end. The mid-Cretaceous M-wP granitoids extend to lower ϵ_{Nd} and higher ϵ_{Sr} , into the field for Precambrian basement rocks for the southern Omineca Belt, and have similar Sr-Nd isotopic compositions to M-wP granitoids in the Cordilleran interior of the western United States (Fig. 5.9). The sP granites and associated aplites from the White Creek and Fry Creek plutons plot

in a distinct field at higher ϵ_{Sr} and lower ϵ_{Nd} and completely within the field for basement rocks and overlapping the field for sP granites from the Cordilleran interior. For the Precambrian basement gneiss data, there is no systematic change in ϵ_{Nd} and ϵ_{Sr} with lithologic composition (Fig. 5.9). The complicated lithologic relationships within the basement exposures for these gneisses (Chamberlain 1983, Chamberlain et al. 1988, Armstrong et al. 1991, McDonough and Parrish 1991), precludes any direct correlation of any of the Mesozoic granitoid types with a distinct basement lithology as a possible source by isotopic distinctions alone. It can only be qualitatively ascertained that an increase in crustal contribution occurred from the Middle Jurassic granitoids to the M and wP mid-Cretaceous granitoids. The mid-Cretaceous sP granites have the greatest amount of a crustal component and these rocks are likely the result of crustal melting without a mantle-derived mafic magma precursor (Brandon and Lambert 1992b, 1992c).

Table 5.3 lists the U-Th-Pb isotopic compositions for the Raft, Galena Bay, and Mt. Toby plutons. The initial Pb isotopic compositions for all of the Mesozoic granitoids plot as bands above the NRHL (Hart 1984) along mixing zones between upper crust with high time-integrated U/Pb and lower crust with a low time-integrated U/Pb (Fig. 5.10). Pb isotope ratios for galenas from Eocene Ag-Pb-Zn-Au veins found crosscutting and extending beyond the north boundary of the Nelson batholith into the country rock, have been interpreted as a lower crust Pb component (Beaudoin et al. 1992), and provides evidence for this type of lower crust underlying SEBC. For $^{207}Pb/^{204}Pb$ versus $^{206}Pb/^{204}Pb$, the band for the SEBC granitoids has a slope of 0.085 and corresponds to a Pb model age of 1.33 Ga (Ghosh 1986). A regression line for Pb in feldspar of Cordilleran interior granitoids from the western United States which plot in a band overlapping the SEBC granitoids and gives a 1.6 Ga model

age (Fig. 5.10). There is too much scatter in $^{208}\text{Pb}/^{204}\text{Pb}$ and $^{206}\text{Pb}/^{204}\text{Pb}$ for a single model age regression line (Fig. 5.10), and the data fall between regression lines that which have Pb model ages of 1.0 and 2.3 Ga (Ghosh 1986). Data for the M-wP granitoids from both suites show nearly complete overlap with the Middle Jurassic suite extending to lower $^{206}\text{Pb}/^{204}\text{Pb}$, $^{207}\text{Pb}/^{204}\text{Pb}$, and $^{208}\text{Pb}/^{204}\text{Pb}$. The mid-Cretaceous sP granites extend to higher initial Pb isotopic compositions than M-wP granitoids from both suites. Available data for Proterozoic metasediments (no data are available for basement gneisses) generally plot along the bands for the Mesozoic granitoids, and extend to much higher $^{206}\text{Pb}/^{204}\text{Pb}$, $^{207}\text{Pb}/^{204}\text{Pb}$, and $^{208}\text{Pb}/^{204}\text{Pb}$ beyond the bounds of Figure 5.10. The initial Pb isotope characteristics for the Mesozoic granitoids therefore appear to reflect the Pb isotopic composition of the Precambrian basement in the southern Omineca Belt and do not yield any evidence for the role of mantle-derived mafic magmas in their petrogeneses.

Figures 5.11 and 5.12 display Nd and Pb isotopic variation with SiO_2 . The M-wP granites show little variation in ϵ_{Nd} for the range in SiO_2 from both suites (Fig. 5.11). The mid-Cretaceous M-wP rocks show an increase in $^{206}\text{Pb}/^{204}\text{Pb}$ with increasing SiO_2 , and plot in a distinct field from the Middle Jurassic M-wP rocks (Fig. 5.12), suggesting that distinct processes resulted in their isotopic character. The mid-Cretaceous sP granitoids plot as distinct fields with restricted ranges in SiO_2 . Crustal rocks and basaltic magmas have similar abundances in Nd, and Nd isotopic compositions of igneous rocks are a more realistic indication (as opposed to Sr and Pb isotopes) of the proportions of mantle and crust contributing to their petrogeneses (Johnson 1991). The Middle Jurassic granitoids extend to higher values of ϵ_{Nd} than the basement rocks in the Omineca Belt, and require a contribution from a high ϵ_{Nd} , mantle-derived basaltic component (Fig. 5.11). The mid-Cretaceous granitoids

completely overlap the range of ϵ_{Nd} for the SEBC basement and are the result of a higher contribution of this crust relative to the Middle Jurassic granitoids.

Discussion

Origin of the southern Omineca Belt Mesozoic granitoids

The chemistry of the SE British Columbia granitoids suggests the occurrence of two distinct magmatic events with unique petrogenetic histories and within different tectonic settings in the Mesozoic. The Middle Jurassic magmas formed in a volcanic arc and the granitoids were evolved from mantle-derived magma which interacted with and were contaminated by Precambrian crust. Evidence to support this origin for the Middle Jurassic granitoids includes observations on the lithologies and geochemistry of these rocks. Abundant tonalites, low-K granodiorites, and diorites, and the presence of gabbroic rocks within this suite are characteristic of Phanerozoic volcanic arc granitoid suites throughout the Cordillera including the Andes, Peninsular Ranges in California and Mexico, Sierra Nevada in California, and the Coast Ranges batholith in British Columbia, Yukon, and Alaska (Pitcher 1984, Gromet and Silver 1987, Bateman 1983, Barker and Arth 1990). The trace element compositions, including spidergram patterns, the clustering within the VAG fields in Figures 5.6 and 5.7, and the Ba/Nb and Ce/Nb abundances overlapping those for volcanic arc granitoids formed within Proterozoic crust in the Pacific Northwest, are consistent with a volcanic arc origin for the Middle Jurassic granitoids. Voluminous amounts of basaltic magmas, providing heat for crustal anatexis and as parental magmas to more silicic members, are a characteristic of arc tectonic settings. Abundant basaltic dikes related to the Middle Jurassic Nelson batholith (Little 1960), attests to the presence of mantle-derived magmas associated with these granitoids.

The Sr and Nd isotopic compositions for the Middle Jurassic granitoids plot in a region between the field for low ϵ_{Sr} and high ϵ_{Nd} oceanic mantle array and SEBC crust, and overlap the field for granitoids from Phanerozoic volcanic arcs in southwest North America, and these features are also consistent with a volcanic arc tectonic setting origin where the granitoids represent the end-product of interaction of basaltic magmas with continental crust. Ghosh (1986) used assimilation and fractional crystallization (AFC) modelling to successfully reproduce the isotopic compositions for the Nelson batholith. Such models predict a change in isotopic composition with a change in SiO_2 . Figures 5.11 and 5.12 show that the isotopic composition remains virtually unchanged with increasing SiO_2 , and suggests that contamination and fractional crystallization were decoupled, a more likely scenario for producing evolved silicic magmas (Johnson 1989). The Pb isotopic compositions do not appear to reflect a mantle component (i.e. a component lying along the NHRL) but instead show characteristics of lower and upper crust (Fig. 5.10). Because of the low Pb abundances in basalts and the high abundances of Pb in crustal rocks, magmas which are mixtures from these sources overemphasize the crustal component(s) in the Pb isotopic ratios (Johnson 1991). In open system interaction of basaltic magma with crust in mixing, assimilation, storage and homogenization (MASH) zones in the lower crust underneath volcanic arcs, the Pb isotopic compositions of evolved magmas reflect the crustal component (Hildreth and Moorbath 1988). The crustal Pb isotopic signatures observed in the Middle Jurassic rocks probably reflect this process of contamination and do not preclude a mantle-derived basalt precursor. In summary, the geochemical characteristics of the Middle Jurassic plutonic suite are in accordance with a ~~model~~ where mantle magmas intrude and interact with lower crust in MASH zones, and then differentiate to

produce a range in isotopically similar mafic to silicic granitoids at the intrusion level, a scenario consistent with a volcanic arc tectonic setting.

The mid-Cretaceous suite has lithologic characteristics of granitoids found within a Phanerozoic belt in the Cordilleran interior to the south in the United States. With the exception of the Idaho batholith which appears to be a remnant volcanic arc, M-wP, and sP granodiorites and granites predominate in both the Cordilleran interior and the Omineca Belt mid-Cretaceous suite, and low-K tonalites are minor to absent in both suites (Miller and Barton 1990, Brandon and Lambert 1992b, 1992c). The low Ba, and high Rb and Nb abundances of the mid-Cretaceous suite within the Omineca Belt are indicative of within-plate and collisional tectonic settings and a larger crustal component contribution in these granitoids relative to the Omineca Belt Middle Jurassic granitoids.

The Sr and Nd isotopic compositions also suggest a larger contribution of a crustal component in the mid-Cretaceous suite. The Sr-Nd-Pb isotopic compositions for the M-wP, and sP rock types are indistinct from the analogous rock types within the Cordilleran interior (Fig. 5.9) and suggest a similar petrogenesis. As shown in Figure 5.12, the Pb isotopic variation versus SiO₂ in the mid-Cretaceous suite is distinct from the Middle Jurassic suite, indicating that the crustal Pb isotopic composition for these 2 suites were acquired in different manners. Brandon and Lambert (1992b, 1992c) favor a model where the mid-Cretaceous granitoids were the result of partial melting of different crustal lithologies. Geochemical characteristics which favor this model are: 1 - the complete overlap in Sr, Nd, Pb, and O isotopic compositions for basement lithologies and granitoids; 2 - REE patterns in the granitoids which can be produced by melting of basement lithologies predicted by their major element compositions including amphibolites and tonalites (producing

M-wP granitoids), and pelites (producing sP granites); 3 - Sr and O isotopes, and Sr abundance relationships, which can be most simply modeled with AFC and mixing as interactions of melts derived from the crustal components required by major element compositions and REE patterns; 4 - Eu/Eu* ratios, and Cr and Ni abundances in the most primitive rocks types in the White Creek batholith inconsistent with fractional crystallization from basaltic melts to produce more silicic melts; and 5 - the absence of early- to mid-Cretaceous mafic igneous rocks in the region of Figure 5.2. In conjunction with the evidence cited earlier in the paper, these points preclude a major contribution from a mafic, mantle-derived magma being parental to the intermediate and silicic mid-Cretaceous granitoids, and support a model for crustal melting. Miller and Barton (1990) also note the absence of mantle-derived magma in the Cretaceous to early Paleogene episode of magmatism in the Cordilleran interior, and combined with geochemical evidence, these features favor a model for crustal melting to produce granitoids analogous to the mid-Cretaceous suite in the Omineca Belt.

Development of the Omineca Belt in the late-Mesozoic

The Middle Jurassic and mid-Cretaceous magmatism in the Omineca Belt was produced during a time of growth of western Canada to the west by accretion of exotic terranes (Monger et al. 1982). Intrusion of the Middle Jurassic granitoids overlaps the final stages of amalgamation of Terrane I in Figure 5.1. Amalgamation likely commenced in the Late Triassic with the eastward subduction of oceanic crust, now represented by the Cache Creek terrane, beneath Quesnellia. Imbrication of this subduction zone in the Early Jurassic resulted in the obduction of the Cache Creek terrane and the accretion of Stikinia. These terranes were accreted to the Barkerville and Kootenay

terrane by the closure of a marginal basin, now preserved in the Slide Mountain terrane, in the Early Jurassic (Monger et al. 1982). Contemporaneous with this later event was the accretion of several small terranes (Bridge River, Cadwallader) to the western margin of Terrane I (Rusmore et al. 1988). The Middle Jurassic granitoids may partly represent a magmatic arc related to either of the latter two events. The intrusion of several Middle Jurassic batholiths (the "pinning" batholiths - Nelson, Kuskanax, and Raft, Lambert and Chamberlain 1988) along the suture between Quesnellia and terranes to the east shown in Fig. 5.2, requires that the position of Terrane I and the terranes to the east remained fixed relative to each other thereafter. Paleomagnetic evidence suggests a position of about 23°N for Terrane I in the Middle Jurassic (Monger and Irving, 1980). However, paleomagnetic evidence from the Cache Creek terrane (Cole et al. 1992), and isotopic evidence from rocks within Quesnellia (Smith et al. 1992), both of which are part of Terrane I, suggest that these rocks were in their present position by the Middle Jurassic.

Paleomagnetic evidence from Cretaceous plutons in the southern Coast Range in British Columbia (Spuzzum pluton, Butler et al. 1989, Fig. 5.1) and in the Omineca Belt (Bardoux and Irving 1989) indicates that Terrane I and units to the east were in their present position by the mid-Cretaceous, in agreement with the evidence cited above for these rocks being in place by Early Jurassic. Mid-Cretaceous granitoids in the southern Omineca Belt were emplaced inboard of the Spences Bridge volcanic arc which formed along the western edge of Terrane I (Fig. 5.1, Thorkelson and Smith 1989). These granites formed near the onset of crustal shortening during the late-Mesozoic Sevier Orogeny. The fold and thrust system of the Sevier Orogeny occurred in the Cordilleran interior in association with a belt of coeval granitoid plutons from Arizona and southern California in the south, extending through Nevada and Idaho, and

into SEBC in the Omineca Belt. Prior to the Sevier Orogeny, there was a magmatic quiet period in the southern Omineca Belt (Armstrong 1988). If the mid-Cretaceous granitoids are a result of crustal melting rather than evolved magmas from parental basalt as supported by petrological and geochemical evidence, a thermal event in the lithosphere is needed for crustal anatexis to generate these granitoids. Several mechanisms have been invoked to explain anatexis during the Sevier Orogeny in the Cordilleran interior granitoid belt. These include intrusion of mantle-derived mafic magmas into the crust (Hyndman and Foster 1988), fluid flux from the mantle (Hoisch and Hamilton 1990), increased deep heat flux (Barton 1990), and crustal thickening during thrusting (Patiño Douce et al. 1990).

Evidence for intrusion of mantle-derived magmas in the Idaho Batholith includes syn-plutonic mafic dikes and early tonalite and quartz diorite plutons (Hyndman and Foster 1988). The Idaho batholith was generated above an easterly dipping subduction zone in a volcanic arc (Hyndman and Foster 1988), in a similar situation to what occurred to produce Middle Jurassic magmatism in the Omineca Belt. As discussed above, mafic dikes, low-K tonalite, and quartz diorite are absent in the mid-Cretaceous plutons in SEBC. Also, the OCB mid-Cretaceous granitoids are geochemically distinct from those in the Idaho batholith and from other volcanic arcs.

Fluid flux from the mantle, presumably from dehydration of subducted crust (Hoisch and Hamilton 1990), is an unlikely process to generate anatexis and hence mid-Cretaceous granitoid melts in SEBC. Ce/Nb ratios in the mid-Cretaceous granitoids are too small to be accounted for by subduction-derived fluids (Fig. 5.8). During the Albian (~110 Ma), dehydration of a subducted slab would have occurred much farther west underneath or in the forearc to the Spences Bridge volcanic arc which arose during subduction of an oceanic

basin, the remnants of which are represented by the Methow Tyaughton trough (Thorkelson and Smith 1989).

Increased deep heat flux as a result of mantle upwelling or magmatic underplating, which would heat the lower crust and generate anatexis (Bergantz 1989, Barton 1990), may explain the origin of the mid-Cretaceous granitoids. An increase in the temperature of the lower crust via this process produces a larger crustal component in the granitoids with time, and explains the change in composition for Cretaceous Basin and Range granitoids from early quartz diorites (~110 to 130 Ma) to late sP granites (~70 to 105 Ma) as suggested by Barton (1990). Although a larger contribution of a crustal component is inferred isotopically in the sP granites relative to the M-wP granites, such a model must take into account the nearly contemporaneous M-wP and sP granites in the SEBC mid-Cretaceous plutons, as exemplified by the White Creek batholith (Reesor 1958, Brandon and Lambert 1992c), and the narrow range of crystallization ages for these plutons (about 10-15 m.y., Brandon and Lambert, 1992a) to be valid for the mid-Cretaceous event in SEBC.

The lack of evidence for basaltic magmatism in the early- to mid-Cretaceous in SEBC lends no support for a contemporaneous underplating mechanism. Densities for basaltic melts from 15 to 20 kbar are from 2.85 to 2.8 g/cm³, respectively, and decrease to 2.75 g/cm³ at 0 kbar (Stolper et al. 1981). In continental crust typical for western North America, basaltic magmas become neutrally buoyant and are trapped at about 20 km depth (Glazner and Ussler 1988). For denser crust, intrusion of basalt into the upper crust by basalt would be expected. The Malton gneiss complex consists of approximately 50 volume percent mafic gneiss making it denser than typical basaltic melt. These arguments suggest, therefore, that a basaltic underplate would manifest itself as dikes intruding the overlying Proterozoic metapelites. Basic dikes

associated with the Middle Jurassic Nelson batholith have intruded into crust overlying the basement gneisses (Little 1960), but no mid-Cretaceous dikes are observed at the crustal levels presently exposed.

Alternatively, crustal thickening may be the process which generated the mid-Cretaceous granitoids in SEBC. Thrusting would thicken the crust, which would in turn result in Barrovian metamorphism and crustal anatexis (i.e. dehydration melting) in the presence of hydrous minerals in the protolith (Zen 1988, Patiño Douce et al. 1990). The magmatic episode during the mid-Cretaceous was relatively short (~10 to 15 m.y.), which suggests that heating of the crust occurred over a time interval that was only long enough to generate granitoids in a single magmatic pulse. In crustal thickening via thrusting, it may take as much as 20 to 50 m.y. to generate a melt zone with the critical melt fraction (30-40%, Wickham 1987, Miller et al. 1988) necessary for separation from the source into discrete magma bodies to occur (Zen 1988, Patiño Douce et al. 1990). Melt zones capable of segregation into discrete bodies have been modelled to be at ~35 to 38 Km depth and 800 to 850°C (biotite induced dehydration melting) after 30 to 40 m.y. with an initial/final thickening ratio of about 1.4 (from an initial 36 Km to a final 50 Km, Patiño Douce et al. 1990). Although not strictly applicable to granitoid generation in SEBC, these models demonstrate that conditions favorable for crustal anatexis can occur by crustal thickening in analogous situations.

Hornblende dehydration melting reactions require temperatures of 850 to 920°C at 10 kbar (Clemens and Vielzeuf 1987, Wolff and Wyllie 1991) and higher temperatures at higher pressures. Temperatures in this range would be required to produce the mid-Cretaceous hornblende bearing granitoids by vapor-absent melting of amphibole-rich protoliths. These temperatures are not predicted in the models of Patiño Douce et al. (1990) for the parameters

which they selected. The initial geotherm used by Patiño Douce et al. (1990) was derived using heat production values for an idealized section of Cordilleran crust. Patiño Douce et al. (1990) used a conservative heat flow value through the Moho from the mantle (28 mW/m^2), resulting in a surface heat flow of 60 mW/m^2 , which is an intermediate value for sedimentary basins. A slightly higher heat flow of 69 mW/m^2 , resulting in a higher starting geotherm, can produce from 50 to 75°C hotter temperatures, well within the melting zone (Patiño Douce et al. 1990) and within the range required for hornblende melting reactions. Possible reasons for a higher starting geotherm could be higher crustal heat generation from higher abundances of U, Th, and K, higher mantle heat flow, or a "preconditioned" crust. Volcanic arc formation on continents is accompanied by magmatic underplating (Furlong and Fountain 1986). Underplating probably occurred in the Middle Jurassic in association with the magmatic arc and its plutons in the Omineca Belt, resulting in a hotter crust. Intrusion of 1 to 5 Km thick basaltic sills in the middle to lower crust can readily produce 200 to 300°C temperature increases in the surrounding country rocks, and depending on the original geothermal gradient of the crust, can induce anatexis (Lambert 1983). Furthermore, intrusion of several Km thick sills can raise the ambient temperatures of overlying crust as much as 100°C for time periods of 20 to 40 m.y. and longer after underplating (as constrained using the heat transfer program of Spear and Peacock 1990). As no magmatism occurred between the Middle Jurassic and the mid-Cretaceous, the crust was not heated enough to produce large amounts of melt during this time interval. However, after the onset of crustal thickening, higher temperature melts would be predicted. We suggest, therefore, that the mid-Cretaceous granitoids may have been generated in a preconditioned lower to middle crust by crustal thickening

either associated with the Sevier Orogeny or resulting from the resumption of subduction which eventually led to the closure of the Methow-Tyauhton basin and collision of Terrane II with Terrane I. Underplating associated with the mid-Cretaceous magmatic pulse cannot be completely ruled out, but no geologic evidence is present to support this process for increasing the ambient temperature of the crust during this time interval.

On the basis of geochemical evidence, Brandon and Lambert (1992c) have concluded that the progression in magmatism from M-wP granodiorites to sP 2-mica granites in the White Creek batholith resulted in a melt zone moving upward through the crust, melting hornblende bearing mafic and tonalitic basement gneisses, followed by melting of the overlying metapelites as the sources for these granites, respectively. These conclusions are in accordance with crustal thickening occurring with an initial high ambient temperature in the lower and middle crust, which would result in early high temperature melting followed by lower temperature melting upward as thickening progressed.

Conclusions

Within the Omineca Belt, granitoid magmatism was produced in two pulses in the Middle Jurassic and mid-Cretaceous, followed by late-Cretaceous magmatism at the onset of crustal extension, regional uplift, and core complex formation (Armstrong 1988, Parrish et al. 1988). Recent paleomagnetic evidence suggests that these magmatic pulses occurred after amalgamation and accretion of allochthonous units from the western edge of Terrane I to those bordering the North American hinterlands. The lithologic character, major and trace element, and isotopic compositions for the Middle Jurassic granitoids all support the conclusion that these granites formed in a volcanic

arc, over an easterly-dipping subduction zone on the western edge of Terrane I. These granites were formed by open system mixing between mantle-derived basalts and continental crust. The Pb isotopic compositions for the Middle Jurassic granitoids do not reflect the contribution of a basalt component, and these relations are best explained by acquisition of lower crust Pb isotopic compositions in MASH zones followed contamination of upper crust Pb during ascent to the intrusion level.

The mid-Cretaceous granitoids are geochemically distinct from the Middle Jurassic granitoids in the southern Omineca Belt. Their compositions are characteristic of granitoids formed within continental interiors and in particular are geochemically and petrologically indistinguishable from analogous Phanerozoic granites in the Cordilleran interior of western United States. A larger crustal component is inferred by the isotopic compositions of the mid-Cretaceous granitoids relative to the Middle Jurassic granitoids. Geological and geochemical evidence best conform to a model where the mid-Cretaceous granitoids were the result of melting the crust, with little or no direct input of mantle-derived magmas. Thermal and tectonic considerations suggest a scenario where initial thermal preconditioning of the SEBC lower crust by basaltic underplating in the Jurassic was followed by crustal thickening in the early- to mid-Cretaceous to produce anatexis in the crust.

The shift in compositional variation of granitoid magmatism within the Omineca Belt in the Mesozoic yield important clues to the thermal and tectonic controls for magmatism in the North American Cordillera. Further characterization of magmatism in the Omineca Belt, which occurred in the late-Cretaceous and early Cenozoic is needed to understand in more detail the development of this Phanerozoic orogenic belt through time and its relationship to orogenic belts elsewhere.

Acknowledgements. This research was supported from NSERC operating and Lithoprobe grants to R.StJ. Lambert (1988-1991). Reviews from Rob Creaser, Bob Luth, Tom Chacko, Jonathan Patchett, George Cumming, and Reidar Trønnes improved the paper.

Table 5.1. Major and trace element abundances for samples from the Raft, Galena Bay, and Mt. Toby plutons.

Sample Type	Raft								
	ERa-2 Gr	ERa-3a Gr	ERa-3b Apl	ERa-4 QMD	ERa-5 Gd	ERa-6 QD	ERa-7a Ton	ERa-7b Ton	ERa-8a Gd
SiO ₂	74.29	73.82	74.89	60.79	64.90	52.03	63.83	58.77	66.31
TiO ₂	0.128	0.051	0.065	0.827	0.633	1.245	0.494	1.066	0.590
Al ₂ O ₃	14.52	14.76	14.44	17.47	16.74	18.05	18.63	17.84	16.17
FeO*	0.91	0.29	0.37	4.90	3.98	7.61	3.04	5.95	3.74
MnO	0.033	0.012	0.017	0.115	0.078	0.146	0.058	0.111	0.087
MgO	0.14	0.00	0.02	2.73	2.17	5.53	1.66	3.36	1.98
CaO	1.08	0.43	1.15	5.32	4.18	8.87	4.82	5.67	3.38
Na ₂ O	3.72	3.28	4.12	4.09	4.40	3.88	5.11	4.47	4.16
K ₂ O	5.11	7.28	4.87	3.37	2.62	2.00	2.14	2.27	3.29
P ₂ O ₅	0.060	0.062	0.048	0.385	0.299	0.639	0.230	0.490	0.296
TTL	99.99	99.99	99.99	100.00	100.00	100.00	100.01	100.00	100.00
ASI	1.077	1.061	1.029	0.912	0.986	0.779	0.982	0.941	1.020
FeRatio	0.867	1.000	0.935	0.642	0.647	0.579	0.647	0.639	0.654
XRF									
Ni	11	12	11	17	14	19	14	18	14
Rb	209	234	171	59	77	47	46	72	102
Sr	169	144	153	875	818	1260	1202	1017	629
Ba	796	331	367	2993	1579	1513	2031	1273	1193
Y	19	6	17	47	20	27	12	29	18
Zr	92	19	48	230	202	124	199	226	190
Nb	19.6	9.6	9.7	50.4	23.2	29.9	11.2	34.5	23.7
Ce	59	10	10	150	110	99	67	98	119
INAA									
Hf	3.36			5.53		2.00		5.20	
Ta	4.54			3.23		1.51		0.84	
Cr	BD			44.1		42.7		43.7	
Co	BD			11.1		25.7		14.7	
Sc	2.93			16.9		22.6		14.6	
La	27.8			75.8		66.5		49.6	
Ce	57.8			148.2		117.8		98.7	
Nd	23.0			74.7		51.8		51.2	
Sm	4.38			11.97		8.09		8.18	
Eu	0.45			2.58		2.27		1.98	
Tb	0.40			1.11		0.90		0.63	
Yb	1.54			4.24		2.11		2.55	
Lu	0.24			0.56		0.34		0.38	

Sample Type	Raft								
	ERa-10 Apl	ERa-11 Gd	ERa-12 Apl.	ERa-13 Gr	ERa-14 Apl	ERa-15 Apl	ERa-16 Gd/Ton	ERa-18 Gd/Ton	ERa-19 Apl
SiO ₂	74.72	65.28	74.98	70.41	73.83	74.11	65.11	68.22	74.36
TiO ₂	0.138	0.628	0.145	0.370	0.174	0.159	0.598	0.486	0.155
Al ₂ O ₃	14.20	16.55	14.24	15.72	14.71	14.36	16.92	15.78	14.26
FeO*	0.64	3.92	0.91	2.33	1.07	0.92	3.66	3.12	1.02
MnO	0.022	0.076	0.033	0.048	0.034	0.036	0.074	0.065	0.032
MgO	0.15	2.01	0.15	1.12	0.18	0.18	1.92	1.58	0.10
CaO	0.98	3.99	1.18	2.63	1.33	1.18	4.15	3.70	1.09
Na ₂ O	3.69	4.33	3.69	3.63	3.78	3.82	4.56	4.37	3.61
K ₂ O	5.39	2.90	4.62	3.56	4.84	5.17	2.71	2.41	5.30
P ₂ O ₅	0.063	0.306	0.049	0.168	0.048	0.067	0.294	0.267	0.061
TTL.	99.99	99.99	100.00	99.99	100.00	100.00	100.00	100.00	99.99
ASI	1.049	0.985	1.087	1.106	1.068	1.035	0.978	0.992	1.055
FeRatio	0.810	0.661	0.858	0.675	0.856	0.836	0.656	0.664	0.911
XRF									
Ni	10	16	11	13	10	13	15	16	12
Rb	155	85	190	79	188	176	75	72	190
Sr	150	787	218	674	283	253	841	736	214
Ba	694	1660	1318	1754	1462	1362	1630	1317	1167
Y	16	22	17	17	11	14	20	19	15
Zr	62	199	98	145	122	95	202	161	114
Nb	16.9	24.4	13.1	20.8	12.9	18.0	21.9	20.2	12.7
Ce	38	95	62	72	69	48	114	57	55
INAA									
Hf			3.04		3.61		4.40	3.87	
Ta			0.84		1.14		1.09	1.16	
Cr			BD		2.56		33.7	26.4	
Co			0.81		1.06		8.15	7.07	
Sc			3.06		2.39		8.93	7.22	
La			31.6		40.9		67.5	43.7	
Ce			55.3		71.3		111.3	74.9	
Nd			21.8		28.4		44.6	30.1	
Sm			3.76		4.32		6.27	4.62	
Eu			0.55		0.58		1.43	1.13	
Tb			0.35		0.31		0.58	0.59	
Yb			1.17		1.02		1.86	1.76	
Lu			0.17		0.16		0.25	0.22	

Sample Type	Raft								
	ERa-19 Rpt	ERa-20 Gd	ERa-21 Apl	ERa-22 Ton	8130 Gr	8130 Rpt	8131 Gr	8131 Rpt	11.6 Gr
SiO ₂	74.32	64.35	74.53	64.90	75.75	76.01	71.97	72.45	75.43
TiO ₂	0.161	0.593	0.138	0.654	0.144	0.139	0.252	0.249	0.189
Al ₂ O ₃	14.27	17.61	14.36	17.16	13.55	13.53	14.47	14.33	13.35
FeO*	1.04	3.64	0.86	4.04	1.15	1.14	2.51	2.54	1.16
MnO	0.031	0.071	0.027	0.088	0.038	0.039	0.063	0.064	0.072
MgO	0.15	1.94	0.20	2.22	0.18	0.00	0.70	0.53	0.33
CaO	1.11	3.35	0.98	4.59	0.55	0.50	1.98	1.95	1.14
Na ₂ O	3.57	3.65	3.69	3.94	3.93	3.85	3.97	3.77	3.86
K ₂ O	5.30	4.53	5.17	2.09	4.67	4.75	3.98	4.00	4.40
P ₂ O ₅	0.060	0.266	0.041	0.312	0.045	0.046	0.116	0.116	0.074
TTL	100.01	100.00	100.00	99.99	100.01	100.00	100.01	100.00	100.01
ASI	1.058	1.075	1.075	1.049	1.091	1.102	1.021	1.038	1.026
FeRatio	0.874	0.652	0.811	0.645	0.865	1.000	0.782	0.827	0.779
XRF									
Ni	13	18	12	19	15	13	16	18	10
Rb	190	114	200	83	217	216	135	135	156
Sr	216	827	169	848	97	95	391	389	196
Ba	1154	4262	1098	1880	468	470	887	892	595
Y	15	20	14	19	20	20	15	13	19
Zr	144	181	66	230	75	75	102	101	104
Nb	11.8	25.3	21.8	22.4	50.1	52.3	27.4	28.9	40.0
Ce	65	75	39	120	48	43	62	59	62
INAA									
Hf		4.44	2.40				2.75		3.71
Ta		1.03	1.82				1.49		2.54
Cr		32.6	BD				27.8		BD
Co		8.23	BD				3.23		NA
Sc		8.29	2.92				3.83		3.90
La		66.8	26.0				35.0		39.6
Ce		112.9	50.8				63.2		75.5
Nd		47.7	20.2				21.7		25.0
Sm		5.83	3.51				3.18		4.49
Eu		1.39	0.51				0.75		0.73
Tb		0.59	0.36				0.38		0.40
Yb		1.68	1.21				1.46		1.80
Lu		0.24	0.18				0.20		0.29

Sample Type	Raft							
	27.1 Gd	60.0 Gr	64.9 Gd	17.4 Gr	146.9 Apl	238.0 Gr	249.2 Gd	40.2 Apl
SiO ₂	66.67	76.76	66.83	71.83	80.50	74.43	67.28	76.63
TiO ₂	0.506	0.119	0.550	0.313	0.116	0.263	0.505	0.097
Al ₂ O ₃	15.66	13.27	15.82	14.66	13.44	14.04	15.65	12.90
FeO*	3.49	0.71	3.46	1.95	0.31	1.26	3.20	0.65
MnO	0.073	0.066	0.072	0.056	0.025	0.051	0.069	0.029
MgO	2.26	0.08	2.03	0.92	0.09	0.26	1.78	0.15
CaO	3.81	0.87	3.78	1.84	0.10	1.54	3.65	0.71
Na ₂ O	3.90	3.63	4.27	3.95	0.57	3.82	3.96	3.63
K ₂ O	3.39	4.47	2.95	4.35	4.83	4.23	3.69	5.17
P ₂ O ₅	0.258	0.027	0.252	0.126	0.023	0.106	0.224	0.023
TTI.	100.02	100.00	100.01	100.00	100.00	100.00	100.01	99.99
ASI	0.954	1.076	0.959	1.028	2.135	1.046	0.941	1.007
FeRatio	0.607	0.899	0.630	0.679	0.775	0.829	0.643	0.813
XRF								
Ni	18	10	16	9	12	9	18	11
Rb	107	176	99	166	141	152	110	176
Sr	563	120	573	333	55	283	586	48
Ba	1306	1028	989	1176	148	917	1475	105
Y	17	20	18	17	26	19	17	9
Zr	152	78	166	135	73	130	147	67
Nb	27.6	79.2	27.6	27.5	47.6	28.8	26.4	37.4
Ce	58	73	62	61	59	60	72	43
INAA								
Hf	3.96	3.23	4.40	4.07	3.79			
Ta	2.00	4.61	1.58	2.24	4.54			
Cr	43.6	BD	42.3	12.8	BD			
Co	NA	NA	NA	NA	NA			
Sc	9.84	3.83	8.30	5.01	3.33			
La	46.5	33.0	50.0	41.4	20.4			
Ce	81.9	64.2	85.7	73.8	45.6			
Nd	31.7	16.3	32.3	26.8	17.6			
Sm	4.82	4.22	4.80	4.24	3.87			
Eu	1.14	0.52	1.15	0.80	0.36			
Tb	0.50	0.31	0.45	0.41	0.34			
Yb	1.64	2.15	1.82	1.63	2.60			
Lu	0.27	0.32	0.26	0.26	0.37			

Sample Type	Galena Bay		GB-3 Apl	Mt. Toby	
	GB-1 Gr	GB-2 Apl		Tob-1 Gd	Tob-2 QMD
SiO ₂	73.63	75.09	75.23	61.96	55.09
TiO ₂	0.157	0.023	0.030	0.695	0.864
Al ₂ O ₃	15.25	14.93	14.61	15.55	14.27
FeO*	0.84	0.37	0.34	6.02	8.22
MnO	0.026	0.072	0.083	0.13	0.171
MgO	0.15	0.00	0.00	2.71	5.98
CaO	1.81	0.76	0.90	5.09	8.02
Na ₂ O	4.57	4.04	4.11	3.29	3.35
K ₂ O	3.52	4.68	4.68	4.27	3.60
P ₂ O ₅	0.039	0.028	0.021	0.287	0.436
TTL	99.99	99.99	100.00	100.00	100.00
ASI	1.049	1.146	1.089	0.835	0.621
FeRatio	0.848	1.000	1.000	0.690	0.579
XRF					
Ni	8	13	12	22	62
Rb	129	261	269	147	101
Sr	662	62	168	1062	1171
Ba	1318	91	436	913	804
Y	5	23	23	28	23
Zr	104	39	43	234	160
Nb	5.1	19.3	22.8	34.7	24.0
Ce	39	2	23	67	80
INAA					
Hf	2.79	2.19		6.18	3.51
Ta	0.40	2.40		1.43	0.87
Cr	BD	BD		44.3	180
Co	0.62	BD		14.7	29.1
Sc	1.36	1.65		14.7	20.5
La	22.2	5.37		40.5	43.4
Ce	37.0	12.8		83.7	81.1
Nd	15.2	6.34		38.9	39.4
Sm	2.08	2.05		7.08	6.71
Eu	0.55	0.10		1.77	1.79
Tb	0.16	0.25		0.88	0.78
Yb	0.40	1.40		2.88	2.08
Lu	0.05	0.17		0.40	0.31

Major element analyses are normalized on a volatile-free basis. All Fe expressed as Fe⁺² (FeO*). Ni, Rb, Sr, Ba, Y, Zr, Nb, and Ce were analyzed by XRF, and the Hf, Ta, Cr, Co, Sc, La, Ce, Nd, Sm, Eu, Tb, Yb, and Lu were analyzed by INAA. Abbreviations: Gr - granite; Apl - Aplite; Gd - granodiorite; Ton - tonalite; QMD - quartz monzodiorite; QD - quartz diorite; and Rpt - repeat analysis.

Table 5.2. Rb-Sr and Sm-Nd isotopic compositions for samples from the Raft, Galena Bay, and Mt. Toby plutons

Type	Sample	Rb	Sr	$^{87}\text{Rb}/^{86}\text{Sr}$	$^{86}\text{Sr}/^{87}\text{Sr}_0$	$^{86}\text{Sr}/^{87}\text{Sr}_T$	$\epsilon_{\text{Sr}T}$
Raft							
Gr	8131	135	391	0.999	0.707700(40)	0.70536	+11.2
Gr	11.6	156	196	2.304	0.709549(40)	0.70416	-8.8
Gr	17.4	166	333	1.443	0.707839(38)	0.70446	-1.6
Gr	60.0	176	120	4.243	0.712604(20)	0.70265	-27.4
Gd	64.9	99	573	0.500	0.706287(44)	0.70512	-7.7
Gr	ERa-2	209	169	3.581	0.713064(50)	0.70467	+1.4
QMD	ERa-4	59	875	0.195	0.705928(62)	0.70547	+12.7
Q	ERa-6	47	1260	0.108	0.704906(28)	0.70465	+1.1
Ton	ERa-18	72	736	0.283	0.705744(20)	0.70508	+7.2
Gd	ERa-20	114	827	0.399	0.705990(18)	0.70506	+6.8
Aplite	Era-21	200	169	3.424	0.713509(38)	0.70548	+12.8
Galena Bay							
Gr	GB-1	129	662	0.561	0.706814(42)	0.705497	+13.1
Mt. Toby							
Gd	Tob-1	147	1062	0.400	0.707833(16)	0.70690	+32.9
QMD	Tob-2	101	1171	0.249	0.706199(40)	0.70562	+14.5

Sample	Sm	Nd	$^{147}\text{Sm}/^{144}\text{Nd}$	$^{143}\text{Nd}/^{144}\text{Nd}_0$	$^{143}\text{Nd}/^{144}\text{Nd}_T$	ϵ_{Nd_T}
Raft						
8131	3.18	21.7	0.0887	0.512345(4)	0.512249	-3.4
11.6	4.49	25.0	0.1087	0.512362(11)	0.512245	-3.5
17.4	4.24	26.84	0.0956	0.512405(5)	0.512302	-2.4
60.0	4.22	16.3	0.1566	0.512353(7)	0.512184	-4.7
64.9	4.80	32.3	0.0899	0.512400(23)	0.512303	-2.4
146.9	3.87	17.62	0.1329	0.512368(23)	0.512225	-3.9
ERa-2	4.38	23.0	0.1152	0.512191(8)	0.512076	-6.8
				0.512209(8)		
ERa-4	11.97	74.7	0.0969	0.512382(32)	0.512277	-2.9
ERa-6	8.09	51.8	0.0945	0.512534(6)	0.512432	+0.1
ERa-12	3.76	21.8	0.1043	0.512306(9)	0.512193	-4.5
ERa-18	4.62	30.1	0.0930	0.512426(6)	0.512326	-2.0
ERa-20	5.83	47.7	0.0739	0.512374(9)	0.512294	-2.6
ERa-21	3.51	20.2	0.1054	0.512226(7)	0.512112	-6.1
Galena Bay						
GB-1	2.08	15.2	0.0828	0.512251(25)	0.512162	-5.2
Mt. Toby						
Tob-1	7.08	38.9	0.1101	0.512239(8)	0.512120	-6.0
Tob-2	6.71	39.4	0.1030	0.512286(4)	0.512175	-4.9

Rb and Sr abundances by XRF, and Sm and Nd abundances by INAA; all ratios and ϵ values relative to $^{86}\text{Sr}/^{88}\text{Sr} = 0.1194$ and $^{144}\text{Nd}/^{146}\text{Nd} = 0.7219$; $^{87}\text{Rb}/^{86}\text{Sr}_{\text{UR}} = 0.0827$; $\lambda^{87}\text{Rb} = 1.42 \cdot 10^{-11}/\text{yr}$; $^{87}\text{Sr}/^{86}\text{Sr}_{\text{UR}}$ at 0 = 0.70478; $\lambda^{147}\text{Sm} = 6.54 \cdot 10^{-12}/\text{yr}$; $^{147}\text{Sm}/^{144}\text{Nd}_{\text{CHUR}} = 0.1967$; $^{143}\text{Nd}/^{144}\text{Nd}_{\text{CHUR}}$ at 0 Ma = 0.512638. The 2σ precision in the last listed place for each measured isotopic ratio is listed in parentheses. ϵ_{Sr} , ϵ_{Nd} , and initial Sr and Nd ratios calculated at T = 165 Ma, using the chondritic uniform reservoir ratios listed above (UR, Allegre and Ben Othman, 1980; CHUR, Jacobsen and Wasserburg, 1984).

Table 5.3. U-Th-Pb isotopic compositions of samples from the Raft, Galena Bay, and Mt. Toby plutons.

Sample	U	Th	Pb	$^{238}\text{U}/^{204}\text{Pb}$		$^{206}\text{Pb}/^{204}\text{Pb}$		$^{207}\text{Pb}/^{204}\text{Pb}$		$^{208}\text{Pb}/^{204}\text{Pb}$	
				Meas.	Init.	Meas.	Init.	Meas.	Init.		
Raft											
ERa-2	7.36	19.27	40	11.9	19.350	19.041	15.690	15.674	39.149	38.884	
ERa-4	3.70	16.61	12	20.0	19.331	18.812	15.663	15.638	39.444	38.683	
ERa-6	1.98	6.54	6	21.4	19.528	18.974	15.685	15.658	39.537	38.937	
ERa-12	4.39	16.10	30	9.49	19.317	19.061	15.692	15.680	39.206	38.911	
ERa-18	1.54	9.29	12	8.32	19.266	19.050	15.665	15.654	39.333	38.907	
ERa-20	1.95	13.76	12	9.73	19.392	19.140	15.671	15.659	39.470	38.887	
ERa-21	5.54	14.45	39	9.21	19.329	19.091	15.683	15.671	39.167	38.933	
8131	3.46	19.20	22	10.20	19.580	19.316	15.730	15.717	39.464	38.984	
11.6	11.87	36.3	24	32.06	19.896	19.069	15.716	15.675	39.801	39.045	
17.4	9.62	16.97	20	31.18	19.767	18.959	15.712	15.672	39.383	38.916	
27.1	5.92	16.51	17	22.58	19.620	19.035	15.693	15.664	39.457	38.923	
60.0	14.20	26.11	22	41.84	20.347	19.262	15.770	15.717	39.727	39.074	
64.9	6.06	21.59	15	26.19	19.564	18.885	15.693	15.659	39.445	39.653	
146.9	21.66	29.81	26	54.00	19.812	19.133	15.720	15.651	40.380	39.749	
Galena Bay											
GB-1	2.59	10.54	22	7.63	19.564	19.366	15.697	15.687	39.237	38.974	
GB-2	4.20	7.24	27	10.08	19.704	19.443	15.695	15.683	39.218	39.070	
Mt. Toby											
Tob-1	2.27	14.27	13	11.32	19.410	19.117	15.644	15.630	39.622	38.917	
Tob-2	0.46	2.77	15	2.00	18.933	18.881	15.634	15.631	38.963	38.862	

U and Th abundances by INAA, and Pb abundances by XRF; Meas. Pb ratios listed are the present day measured ratios which have a precision of 0.05% (2σ) for each ratio. Init. Pb ratios are the initial ratios corrected to 165 Ma using the following decay constants: $\lambda^{238}\text{U} = 1.55125 \times 10^{-10}$; $\lambda^{235}\text{U} = 9.8485 \times 10^{-10}$; and $\lambda^{232}\text{Th} = 4.9475 \times 10^{-11}$. The U abundance for Tob-2 is estimated.

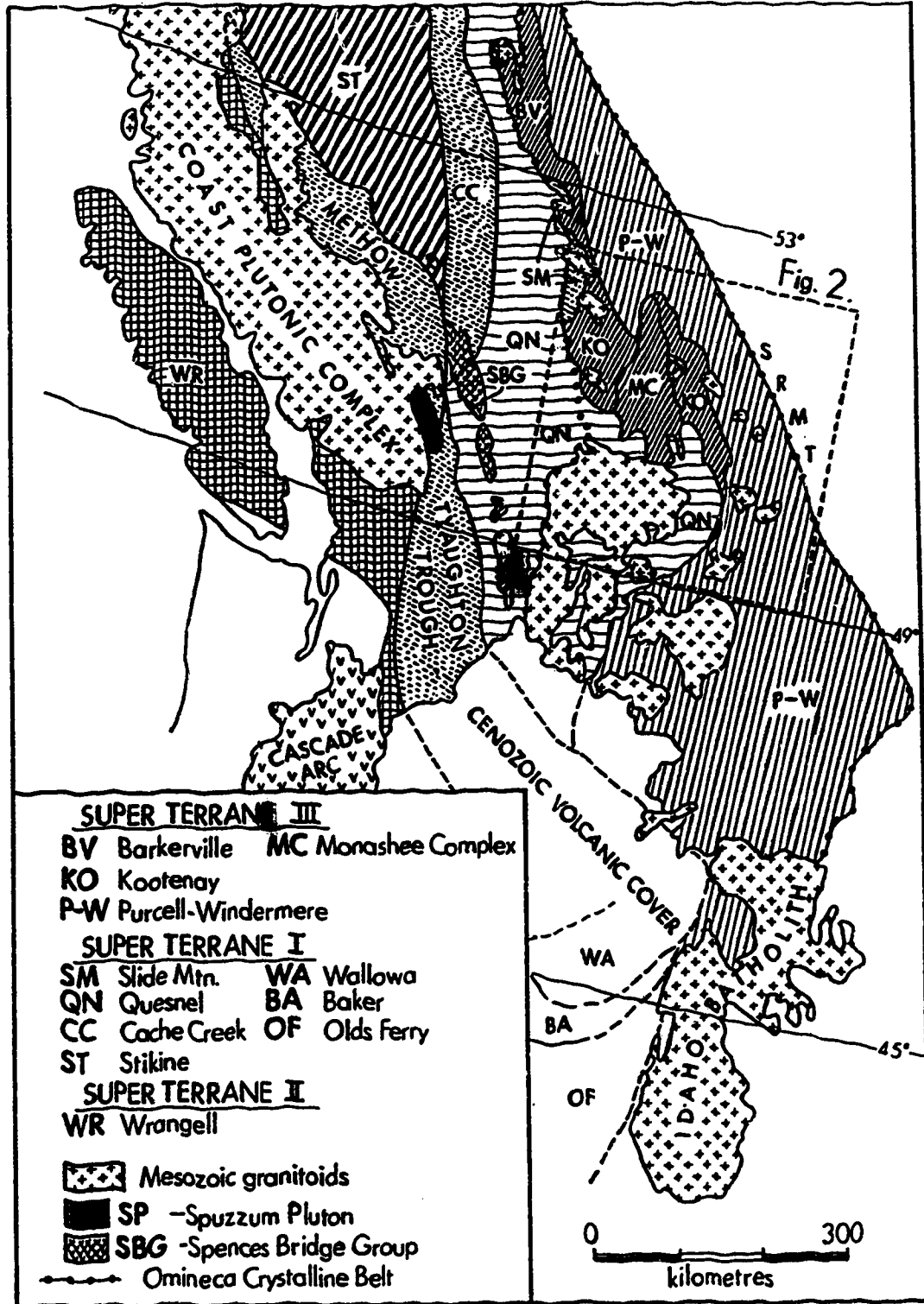


Figure 5.1. Tectono-magmatic map of southern British Columbia and surrounding region (modified from Monger and Berg 1987).

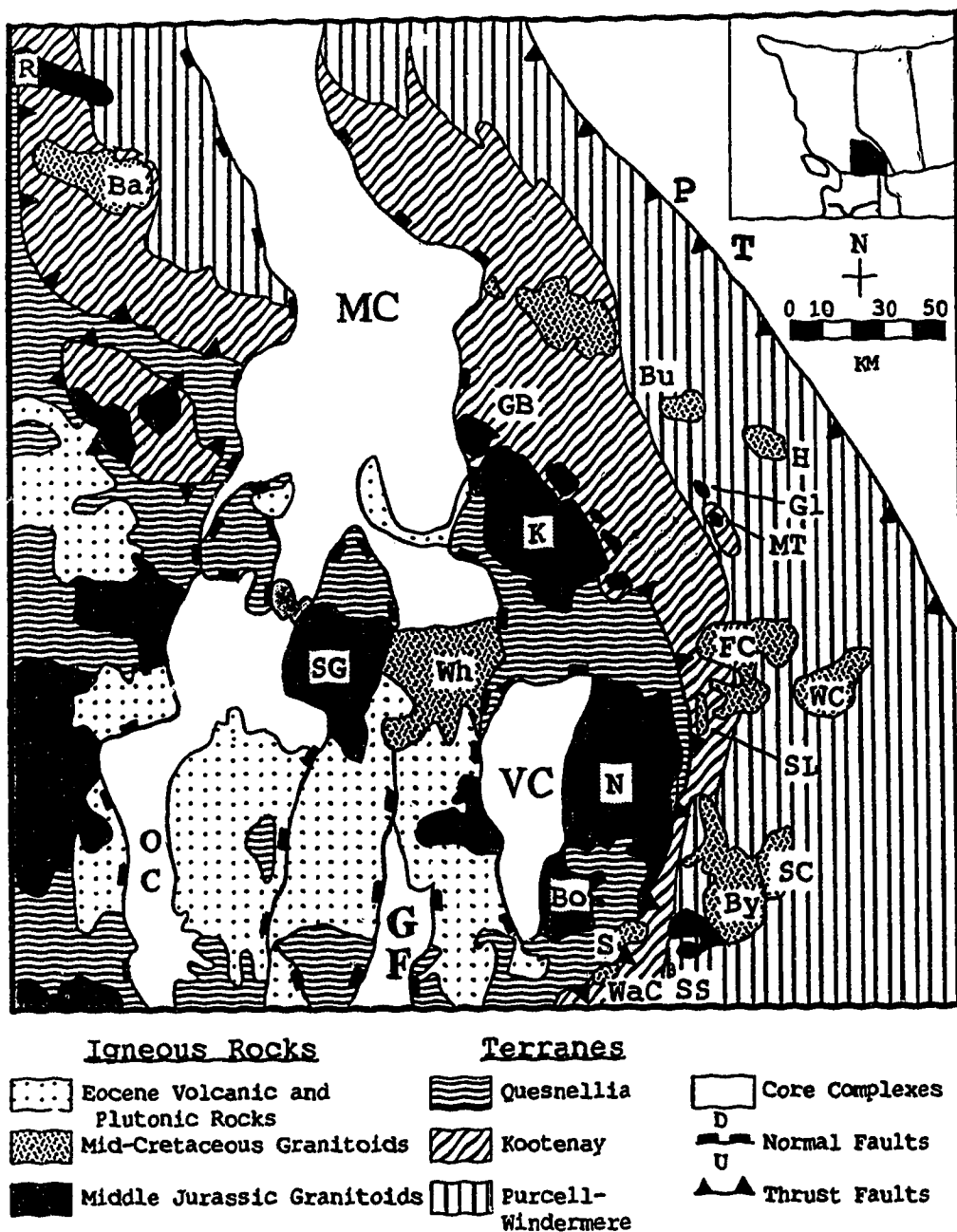


Figure 5.2. Tectono-magmatic map of the southern Omineca Crystalline Belt (modified from Parrish et al. 1988, Lambert and Chamberlain 1988, and Monger and Berg 1987). Several of the metamorphic core complexes include GF - Kettle-Grand Forks complex, MC - Monashee complex, OC - Okanagan complex, and VC - Valhalla complex. The plutons include Ba - Mt. Baldy, Bo - Bonnington, Bu - Bugaboo, By - Bayonne, FC - Fry Creek, GB - Galena Bay, Gl - Glacier Stock, H - Horsethief Creek, K - Kuskanax, MT - Mt. Toby, N - Nelson, R - Raft, S - Salmo, SC - Skelly Creek, SL - Shore Line Stock, SS - Summit Stock, WaC - Wallack Creek, WC - White Creek, and Wh - Whatshan. The Purcell Thrust is labelled PT.

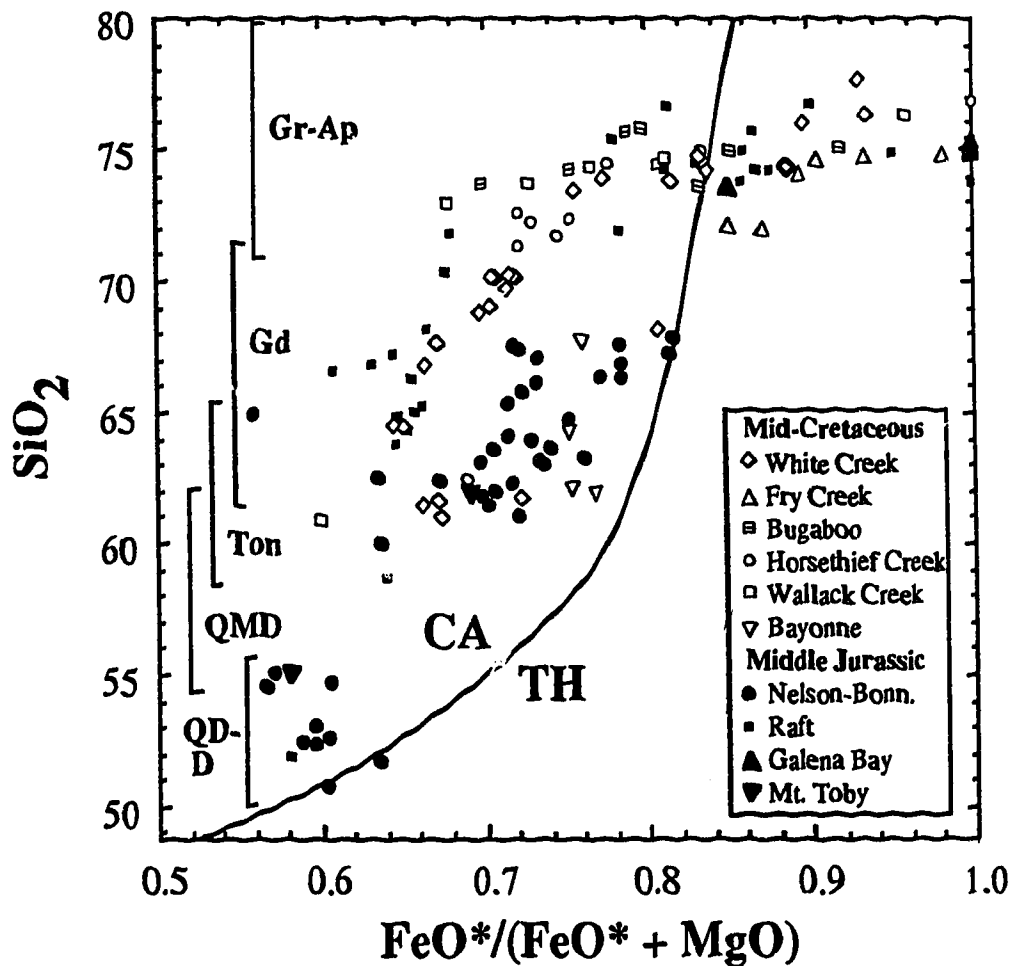


Figure 5.3. SiO_2 versus $\text{FeO}^*/(\text{FeO}^* + \text{MgO})$ for the Mesozoic granitoids in SEBC (after Miyashiro 1974). CA and TH are for calc-alkaline and tholeiitic, respectively. The range in silica contents for different lithologies - QD-D, quartz diorite-diorite; QMD, quartz monzodiorite; Ton, tonalite; GD, granodiorite; and Gr-Ap, granite-aplite are also shown. The mid-Cretaceous data for White Creek, Bugaboo, Horsethief Creek, and Fry Creek are from Brandon and Lambert (1992b, 1992c), and for Bayonne and Wallack Creek from Brandon and Lambert (unpublished data). The Middle Jurassic Nelson and Bonnington (Bonn.) data are from Ghosh (1986).

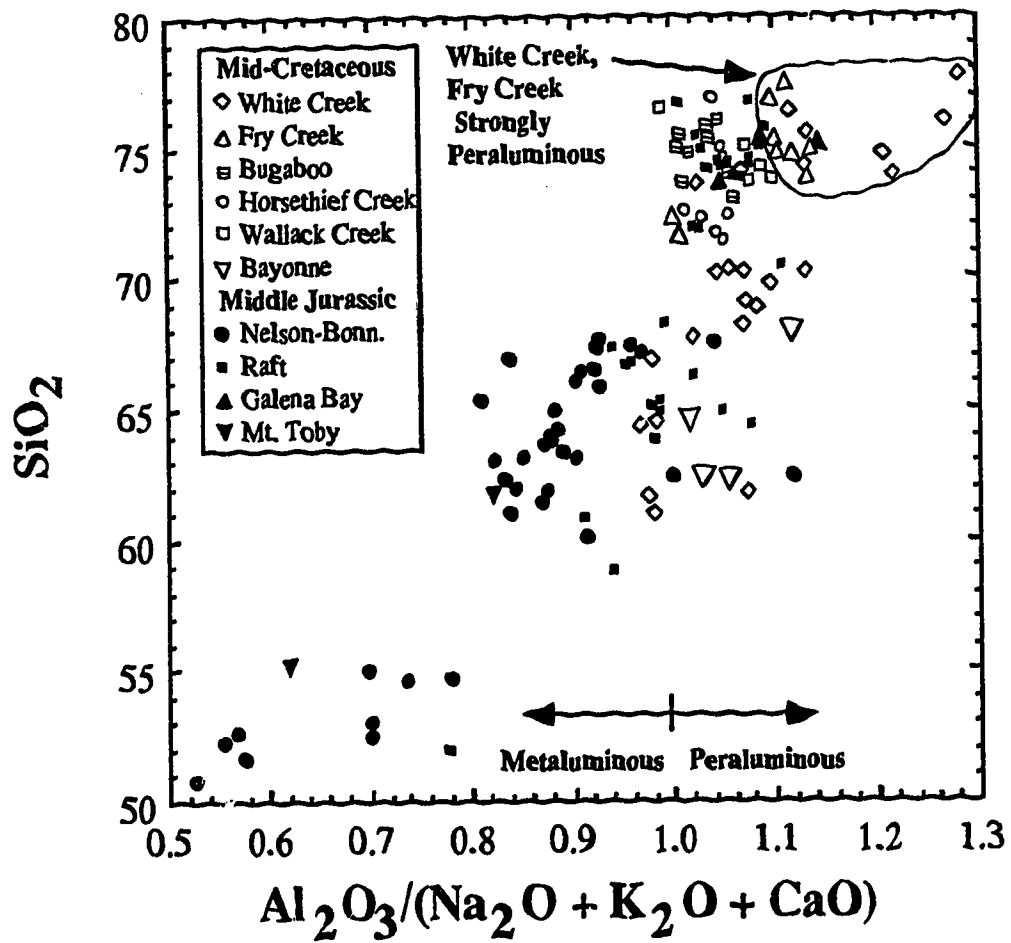


Figure 5.4. SiO_2 versus $\text{Al}_2\text{O}_3/(\text{Na}_2\text{O} + \text{K}_2\text{O} + \text{CaO})$ for the Mesozoic granitoids in SEBC.

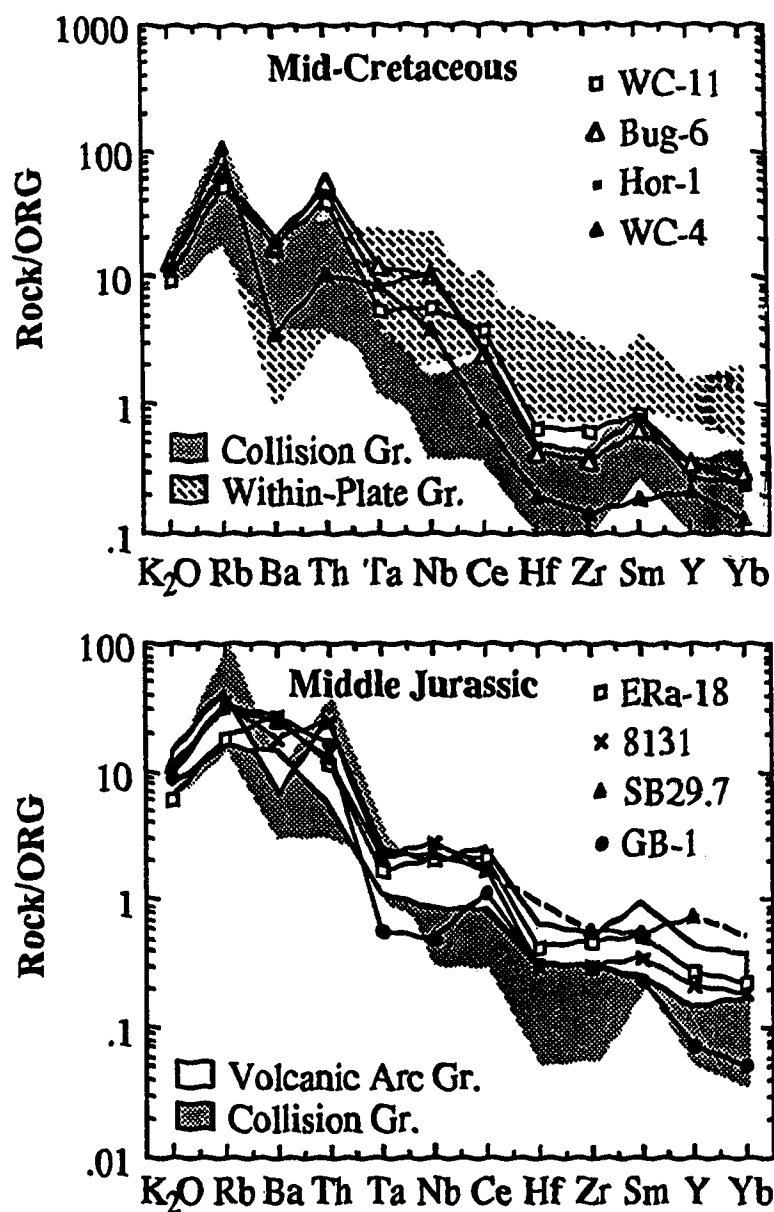


Figure 5.5. Incompatible trace element normalized plots for representative Middle Jurassic and mid-Cretaceous granitoids. Abundances are normalized to ocean ridge granite (ORG) of Pearce et al. (1984). Also shown are the patterns for collision granites, within-plate granites and volcanic arc granites (data compiled by Pearce et al. 1984). WC-11 and WC-4 are from the White Creek batholith and are a porphyritic hornblende-biotite granodiorite and a sP, 2-mica granite respectively (Brandon and Lambert 1992c). Hor-1 is from Horsethief Creek, and Bug-6 is from Bugaboo, and both are hornblende-biotite granites (from Brandon and Lambert 1992b). SB 29.7 is a hornblende-biotite granodiorite from the Nelson batholith (from Ghosh 1986).

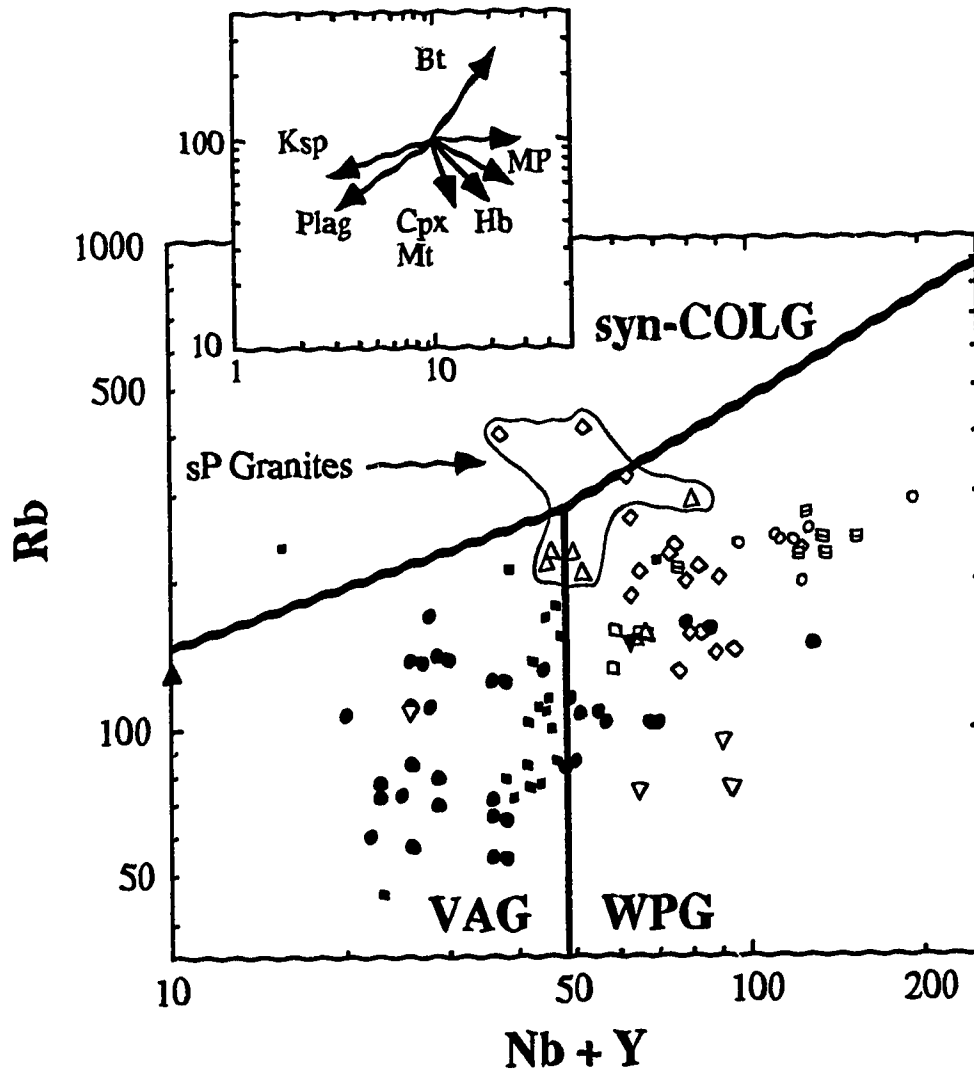


Figure 5.6. Rb versus Nb + Y diagram of Pearce et al.(1984), showing abundances from SEBC granodiorites and granites (62 - 78 wt.% SiO₂) with symbols as in Figure 5.3. The regions for syn-COLG - syn-collision granitoids, VAG - volcanic arc granitoids, and WPG - within-plate granitoids are delineate. The inset shows vectors for 50% addition of the cumulate mineral for the major phases and qualitative trends for minor phases found within granitoids (Pearce et al. 1984) and abbreviations are for: Ksp - alkali feldspar, Bt - biotite, MP - minor phases (apatite, zircon, and sphene), Hb - hornblende, Cpx - clinopyroxene, and Mt - magnetite. Fractional crystallization vectors would have the opposite direction for each mineral phase accumulation vector.

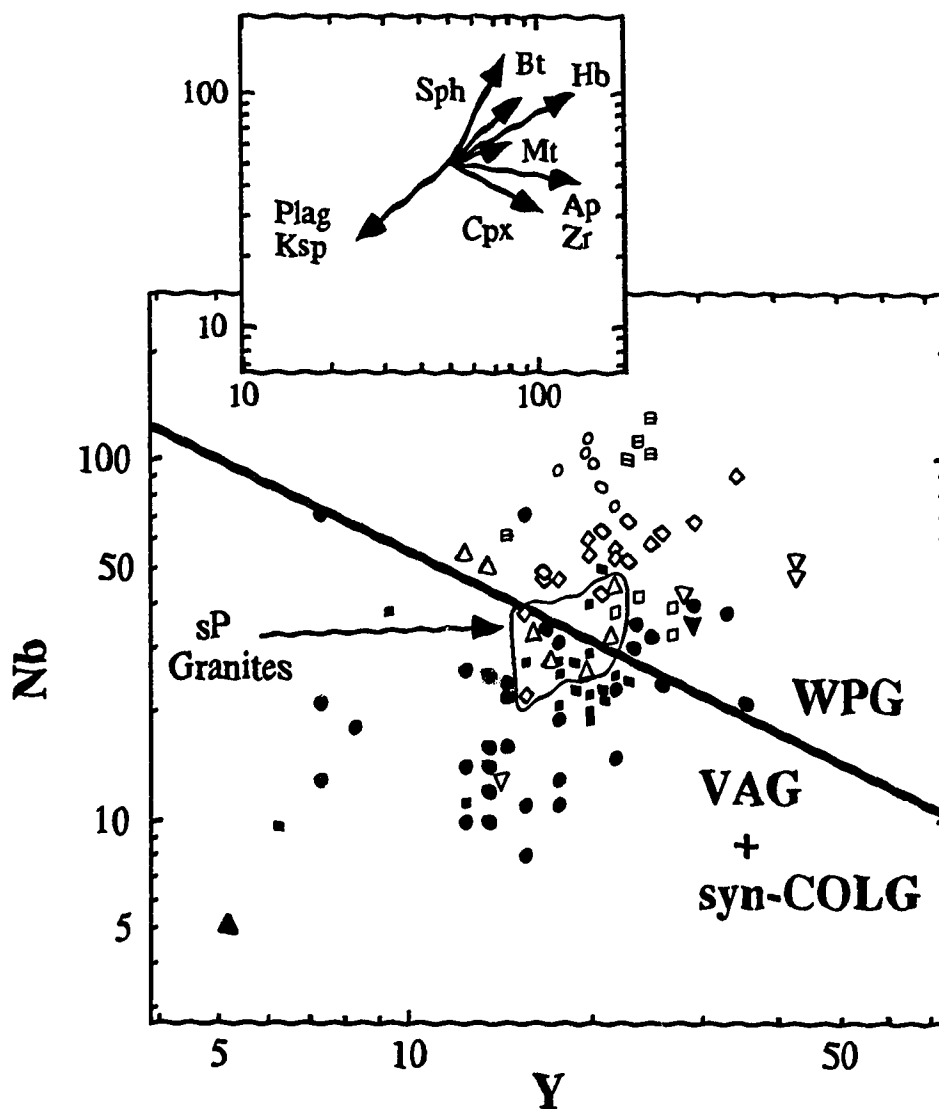


Figure 5.7. Nb versus Y diagram of Pearce et al. (1984), showing the abundances for SEBC granodiorites and granites with symbols as in Figure 5.3. The inset shows accumulations trends with the parameters discussed in Figure 6.

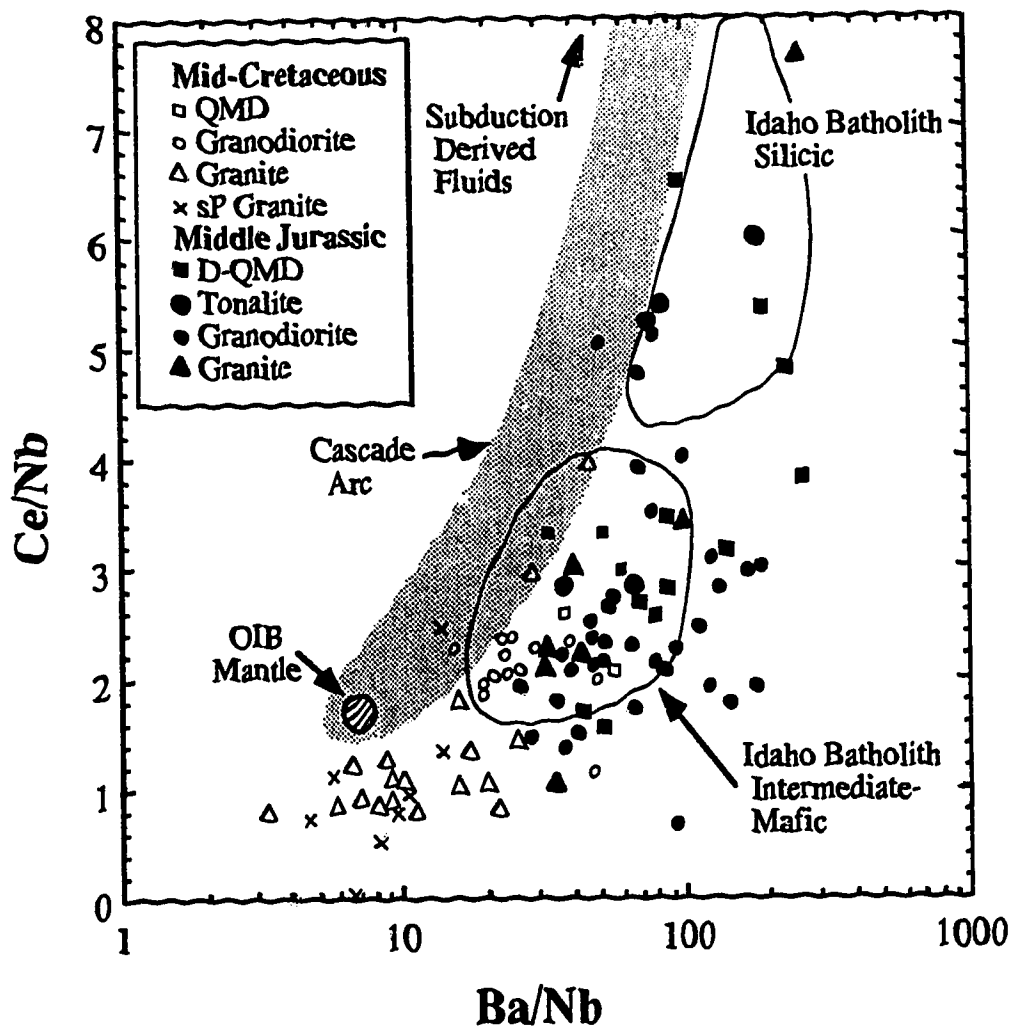


Figure 5.8. Ce/Nb versus Ba/Nb. Data sources for SEBC Mesozoic granitoids as in Figure 5.3. Idaho batholith rocks are from Foster and Hyndman (1990). The Cascade arc data is from Bullen and Clynne (1990), Hughes (1990), and Leeman et al. (1990). Ocean island basalt mantle (OIB mantle) is after Saunders et al. (1988).

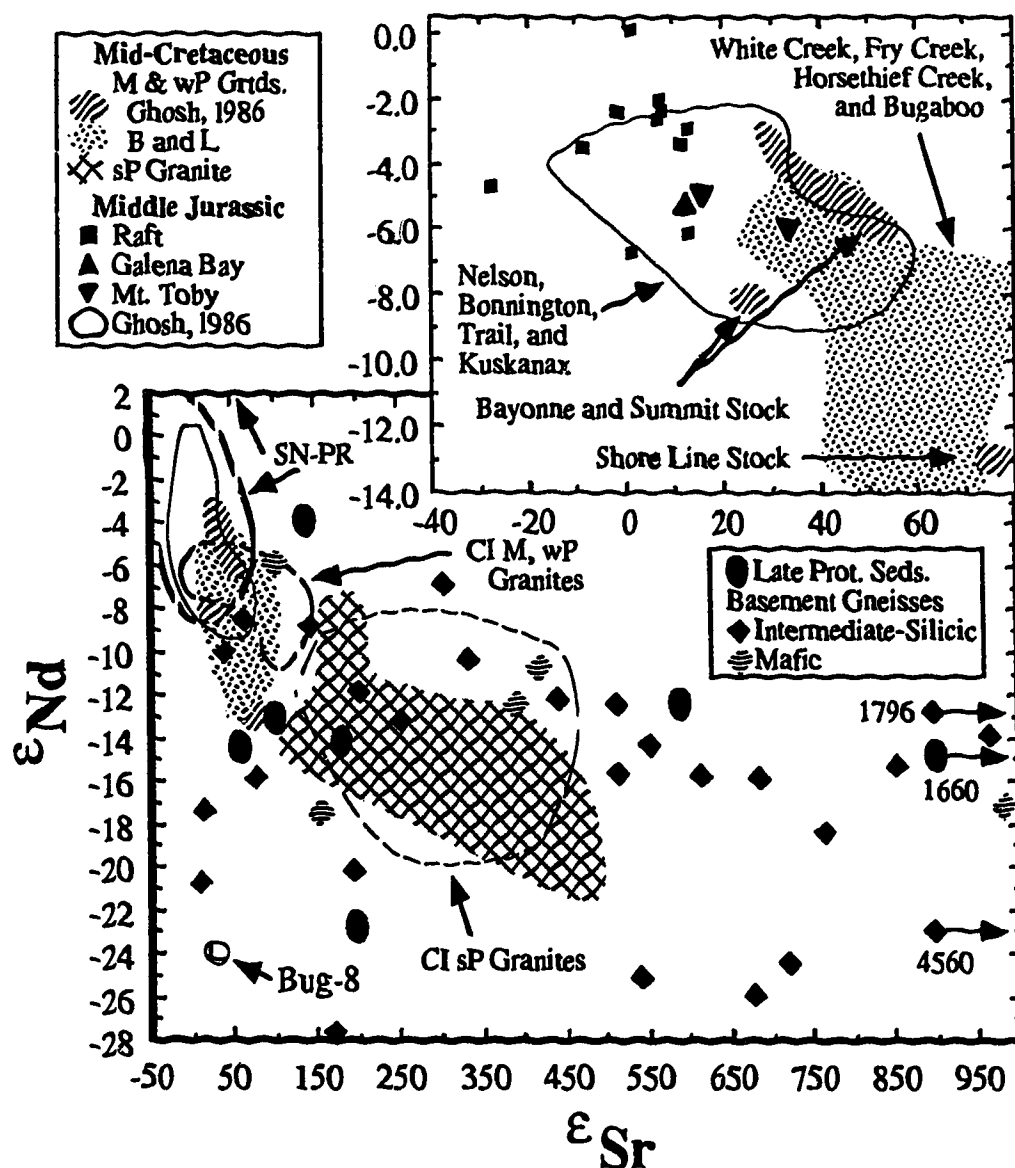


Figure 5.9. ϵ_{Nd} versus ϵ_{Sr} for the SEBC granitoids. The Middle Jurassic data for Nelson, Bonnington, Trail and Kuskanax and the mid-Cretaceous data for Bayonne, Summit Stock and Shore Line Stock are from Ghosh (1986). The mid-Cretaceous data from White Creek, Bugaboo, Horsethief Creek, and Fry Creek are from Brandon and Lambert (B and L, 1992b, 1992c). Also plotted are fields for granitoids from the Cordilleran interior (CI) of the western United States, and the Sierra Nevada and Peninsular Ranges batholiths (data compiled by Miller and Barton 1990). Basement rocks from the Omineca Belt, including Late Proterozoic metapelites (Ghosh and Lambert 1989), and Precambrian basement gneisses from the Malton complex near Valemount, British Columbia, and Pre-Belt gneisses from northern Idaho (Lambert and Chamberlain 1990), and gneisses from Frenchman Cap in the Monashee complex, Grand Forks gneiss from the Kettle-Grand Forks complex, and gneisses from the Spokane, Washington area (Armstrong et al. 1991), are plotted as individual data points and are corrected to 110 Ma. Bug-8 is a metapelite xenolith collected from the Bugaboo pluton (Brandon and Lambert 1992b).

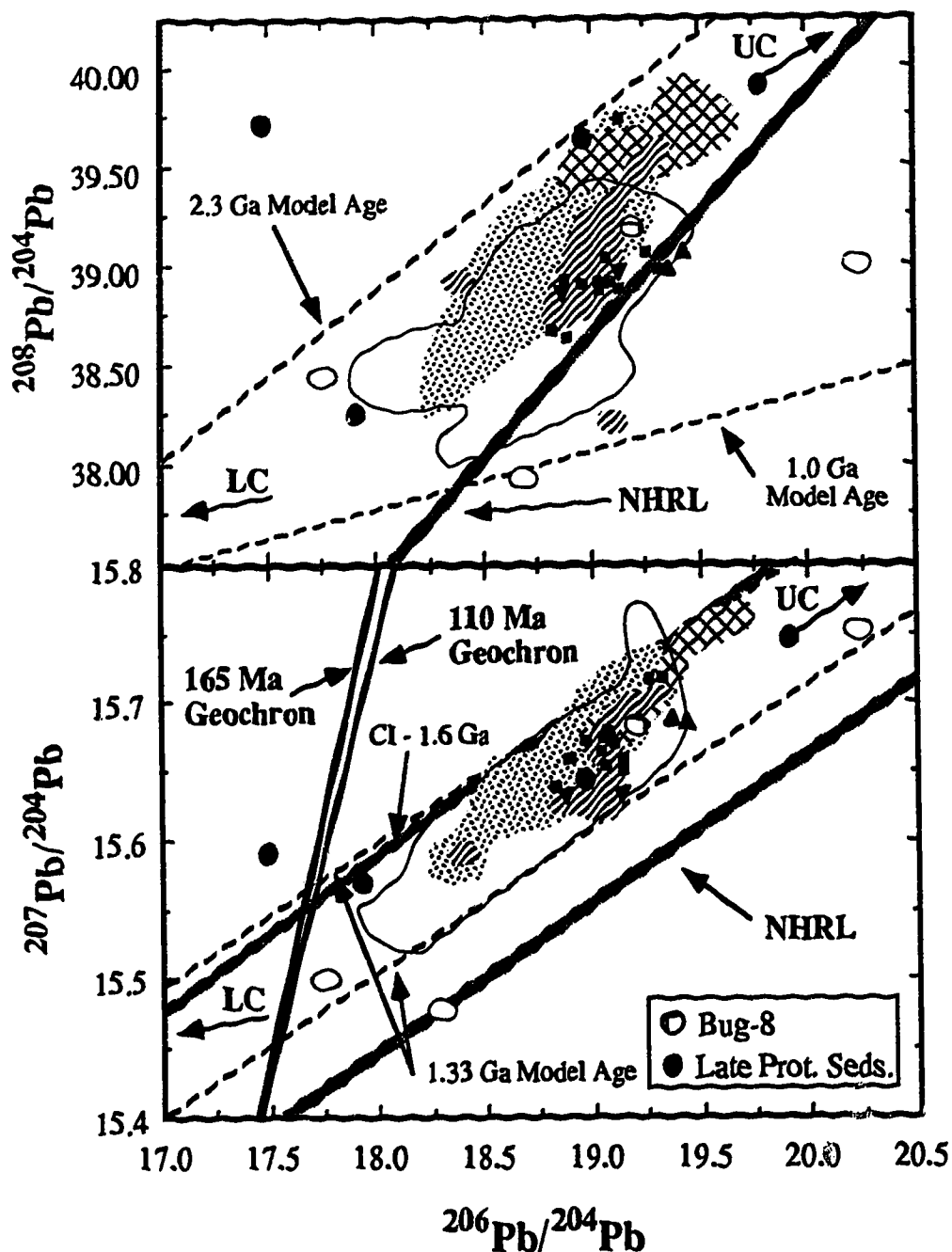


Figure 5.10. Initial $^{208}\text{Pb}/^{204}\text{Pb}$ and $^{207}\text{Pb}/^{204}\text{Pb}$ versus $^{206}\text{Pb}/^{204}\text{Pb}$ for the Mesozoic granitoids in the Omineca Belt with symbols, fields, and data sources as in Figure 5.9. Model age regression lines follow Ghosh (1986) except for the CI -1.6 Ga line from Miller and Barton (1990) for the Cordilleran interior granitoids. Also shown are arrows pointing to lower crust (LC) and upper crust (UC) Pb compositions. The northern hemisphere regression line (NHRL) for oceanic basalts is from Hart (1984).

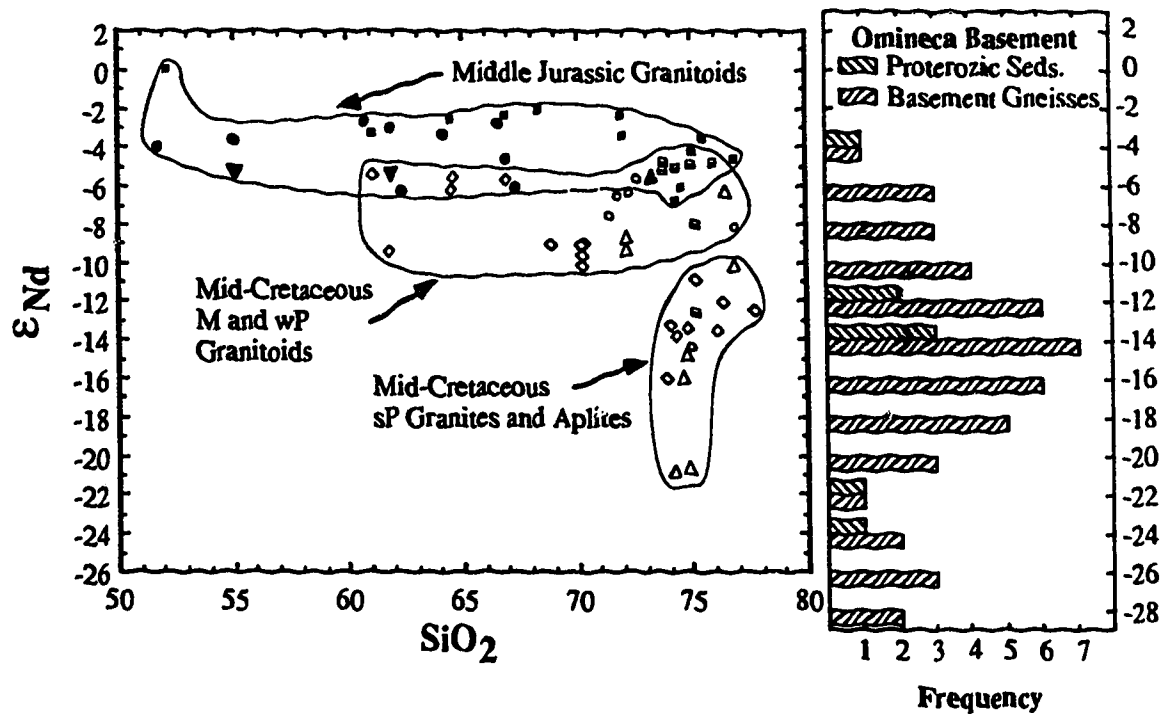


Figure 5.11. ϵ_{Nd} versus SiO_2 for Mesozoic granitoids in the Omineca Belt with symbols as in Figure 5.3, and an accompanying histogram for ϵ_{Nd} at 110 Ma for basement rocks with data sources as in Figure 5.9.

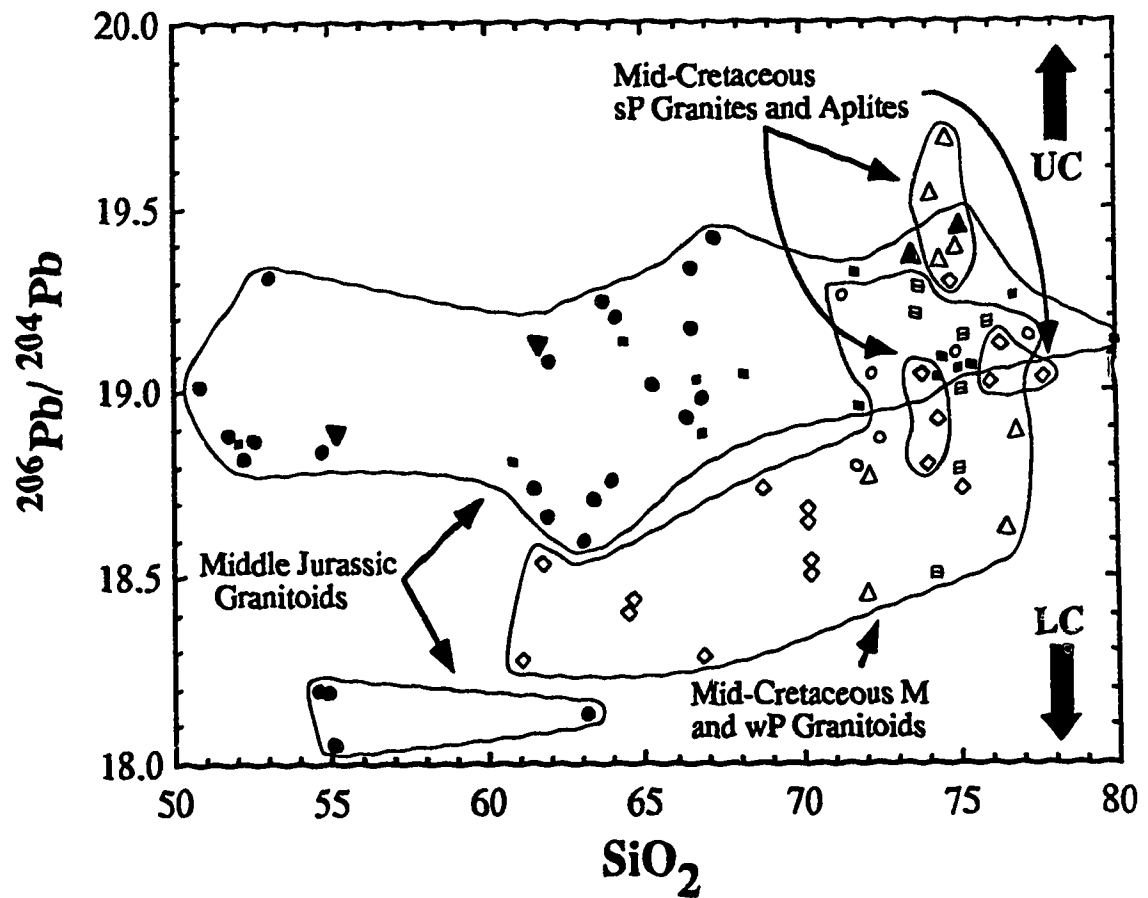


Figure 5.12. $^{206}\text{Pb}/^{204}\text{Pb}$ versus SiO_2 for Mesozoic granitoids from the Omineca Belt with symbols as in Figure 5.3. Arrows point toward lower crust (LC) and upper crust (UC) Pb isotopic compositions.

Appendix 5.1

Sample locales, rock types, and estimated modal proportions (%) of mineralogy.

Raft											
Sample	Latitude	Longitude	Type	Pl	Ksp	Qtz	Bt	Hb	Ep	Ms	
ERa-2	51°41'41"N	119°56'18"W	Gr	23	49	24	2			2	
ERa-3a	"	"	Gr	20	45	35	X				
ERa-3b	"	"	Apl	27	47	26	X			X	
ERa-4	"	"	QMD	50	12	12	7	17	X		
ERa-5	51°41'30"N	119°56'05"W	Gd	50	14	16	10	10	X		
ERa-6	51°41'45"N	119°52'57"W	QD	45	2	3	15	35	X		
ERa-7a	"	"	Ton	55	2	28	11	4	X		
ERa-7b	"	"	Ton	49		20	12	19	X		
ERa-8a	"	"	Gd	40	30	19	8	3	X		
ERa-10	"	"	Apl	23	53	24	X		X	X	
ERa-11	51°41'29"N	119°53'45"W	Gd	48	12	22	11	7	X		
ERa-12	"	"	Apl	10	60	25	3		X	2	
ERa-13	51°41'21"N	119°53'59"W	Gr	15	45	25	15	X	X	X	
ERa-14	51°41'17"N	119°54'19"W	Apl	12	60	23	3			2	
ERa-15	"	"	Apl	8	61	20	3		X	X	
ERa-16	"	"	Gd/Ton	50	7	17	16	10	X		
ERa-18	51°41'18"N	119°54'40"W	Gd/Ton	60	8	21	12	8	X		
ERa-19	"	"	Apl	8	62	28	2			X	
ERa-20	"	"	Gd	46	12	19	16	7	X		
ERa-21	51°40'24"N	119°52'03"W	Ap	5	62	30	3			X	
Era-22	"	"	Ton	56	2	20	12	10	X		
8130	51°44'35"N	120°01'30"W	Gr	26	48	25	1			X	
8131	51°43'21"N	120°01'45"W	Gr	36	39	21	4				
Galena Bay											
Sample	Latitude	Longitude	Type	Pl	Ksp	Qtz	Bt	Ms	Gnt		
GB-1	50°38'06"N	117°55'24"W	Gr	33	25	36	4	2	X		
GB-2	"	"	Apl	25	34	34		5	2		
GB-3	"	"	Apl	29	32	33	X	6	X		
Mt. Toby											
Sample	Latitude	Longitude	Type	Pl	Ksp	Qtz	Bt	Hb	Opx	Cpx	Ep
Tob-1	50°11'37"N	116°34'29"W	Gd	22	25	15	14	21			3
Tob-2	"	"	QMD	38	9	3	12	18	6	14	X

The Accessory phases zircon, apatite, and magnetite are nearly ubiquitous in all of the rocks, and sphene was always found in the rocks with hornblende. Abbreviations: Gr - granite; Apl - aplite; Gd - granodiorite; Ton - Tonalite; QMD - quartz monzodiorite, QD - quartz diorite; Pl - plagioclase; Ksp - alkali feldspar; Qtz - quartz; Bt - biotite; Hb - hornblende; Ep - epidote; Ms - muscovite; Gnt - garnet; Opx - orthopyroxene; Cpx - clinopyroxene. X denotes present in 1% or less.

References

- Allegre, C.J., and Ben Othman, D., 1980. Nd-Sr isotopic relationships in granitoid rocks and continental crust development: A chemical approach to orogenesis. *Nature*, **286**, 335-342.
- Archibald, D.A., Glover, J.K., Price, R.A. Farrar, E., and Carmichael, D.M., 1983. Geochronology and tectonic implications of magmatism and metamorphism, southern Kootenay Arc and neighbouring regions, southeastern British Columbia. Part I: Jurassic to Mid-Cretaceous. *Canadian Journal of Earth Sciences*, **20**, 1891-1913.
- Archibald, D.A., Krogh, T.E., Armstrong, R.L., and Farrar, E., 1984. Geochronology and tectonic implications of magmatism and metamorphism, southern Kootenay Arc and neighbouring regions, southeastern British Columbia. Part II: Mid-Cretaceous to Eocene. *Canadian Journal of Earth Sciences*, **21**, 567-583.
- Armstrong, R.L., 1982, Cordilleran metamorphic core complexes: *Annual Reviews of Earth and Planetary Sciences*, **10**, 129-154.
- Armstrong, R.L., 1988. Mesozoic and Early Cenozoic magmatic evolution of the Canadian Cordillera. *In Processes In Continental Lithospheric Deformation*, Edited by S.P.Clark, B.C. Burchfiel, and J. Suppe. Geological Society of America, Special Paper 218, 55-91.
- Armstrong, R.L., Parrish, R.R., van der Heyden, P., Scott, K., and Runkle, D., 1991. Early Proterozoic basement exposures in the southern Canadian Cordillera core gneiss of Frenchman Cap, Unit I of the Grand Forks gneiss, and the Vaseaux Formation. *Canadian Journal of Earth Sciences*, **28**, 1169-1201.
- Armstrong, R.L., van der Heyden, P., and Ghosh, D, 1989. The 2.1 to 2.3 Ga basement under Quesnellia between 47° and 53° N. *Proceedings of the*

- Cordilleran Workshop, University of Calgary Publications, p.60.
- Barker, F., and Arth, J.G., 1990. Two traverses across the Coast batholith, southeastern Alaska. *In* The nature and origin of Cordilleran magmatism, *Edited by* J.L. Anderson. Geological Society of America, Memoir 174, 395-405
- Barton, M.D., 1990. Strongly peraluminous granites in the western United States as part of a temporal continuum. Transactions of the American Geophysical Union, 71, 694-696.
- Bateman, P.C., 1983. A summary of critical relations in the central part of the Sierra Nevada batholith, California, U.S.A. Geological Society of America, Memoir 159, 241-254.
- Beaudoin, G.A., Sangster, and C.I. Godwin, 1992. Isotopic evidence for complex Pb sources in the Ag-Pb-Zn-Au veins of the Kokanee Range, southeastern British Columbia. Canadian Journal of Earth Sciences, 29, 418-431.
- Bergantz, G.W., 1989. Underplating and partial melting: Implications for melt generation and extraction. Science, 245, 1093-1095.
- Brandon, A.D., 1989. Constraints on magma genesis behind the Neogene Cascade arc: Evidence from major and trace element variation of high-alumina and tholeiitic volcanics of the Bear Creek area. Journal of Geophysical Research, 94, 7775-7798.
- Brandon, A.D., and Goles, G.G., 1988. A Miocene subcontinental plume in the Pacific Northwest: Geochemical evidence. Earth and Planetary Science Letters, 88, 273-283.
- Brandon, A.D., and Lambert, R.St.J., 1990. Geochemistry of the 115 Ma White Creek batholith of southeast British Columbia: Implications for the origin of granitoids in the Omineca Crystalline Belt. Geological

- Association of Canada and Mineralogical Association of Canada, Annual Meeting, Program with Abstracts, 15, p. A14.
- Brandon, A.D., and Lambert, R.StJ., 1992a. Geochronology of Mesozoic granitoids in the southern Canadian Cordillera. *In* Project Lithoprobe Southern Cordillera Transect, Report no. 24, 95-104.
- Brandon, A.D., and Lambert, R.StJ., 1992b. Geochemical characterization of mid-Cretaceous granitoids in the Kootenay Arc in the southern Canadian Cordillera. *Canadian Journal of Earth Sciences*, submitted.
- Brandon, A.D., and Lambert, R.StJ., 1992c. Crustal melting Cordilleran interior: The mid-Cretaceous White Creek batholith in the southern Canadian Cordillera. *Journal of Petrology*, submitted.
- Bullen, T.D., and Clynne, M.A., 1990. Trace element and isotopic constraints on magmatic evolution at Lassen volcanic center. *Journal of Geophysical Research*, 95, 19671-19692.
- Butler, R.F., Gehrels, G.E., McClelland, W.C., May, S.R., and Klepacki, D., 1989. Discordant paleomagnetic poles for the Canadian Coast Plutonic Complex: Regional tilt rather than large-scale displacement? *Geology*, 17, 691-694.
- Calderwood, A.R., van der Heyden, P., and Armstrong, R.L., 1990. Geochronometry of the Thuya, Takomkane, Raft, and Baldy batholiths, south-central British Columbia. *Geological Association of Canada, Program with Abstracts*, 15, p.A19.
- Carr, S.D., 1991a. Tectonic evolution of the Thor-Odin - Pinnacles area, southern Omineca Belt, British Columbia. *Proceedings of the Lithoprobe Cordilleran Workshop, University of Calgary Publications*, 61-75.
- Carr, S.D., 1991b. U-Pb zircon and titanite ages from three Mesozoic igneous rocks of the Thor-Odin - Pinnacles area, southern Omineca Belt, British

- Columbia. *Canadian Journal of Earth Sciences*, **28**, 1877-1882.
- Carr, S.D., and Brown, R.L., 1990, Southern Cordilleran Lithoprobe transect lines 6 to 10: Crustal structure and tectonic chronology. *Proceedings of the Cordilleran Workshop, University of Calgary Publications*, 10-19.
- Chamberlain, V.E., 1983. The Malton gneiss complex, Valemount, B.C., Ph.D. Thesis, University of Alberta.
- Chamberlain, V.E., and Lambert, R.StJ., 1985. Cordilleria, a newly defined Canadian microcontinent. *Nature*, **314**, 707-713.
- Chamberlain, V.E., and Lambert, R.StJ., and Holland, J.G., 1988. Geochemistry of the gneissic basement complex near Valemount, British Columbia: further evidence for a varied origin. *Canadian Journal of Earth Sciences*, **25**, 1725-1739.
- Clemens, J.D., and Vielzeuf, D., 1987. Constraints on melting and magma production in the crust. *Earth and Planetary Science Letters*, **86**, 287-306.
- Cole, F., Butler, R.F., and Gehrels, G.E., 1992. Paleomagnetism of late Paleozoic rocks in the northern Cache Creek terrane near Atlin, British Columbia. *Canadian Journal of Earth Sciences*, **29**, 486-498.
- Cook, F.A., Green, A.G., Simony, P.S., Price, R.A., Parrish, R.R., Milkereit, B., Gordy, P.L., Brown, R.L., Coflin, K.C., and Patenaude, C., 1988. Lithoprobe seismic reflection structure of the southeastern Canadian Cordillera. *Tectonics*, **7**, 157-180.
- Cook, F.A., Varsek, J., Clowes, R., Kanasevich, E., Spencer, C., Brown, R., Carr, S., Parrish, R., Johnson, B., Price, R., and Moore, J., 1990. Reflection crustal structure of the southern Canadian Cordillera interior: Omineca crystalline belt and intermontane belt. *Proceedings of the Cordilleran Workshop, University of Calgary Publications*, 1-19.

- DePaolo, D.J., 1988. Neodymium Isotope Geochemistry, An Introduction. Springer-Verlag, Berlin.
- Einarsen, J.M., 1990. Structural setting and geochemistry of granitic stocks in the Quesnellia-North America boundary of southeastern B.C. Geological Society of America, Abstracts with Programs, 22, no.3, 20-21.
- Fleck, R.J., 1990. Neodymium, strontium, and trace-element evidence of crustal anatexis and magma mixing in the Idaho batholith. *In* The Nature and Origin of Cordilleran Magmatism, Edited by J.L. Anderson, Geological Society of America, Memoir 174, 359-373.
- Foster, D.A., and Hyndman, D.W., 1990. Magma mixing and mingling between synplutonic mafic dikes and granite in the Idaho-Bitterroot batholith. *In* The Nature and Origin of Cordilleran Magmatism, Edited by J.L. Anderson, Geological Society of America, Memoir 174, 359-373.
- Furlong, K.P., and Fountain, D.M., 1986. Continental crustal underplating: Thermal considerations and seismic-petrologic consequences. Journal of Geophysical Research, 91, 8285-8294.
- Gordon, G.E., Randle, K., Goles, G.G., Corliss, J.B., Beeson, M.H., 1968. Instrumental activation analysis of standard rocks with high-resolution gamma-ray detectors. Geochimica et Cosmochimica Acta, 32, 369-396.
- Ghosh, D., 1986. Geochemistry of the Nelson-Rossland area, B.C. Ph.D. thesis, University of Alberta.
- Ghosh, D., 1990. Isotopic evidence for 1.8-2.3 Ga crust under Quesnellia. Geological Association of Canada and Mineralogical Association of Canada, Annual Meeting, Programs with Abstracts, 15, p.A46.
- Ghosh, D., 1991. Nd and Sr isotopic constraints on the timing of obduction of Quesnellia onto the western edge of North America. Proceedings of the Cordilleran Workshop, University of Calgary Publications, 113-127.

- Ghosh, D., and Lambert, R.StJ., 1989. Nd-Sr isotope study of Proterozoic to Triassic sediments from southeastern British Columbia. *Earth and Planetary Science Letters*, **94**, 29-44.
- Glazner, A.F., and Ussler, W., 1988. Trapping of magma at midcrustal density discontinuities. *Geophysical Research Letters*, **15**, 673-675.
- Gromet, L.P., and Silver, L.T., 1987. REE variations across the Peninsular Ranges batholith: Implications for batholithic petrogenesis and crustal growth in magmatic arcs. *Journal of Petrology*, **28**, 75-125.
- Hart, S., 1984. A large-scale isotopic anomaly in the Southern Hemisphere mantle. *Nature*, **47**, 753-757.
- Hawkesworth, C.J., 1979. $^{143}\text{Nd}/^{144}\text{Nd}$, $^{87}\text{Sr}/^{86}\text{Sr}$ and trace element characteristics of magmas along destructive plate margins. *In* *Origin of Granite Batholiths*, Edited by M.P. Atherton and J. Tarney, Shiva, Chesire, 76-89.
- Hildreth, W., and Moorbath, S., 1988. Crustal contributions to arc magmatism in the Andes of central Chile. *Contributions to Mineralogy and Petrology*, **98**, 455-489.
- Hoisch, T.D., and Hamilton, W.B., 1990. Granite generation by fluid-induced anatexis. *Transactions of the American Geophysical Union*, **71**, 694-696.
- Hooper, P.R., and Johnson, D., 1987. Major and trace element analyses of rocks and minerals by automated X-ray spectrometry. In house report, Department of Geology, Washington State University, Pullman.
- Hughes, S.S., 1990. Mafic magmatism and associated tectonism of the central High Cascade Range, Oregon. *Journal of Geophysical Research*, **95**, 19623-19638.
- Hyndman, D.W., and Foster, D.A., 1988. The role of tonalites and mafic dikes in the generation of the Idaho batholith. *Journal of Geology*, **96**, 31-46.

- Irving, E., and Archibald, D.A., 1990. Bathozonal tilt corrections to paleomagnetic data from mid-Cretaceous plutonic rocks. Examples from the Omineca belt, British Columbia. *Journal of Geophysical Research*, **95**, 4579-4585.
- Jacobsen, S.B., and Wasserburg, G.J., 1984. Sm-Nd isotopic evolution of chondrites and achondrites, 2. *Earth and Planetary Science Letters*, **67**, 137-150.
- Johnson, C.M., 1989. Isotopic zonations in silicic magma chambers. *Geology*, **17**, 1136-1139.
- Johnson, C.M., 1991. Large-scale crust formation and lithosphere modification beneath Middle to Late Cenozoic calderas and volcanic fields, western North America. *Journal of Geophysical Research*, **96**, 13485-13507.
- Lambert, R.StJ., 1983. Metamorphism and thermal gradients in the Proterozoic continental crust. *In Proterozoic Geology, Selected Papers from an International Symposium, Edited by L.G. Medaris, C.W. Byers, D.M. Mickelson, and W.C.Shanks. Geological Society of America, Memoir 161, 155-165.*
- Lambert, R.StJ., and Chamberlain, V.E., 1988. Cordillera revisited, with a three-dimensional model for Cretaceous tectonics in British Columbia. *Journal of Geology*, **96**, 47-60.
- Lambert, R.StJ., and Chamberlain, V.E., 1990. Isotopic studies on Mesozoic and Tertiary granitoids and their Precambrian basement, BC, Washington, and Idaho. *Proceedings of the 1990 Lithoprobe Cordilleran Workshop, University of Calgary*, 91-98.
- Little, H.W., 1960. Nelson map area, west half, British Columbia. *Geological Survey of Canada, Memoir 308.*
- Leeman, W.P., Smith, D.R., Hildreth, W., Palacz, Z., and Rogers, N., 1990.

- Compositional diversity of the Late Cenozoic basalts in a transect across the southern Washington Cascades: Implications for subduction zone magmatism. *Journal of Geophysical Research*, **95**, 19561-19582.
- McDonough, M.R., and Parrish, R.R., 1991. Proterozoic gneisses of the Malton Complex, near Valemount, British Columbia: U-Pb ages and Nd isotopic signatures. *Canadian Journal of Earth Sciences*, **28**, 1202-1216.
- Menzies, M.A., 1989. Cratonic, circumcratonic, and oceanic mantle domains beneath the western United States. *Journal of Geophysical Research*, **94**, 7899-7915.
- Miller, C.F., and Barton, M.D., 1990. Phanerozoic plutonism in the Cordilleran interior, USA. *In Plutonism from Antarctica to Alaska, Edited by S.M. Kay and C.W. Rapela, Geological Society of America, Special Paper 241*, 213-131.
- Miller, C.F., Watson, E.B., and Harrison, T.M., 1988. Perspectives on the source, segregation and transport of granitoid magmas. *Transactions of the Royal Society of Edinburgh, Earth Sciences*, **79**, 135-156.
- Miyashiro, A., 1974. Volcanic rock series in island arcs and active continental margins. *American Journal of Science*, **274**, 321-355.
- Monger, J.W.H., and Berg, H.C., 1987. Lithotectonic terranes of Western Canada and Southeastern Alaska. Map MF-1874B, United States Geological Survey, 1-12.
- Monger, J.W.H., and Irving, E., 1980. Northward displacement of north-central British Columbia. *Nature*, **285**, 289-293.
- Monger, J.W.H., and Price, R.A., 1979. Geodynamic evolution of the Canadian Cordillera - progress and problems. *Canadian Journal of Earth Sciences*, **16**, 770-791.
- Monger, J.W.H., Price, R.A., and Tempelman-Kluit, D.J., 1982. Tectonic accretion

- and the origin of the two major metamorphic and plutonic belts in the Canadian Cordillera. *Geology*, **10**, 70-75.
- Parrish, R.R., and Armstrong, R.L., 1987. The ca. 162 Ma Galena Bay stock and its relationship to the Columbia River fault zone, southeast British Columbia. *In Radiogenic Age and Isotopic Studies, Report 1, Geological Survey of Canada, Paper 87-2*, 25-32.
- Parrish, R.R., and Wheeler, J.O., 1983. U-Pb zircon age for the Kuskanax batholith, southeastern British Columbia. *Canadian Journal of Earth Sciences*, **20**, 1751-1756.
- Parrish, R.R., Carr, S.D., and Parkinson, D.L., 1988. Eocene extensional tectonics and geochronology of the southern Omineca Belt, British Columbia and Washington. *Tectonics*, **7**, 181-212.
- Patiño Douce, A.E., Humphreys, E.D., and Johnston, A.D., 1990. Anatexis and metamorphism in tectonically thickened continental crust exemplified by the Sevier hinterland, western North America. *Earth and Planetary Science Letters*, **97**, 290-315.
- Pearce, J.A., Harris, N.B.W., and Tindle, A.G., 1984. Trace element discrimination diagrams for the tectonic interpretation of granitic rocks. *Journal of Petrology*, **25**, 956-983.
- Pitcher, W.S., 1984. Phanerozoic plutonism in the Peruvian Andes. *In Andean Magmatism, Chemical and Isotopic Constraints, Edited by R.S. Harmon and B.A. Barreiro, Shiva Publications, Chesire*, 152-167.
- Reesor, J.E., 1958. Dewar Creek map-area with special emphasis on the White Creek batholith, British Columbia. *Geological Survey of Canada, Memoir 292*.
- Reesor, J.E., 1973. Geology of the Lardeau map-area, east half, British Columbia. *Geological Survey of Canada, Memoir 369*.

- Rubin, C.M., Saleeby, J.B., Cowan, D.S., Brandon, M.T., and McGroder, M.F., 1990. Regionally extensive Mid-Cretaceous west-vergent thrust system in the northwestern Cordillera. Implications for continent-margin tectonism. *Geology*, v.18, p.276-280.
- Rusmore, M.E., Potter, C.J., and Umhoefer, P.J., 1988. Middle Jurassic terrane accretion along the western edge of the Intermontane Superterrane, southwestern British Columbia. *Geology*, 16, 891-894.
- Saunders, A.D., Norry, M.J., and Tarney, J., 1988. Origin of MORB and chemically depleted mantle reservoirs: Trace element constraints. *Journal of Petrology*, Special Lithosphere Issue, 415-445.
- Shand, S.J., 1949. *Eruptive Rocks*. John Wiley and Sons, New York.
- Smith, A.D., 1992. Back-arc convection model for Columbia River Basalt genesis. *Tectonophysics*, in press.
- Smith, M.T., Gehrels, G.E., and Klepacki, D.W., 1992. 173 Ma U-Pb age of felsite sills (Kaslo river intrusive) west of Kootenay Lake, southeastern British Columbia. *Canadian Journal of Earth Sciences*, 29, 531-534.
- Spear, F.S., and Peacock, S.M., 1990. Program manual and computer exercises for the calculation of metamorphic phase equilibria, pressure-temperature-time paths and thermal evolution of orogenic belts. In-house publication by Frank Spear, Rensselaer Polytechnic Institute, Troy, New York.
- Stolper, E.D., Walker, D., Hager, B.D., and Hays, J.F., 1981. Melt segregation from partially molten source regions: The importance of melt density and source region size. *Journal of Geophysical Research*, 86, 6261-6271.
- Tatsumi, Y., Hamilton, D.L., and Nesbitt, R.W., 1986. Chemical characteristics of fluid phase released from a subducted lithosphere and origin of arc magmas: Evidence from high-pressure experiments and natural rocks.

- Journal of Volcanology and Geothermal Research*, **29**, 293-309.
- Thorkelson, D.J., and Smith, A.D., 1989. Arc and intraplate volcanism in the Spences Bridge Group: Implications for Cretaceous tectonics in the Canadian Cordillera. *Geology*, **17**, 1093-1096.
- Trønnes, R.G., and Brandon, A.D., 1992. Mildly peraluminous high-silica granites in a continental rift: The Drammen and Finnemarka batholiths, Oslo Rift, Norway. *Contributions to Mineralogy and Petrology*, **109**, 275-294.
- Wanless, R.K., Loveridge, W.D., and Mursky, G., 1968. A geochronological study of the White Creek batholith, southeastern British Columbia. *Canadian Journal of Earth Sciences*, **5**, 375-386.
- Wickham, S.M., 1987. The segregation and emplacement of granitic magmas. *Journal of the Geological Society of London*, **144**, 281-297.
- Wolff, M.B., and Wyllie, P.J., 1991. Dehydration-melting of solid amphibolite at 10 kbar: Textural development, liquid interconnectivity and applications to the segregation of magmas. *Mineralogy and Petrology*, **44**, 151-179.
- Zen, E.A., 1986. Aluminum enrichment in silicate melts by fractional crystallization: Some mineralogic and petrographic constraints. *Journal of Petrology*, **27**, 1095-1117.
- Zen, E.A., 1988. Thermal modelling of stepwise anatexis in a thrust-thickened sialic crust. *Transactions of the Royal Society of Edinburgh. Earth Sciences*, **79**, 223-235.
- Zen, E.A., 1984, and Hammarstrom, J.M., 1984. Magmatic epidote and its petrologic significance. *Geology*, **12**, 515-518.

Chapter 6

Concluding Remarks

Within southeast British Columbia (SEBC), Middle Jurassic and mid-Cretaceous granitoid batholiths are exposed in the Omineca Belt, a N-S trending metamorphic and plutonic orogenic belt which formed as the result of compressional tectonics in the Mesozoic during terrane accretion, and extensional tectonics in the Paleocene and Eocene. In this study, I determined the ages, lithological, and geochemical characteristics of several of the batholiths in order to constrain the possible mechanisms for granitoid generation with the Omineca Belt. Understanding the petrogeneses for granitoids in this region has yielded insight into the processes for granitoid production during the Mesozoic in the Cordilleran interior of western North America.

In Chapter 2, Rb-Sr isochrons for several of the batholiths give the following ages : Raft - 164 +/- 4 Ma for whole rock; Bugaboo - 107 +/- 1 Ma for whole rock-apatite (WRA); Horsethief Creek - 109 +/- 14 Ma for WRA; Fry Creek - 115 +/- 7 Ma for WRA; and White Creek - 106 +/- 1 Ma for WRA. Most of the isochrons were improved by using apatite in conjunction with the whole rock data from each batholith. Apatite's utility in pinpointing the initial $^{87}\text{Sr}/^{86}\text{Sr}$ ratio for the isochrons was demonstrated. These ages fall within the ranges for a Middle Jurassic magmatic pulse from approximately 175 to 160 Ma and a mid-Cretaceous magmatic pulse from 115 to 105 Ma defined from a compilation of crystallization ages for all granitoid rocks from southeast British Columbia. Defining the durations of these two magmatic pulses is

important in constraining the mechanisms for granitoid production in the Omineca Belt.

In Chapters 3 and 4, batholiths from the mid-Cretaceous magmatic pulse from the Omineca Belt are considered. The mid-Cretaceous Bugaboo, Horsethief Creek, Fry Creek, and White Creek batholiths are post-kinematic with respect to regional metamorphism which affected their host rocks and are composed calc-alkaline quartz monzodiorite, hornblende-biotite granodiorite and granite, and 2-mica granite. This range of lithologies is similar to the range displayed by calc-alkaline granitoids in the Cordilleran interior in the United States. The White Creek batholith is a zoned pluton with quartz monzodiorite on the rim grading into hornblende-biotite granodiorite, which in turn is crosscut by 2-mica granites. The hornblende-biotite granitoids have initial ϵ_{Sr} ranging from +36 to +80, initial ϵ_{Nd} ranging from -5 to -9 and overlap the range of Nd-Sr isotopic compositions for Precambrian basement gneisses and Proterozoic metasediments found in SEBC. The initial $^{206}Pb/^{204}Pb$, $^{208}Pb/^{204}Pb$, and $^{207}Pb/^{204}Pb$ for these granitoids lie in a band between model lower and upper crustal Pb isotopic compositions above the Northern Hemisphere Reference Line for oceanic basalts. These granitoids have high Nb and Rb, and low Ba abundances relative to granites found in volcanic arcs, and other trace element characteristics which are not in accordance with differentiation from mafic magmas to produce more evolved silicic magmas. The 2-mica granites are strongly peraluminous and have ϵ_{Sr} ranging from +150 to +470, ϵ_{Nd} ranging from -12 to -21, and more radiogenic initial Pb isotope ratios than the hornblende-biotite granitoids. Their trace element compositions are similar to strongly peraluminous granites found in continental interiors.

Oxygen and Sr isotopes, REE modelling of granitoid compositions, and phase equilibrium considerations are consistent with a model for crustal anatexis of Precambrian basement gneisses and Proterozoic metapelites to produce the mid-Cretaceous hornblende-biotite granitoids and 2-mica granites, respectively. The sequence of intrusion in the White Creek batholith, where the most mafic hornblende-biotite granitoids intruded earliest, followed by more silicic magmas and ending with strongly peraluminous granites, constrains the timing of melting in the mid-Cretaceous crust. A scenario where a melt zone migrated upwards in the crust beneath the intrusion level of the Cretaceous batholiths, likely as the result of dehydration melting in response to crustal thickening, produced melting of the basement gneisses followed by melting of overlying metapelites. Crustal thickening occurred during the Mesozoic in SEBC as exotic terranes collided with and were accreted to the western edge of the North American continent.

Trace element and isotopic compositions of the mid-Cretaceous granitoids are consistent with a petrogenesis where the geochemical influence of mantle-derived magma on these granitoid magmas is minimal. However, in crustal thickening models for the Cordilleran interior, temperatures only high enough to induce biotite dehydration melting have been favored. In order to achieve the slightly higher temperatures required for hornblende dehydration melting, and to produce the mid-Cretaceous hornblende-bearing granitoids by crustal anatexis, an additional heat source, probably in the form of heat transfer from the mantle, is needed. In Chapter 5, I consider several mechanisms for producing higher temperatures in the mid-Cretaceous crust and conclude that the most likely mechanism is by basaltic underplating during the Middle Jurassic magmatic pulse which left

the crust in SEBC at a higher temperature for the rest of the Mesozoic. This model is in accordance with geologic constraints.

Also in Chapter 5, the petrogenesis of the Middle Jurassic granitoids is considered. I analyzed samples from the the Middle Jurassic Raft, Galena Bay, and Mt. Toby plutons. These plutons have compositional features similar to other Middle Jurassic granitoids in SEBC. They generally have lower initial ϵ_{Sr} and higher ϵ_{Nd} and less radiogenic initial $^{206}Pb/^{204}Pb$, $^{208}Pb/^{204}Pb$, and $^{207}Pb/^{204}Pb$ ratios than the mid-Cretaceous granitoids. These isotopic features are consistent with mixing between mantle-derived basalt and Precambrian crust. Their trace element compositions are similar to granitoids found within volcanic arcs. In particular, they have high Ba and low Rb and Nb relative to the mid-Cretaceous granitoids. The compositional relationships for the Middle Jurassic granitoids are consistent with an origin where these rocks were formed in a volcanic arc. This arc formed on Terrane I as subduction of ocean crust and accretion of Terrane II occurred westwards from Early to Middle Jurassic. It is possible that these Middle Jurassic batholiths are related to the Jurassic Hazelton volcanic group, which spans across Terrane I in a N-S belt for several hundred kilometers in British Columbia. Further study is needed in order to test this hypothesis, and to ascertain its implications to the tectonics which formed the Phanerozoic Cordilleran orogenic belt in western Canada.

In conclusion, the diverse magmatism and the excellent exposure of igneous rocks in the Omineca Belt in SEBC provides an outstanding laboratory for studying igneous petrology and geochemistry. This, and earlier studies have only begun to unravel the complex magmatic history and the clues these rocks have for the genesis of magmas in continental orogenic belts.